Neutron Scattering Principal Investigators' Meeting

Virtual Meeting, December 15–17, 2021

Program and Abstracts

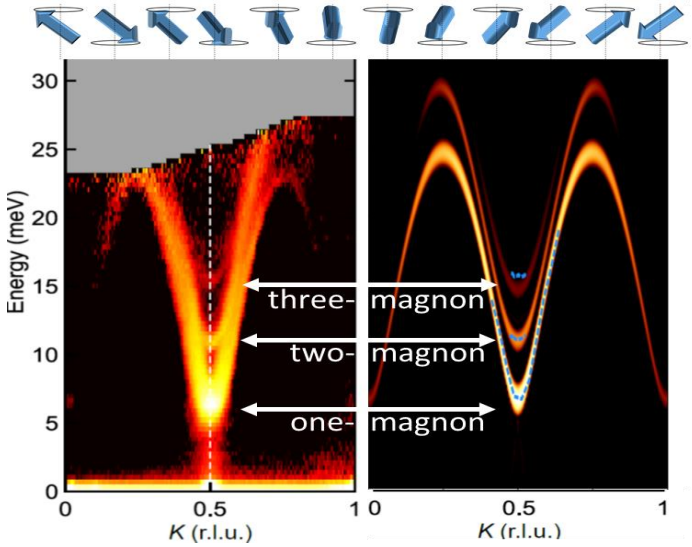

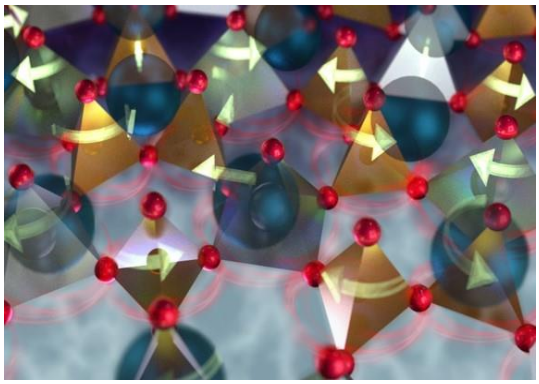

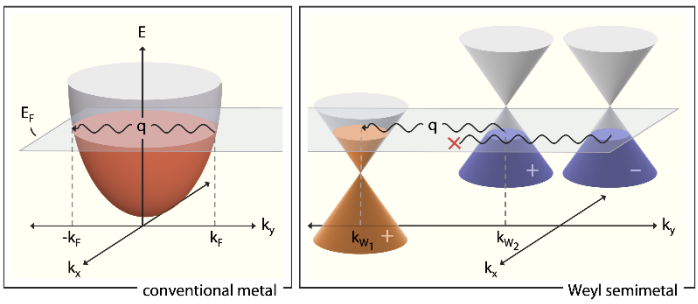

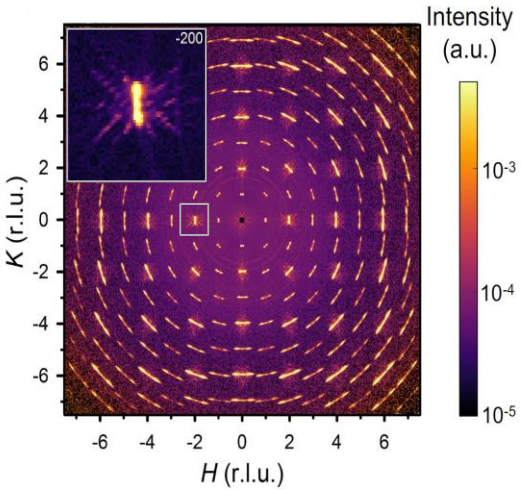

Office of Basic Energy Sciences
Division of Materials Sciences and Engineering

U.S. DEPARTMENT OF ENERGY | Office of Science

On the Cover

Top Left: Oscillating moments in a spin chain, forming a magnon (top). Neutron scattering data (left) and corresponding theoretical models (right) in $NaMnO_2$ corresponding to one-, two-, and three-magnon bound states. $NaMnO_2$ represents the first antiferromagnetic (antiparallel alignment of magnetic moments) material that hosts a three-magnon bound state, demonstrating that such quasiparticles are stable enough to form. Using multiple-magnon bound states as carriers of quantum information is of interest in future quantum technologies and provides a model material for studying the formation and properties of these new multiple-magnon quasiparticles. (Image courtesy of Stephen Wilson and Rebecca Dally.)

Top Right: Heat usually moves by atomic vibrations that are limited by the speed of sound. Heat also can move by quasiparticles (phasons) related to atomic rearrangements that change with the movement of waves in the crystal structure. Using neutron scattering, this research discovered supersonic phasons that could remove harmful heat in electronics and send signals faster. Phasons were observed in a mineral containing titanium (gray) and silicate (orange) polyhedrons linked at their corners. (Oxygen is red, while barium is the large blue spheres.) Below a critical temperature, the polyhedrons began to twist and slide (arrows). (Image courtesy of the Oak Ridge National Laboratory.)

Bottom Left: Energy versus momentum depiction of different conditions that give rise to a Kohn anomaly in conventional metals (left), versus a Weyl semimetal (right). Theoretical research has shown that the topology of the *electronic* states in a Weyl semimetal (a topological material) can leave fingerprints on their *phonon* spectral properties. This happens due to electron-phonon interactions called the Kohn anomaly that impacts how electrons screen phonons through a material. Using a novel combination of neutron and x-ray scattering and theory, topological electronic states were shown to alter the phonon spectra in materials, which hold promise for future quantum applications. (Image courtesy of Mingda Li, Massachusetts Institute of Technology.)

Bottom Right: Neutron diffraction from a lightly-doped $SrTiO_3$ crystal that was plastically and compressively deformed by 4.5% along [010]. Note that instead of spots at integer positions, the Bragg peaks are arc-like, with a fine pattern indicative of periodic dislocation walls. Inset: Zoomed spot from the marked square showing a complex pattern indicative of ordering in the material. Strontium titanate is an archetypical quantum material with intriguing ferroelectric and superconducting properties. Superconductivity is characterized by zero electrical resistance and the complete expulsion of magnetic fields, whereas ferroelectricity signifies a spontaneous electric polarization that can be reversed by an electric field. This research shows that plastic deformation of the material induces extended defects (known as dislocations) to self-organize into periodic structures. These structural changes lead to surprisingly enhanced superconducting and ferroelectric properties. (Image courtesy of Martin Greven, University of Minnesota.)

This document was produced under contract number DE-SC0014664 between the U.S. Department of Energy and Oak Ridge Associated Universities.

The research grants and contracts described in this document are supported by the U.S. DOE Office of Science, Office of Basic Energy Sciences, Materials Sciences and Engineering Division.

Foreword

This abstract book is a compilation of the scientific content presented at the 2021 Neutron Scattering Principal Investigators' (PI) Meeting (virtual due to Covid-19 pandemic) sponsored by the Division of Materials Sciences and Engineering (MSED) in the U.S. Department of Energy Office of Basic Energy Sciences (BES).

This biennial PI meeting held on December 15–17, 2021, is seventh in the series for the Neutron Scattering program. The purpose of the meeting is to bring together all the PIs supported by the program on a periodic basis to facilitate discussions of recent research accomplishments of the projects, to nucleate new ideas and to encourage collaborations among the groups, and to identify new research opportunities. The meeting also serves BES to assess the state of the program, to chart new research directions and to identify programmatic needs.

The program addresses the increasing complexity of DOE mission-relevant materials for various energy applications requiring sophisticated experimental and computational tools to investigate the structure and dynamics at relevant length and time scales. Its goal aligns well with the BES mission in supporting fundamental research to understand, predict, and ultimately control matter and energy at the electronic, atomic, and molecular levels in order to provide the foundations for new energy technologies and to support DOE missions in energy, environment, and national security. It supports projects at national laboratories and universities with scientific scopes on transformative research on materials and phenomena using neutron scattering as a major tool, coupled with the advancement of neutron scattering techniques and approaches primarily at the BES user facilities. A continuing theme of the program is the integration of high-quality material synthesis, single crystal growth, advanced neutron scattering measurements and computational modeling needed for an in-depth understanding of the structure and dynamics of materials and their relationship to macroscopic properties.

The co-chairs, Dr. Raphaël Hermann from ORNL and Professor YZ from UIUC, are highly appreciated for their effort in reading the abstracts to develop an effective agenda and in conducting the virtual meeting smoothly. Dr. Helen Kerch and Teresa Crockett from BES and Tia Moua and Linda Severs from the Oak Ridge Institute for Science and Education (ORISE) are thanked for their outstanding support from planning to the execution of the meeting.

Thiyaga P. Thiyagarajan
MSED, BES, Office of Science
U.S. Department of Energy

Table of Contents

Agenda ix

Poster Lists xv

Invited Talks

Neutron Facilities in the USA and Around the World
Ken Andersen 3

Neutron Scattering: The Next Decade
Sunil K. Sinha 4

Scientific Computing and Research Data Management as Tools for Accelerating Scientific Discovery at Research Infrastructures
Jonathan Taylor 5

University Abstracts

Investigation of Short-Range Ordering in Transition Metal Compounds by Diffuse Scattering
Jared M. Allred 9

Dynamic Modulation of Structure and Phase Transformations in Asymmetric Crystalline Colloidal Brush Alloys
Michael R. Bockstaller, Krzysztof Matyjaszewski, and Alamgir Karim 13

***In Operando* Neutron Diffraction Study of Phase Transitions in Si Electrode Morphologies Using a Novel Electrochemical Cell**
K. S. Ravi Chandran 17

Non-Reciprocal Effects in Non-Centrosymmetric Magnets: Neutron and Optical Studies
S.-W. Cheong, V. Kiryukhin, and A. Sirenko 22

Using Neutron as a Probe to Study Magnetic Excitations in Strongly Correlated Electron Materials
Pengcheng Dai 28

Flow-Through Neutron Reflectometry – An *In Operando* Sample Environment for Active Polymer Interface Studies
Steven C. DeCaluwe 34

Neutron Scattering Studies of Phonon Anharmonicity and Coupling with Spin and Charge Degrees of Freedom
Olivier Delaire 38

Equilibrium and Non-Equilibrium Vortex and Skyrmion Lattices
Morten R. Eskildsen 43

Probing Short-Range Structure and Magnetism in Next-Generation Energy Conversion Materials
Benjamin Frandsen 48

Inelastic Neutron Scattering Studies of Quantum Anharmonicity and Nonlinear Phonons
Brent Fultz 52

Exotic Uses of Neutrons and X-rays as Probes for Chiral Magnets
Dustin A. Gilbert 56

University of Minnesota Center for Quantum Materials (CQM)
Martin Greven, Turan Birol, Rafael Fernandes, Bharat Jalan, and Chris Leighton 61

Precise Chain Conformation and Dynamics Control for Conjugated Polymers in Organic Electronic Thin Film Devices
Xiaodan Gu 69

Understanding the Structure and Dynamics of Conjugated Polymers by Advancing Deuteration Chemistry and Neutron Scattering
Xiaodan Gu and Jason Azoulay 73

Understanding the Role of Polymer Topology on Molecular Deformation and Scission under Extreme Shear using *In Situ* Neutron Scattering
Matthew E. Helgeson and Patrick T. Underhill 80

Novel Quantum Phenomena in Geometrically Frustrated Magnets Near the Metal-Insulator Phase Boundary
Xianglin Ke 85

Role of Organic Cations in Organic-Inorganic Perovskite Solar Cells
Seung-Hun Lee and Joshua J. Choi 89

Scattering and Spectroscopic Studies of Quantum Materials
Young Lee, Hongchen Jiang, and Jiajia Wen 92

Tracing the Topological Fingerprint of Weyl Semimetals Using Neutron Probes
Mingda Li 97

Machine Learning-Augmented Multimodal Neutron Scattering for Emergent Topological Materials
Mingda Li 102

Structure and Dynamics of Ion-Containing Nanostructured Ternary Polymer Blend
Timothy P. Lodge and Frank S. Bates 106

Quantum Materials with Non-trivial Electronic Topologies and Flat Bands Studied via Neutron Scattering
Despina Louca 111

Quantification of Dynamic Disorder in Electronic and Excitonic Organic Materials
Adam J. Moulé 114

Quantum Multipolar Fluctuations in Spin-Orbit Magnets
Martin Mourigal and Cristian Batista 119

Encoding Material Structure Into the Primary Sequence of Polymers
Bradley D. Olsen 124

Ionic Polymers Under Dynamic Conditions
Dvora Perahia 129

Deciphering Low Energy Spin and Orbital Dynamics in Frustrated Quantum Magnets
Kemp Plumb 135

Neutron Analysis of Structure-Property Relationships in Conductive Polymer Plastic Composites
Lilo D. Pozzo and Christine Luscombe 138

Inelastic Neutron and X-ray Scattering Investigation of Electron-Phonon Effects in Quantum Materials
Dmitry Reznik 142

Structure-Property Relationships in Porous Electrodes for Electrochemical Energy Storage
Jeffrey J. Richards 147

Discovering Toroidal Materials with Spherical Neutron Polarimetry
Efrain E. Rodriguez 151

Non-Equilibrium Effects in Quantum Magnets
Kate A. Ross 156

Fundamental Understanding of Bottlebrush Polymers Based on Structure and Dynamics
Gerald J. Schneider 159

Neutron and X-Ray Studies of Spin and Change Manipulation in Magnetic Nanostructures
Sunil K Sinha and Eric Fullerton 164

Revealing the Molecular Origin of Interactions between Nanocrystals
William Tisdale and James Swan 170

Orbitally Active AMX_2 as a Platform for Novel Magnetism and Entangled Electronic States
Stephen D. Wilson 174

Bound Layer Exchange in Polymer Nanocomposite Melts
Karen I. Winey and Robert A. Riggleman 178

Unraveling Emergent Quantum States in Magnetic Topological Insulators using High Pressure Neutron Scattering
Weiwei Xie 182

Exotic Magnetic Orders and Dynamics in Chiral Magnets
Junjie Yang 188

Universality of Collective Dynamics in Liquids At and Away from Equilibrium
Yang Zhang 192

Laboratory Abstracts

Local Site Magnetic Susceptibility for Quantum Materials
Huibo Cao 201

Understanding Quantum Matter Beyond the Unit Cell
Andrew Christianson, Joseph Paddison, Andrew May, Gábor Halász, and David Mandrus 207

Neutron Studies of Hybrid Excitations
R. P. Hermann, M. E. Manley, and R. S. Fishman 214

Realization of Full Neutron Polarization Control: Next Generation Spherical Neutron Polarimetry for Neutron Scattering
Chenyang Jiang 220

Resolving the Structure and Dynamics of Advanced Materials with Unprecedented Resolution
Fankang Li 223

Neutron and X-ray Scattering Investigations of the Influence of Short-Range Correlations, Interfaces, and Complex Disorder on Materials Properties
S. Rosenkranz, O. Chmaissem, R. Osborn, D. Phelan, and S. G. E. te Velthuis 226

National School on Neutron and X-ray Scattering
Stephan Rosenkranz, Matthias Frontzek, Bianca Haberl, Michael Manley, and Uta Ruett 232

Neutron Scattering Studies of Unconventional Superconductors
John M. Tranquada, Genda D. Gu, Cedomir Petrovic, and Igor A. Zaliznyak 237

Fingerprinting Macromolecular Flow and Deformation with Neutrons
Yangyang Wang 253

Author Index 261

Participants List 265

DOE BES Neutron Scattering
Virtual Principal Investigators' Meeting Agenda
December 15 – 17, 2021
Co-Chairs: Raphaël Hermann (ORNL) and Y Z (UIUC)
(Times listed in Eastern Time Zone)

Wednesday, December 15, 2021

Opening Session

11:00–11:15	**Thiyaga P. Thiyagarajan**, Department of Energy *Welcome and Introductory Remarks*
11:15–11:30	**Andrew Schwartz**, Department of Energy *Remarks from BES*
Oral Session 1 (Solid State 1)	Chair: **Raphaël Hermann**
11:30–11:45	**Stephen Wilson**, *University of California, Santa Barbara* *Orbitally-active AMX_2 as a platform for novel magnetism and entangled electronic states* (*Poster:* Quantum disorder in the magnetism of orbitally active AMO_2 compounds)
11:45–12:00	**Olivier Delaire**, *Duke University* *Neutron scattering studies of phonon anharmonicity and coupling with spin and charge degrees of freedom* (*Poster:* Same as above)
12:00–12:15	**Stephan Rosenkranz**, *Argonne National Laboratory* *Neutron and x-ray scattering investigations of the influence of short-range correlations, interfaces, and complex disorder on materials properties* (*Poster 1:* The role of spin, charge, and lattice correlations on materials properties) (*Poster 2:* The role of ionic and lattice correlations on materials properties)
12:15–12:20	**5-Minute Break**
12:20–12:40	**Invited Talk, Ken Andersen, Oak Ridge National Laboratory,** *Neutron facilities in the USA and around the world*
12:40–1:10	**Round-table discussion. Moderator: Raphaël Hermann** **Panel: K. Andersen, C. Leighton, A. Christianson, J. Richards**
1:10–1:25	**15-Minute Break**
1:25–1:30	**Poster Sessions – Introduction to Gathertown**
1:30–2:45	**Poster Session 1 (GatherTown)**
2:45–2:50	**5-Minute Break**

Oral Session 2 (Quantum and Magnetism 1) Chair: **Despina Louca**

2:50–3:05 **Martin Greven**, *University of Minnesota*
University of Minnesota Center for Quantum Materials (*CQM*)
(*Poster 1:* Understanding rare-earth titanates)
(*Poster 2:* Strain and plastic deformation studies)

3:05–3:20 **Morten Eskildsen**, *University of Notre Dame*
Equilibrium and non-equilibrium vortex and skyrmion lattices
(*Poster:* Same as above)

3:20–3:35 **Sang-Wook Cheong**, *Rutgers University*
Non-reciprocal effects in non-centrosymmetric magnets: Neutron and optical studies
(*Poster:* Same as above)

3:35–3:50 **Andrew Christianson**, *Oak Ridge National Laboratory*
Understanding quantum matter beyond the unit cell
(*Poster 1:* Magnetic interactions of the skyrmion material Gd_2PdSi_3)
(*Poster 2*: Emergent spin clusters in breathing pyrochlore magnets)

3:50–4:05 **Martin Mourigal**, *Georgia Institute of Technology*
Quantum multipolar fluctuations in spin-orbit magnets
(*Poster:* Same as above)

4:05-4:15 **10-Minute Break**

4:15–5:30 **Poster Session 2 (GatherTown)**

Thursday, December 16, 2021

11:00–11:05 **Welcome to Day Two – Thiyaga P. Thiyagarajan**, Department of Energy

Oral Session 3 (Solid State 2 and Energy Materials) Chair: **Ray Osborn**

11:05–11:20 **Dmitry Reznik**, *University of Colorado – Boulder*
Inelastic neutron and x-ray scattering investigation of electron-phonon effects in quantum materials
(*Poster:* Effect of site occupation disorder on thermal conductivity in the clathrate $Ba_8Ga_{16}Ge_{30}$)

11:20–11:35 **Raphaël Hermann**, *Oak Ridge National Laboratory*
Neutron studies of hybrid excitations
(*Poster 1:* Giant isotopic shift in phonons keeps charge carriers hot longer in a photovoltaic perovskite)
(*Poster 2:* Doping-driven transport and magnetism in MnTe)

11:35–11:50	**Adam Moulé**, *University of California, Davis* *Quantification of dynamic disorder in electronic and excitonic organic materials* (*Poster:* Validating phonon simulations with inelastic neutron scattering)
11:50–12:05	**Seung-Hun Lee**, *University of Virginia* *Role of organic cations in organic-inorganic perovskite solar cells* (*Poster:* Structural dynamics and optoelectronic properties of a two-dimensional hybrid organic-inorganic perovskite)
12:05–12:25	**Invited Talk, Jonathan Taylor, European Spallation Source,** *Scientific computing and research data management as tools for accelerating scientific discovery at research infrastructures*
12:25–12:50	**Round-table discussion. Moderator: Ray Osborn** **Panel: J. Taylor, L. Pozzo, M. Li, M. Manley**
12:50–1:05	**15-Minute Break**
1:05–2:20	**Poster Session 3 (GatherTown)**
2:20–2:25	**5-Minute Break**

Oral Session 4 (Soft Matter 1/ Methods and Instrumentation)	Chair: **Yang Zhang (YZ)**
2:25–2:40	**Yangyang Wang**, *Oak Ridge National Laboratory* *Fingerprinting macromolecular flow and deformation with neutrons* (*Poster:* Molecular view on mechanical reinforcement in polymer nanocomposites)
2:40–2:55	**Timothy Lodge**, *University of Minnesota* *Structure and dynamics of ion-containing nanostructured ternary polymer blend* (*Poster:* Same as above)
2:55–3:10	**Lilo Pozzo**, *University of Washington – Seattle* *Neutron analysis of structure-property relationships in conductive polymer plastic composites* (*Poster:* Small angle neutron scattering analysis of conjugated-polymer polymer blends)
3:10–3:15	**5-Minute Break**
3:15–3:30	**Huibo Cao**, *Oak Ridge National Laboratory* *Local Site Magnetic Susceptibility for Quantum Materials* (*Poster:* Same as above)

3:30–3:45	**Weiwei Xie**, *Rutgers University* *Unraveling emergent quantum states in magnetic topological insulators using high pressure neutron scattering* (*Poster:* Same as above)
3:45–4:00	**Fankang Li**, *Oak Ridge National Laboratory* *Resolving the structure and dynamics of advanced materials with unprecedented resolution* (*Poster:* Ultra-high resolution neutron scattering platform for advanced material)
4:00–4:15	**15-Minute Break**
4:15–5:30	**Poster Session 4 (GatherTown)**

Friday, December 17, 2021

11:00–11:05	**Welcome to Day Three – Thiyaga P. Thiyagarajan**, Department of Energy
Oral Session 5 (Soft Matter 2)	Chair: **Alamgir Karim**
11:05–11:20	**Xiaodan Gu**, *The University of Southern Mississippi* *Understanding the structure and dynamics of conjugated polymers by advancing deuteration chemistry and neutron scattering* (*Poster 1:* Same as above*)* *(Poster 2:* Early Career: Precise chain conformation and dynamics control for conjugated polymers in organic electronic thin film devices)
11:20–11:35	**Matthew Helgeson**, *University of California, Santa Barbara* *Understanding the role of polymer topology on molecular deformation and scission under extreme shear using in situ neutron scattering* (*Poster: Same as above*)
11:35–11:50	**Bradley Olsen**, *Massachusetts Institute of Technology* *Encoding material structure into the primary sequence of polymers* (*Poster:* A novel self-consistent field theory formalism for sequence-defined polymers)
11:50–12:05	**Yang Zhang (YZ)**, *University of Illinois at Urbana-Champaign* *Universality of collective dynamics in liquids at and away from equilibrium* (*Poster:* Same as above)
12:05–12:25	**Invited Talk, Sunil Sinha, U.C. San Diego,** *Neutron scattering: The next decade*
12:25–12:50	**Round-table discussion. Moderator: A. Karim** **Panel: S. Sinha, B. Fultz, M. Mourigal, V. Kiryukhin**
12:50–1:05	**15-Minute Break**

1:05–2:20	**Poster Session 5 (GatherTown)**
2:20–2:25	**5-Minute Break**
Oral Session 6 (Quantum and Magnetism 2)	Chair: **Suzanne te Velthuis**
2:25–2:40	**John Tranquada**, Brookhaven National Laboratory *Neutron scattering studies of unconventional superconductors* (*Poster 1:* Neutron scattering studies of unconventional superconductors*)* *(Poster 2:* Coupling of magnetism and charge carriers in Dirac semimetals)
2:40–2:55	**Young Lee**, Stanford University *Scattering and spectroscopic studies of quantum materials* (*Poster 1:* Scattering study of charge and spin density wave orders in high-T_c cuprate superconductors) *(Poster 2:* Superconductivity, pair density wave and quantum spin liquid)
2:55–3:10	**Pengcheng Dai**, *Rice University* *Using neutron as a probe to study magnetic excitations in strongly correlated electron materials* (*Poster:* Resonance from antiferromagnetic spin fluctuations in the spin-triplet superconductor candidate UTe_2)
3:10–3:25	**Xianglin Ke**, Michigan State University *Novel quantum phenomena in geometrically frustrated magnets near the metal-insulator phase boundary* (*Poster:* Same as above)
3:25–3:40	**Deepak Kumar Singh**, University of Missouri – Columbia *Study of magnetic charge dynamics and correlation in artificial magnetic honeycomb lattice* (*Poster:* Same as above)
3:40–3:55	**15-Minute Break**
3:55–5:10	**Poster Session 6 (GatherTown)**
5:10–5:15	**5-Minute Break**
Closing Session	
5:15–5:30	**Thiyaga P. Thiyagarajan**, Department of Energy *Concluding Remarks*
5:30	**Meeting Adjourns**

POSTER SESSION 1 – Solid State 1

Wednesday, December 15, 2021

1:30–2:45PM

1. Neutron scattering studies of phonon anharmonicity and coupling with spin and charge degrees of freedom
   Olivier Delaire

2. Studies on the role of ionic and lattice correlations on materials properties
   Stefan Rosenkranz

3. The role of spin, charge, and lattice correlations on materials properties
   Stefan Rosenkranz (2)

4. Quantum disorder in the magnetism of orbitally active AMO2 compounds
   Stephen Wilson

5. Inelastic neutron scattering studies of quantum anharmonicity and nonlinear phonons
   Brent Fultz

6. Investigation of short-range ordering in transition metal compounds by diffuse scattering
   Jared Allred

7. Quantized thermoelectric Hall effect induces giant power factor in a topological semimetal
   Mingda Li

8. Gapless Dirac magnons in CrCl3
   Despina Louca

9. Exploring toroidal materials with neutron scattering
   Efrain Rodriguez

POSTER SESSION 2 – Quantum and Magnetism 1

Wednesday, December 15, 2021

4:15–5:30PM

1. University of Minnesota Center for Quantum Materials (CQM): Understanding rare-earth titanates
   Martin Greven

2. University of Minnesota Center for Quantum Materials (CQM): Strain and plastic deformation studies
   Martin Greven (2)

3. Magnetic interactions of the skyrmion material Gd_2PdSi_3
   Andy Christianson

4. Emergent spin clusters in breathing pyrochlore magnets
   Andy Christianson (2)

5. Quantum multipolar fluctuations in spin-orbit magnets
   Martin Mourigal

6. Nonreciprocal effects in noncentrosymmetric magnets: Neutron and optical studies
   S. W. Cheong

7. Equilibrium and nonequilibrium vortex and skyrmion lattices
   Morten Eskilden

8. Nonequilibrium effects in quantum magnets
   Kate Ross

9. Exotic magnetic orders and dynamics in chiral magnets
   Junjie Yang

10. Exotic uses of neutrons and x-rays as probes for chiral magnets
    Dustin Gilbert

POSTER SESSION 3 - Solid State 2 and Energy Materials

Thursday, December 16, 2021

1:05–2:20PM

1. Effect of site occupation disorder on thermal conductivity in the clathrate $Ba_8Ga_{16}Ge_{30}$
   Dmitry Reznik

2. Giant isotopic shift in phonons keeps charge carriers hot longer in a photovoltaic perovskite
   Raphaël Hermann

3. Doping-driven transport and magnetism in MnTe
   Raphaël Hermann (2)

4. Elucidating proximity magnetism through polarized neutron reflectometry and machine learning
   Mingda Li

5. Structural dynamics and optoelectronic properties of a two-dimensional hybrid organic-inorganic perovskite
   Seung-Hun Lee

6. Validating phonon simulations with inelastic neutron scattering
   Adam Moulé

7. In operando neutron diffraction study of phase transitions in Si electrode morphologies using a novel electrochemical cell
   K. S. Ravi Chandran

8. Structure-property relationships in porous electrodes for electrochemical energy storage
   Jeffrey Richards

9. National School on Neutron and X-ray Scattering
   Stefan Rosenkranz

POSTER SESSION 4 - Soft Matter 1 / Methods and Instrumentation

Thursday, December 16, 2021

4:15–5:30PM

1. Ultra-high resolution neutron scattering platform for advanced material
   Fankang Li

2. Unraveling emergent quantum states in magnetic topological insulators using high pressure neutron scattering
   Weiwei Xie

3. Local site magnetic susceptibility for quantum materials
   Huibo Cao

4. Flow-through neutron reflectometry – an *operando* sample environment for active polymer interface studies
   Steven DeCaluwe

5. Realization of full neutron polarization control: Next-generation spherical neutron polarimetry for neutron scattering
   Chenyang Jiang

6. Molecular view on mechanical reinforcement in polymer nanocomposites
   Yangyang Wang

7. Small angle neutron scattering analysis of conjugated-polymer polymer blends
   Lilo Pozzo

8. Structure and dynamics of ion-containing nanostructured ternary polymer blends
   Timothy Lodge

9. Precise chain conformation and dynamics control for conjugated polymers in organic electronic thin film devices
   Xiaodan Gu

POSTER SESSION 5 - Soft Matter 2

Friday, December 17, 2021

1:05–2:20PM

1. Understanding the backbone rigidity of conjugated polymers by advancing deuteration chemistry and neutron scattering
   Xiaodan Gu

2. A novel self-consistent field theory formalism for sequence-defined polymers
   Bradley Olsen

3. Bound layer formation and exchange in polymer nanocomposites (PNCs): A combined simulation and experimental study
   Karen Winey

4. Revealing the molecular origin of interactions between nanocrystals
   William Tisdale

5. Elucidation and modulation of ligand-driven segregation in multicomponent hybrid particles for dynamic assembly of nanostructures
   Michael Bockstaller

6. Understanding the role of polymer topology on molecular deformation and scission under extreme shear using in situ neutron scattering
   Matthew Helgeson

7. Fundamental understanding of bottlebrush polymers based on structure and dynamics
   Gerald Schneider

8. Ionic polymers under dynamic conditions: shear and electrical field response
   Dvora Perahia

9. Universality of collective dynamics in liquids at and away from equilibrium
   Yang Zhang

POSTER SESSION 6 - Quantum and Magnetism 2

Friday, December 17, 2021

3:55–5:10PM

1. Neutron scattering studies of unconventional superconductors
   John Tranquada

2. Coupling of magnetism and charge carriers in Dirac semimetals
   John Tranquada (2)

3. Resonance from antiferromagnetic spin fluctuations in the spin-triplet superconductor candidate UTe_2
   Pencheng Dai

4. Scattering study of charge and spin density wave orders in high-Tc cuprate superconductors
   Lee Young

5. Superconductivity, pair density wave and quantum spin liquid
   Lee Young (2)

6. Study of magnetic charge dynamics and correlation in artificial magnetic honeycomb lattice
   Deepak Kumar Singh

7. Novel quantum phenomena in geometrically frustrated magnets near the metal-insulator phase boundary
   Xianglin Ke

8. Neutron and x-ray studies of spin and charge manipulation in magnetic nanostructures
   Sunhil Sinha

9. Probing short-range structure and magnetism in next-generation energy conversion materials
   Benjamin Frandsen

10. Deciphering spin and orbital dynamics in frustrated quantum magnets
    Kemp Plumb

Invited Talks

Neutron Facilities in the USA and around the World

Ken Andersen
Associate Laboratory Director for Neutron Sciences
Oak Ridge National Laboratory, Oak Ridge, TN

Neutron scattering is an essential element in the materials science toolkit, providing unique structural and dynamic information. It relies on an ecosystem of neutron facilities, which provide access to researchers covering a vast range of scientific problems. This talk will provide an overview of the current neutron landscape, both in the USA and in the global context, covering source performance, publication output, instrument capacity, and ongoing upgrade projects.

Neutron Scattering: The Next Decade

BES Neutron Scattering Program Contractors Meeting

Sunil K Sinha, Univ. of California San Diego

ABSTRACT

It is of course almost impossible to predict the future. Our field may be transformed by developments we are currently unaware of. Nevertheless, one can make guesses based on current trends. The various scientific fields which are impacted by neutron scattering can be expected to turn up exciting new materials and problems with regularity, as they have done for decades, and as before, neutron scattering may be expected to provide key information. Current examples are exotic superconductors, quantum spin liquids, manifestation of exotic quasiparticles such as Majorana fermions, etc. In the absence of huge increases in source flux, this will lead to emphasis on greater efficiencies on developments in neutron instrumentation and more sophisticated data collection and analysis. This will involve rapid handling, collection, analysis and transmission of massive amounts of data, and perhaps the application of AI and Machine Learning, as well as advances in scattering theory.

We must also bear in mind that our world is facing serious challenges, and how these are tackled will determine the fate of humanity. Thus, obviously our Science will be increasingly directed to tackling these challenges, ranging from research on alternative energy sources, to pollution remediation, to combating deadly diseases such as COVID or security threats to the country. Neutron scattering has played and will continue to play a crucial role in these areas. In my talk, I will try to develop these ideas using specific examples.

Scientific computing and research data management as tools for accelerating scientific discovery at research infrastructures

Jonathan Taylor
European Spallation Source, Lund, Sweden

Research data management and scientific computing have become a fundamental core component of research infrastructure operations. It is widely accepted that excellence in this area can positively influence the scientific output of both photon and neutron facilities, such that facilities can execute their mission of delivery of high impact scientific discovery across a broad thematic range.

- Collaborative development and the open-source community have over the last 20 years changed the scientific computing landscape at facilities. Examples such as the Mantid project and the nexus data standard are excellent examples.
- The movement towards FAIR data and data services catalyzes development of research data management process and access to data services. Providing cloud like remote access to data and compute for facility users and prompting structural developments such as the European Open Science Cloud.
- Advances in underlying scientific computing technologies, such as machine learning and AI are now being applied to complex scattering experiments and data analysis workflows.

In this presentation these advances will be discussed within the context of an evolving community of research infrastructures, facility users, source and instrument development in Europe and the USA, highlighting some of the key requirements for accelerating scientific discovery and maximizing the experimental opportunities provided by high brightness sources and next generation instrumentation.

University Abstracts

Investigation of Short-Range Ordering in Transition Metal Compounds by Diffuse Scattering

Jared M. Allred, Department of Chemistry and Biochemistry, University of Alabama

Program Scope

X-ray and neutron total scattering measurements are used to study the relationship between observed electronic properties and the short-range, medium-range, and long-range order. The main activity is associated with the structural instability component of the metal to insulator transition (MIT) in rutile VO_2, especially focusing on effects that doping can cause on the local structure. Methods of diffuse scattering analysis include 3D-ΔPDF and using isotropic group-subgroup relations to simplify structural models.

Besides the structural instability in VO_2, the program applies the same methods to other correlated-electron quantum materials. For example, the relationship between superconductivity and the hidden ordering in condensed Chevrel phases $A_nM_6X_6$ (n =2,4; M = Cr,Mo, X = As, S, Se, Te).

Recent Progress

The metal-insulator-transition in VO_2 comes with a simultaneous structural phase transition. Understanding how the two are linked is a significant portion of the ongoing effort to understand the underlying physics driving the electronic properties. One of the biggest remaining puzzles surrounding the structural instability is the fragile ordering in VO_2—that is the way that the low-temperature monoclinic (M1) phase in VO_2 is rapidly suppressed by almost any external perturbation despite the strong interatomic interactions that apparently drive the instability. For example, Nb, Mo, and W as dopants in VO_2 all rapidly suppress all structural distortions despite the fact that all of the pure dioxides are distorted rutiles themselves.[1]

For the past 40 years, the most widely accepted model explaining this apparent contradiction is that impurity ions act as electron-localizing, charge-ordered d^0 defects, which weaken ordering in a percolative manner..[2] The most notable recent progress in this program has been concerned with fully overturning this model and replacing it with a geometric frustration model. This newer model, which had only been proposed theoretically until now, has important implications on pure VO_2 itself, and it is a necessary step toward a complete model for the structural instability.

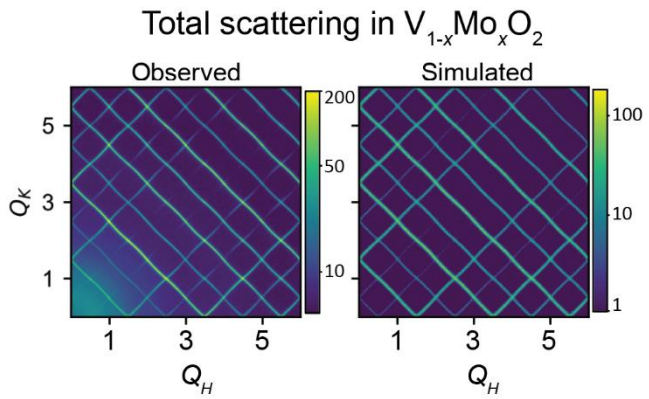

Figure 1: Geometric frustration simulation compared to experimental total scattering plot

We have arrived at the new solution to this problem by systematically studying the total neutron scattering and x-ray scattering maps of compounds in the phase diagrams $V_{1-x}Mo_xO_2$ ($0 \leq x \leq 0.56$) and $Nb_xV_{1-x}O_2$ ($0 \leq x \leq 1$). Firstly, the neutron total scattering on Corelli (Oak Ridge National Lab, Spallation Neutron Source) combined with x-ray total scattering collected on 6-ID-D (Argonne National Lab, Advanced Photon Source) together found that the bonding environment of the V and Mo atoms are quite similar, which fully invalidates the reigning percolative charge-ordered defects model for the Mo compounds.

We also found that the loss of long-range ordering in both sub families is accompanied by *strengthened* symmetry-breaking correlations on nanometer length scales. This means that the local correlations in the non-ordered rutile phase are paradoxically stronger than they are just above the phase transition in the long-range ordered M1 phases for $x < 0.19$ for Mo- and $x < 0.10$ for Nb-substituted VO_2. This appears to be an example of frustrated ordering.

Frustration occurs when the primary interactions compete so strongly that they inhibit long-range ordering, and geometric frustration applies to examples where the interaction geometry itself forces the frustration. While this model is normally used on magnetic systems, it can just as easily be applied to displacive frustration, which was first done for VO_2 in 2017.[3]

In addition to these findings, we discovered at least three new short-range ordered phases in both the Mo and Nb substituted phase diagrams.[4, 5] At 19% Mo doping geometric frustration suppresses long-range ordering in only one dimension, giving a two-dimensionally ordered phase, which we named 2D-M2 to describe the dimensionality and type of ordering. The unique pattern of sharp, wavey scattering rods were successfully simulated using a simple three unique J interaction model drawn from theory, which supports this interpretation (Figure 1). Another short-range ordered phase occurs around 50% Mo, and appears to be an isotropic version of the 2D-M2 phase.[4]

In the early 70s, similar scattering patterns were observed in 10% Nb doped VO2, which was also described as a 2D-M2 like model. However, the complex rod shapes were not observed and no geometric frustration model was used. We reproduced the same scattering experiments in these phases from 11 to 22% Nb doping and showed that they are indeed the same phase as the Mo 2D-M2 phase, showing that geometric frustration dominates the Nb-doped VO_2 phase diagram as well. Additionally, we found a *different* 2D-correlated phase (2D-u, for unknown) at

90% Nb, 10% V. This one shows different rod dispersions than the 2D-M2 and may be related to the different time of structural ordering present in NbO_2. In this work, we were able to fully redraw the electronic and structural phase diagram of $Nb_xV_{1-x}O_2$

This work shows that the structural instability in VO_2 is itself unstable. The long-range ordering of metal atom displacements to form dimers is frustrated, which is why small perturbations tend to push it over the edge into a strongly correlated short-range only regime. This new perspective will have major ramifications on how the MIT and structural transitions in VO_2 are linked.

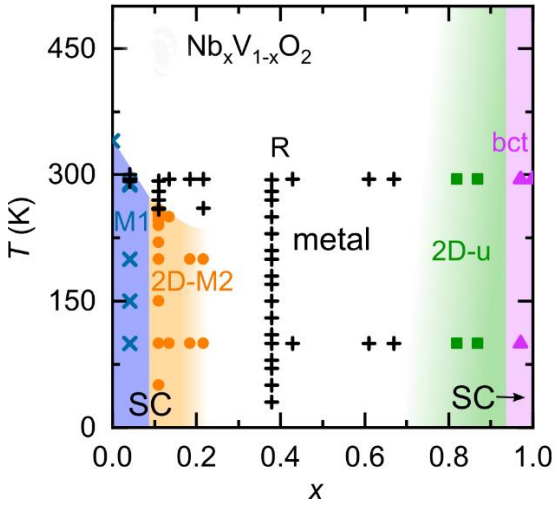

Figure 2: Revised electrostructural phase diagram of NbxV1-O2.

Future Plans

Despite the major progress we have made, there are still many remaining questions about the details in the local structure in the Nb and Mo substituted VO_2 total scattering data. The size effect scattering is quite different between similarly ordered compounds in each sub family. Efforts to model the size effect scattering are ongoing, but overall support the idea that the local metal-oxygen octahedral bond anisotropy differs between V, Mo, and Nb.

We are also in the process of completing a complete analysis of the correlation lengths of different ordering types in the Mo-substituted VO_2 compounds.

Additionally, using isotropy, we have categorized all of the known rutile subtypes in order to better understand the potential structural distortions. The preliminary analysis has shown that at least 6 of the 22 reported subtypes are probably incorrect and a many compounds' structures are probably misidentified.

References

1. Hiroi, Z., Structural instability of the rutile compounds and its relevance to the metal–insulator transition of VO2. *Progress in Solid State Chemistry* **2015,** *43* (1–2), 47-69.
2. Pouget, J. P., Basic aspects of the metal–insulator transition in vanadium dioxide VO_2: a critical review. . *Comptes Rendus Physique* **2021,** *22* (1), 37-87.
3. Lovorn, T.; Sarker, S. K., Complex Quasi-Two-Dimensional Crystalline Order Embedded in VO_2 and Other Crystals. *Physical Review Letters* **2017,** *119* (4), 045501.
4. Davenport, M. A.; Allred, J. M., A crystallographic approach to the short-range ordering problem in V1−xMoxO2 (0.50 ≤ x ≤ 0.60). *Journal of Materials Chemistry C* **2020,** *8* (31), 10907-10916.

5. Davenport, M. A.; Krogstad, M. J.; Whitt, L. M.; Hu, C.; Douglas, T. C.; Ni, N.; Rosenkranz, S.; Osborn, R.; Allred, J. M., Fragile 3D Order in $V_{1-x}Mo_xO_2$. *Physical Review Letters* **2021,** *127* (12), 125501.

Publications

1. Davenport, M. A., Krogstad, M. J.; Whitt, L. M.; Hu, C.; Douglas, T.C. Douglas; Ni, N.; Rosenkranz, S; Osborn, R.; Allred, J. M.; *Fragile 3D Order in $V_{1-x}Mo_xO_2$,* Phys. Rev. Lett.,**127**, 125501 (2021) 10.1103/PhysRevLett.127.125501
2. Davenport, Mathew A.; Allred, J.M.; *A crystallographic approach to the short-range ordering problem in $V_{1-x}Mo_xO_2$ ($0.50 \leq x \leq 0.60$),* Journal of Materials Chemistry C, **8**, 10907-10916, (2020) DOI: 10.1039/D0TC01173H
3. Davenport, Matthew A., Confer, Matthew P, Douglas, Tyra C, Rawot Chhetri, Top B., Allred, Jared M.; *Large single crystals of $V_{1-x}Mo_xO_2$ from a two-step, chemical vapor transport synthesis*. Crystal Growth & Design, 20, 6, 2625-2640 (2020) DOI: 10.1021/acs.cgd.9b01296
4. Rawot Chhetri, T.B., Douglas, T. C., Davenport, M. A., Rosenkranz, S., Osborn, R., Krogstad, M. J., Allred, J. M., Geometric frustration suppresses long-range structural distortions in $Nb_xV_{1-x}O_2$, J. Phys. Chem. C (2021) *Pending minor revisions.*
5. Whitt, L.M, Douglas, T. C., Chi, S., Taddei, K.M., Allred, J.M. *A magnetic excitation linking quasi-1D Chevrel-type selenide and arsenide superconductors,* Submitted to Physical Review B, arXiv: 2110:10226

Collaborative Proposal: Dynamic Modulation of Structure and Phase Transformations in Asymmetric Crystalline Colloidal Brush Alloys

Michael R. Bockstaller, Department of Materials Science and Engineering, Carnegie Mellon University

Krzysztof Matyjaszewski, Chemistry Department, Carnegie Mellon University

Alamgir Karim, Department of Chemical and Biomolecular Engineering, University of Houston

Program Scope

Progress in the chemistry and physics underlying the organization of surfactant-modified particles now provides a framework for the controlled assembly of multi-component particle systems into a range of superlattice structures that mimic atomic crystals [1]. The opportunities for property engineering that are afforded by these processes suggest a new era for the fundamental science and engineering of particle-based materials [2]. Recent advances in surface-initiated polymerization have extended the range of possible ligand compositions to encompass polymer chains of diverse structure and composition [3]. Polymeric ligands present new opportunities to smoothly vary interparticle potentials, to selectively vary relevant material characteristics or to reversibly switch from attractive to repulsive interactions between constituents that could advance the development of a generalized physics framework for interpreting structure formation in particle-based materials. The overarching scope of this collaborative research project is to elucidate the governing parameters that control the structure formation in mixed polymer-modified colloidal systems and to demonstrate that modulated interactions between polymer ligands can drive the reversible transition between distinct ordered states. Two material realizations to validate this hypothesis are (1) mixtures of polymer-modified nanoparticles undergoing spinodal decomposition to form bicontinuous superstructures (Fig.1a) and (2) thermal-induced polymorphic transitions of colloidal brush crystal alloys (Fig. 1b). The scientific goals are to elucidate the role of brush architecture (dense vs. sparse), composition, segment asymmetry, interaction parameter as well as geometric constraints on structure formation and transitions.

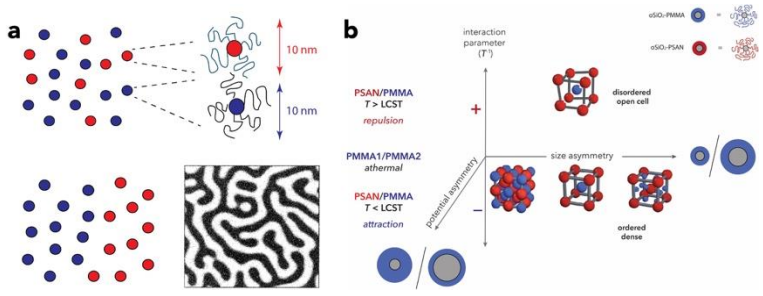

Figure 1. Illustration of material system and scope. Blue and red indicate distinct SLD of organosilica NPs.

Neutron scattering in conjunction with deliberate SLD variation is being used to evaluate the energetics and isolate the contribution of polymer ligands to structure formation processes.

Recent Progress

To enable contrast matched conditions for neutron scattering experiments, we have developed a novel chemistry to synthesize organosilica ($oSiO_2$)-hybrid particles (via crosslinking of organosiloxanes) with a tunable and narrow disperse size in the range of d = 3-10 nm and temperature stability up to T = 230 ºC (Fig. 2a) [a, b]. By variation of the (H/D)-isotope composition of the organic component, the scattering length density of the hybrid particles can be tailored to be within the range SLD = 3.11 10^{10} cm^{-2} (corresponding to fully deuterated $oSiO_2$ core) and SLD = 1.23 10^{10} cm^{-2} (corresponding to a fully hydrogenated $oSiO_2$ core). SLD values were validated using systematic contrast variation of solvent media (Fig. 2b).

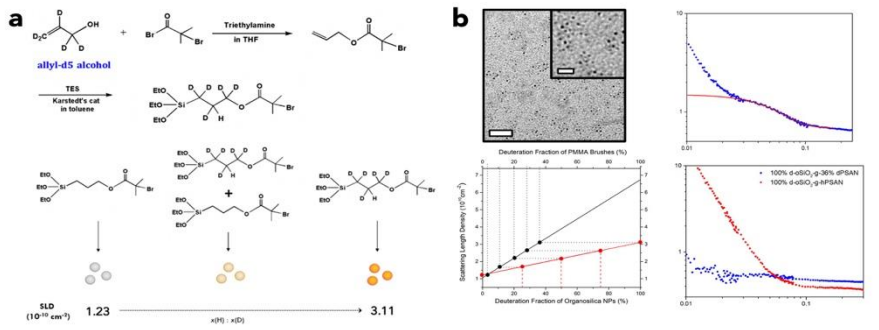

Figure 2. (a) Synthetic scheme towards organosilica nanoparticles with controlled SLD through condensation of deuterated particle precursor [1, 2]. (b) TEM and SANS curves of $oSiO_2$ NPs as well as accessible SLD range [3].

LCST-phase separation of $oSiO_2$-PMMA/$oSiO_2$-PSAN blends was demonstrated in the thin film form using TEM (Fig 3a, b) and in the bulk state using SANS (Fig. 3c). Phase separation was induced by thermal annealing at varying quench depth and subsequent rapid vitrification at 25°C. Figure 3c displays the evolution of the scattered intensity from the initial (uniform) state (red curve) after 48 h of quenching into the two-phase region (blue curve). Interestingly, the domain growth kinetics inferred from the low-q peak position reveals two regimes that are distinguished by a growth exponent of 0.2 and 0.3, respectively (Fig. 3d). The growth kinetics is consistent with anomalous growth behavior that is induced by entanglements in brush particle films that act as constraints to the phase separation process and represents the first demonstration of anomalous phase separation kinetics in polymer blend films [4].

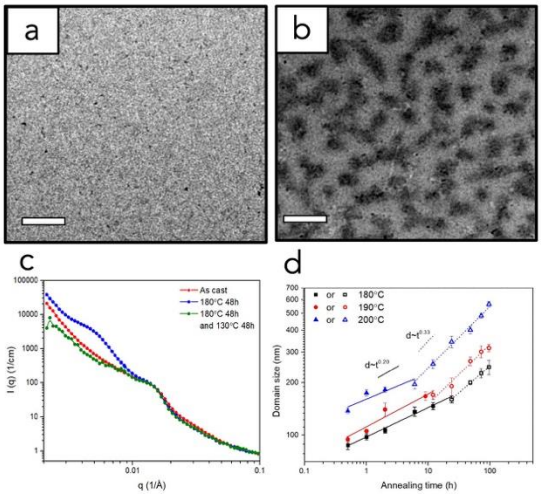

Figure 3. TEM images for $oSiO_2$-g-PSAN and $oSiO_2$-g-PMMA blend after a) annealing at 130 °C for 24h and b) annealing at 180 °C for 48h. Scale bar is 200nm; c) scattered intensity profile I(q) for contrast matched system after annealing at 180 °C for 0h, 48h and then 130°C for 48h (EQ-SANS experiments were performed by W.-R. Chen and C. Do at ORNL); d) domain growth kinetics of symmetric blends at various quench depths. Diffusion controlled growth ($d \sim t^{0.3}$) is preceded by anomalous growth ($d \sim t^{0.2}$).

We developed a dry processing methodology to achieve reversible control of the ordering of PGNPs under topographic confinement. The application of topographic constraints onto the polymer thin films and subsequent annealing near the lower-critical solution temperature (LCST) induced pattern formation. The positive enthalpic force (χN > critical value) drives the larger-sized PGNPs to selectively segregate to the less confined 'mesa' region (Fig. 4). More interestingly, after annealing of the selective partitioned films below LCST (in the presence of topographic constraints), enthalpic forces (χN < critical value) caused the polymer blends to homogenize and the PGNPs redistribute evenly in the patterned films (Fig. 4). This provides for new opportunities to enable the reversible switching of ordered/disordered microstructure states.

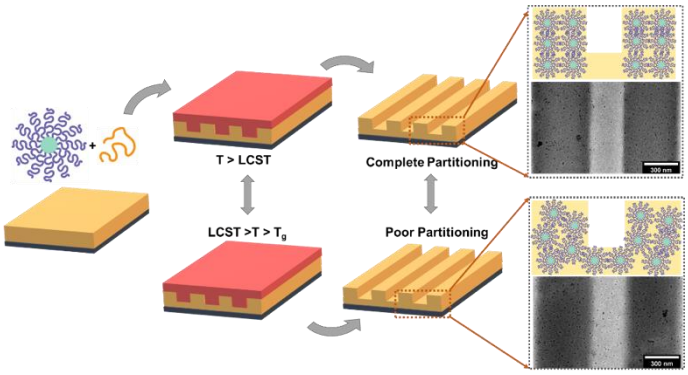

Figure 4. Reversible partitioning of topogr. patterned films.

Future Plans

Current research is focused on the synthesis of particle model systems with diameter in the 30-40 nm range, size dispersity less than 5% and tunable SLD. Two strategies are currently being pursued, i.e., the synthesis of $oSiO_2$ in more polar solvent media and in the presence of tetraethoxysilane (Fig. 5a) as well as all-organic colloids through mini-emulsion method (Fig. 5b, 5c). Silane crosslinkers are introduced to raise the crosslink density and hence modulus of the

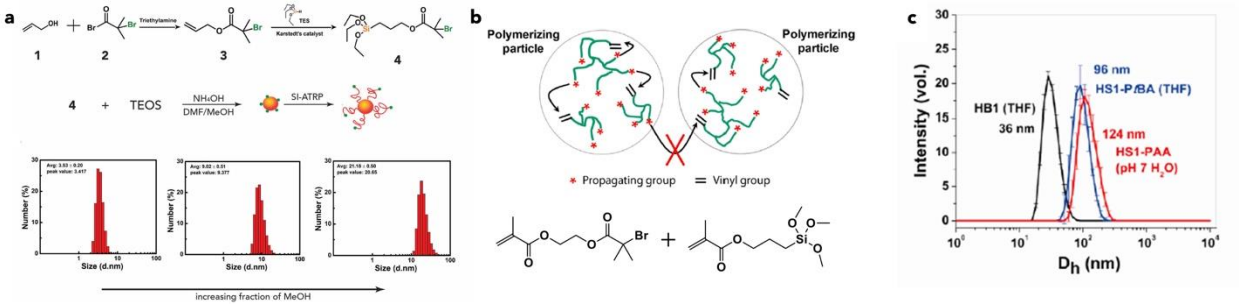

Figure 5. Illustration of synthetic pathways to organosilica (a) and organic (b) colloids for variable size control.

resulting hybrid particles. Both methods involve the inimer method, i.e., the polymerization of ATRP-initiator-modified precursor. The inimer method is expected to result in particle systems that are readily accessible to surface polymerization of PMMA and PSAN via SI-ATRP. Concurrent research focuses on establishing the conditions for crystallization of brush particle colloids. Advanced neutron methods will be employed to reveal the correlation between the inner structures of polymer brushes and the corresponding microstructure changes in crystallized colloidal crystal alloys. The instruments involved will be Neutron Scattering (R-SANS, GISANS, vSANS, uSANS, SANS) and Neutron Reflectivity (NR).

References

[1] Boles, M. A., Engel, M., Talapin, D. V. Self-Assembly of Colloidal Nanocrystals: From Intricate Structures to Functional Materials. **Chemical Reviews** 116, (2016), 11220-89.

[2] Christine R. Laramy, Matthew N. O'Brien, Chad A. Mirkin Crystal engineering with DNA. **Nature Reviews** 4, (2019), 201-224.

[3] Yan, J., Bockstaller, M., & Matyjaszewski, K. Brush-modified materials: Control of molecular architecture, assembly behavior, properties and applications. **Progress in Polymer Science** 100, (2020), 100, 101180.

[4] De Gennes, P.G. "Dynamics of fluctuations and spinodal decomposition in polymer blends", **Journal of Chemical Physics** 72, (1980).

Publications

[a] Han, Jin et al. Nanosized Organo-Silica Particles with "Built-In" Surface-Initiated Atom Transfer Radical Polymerization Capability as a Platform for Brush Particle Synthesis. **ACS Macro Letters** 9 (2020), 9, 1218−1223.

[b] Zhai, Yue et al. "Processable Sub-5 Nanometer Organosilica Hybrid Particles for Dye Stabilization", **ACS Applied Polymer Materials**, 6 (2021), 3631-3635.

[c] Wu, Wenjie, et al. "Control of Phase Morphology of Binary Polymer Grafted Nanoparticle Blend Films via Direct Immersion Annealing." **ACS Nano** 15.7 (2021): 12042-12056.

[d] Bhadauriya, Sonal, et al. "Observation of General Entropy–Enthalpy Compensation Effect in the Relaxation of Wrinkled Polymer Nanocomposite Films." **Nano Letters** 21.3 (2021): 1274-1281.

[e] Bhadauriya, Sonal, et al. "Enhanced resistance to decay of imprinted nanopatterns in thin films by bare nanoparticles compared to polymer-grafted nanoparticles." **Nanoscale Advances** 3.18 (2021): 5348-5354.

[f] Wang, Xiaoteng, et al. "Nanoimprint Directed Assembly of Associating Polymer-Grafted Nanoparticles for Polymer Thin Films with Enhanced Stability." **ACS Applied Polymer Materials** 1.12 (2019): 3242-3252.

In Operando Neutron Diffraction Study of Phase Transitions in Si Electrode Morphologies Using a Novel Electrochemical Cell

K. S. Ravi Chandran (PI)
Department of Materials Science and Engineering, University of Utah, SLC, UT 84112

Program Scope

The research focuses on the fundamental understanding of the phase transition and diffraction phenomena in Si particle, Si nanowire and Si columnar electrodes for Li-ion batteries, using a simple in situ cell developed in the current project. Particle Si electrodes (micro- and nano-sized particles, nanowires (created by CVD or etching) as well as Si columns with sizes ranging in size from mid-nano to micron scale and with varying wall and pore architectures were prepared for *in operando* experiments in Vulcan diffractometer at SNS, ORNL. Using the *in situ* electrochemical cell, the phase transitions and diffraction phenomena that occur during the reversible lithiation of Si were investigated. The over-arching goal is to explore in detail the unexpected phenomena observed in our recent *in situ* experiments and correlate energy storage capacity of the electrodes to the phase transitions. This will help to resolve many electrochemical limitations which are blocking the realization of very high-capacity energy storage Si electrodes for Li-ion batteries. This research is done in collaboration with ORNL (Dr. Ke An, SNS).

The research mainly investigates the phase transitions in electrodes made of Si micro/nano particles, Si nanowires and photolithographic Si structures. The experiments involve both Vulcan diffractometer and NOMAD diffractometer. The premise is that by understanding the Si morphology (particle vs nanowire vs columns) one can discover electrode microstructures that facilitate reversible phase transformations upon Li insertion and extraction in Si electrode. Going from particles to nanowires to Si columns is expected to vastly change the phase transition behavior of electrodes. These morphologies help to understand (i) the effect of dimensions on lithiation, since diffusion scales as $t=L^2/D$ (L is diffusion length and D is diffusivity), (ii) effects of morphology on electron transport and phase transformation in electrode, (iii) the effect of high size versus surface-to-volume ratio and (iv) mechanisms of volume change accommodation during Li insertion. The research is performed in collaboration with NOMAD and Vulcan scientists at ORNL through beam time allocations.

Recent Progress

I. In situ cell for the study of phase transitions in microcolumnar Si (100) electrode using ND

A major development is that we recently designed and built a modified in situ electrochemical cell, in a very simple form, which has been validated. This cell works exceptionally well and enables capturing of neutron diffraction patterns in VULCAN neutron diffractometer with high signal to noise ratio, thus enabling the study of the lithiation phenomenon in Si columnar electrodes. In recent beam time experiments in Vulcan, this cell was successfully shown to perform well in multiple cell cycles with higher specific capacity (>3000 mAh/g). The simple cell (Figure 1a & 1b) is the primary experimental device now used to study the phase transitions in-situ in columnar Si (100) electrodes. The cell, containing the columnar Si (100) electrodes to be diffracted, is oriented at 45º (Figure 1c) to the VULCAN beam. This is to enable Si (400) and

Si (440)/(220) Bragg reflections to appear in the reflection bank and the transmission bank respectively. Some real time ND patterns, collected during lithiation of Si, are shown in Figure 2 and 3. The intensity of Si (220) (and also (400), (440), not shown here) can be seen to be increasing continuously, whereas that of Cu (200), acting as a standard, remains the same. The resolution of Si (220), (400) and (440) peaks is remarkably high, allowing the study of transformations in Si during lithiation and delithiation. An extensive data set, obtained in beam time experiments in Fall 2021, is being analyzed in detail.

We currently investigating the relationship between the Si (hkl) intensity and the transformations in Si (100) during lithiation. It is thought that, as Li diffuses in Si (100) along <110> direction, the Si-Si bonds across {111} planes will be broken [2]. At the same time, incorporation of Li in Si causes the volume change, leading to strong intensification of spots in Figure 2.

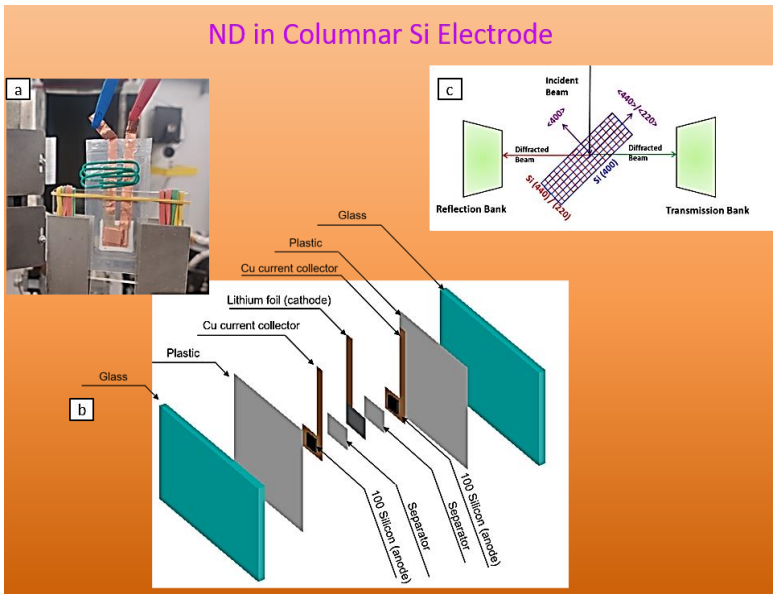

Figure 1(a) Photograph of the new *in-situ* electrochemical cell with columnar Si (100) electrode, in the assembled form, in Vulcan, (b) exploded view of the *in-situ* electrochemical cell, with glass as casing, (c) electrode arrangement with respect to the beam. In the preliminary experiments, the *in-situ* cell was arranged such that the Si (100) electrode makes an angle of 44º with the incident beam (Figure 1(c)) in Vulcan diffractometer. As a result (400) and (440)/(220) planes in Si electrode were Bragg diffracted into the reflection bank and transmission bank, respectively.

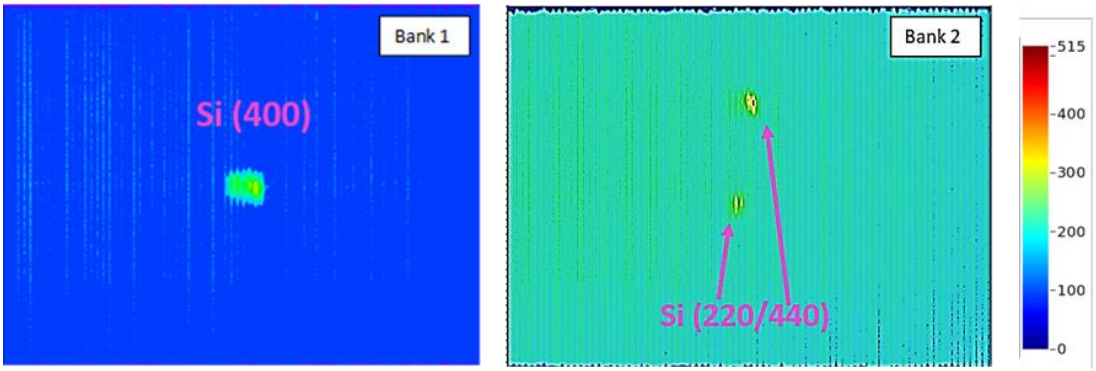

Figure 2. Sharp diffraction signatures, during lithiation of Si electrode, in east and west detectors in Vulcan.

The diffraction signatures recorded in the west (bank 1) and east (bank 2) detectors are shown in Figure 2. The real time ND patterns collected during two charge-discharge cycles with Si (100) electrode are shown in Figure 3. The intensities of the Si (220) reflections increase dramatically

during lithiation and then decrease during delithiation (Figure 3(a)). A similar pattern was observed for Si(400) but it is not shown here. The intensity of Si (220) (and also that of Si(440)) reflection were found to nearly triple toward end of lithiation. Surprisingly, the d-spacing and FWHM of the (400) and (220) Si reflections remained the same through delithiation/lithiation. The intensity of the Cu (200) reflection (Figure 3(c)) in both the banks remained the same, which serves as a reference, indicating that the changes in intensities of (400) and (220) Si reflections are indeed real and are due to lithiation of Si in the *in-situ* cell. This demonstrates the feasibility of *in operando* ND experiments with the simple cell. The question of whether these changes are due to mosaic structure formation due to bond breaking [2] is being investigated.

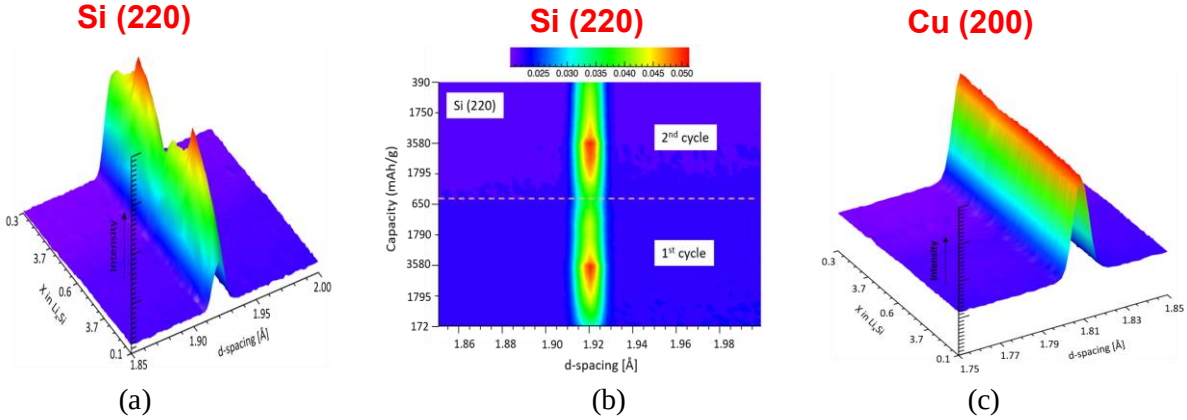

Figure 3. *In-situ* neutron data (extracted from the binned data) collected during the two cycles of PS1 Si, (a) the continuous change in Si (220) peak during lithiation and delithiation, (b) is Si (220) 2D plot of top view of (a) showing an increase during lithiation and decrease during delithiation of 1st and 2nd cycle, and (c) Cu (200) peaks that do not change.

Sample	PS1	PS2	PS3
Average pore diameter(µm)	1.2	1.6	1
Average etched depth(µm)	8	7	9
Pore Fraction	0.57	0.75	0.45
Microstructure	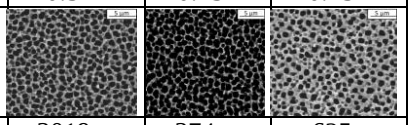		
Average Capacity (mAh/g)	3019	374	625

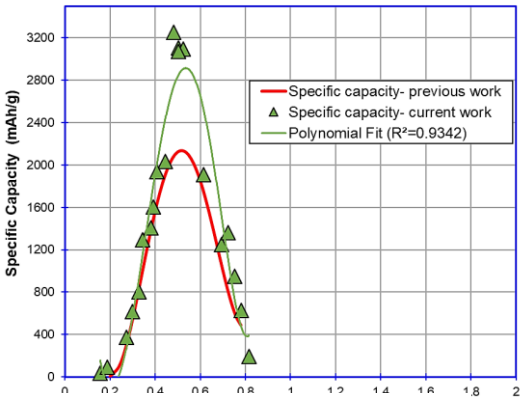

Figure 4. Specific capacity vs Si wall thickness/pore diameter

II. Progress on the optimization of columnar Si electrodes for in operando neutron diffraction:

We have identified three different Si columnar structures (table above), which have different columnar structural parameters and steady state cell cycling capacities. All the three structures have been cycled to 30 cycles in the preliminary evaluation. These samples were obtained from the electrode optimization experiments (figure 4), which have been completed in 2021. The morphology of Si columns greatly impacts the specific capacity. Our primary objectives are to study in Vulcan ND experiments that if any of these structures undergo mosaic pattern behavior, which may explain steady state capacities and cyclic performances of the Si electrodes.

III. Progress on the Si Nanowire and photolothographic patterned structures for Li-ion batteries'

Toward examining the effect of Si morphology, we have successfully prepared a series of Si nanowires with different depth by metal-assisted chemical etching. Figure 5 shows the microstructure of Si nanowire electrode with 9 µm depth. The etching time vs. etching depth and porosity is shown in Figure 6. Figure 7 shows the electrochemical performances of 9 µm Si nanowire electrode. This electrode showed a superior discharge specific capacity of ~3570 mAh/g after 50 cycles, which is quite impressive. Work is in progress to study these in NOMAD/VULCAN.

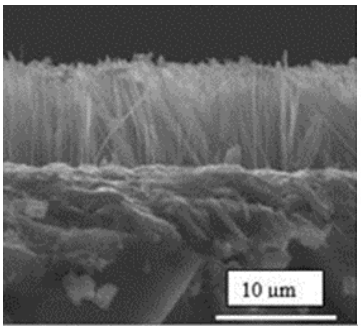

Figure 5: Cross-section of the Si nanowires etched for 15 min

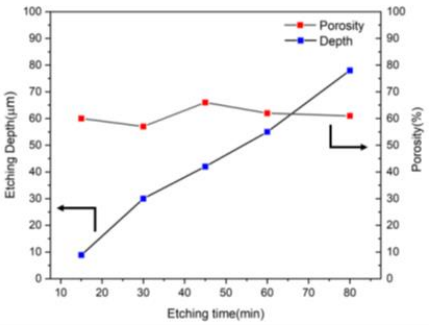

Figure 6: Etching depth vs. etching time (left axis) and porosity (right axis)

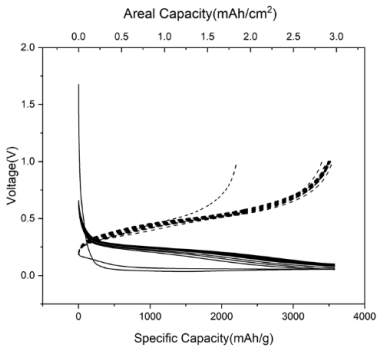

Figure 7: Voltage profiles for SiNW electrode etched for 15 min

We have also prepared various photolithographically patterned Si micro-pillar structures, as shown in Figure 8. The peaks of cyclic voltammogram study of Si micro-pillar structure (Figure 9) indicated the existence of various phase transitions during electrochemical cycling. The discharge specific capacity remained ~3050 mAh/g after 50 cycles, as is shown in Figure 10. This is also quite impressive and will be investigated in NOMAD/VULCAN experiments.

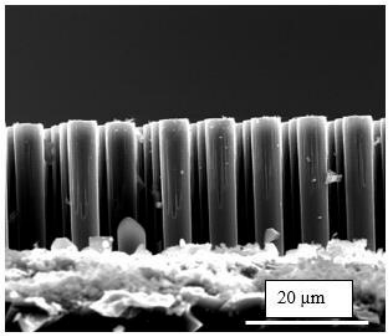

Figure 8: Cross-section of Si pillar (5 µm diameter, 22 µm depth)

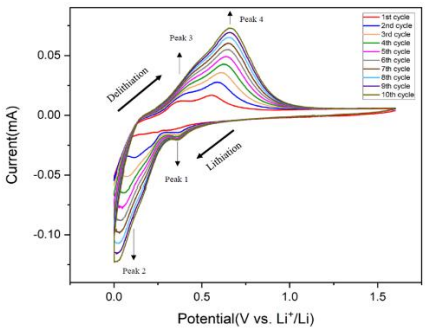

Figure 9: Cyclic voltammogram for Si pillars

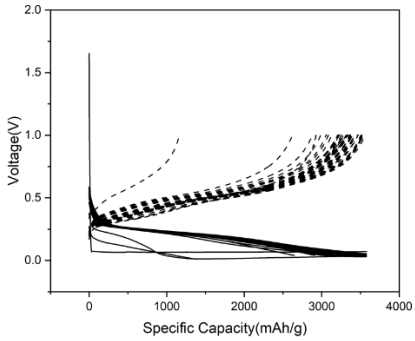

Figure 10: Voltage profiles for Si micro-pillar (5 µm diameter, 22 µm depth)

Future Plans:

In recent beamtime experiments in VULCAN, a nice set of results have been obtained, which enabled us to prepare a manuscript detailing the newly observed phenomenon. Following the success of the simple in-situ cell, now is the opportunity to study, using VULCAN, the effect of various Si column morphologies on the performance of Si electrodes prepared here. We hope to complete all the key experiments by summer of 2022. Electron microscopy of lithiated and delithiated columnar Si (100) electrodes will be performed. We are starting the NOMAD experiments near the end of 2021 or early 2022. Plans are in place to do experiments in NOMAD and perform PDF analysis of data obtained using the Si nanowire and photolithographic structures.

References

1. B. Vadlamani, K. An, M. Jagannathan, K.S.Ravi Chandran, "A Novel In-situ Electrochemical Cell for Neutron Diffraction Studies of Phase Transitions in Small Volume Electrodes of Li-ion Batteries," *J. Electrochem. Soc.*, 161, A1731 (2014)

2. S.W. Lee, M.T. McDowell, J.W. Choi, Y. Cui, Anomalous shape changes of silicon nanopillars by electrochemical lithiation. *Nano Lett.* 11, 3034–3039 (2011)

Publications from this Project

1. Vadlamani, B., M. Jagannathan, J. Palmer, and KS Ravi Chandran. "Large effect of structural variations in the columnar silicon electrode on energy storage capacity and electrode structural integrity in Li-ion cells." *Journal of Materials Research* 35, no. 21 (2020): 2976-2988.

2. Chandran, KS Ravi, and J. Palmer. "A critical review and assessment of 3D columnar silicon electrode architectures and their performance as negative electrodes in Li-ion cells." *Materials Science and Engineering: B* 271 (2021): 115278.

3. R. Srinivasan, K.S. Ravi Chandran, "The Strong Effect of Microporous Column Depth on the Lithiation-Delithiation Behavior in Si Electrodes for Li-ion Cells and the Resistance to Mechanical Damage" Accepted in *J. Electron. Mater.* Nov 2021.

Manuscripts in Preparation

4. R. Srinivasan, K.S. Ravi Chandran, and Ke An, "Investigation of Electrochemical Phase Transformations in 3-D Microporous Columnar (100) Si Electrodes from Neutron Diffraction using a Simple *In-Situ* Cell" Manuscript in preparation, to be completed by Dec 2021.

5. R. Srinivasan, K.S. Ravi Chandran, "Evolution in the Performance of Columnar Microporous Si Electrode through Optimization of Si Wall Thickness/ Pore Diameter Providing Superior Cycling Characteristics for Li-ion Cells" Manuscript in preparation, to be completed by Dec 2021.

Non-Reciprocal Effects in Non-Centrosymmetric Magnets: Neutron and Optical Studies

S.-W. Cheong (Rutgers Univ.), V. Kiryukhin (Rutgers Univ.), and A. Sirenko (NJIT)

Program Scope

Effects lacking symmetry under the exchange of source and detector are called nonreciprocal. They are well-known in optics, but can occur for any (quasi)particles, including neutrons, spin waves etc. Numerous possible applications for these effects are in all-optics computing, quantum cryptography, and spintronics. While the non-reciprocal effects involving magnetic (spin-waves) and mixed (electromagnons) quasiparticles are important for both fundamental and applied science, they are not studied as well as those for photons. Neutron scattering is an ideal probe for magnetic excitations, capable of measuring their spectra with an unprecedented level of details. A team from Rutgers University and NJIT is engaged in a collaborative effort to understand non-reciprocal effects and other exotic dynamic properties utilizing inelastic neutron scattering, advanced crystal growth, and optical spectroscopy. This program focuses on studies of polar magnets and magnets with structural chirality. Among these compounds are toroidal magnets, a spin liquid, and unconventional magnetoelectrics. In these systems, combination of absent inversion, time-reversal, and mirror symmetries leads to non-reciprocal effects revealed, for example, in non-equivalent magnon/electromagnon spectra for the opposite directions of the particle propagation, and as directional dichroism (difference in the light absorption) in the far-infrared optical spectra. The high-quality monodomain single crystals synthesized under this program are crucial for the studies of nonreciprocal and magnetoelectric effects. Spectroscopic studies include utilization of THz vortex beams, which we recently developed as a new probe of magnetism in matter. Combined neutron and optical studies should reveal the physical mechanisms responsible for the exotic dynamic properties in low symmetry materials and help identify prospective quantum materials for novel computational and theoretical techniques.

Recent Progress

Quantum spin liquid (QSL) in a polar magnet. Strong evidence of the QSL behavior is found by inelastic neutron scattering in $TbInO_3$, an antiferromagnet on a nearly triangular lattice[1]. It includes absence of any long-range order at the temperatures two orders of magnitude smaller than the major interaction energy, and a very broad, diffuse inelastic magnetic signal centered at the Brillouin zone boundary of the triangular lattice, see Fig 1. The data taken in the polycrystals (partially supported by this Grant in the previous period) were interpreted as suggesting an emergent honeycomb lattice. This study used single crystals, synthesized for the first time. It shows that the low-energy physics is better approximated by the properties of the frustrated triangular

lattice instead. To prove (or reject) the QSL state in $TbInO_3$, one needs to quantify the possible effects of the disorder. The role of such effects is one of the most important subjects in the field. Even in stoichiometric compounds such as $TbInO_3$, one needs to exclude the disorder effects conclusively for the compound to be a viable QSL candidate. We are currently utilizing one of the possible approaches to this problem: investigation of the magnetic excitations in an applied magnetic field in the (nearly) polarized state. So far, studies in 8 Tesla fields have been done. Significant narrowing of the magnetic excitations was observed (Fig 1), indicating that the disorder is probably irrelevant. We found that higher fields, currently available at the SNS, are needed for a conclusive experiment that may also allow to determine the relevant magnetic interactions (experiments planned). Importantly, $TbInO_3$ is a polar magnet with the symmetry admitting non-reciprocal effects in an applied magnetic field, independent of any magnetic order or lack thereof. Thus, this system presents a unique opportunity: investigation of potential directional nonreciprocal effects in a spin liquid compound. Studies of $TbInO_3$ in the context of nonreciprocal effects is one of our future research directions.

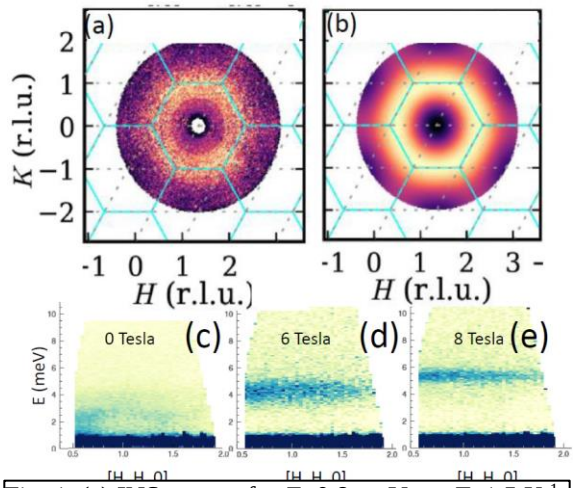

Fig. 1. (a) INS pattern for E=0.8 meV ant T=1.5 K.[1] (b) Theoretical calculation of the uncorrelated valence bond model.[1] (c)-(e) INS spectra in various magnetic fields (unpublished).

Nonreciprocal magnons in iron langasite. Mechanisms for controlling the flow of magnetic excitations, analogous to diodes in electric circuits, have been sought after. Using neutron scattering, we show[2] that the spin waves in antiferromagnetic langasite $Ba_3NbFe_3Si_2O_{14}$ display directional anisotropy. On applying a time-reversal symmetry breaking magnetic field along the c axis, the spin-wave energies differ when the sign is reversed for either the momentum transfer $\pm Q$ or applied magnetic field $\pm H$, see Fig 2. When the field is applied within the crystallographic ab plane, the spin-wave dispersion is directionally isotropic and symmetric, but a directional anisotropy is observed in the spin-wave intensity. While related anisotropies have been previously observed in antiferromagnets, they all involved spin-orbit interaction providing a direct means of coupling the magnetism to an applied magnetic field. We find that nonreciprocal response can also occur in the absence of the Dzyaloshinskii-Moriya (DM) interaction or other effects resulting from spin-orbit coupling, thereby significantly increasing the range of magnets in which such response may occur. $Ba_3NbFe_3Si_2O_{14}$ is structurally and

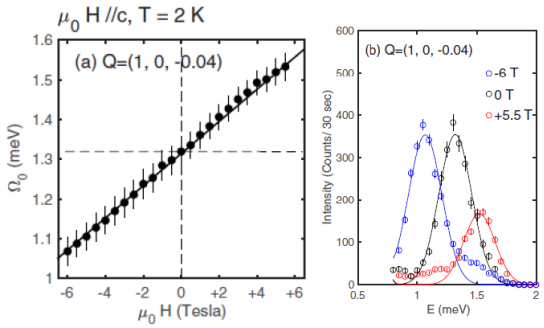

Fig. 2. (a) Linear scaling of Q=(1,0,−0.04) magnon. (b) Representative constant momentum scans[2].

magnetically single-domain chiral with the magnetic helicity induced through competing symmetric exchange interactions. Using combined polarized neutron and x-ray scattering[3], we determine the absolute structural and magnetic chiralities of enantiopure crystals and show that the magnetic handedness is pinned by the structural one.

Imaging fluctuating AFM domains. To observe many of the effects described in this project, monodomain (structural or magnetic) samples are essential. Imaging antiferromagnetic (AFM) domains is a highly nontrivial task. For some domain types, such as antiphase AFM domains in collinear magnets, there were no practical imaging approaches. In 2018, we have invented[4] a new imaging technique for AFM domains which is applicable to many domain types, including the antiphase domains. It is based on magnetic diffraction of coherent soft x-rays. We have now dramatically improved the sensitivity of the method, making possible observation of fluctuating antiferromagnetic domains, see Fig. 3. This is the first observation of this kind done in real space and time. In addition to the obvious scientific interest, these experiments open numerous possibilities for the studies of AFM spintronic devices in real time/space.

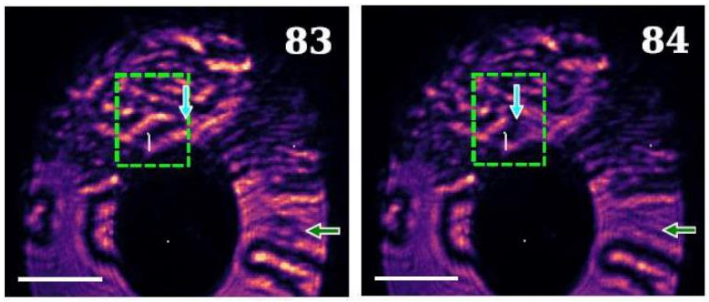

Fig. 3. Two consecutive frames from a video showing fluctuating AFM phase domains in Ni_2MnTeO_6. Dark lines show the domain boundaries. Scale bars are 10 μm. The time interval between the frames is 2×10^{-1} s. Vertical arrows point to a shifting domain boundary. Horizontal arrows show a disappearing bubble domain. Unpublished.

Vortex beam spectroscopy. We have introduced a new spectroscopic probe for magnetism: light beams carrying orbital angular momentum (OAM), also called vortex beams.[5,6] Light beams carrying spin angular momentum (circularly polarized light) are among the most valuable probes of magnetism. We demonstrate that THz vortex beams also couple to magnetism, exhibiting dichroic effects in a magnetic medium. In ferrimagnetic crystals, resonant optical absorption depends strongly on both the handedness of the vortex (vortex dichroism) and the direction of the beam propagation with respect to the sample magnetization. This effect exceeds the conventional magnetic dichroism for circularly polarized light.[5] In antiferromagnets, strong vortex beam dichroism is observed at the AFM resonances,[6] see Fig 4. The selection rules at the AFM resonances are governed by the total angular momentum of the

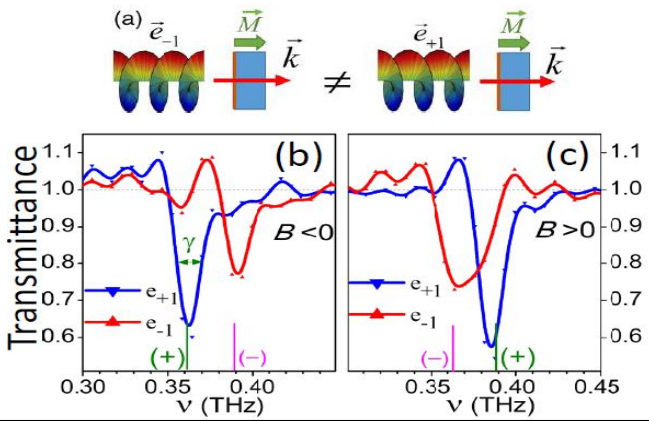

Fig. 4. Vortex dichroism for THz vortex light beams with $l = \pm1$ in antiferromagnetic Ni_3TeO_6. Adapted from Refs. [5,6].

vortex beam: $j = \sigma + l$, where σ and l are the spin and orbital angular momentum, respectively. In particular, for $l = \pm 2$, ± 3, and ± 4, the sign of l is shown to dominate over that for conventional circular polarization σ. Our results demonstrate the high potential of the vortex beams with OAM as a new spectroscopic probe of magnetism in matter. Expanding this project into the x-ray range, we have constructed an experimental setup producing soft x-ray vortex beams at the NSLS-II. It will be used to study vortex dichroism at the x-ray absorption edges, and to search for the forbidden collective magnetic modes that interact with vortex beams but remain invisible for conventional light. This research is complementary to neutron scattering because it can address different types of the nonreciprocal effects (e.g. polarization dichroism), and is applicable to small samples not suitable for INS.

Future Plans

Inelastic neutron scattering experiments will be performed in the reduced-symmetry compounds with expected nonreciprocal effects: enantiopure $M_2Mo_3O_8$, $TbInO_3$, $BaCoSiO_4$, and $(Ni,Mn,Co)_3TeO_6$ crystals in high applied magnetic fields. We will continue sample-growth optimization to obtain large enantiopure crystals, and monitor the most promising excitations for the INS studies by optical spectroscopy, including the development of the vortex-beam spectroscopy of magnetic materials using the listed systems as test subjects. We are expanding the vortex beam spectroscopy into two directions: (1) soft X-rays at the NSLS-II, BNL for dichroism in magnetic oxides, and (2) dichroism of the coherent THz beams, which carry the total angular momentum as a combination of the spin and orbital angular momenta.

References

[1] M. G. Kim *et al*., Spin-liquid-like state in pure and Mn-doped $TbInO_3$ with a nearly triangular lattice. *Phys. Rev. B* **100**, 024405 (2019).

[2] C. Stock *et al*., Spin-wave directional anisotropies in antiferromagnetic $Ba_3NbFe_3Si_2O_{14}$. *Phys. Rev. B* **100**, 134429 (2019).

[3] N. Qureshi *et al.,* Absolute crystal and magnetic chiralities in the langasite compound $Ba_3NbFe_3Si_2O_{14}$ determined by polarized neutron and x-ray scattering. *Phys. Rev. B* **102**, 054417 (2020).

[4] M. G. Kim *et al*., Imaging antiferromagnetic antiphase domain boundaries using magnetic Bragg diffraction phase contrast. *Nature Comm.* **9**, 5013 (2018).

[5] A. A. Sirenko *et al*., Terahertz vortex beam as a spectroscopic probe of magnetic excitations. *Phys. Rev. Lett.* **122**, 237401 (2019).

[6] A. A. Sirenko *et al*., Total angular momentum dichroism of the terahertz vortex beams at the antiferromagnetic resonances. *Phys. Rev. Lett.* **126**, 157401 (2021).

Publications

[1] A. A. Sirenko, P. Marsik, L. Bugnon, M. Soulier, C. Bernhard, T. N. Stanislavchuk, Xianghan Xu, and S.-W. Cheong. Total angular momentum dichroism of the terahertz vortex beams at the antiferromagnetic resonances, *Phys. Rev. Lett.* **126**, 157401 (2021)

[2] M. Songvilay, S. Petit, F. Damay, G. Roux, N. Qureshi, H. C. Walker, J. A. Rodriguez-Rivera, B. Gao, S.-W. Cheong, and C. Stock. From one- to two-magnon excitations in the S=3/2 Magnet β-$CaCr_2O_4$. *Phys. Rev. Lett.* **126**, 017201 (2021).

[3] M. G. Kim, W. Ratcliff, II, D. M. Pajerowski, J.-W. Kim, J.-Q. Yan, J. W. Lynn, A. I. Goldman, and A. Kreyssig. Magnetic ordering and structural distortion in a PrFeAsO single crystal studied by neutron and x-ray scattering. *Phys. Rev. B* **103**, 174405 (2021).

[4] T. N. Stanislavchuk, G. L. Pascut, A. P. Litvinchuk, Z. Liu, S. Choi, M. J. Gutmann, B. Gao, K. Haule, V. Kiryukhin, S.-W. Cheong, A. A. Sirenko. Spectroscopic and first principle DFT+eDMFT study of complex structural, electronic, and vibrational properties of $M_2Mo_3O_8$ (M = Fe, Mn) polar magnets. *Phys. Rev. B* **102**, 115139 (2020).

[5] N. Qureshi, A. Bombardi, S. Picozzi, P. Barone, E. Lelièvre-Berna, X. Xu, C. Stock, D. F. McMorrow, A. Hearmon, F. Fabrizi, P. G. Radaelli, S.-W. Cheong, and L. C. Chapon. Absolute crystal and magnetic chiralities in the langasite compound $Ba_3NbFe_3Si_2O_{14}$ determined by polarized neutron and x-ray scattering. *Phys. Rev. B* **102**, 054417 (2020).

[6] H. Lane, C. Stock, S.-W. Cheong, F. Demmel, R. A. Ewings, and F. Krüger. Nonlinear soliton confinement in weakly coupled antiferromagnetic spin chains. *Phys. Rev. B* **102**, 024437 (2020).

[7] N. N. Giles-Donovan, N. Qureshi, R. D. Johnson, L. Y. Zhang, S.-W. Cheong, S. Cochran, and C. Stock. Imitation of spin density wave order in $Cu_3Nb_2O_8$. *Phys. Rev. B* **102**, 024414 (2020).

[8] Fernando Pomiro, Chris Ablitt, Nicholas C. Bristowe, Arash A. Mostofi, Choongjae Won, Sang-Wook Cheong, and Mark S. Senn. From first- to second-order phase transitions in hybrid improper ferroelectrics through entropy stabilization. *Phys. Rev. B* **102**, 014101 (2020).

[9] Meixia Wu, Xiang Zhou, Mark Croft, Steven Ehrlich, Syed Khalid, Wen Wen, Saul H. Lapidus, Xianghan Xu, Man- Rong Li, Zhongwu Liu, and Sang-Wook Cheong. Single-crystal growth and room-temperature magnetocaloric effect of X-type hexaferrite $Sr_2Co_2Fe_{28}O_{46}$. *Inorg. Chem.* **59**, 6755 (2020).

[10] S-W. Cheong, M. Feibig, W. Wu, L. Chapon, V. Kiryukhin. Seeing is believing: visualization of antiferromagnetic domains. *npj Quantum Materials* **5**, 3 (2020).

[11] Dipanshu Bansal, Jennifer L. Niedziela, Xing He, Tyson Lanigan-Atkins, Ayman Said, Ahmet Alatas, Douglas L. Abernathy, Yang Ren, Bin Gao, Sang-Wook Cheong, and Olivier Delaire. Lattice dynamics of the hybrid improper ferroelectrics $(Ca,Sr)_3Ti_2O_7$. *Phys. Rev. B* **100**, 214304 (2019).

[12] F. Foggetti, S.-W. Cheong, S. Artyukhin. Magnetic monopoles and toroidal moments in $LuFeO_3$ and related compounds. *Phys. Rev. B* **100**, 180408 (2019).

[13] Shuyu Xiao, Yaming Jin, Xiaomei Lu, Sang-Wook Cheong, Jiangyu Li, Yang Li, Fengzhen Huang, Jinsong Zhu. Dynamics and manipulation of ferroelectric domain walls in bismuth ferrite thin films. *Nat. Sci. Rev.* **7**, 278 (2019).

[14] S. Tang, J. H. Zhang, L. Lin, Z. B. Yan, X. P. Jiang, S. W. Cheong, and J.-M. Liu. Abnormal dependence of multiferroicity on high-temperature electro-poling in $GdMn_2O_5$. *J. Appl. Phys.* **126**, 174104 (2019).

[15] C. Stock, R. D. Johnson, N. Giles-Donovan, M. Songvilay, J. A. Rodriguez-Rivera, N. Lee, X. Xu, P. G. Radaelli, L. C. Chapon, A. Bombardi, S. Cochran, Ch. Niedermayer, A. Schneidewind, Z. Husges, Z. Lu, S. Meng, and S.-W. Cheong. Spin-wave directional anisotropies in antiferromagnetic $Ba_3NbFe_3Si_2O_{14}$. *Phys. Rev. B* **100**, 134429 (2019).

[16] S.-W. Cheong. SOS: symmetry-operational similarity. *npj Quantum Mater.* **4**, 53 (2019).

[17] P. Lampen-Kelley, E.M. Clements, B. Casas, M.H. Phan, H. Srikanth, J. Marcin, I. Skorvanek, H.T. Yic , S.W. Cheong. Impact of reduced dimensionality on the correlation length and magnetization dynamics of the spin chain cobaltite $Ca_3Co_2O_6$. *J. Mag. Mag. Mater.* **493**, 165690 (2020).

[18] M. G. Kim, B. Winn, S. Chi, A. T. Savici, J. A. Rodriguez-Rivera, W. C. Chen, X. Xu, Y. Li, J. W. Kim, S.-W. Cheong, and V. Kiryukhin. Spin-liquid-like state in pure and Mn-doped $TbInO_3$ with a nearly triangular lattice. *Phys. Rev. B* **100**, 024405 (2019).

[19] S. Liu, H. Zhang, S. Ghose, M. Balasubramanian, Zhenxian Liu, S. G. Wang, Y.-S. Chen, B. Gao, Jaewook Kim, S.-W. Cheong, and T. A. Tyson. Nature of the structural symmetries associated with hybrid improper ferroelectricity in $Ca_3X_2O_7$ (X = Mn and Ti). *Phys. Rev. B* **99**, 224105 (2019).

[20] M. Kratochvilova, F.-T. Huang, M.-T. Fernandez Diaz, M. Klicpera, S. J. Day, S. P. Thompson, Y.- S. Oh, B. Gao, S.-W. Cheong, and J.-G. Park. Mapping the structural transitions controlled by the trilinear coupling in $Ca_{3-x}Sr_xTi_2O_7$. *J. Appl. Phys.* **125**, 244102 (2019).

[21] A. A. Sirenko, P. Marsik, C. Bernhard, T. N. Stanislavchuk, V. Kiryukhin, and S.-W. Cheong. Terahertz vortex beam as a spectroscopic probe of magnetic excitations. *Phys. Rev. Lett.* **122**, 237401 (2019).

Using neutron as a probe to study magnetic excitations in strongly correlated electron materials

Pengcheng Dai (pdai@rice.edu)

Department of Physics and Astronomy, Rice University, Houston, Texas 77005

Program Scope

Understanding the electronic structure and magnetism in correlated electron materials continues to be at the forefront of modern condensed matter physics. Compounds containing quasi-localized *d*-electrons and extended *f*-electrons exhibit a wide range of phenomena, include high-transition temperature and unconventional superconductivity. Elucidating the microscopic spin excitations in these systems is central to understand their exotic macroscopic properties, which continue to defy description of the conventional Fermi-liquid theory. Neutron scattering plays an important role in determining the dynamical spin properties in these materials. The normal operation of the spallation neutron source and upgraded high-flux isotope reactor at Oak Ridge National Laboratory has created a unique opportunity for us to establish a strong materials synthesis and neutron scattering program at Rice University. The scope of our present program is to study spin excitations in iron-based superconductors, heavy fermion superconductors, and quantum spin liquid candidate materials. In addition, we train the next generation of neutron scattering scientists. We also establish a materials growth laboratory capable of producing some of the best Fe-based superconductors and quantum spin liquid materials for the U.S. condensed matter physics community.

Recent Progress

Resonance from antiferromagnetic spin fluctuations for superconductivity in UTe_2

Superconductivity originates from the formation of bound (Cooper) pairs of electrons that can move through the lattice without resistance below the superconducting transition temperature T_c. While electron Cooper pairs in most superconductors form anti-parallel spin-singlets with total spin $S = 0$, they can also form parallel spin-triplet Cooper pairs with $S = 1$ and an odd parity wavefunction. Spin-triplet pairing is important because it can host

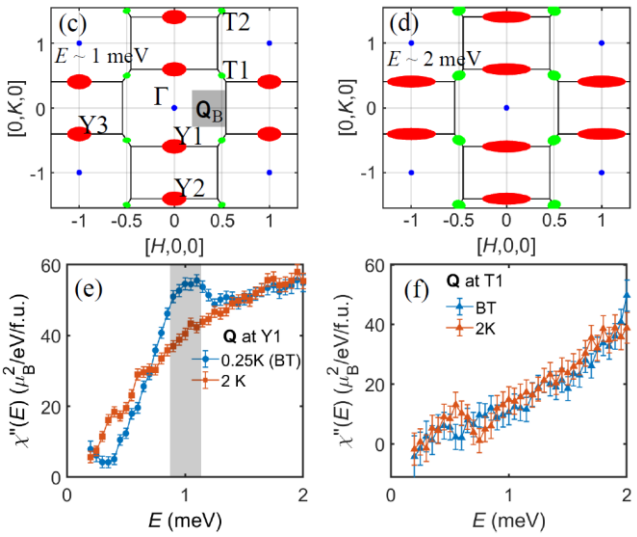

Fig. 1 (c,d) Schematics of the energy dependence of spin fluctuations in UTe2. (e,f) Temperature dependence of the spin fluctuations across T_c at Y1 and T1 points, respectively.

topological states and Majorana fermions relevant for quantum computation. Since spin-triplet pairing is usually mediated by ferromagnetic (FM) spin fluctuations, uranium based materials near a FM instability are considered ideal candidates for realizing spin-triplet superconductivity. Indeed, UTe_2, which has a T_c=1.6 K, has been identified as a candidate for chiral spin-triplet topological superconductor near a FM instability, although it also has antiferromagnetic (AF) spin fluctuations. Here we use inelastic neutron scattering (INS) to show that superconductivity in UTe_2 is coupled with a sharp magnetic excitation, termed resonance, at the Brillouin zone (BZ) boundary near AF order. Since the resonance has only been found in spin-singlet unconventional superconductors near an AF instability, its discovery in UTe_2 suggests that AF spin fluctuations may also induce spin-triplet pairing or that electron pairing in UTe2 has a spin-singlet component. [C. R. Dun *et al.*, *Nature (in press) 2021; Phys. Rev. Lett.* **125**, 237003 (2020)].

Nature of the spin resonance mode in $CeCoIn_5$

Spin-fluctuation-mediated unconventional superconductivity can emerge at the border of magnetism, featuring a superconducting order parameter that changes sign in momentum space. Detection of such a sign-change is experimentally challenging, since most probes are not phase-sensitive. The observation of a spin resonance mode (SRM) from inelastic neutron scattering is often seen as strong phase-sensitive evidence for a sign-changing superconducting order parameter, by assuming the SRM is a spin-excitonic bound state. Here we show that for the heavy fermion superconductor $CeCoIn_5$, its SRM defies expectations for a spin-excitonic bound state, and is not a manifestation of sign-changing superconductivity. Instead, the SRM in $CeCoIn_5$ likely arises from a reduction of damping to a magnon-like mode in the superconducting state, due to its proximity to magnetic quantum criticality. Our findings emphasize the need for more stringent tests of whether SRMs are spin-excitonic, when using their presence to evidence sign-changing superconductivity. [Y. Song *et al.*, *Communications Physics* **3**, 98 (2020)].

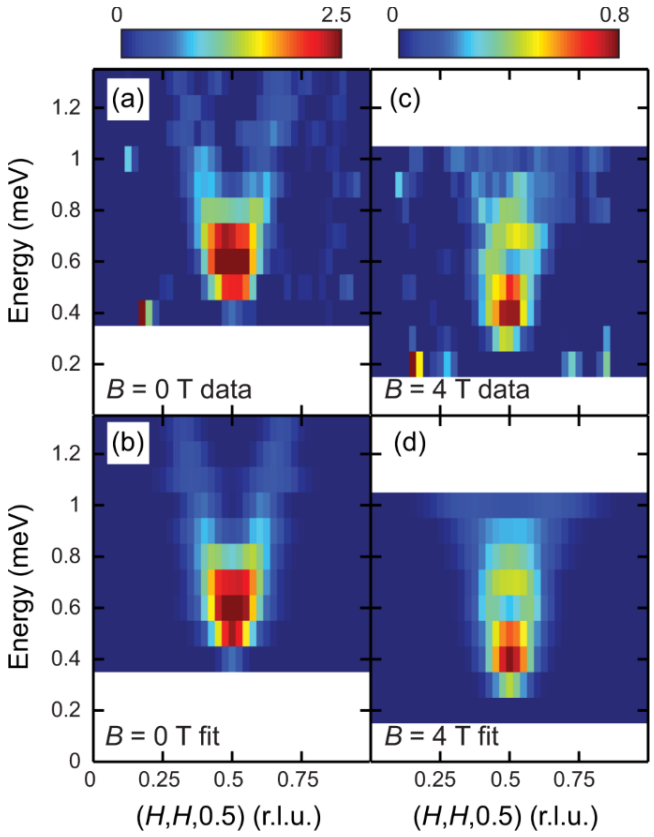

Fig. 2 The effect of a magnetic field on the neutron spin resonance of $CeCoIn_5$.

Orbital selective spin waves in detwinned NaFeAs

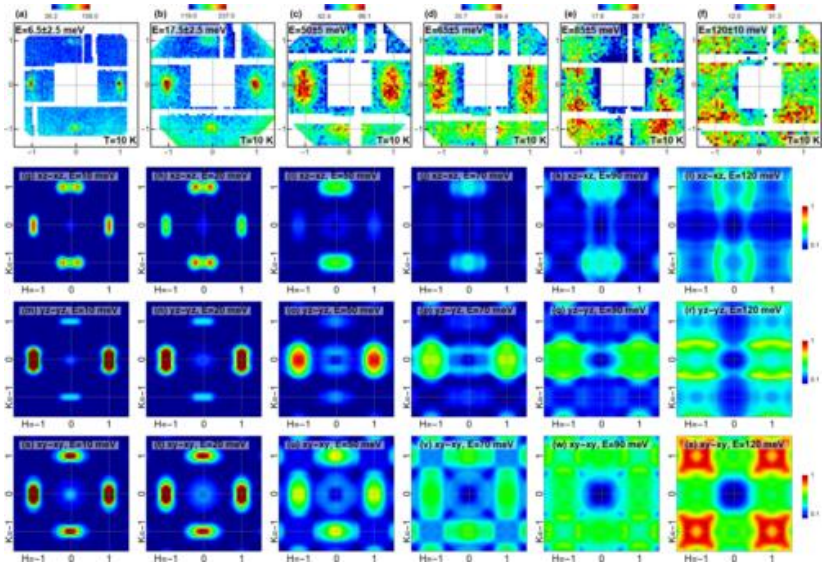

Fig. 3 Comparison of spin waves in detwinned NaFeAs with DFT+DMFT calculations with different orbitals.

The existence of orbital-dependent electronic correlations has been recognized as an essential ingredient to describe the physics of iron-based superconductors. NaFeAs, a parent compound of iron-based superconductors, exhibits a tetragonal-to-orthorhombic lattice distortion below $T_s \approx 60$ K, forming an electronic nematic phase with two 90∘ rotated (twinned) domains, and orders antiferromagnetically below $T_N \approx 42$ K. We use inelastic neutron scattering to study spin waves in uniaxial pressure-detwinned NaFeAs. By comparing the data with combined density functional theory and dynamical mean-field theory calculations, we conclude that spin waves up to an energy scale of $E_{crossover} \approx 100$ meV are dominated by d_{yz}–d_{yz} intraorbital scattering processes, which have the twofold (C2) rotational symmetry of the underlying lattice. On the other hand, the spin wave excitations above $E_{crossover}$, which have approximately fourfold (C4) rotational symmetry, arise from the d_{xy}–d_{xy} intraorbital scattering that controls the overall magnetic bandwidth in this material. In addition, we find that the low-energy ($E \approx 6$ meV) spin excitations change from approximate C4 to C2 rotational symmetry below a temperature $T^* (>T_s)$, while spin excitations at energies above $E_{crossover}$ have approximate C4 rotational symmetry and are weakly temperature dependent. These results are consistent with angle-resolved photoemission spectroscopy measurements, where the presence of a uniaxial strain necessary to detwin NaFeAs also raises the onset temperature $T*$ of observable orbital-dependent band splitting to above Ts, thus supporting the notion of orbital selective spin waves in the nematic phase of iron-based superconductors. [D. W. Tam *et al.*, *Phys. Rev. B* **102**, 054430 (2020)].

Spinon Fermi Surface Spin Liquid in a Triangular Lattice Antiferromagnet $NaYbSe_2$

Triangular lattice of rare-earth ions with interacting effective spin-1/2 local moments is an ideal platform to explore the physics of quantum spin liquids (QSLs) in the presence of strong spin-orbit coupling, crystal electric fields, and geometrical frustration. The Yb delafossites, $NaYbCh_2$ (Ch=O, S, Se) with Yb ions forming a perfect triangular lattice, have been suggested to be candidates for QSLs. Previous thermodynamics, nuclear magnetic resonance, and powder-sample neutron scattering measurements on $NaYbCh_2$ have supported the suggestion of the QSL ground states. The key signature of a QSL, the spin excitation continuum, arising from the spin quantum number fractionalization, has not been observed. Here we perform both

elastic and inelastic neutron scattering measurements as well as detailed thermodynamic measurements on high-quality single-crystal $NaYbSe_2$ samples to confirm the absence of long-range magnetic order down to 40 mK, and further reveal a clear signature of magnetic excitation continuum extending from 0.1 to 2.5 meV. The comparison between the structure of the magnetic excitation spectra and the theoretical expectation from the spinon continuum suggests that the ground state of $NaYbSe_2$ is a QSL with a spinon Fermi surface. [P. L. Dai *et al.*, Phys. Rev. X 11, 021044 (2021)]

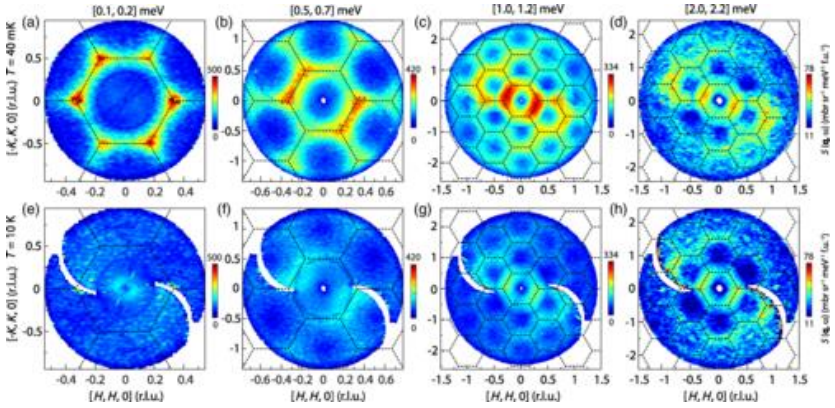

Fig. 4 Energy and temperature dependence of spin excitations within the [H,K,0] plane in NaYbSe2. Spin excitation continuum is seen at the zone boundary.

Future Plans

Our ultimate goal in this DOE supported project is to understand the microscopic origin of superconductivity in the unconventional superconductors. We will continue our successful program to study the interplay between magnetism and superconductivity. In particular, we will focus on spin dynamics in spin triplet candidate UTe_2, which reveal AF spin fluctuations coupled with superconductivity. In the coming years, we will determine crystal field levels of UTe_2, the strength of spin-orbit coupling and magnetic field dependence of the resonance, temperature dependence of the resonance and spin fluctuations, search for vortex lattice, and determine how hydrostatic pressure-induced AF order. Following the work on UTe_2, we used INS to study spin excitations in another spin triple superconductor UPt_3, and also discovered that superconductivity is also coupled with AF spin fluctuations. We will write up these results in the coming months. We will continue our original proposed program to study $(Ni,Co)_2Mo_3O_8$ and associated materials. We already obtained exciting results, and are in the process writing up these results. We will also continue our work on $Ce_2Zr_2O_7$ family of materials in the hope to sort out how disorder will affect the spin excitation continuum discovered a few years ago. Additional work on detwinned FeSe is going well with results likely be published in Nature Physics (second round of review). Very recently, we started to work on CsV_3Sb_5 kagome lattice superconductor, and discovered that phonons are involved in the charge density wave order in the system, this work is submitted and currently under review at PRL. By carrying out systematic measurements on doping dependence of the phonon anomaly, we hope to identify the microscopic origin of the charge density wave and its connection with superconductivity of CeV_3Sb_5.

Publications from DOE support from December 1st, 2019 till November 12, 2021

1. C. R. Dun, R. E. Baumbach, A. Podlesnyak, Y. H. Deng, C. Moir, A. J. Breindel, M. B. Maple, E. M. Nica, Q. Si, and Pengcheng Dai, Nature (in press) Arxiv:2106.14424 (2021).

2. Yaofeng Xie, Lebing Chen, Tong Chen, Qi Wang, Qiangwei Yin, J. Ross Stewart, Matthew B. Stone, Luke L. Daemen, Erxi Feng, Huibo Cao, Hechang Lei, Zhiping Yin, Allan H. MacDonald, and Pengcheng Dai, Communications Physics **4**, 240 (2021).

3. Lebing Chen, Matthew B Stone, Alexander I Kolesnikov, Barry Winn, Wonhyuk Shon, Pengcheng Dai, and Jae-Ho Chung, 2D Mater. **9**, 015006 (2022).

4. Yizhou Xin, Ingrid Stolt, Yu Song, Pengcheng Dai, and W. P. Halperin, Phys. Rev. B **104**, 144421 (2021).

5. Zhiwei Wang, Yu-Xiao Jiang, Jia-Xin Yin, Yongkai Li, Guan-Yong Wang, Hai-Li Huang, Shen Shao, Jinjin Liu, Peng Zhu, Nana Shumiya, Md Shafayat Hossain, Hongxiong Liu, Youguo Shi, Junxi Duan, Xiang Li, Guoqing Chang, Pengcheng Dai, Zijin Ye, Gang Xu, Yanchao Wang, Hao Zheng, Jinfeng Jia, M. Zahid Hasan, and Yugui Yao, Phys. Rev. B **104**, 075148 (2021).

6. Long Tian, Panpan Liu, Tao Hong, Tilo Seydel, Xingye Lu, Huiqian Luo, Shiliang Li, and Pengcheng Dai, Chin. Phys. B **30**, 087402 (2021).

7. Liangzi Deng, Trevor Bontke, Rabin Dahal, Yu Xie, Bin Gao, Xue Li, Ketao Yin, Melissa Gooch, Donald Rolston, Tong Chen, Zheng Wu, Yanming Ma, Pengcheng Dai, and Ching-Wu Chu, PNAS **118**, e2108938118 (2021).

8. Yu Song, Weiyi Wang, Chongde Cao, Zahra Yamani, Yuanji Xu, Yutao Sheng, Wolfgang Löser, Yiming Qiu, Yi-feng Yang, Robert J. Birgeneau, and Pengcheng Dai, npj Quantum Materials **6**, 60 (2021).

9. Peng-Ling Dai, Gaoning Zhang, Yaofeng Xie, Chunruo Duan, Yonghao Gao, Zihao Zhu, Erxi Feng, Zhen Tao, Chien-Lung Huang, Huibo Cao, Andrey Podlesnyak, Garrett E. Granroth, Michelle S. Everett, Joerg C. Neuefeind, David Voneshen, Shun Wang, Guotai Tan, Emilia Morosan, Xia Wang, Hai-Qing Lin, Lei Shu, Gang Chen, Yanfeng Guo, Xingye Lu, and Pengcheng Dai, Phys. Rev. X **11**, 021044 (2021).

10. Yu Song, Weiyi Wang, Eugenio Paris, Xingye Lu, Jonathan Pelliciari, Yi Tseng, Yaobo Huang, Daniel McNally, Marcus Dantz, Chongde Cao, Rong Yu, Robert J. Birgeneau, Thorsten Schmitt, and Pengcheng Dai, Phys. Rev. B **103**, 075112 (2021).

11. Chunruo Duan, Kalyan Sasmal, M. Brian Maple, Andrey Podlesnyak, Jian-Xin Zhu, Qimiao Si, and Pengcheng Dai, Phys. Rev. Lett. **125**, 237003 (2020).

12. David W. Tam, Zhiping Yin, Yaofeng Xie, Weiyi Wang, M. B. Stone, D. T. Adroja, H. C. Walker, Ming Yi, and Pengcheng Dai, Phys. Rev. B **102**, 054430 (2020).

13. Tong Chen, Ming Yi, and Pengcheng Dai, Frontiers in Physics **8**, 314 (2020).

14. Yu Song, Weiyi Wang, John S. Van Dyke, Naveen Pouse, Sheng Ran, Duygu Yazici, A. Schneidewind, Petrermák, Y. Qiu, M. B. Maple, Dirk K. Morr, and Pengcheng Dai, Communications Physics **3**, 98 (2020).

15. Tong Chen, Youzhe Chen, David W. Tam, Bin Gao, Yiming Qiu, Astrid Schneidewind, Igor Radelytskyi, Karel Prokes, Songxue Chi, Masaaki Matsuda, Collin Broholm, and Pengcheng Dai, Phys. Rev. B **101**, 140504(R) (2020).

16. Zhuang Xu, Guangyang Dai, Yu Li, Zhiping Yin, Yan Rong, Long Tian, Panpan Liu, Hui Wang, Lingyi Xing, Yuan Wei, Ryoichi Kajimoto, Kazuhiko Ikeuchi, D. L. Abernathy, Xiancheng Wang, Changqing Jin, Xingye Lu, Guotai Tan, & Pengcheng Dai, npj Quantum Materials **5**, 11 (2020).

17. Yizhou Xin, Ingrid Stolt, Yu Song, Pengcheng Dai, and W. P. Halperin, Phys. Rev. B **101**, 064410 (2020).

18. M. Yi, H. Pfau, Y. Zhang, Y. He, H. Wu, T. Chen, Z.?R. Ye, M. Hashimoto, R. Yu, Q. Si, D.-H. Lee, Pengcheng Dai, Z.-X. Shen, D. H. Lu, and R. J. Birgeneau, Phys. Rev. X **9**, 041049 (2019).

Flow-through Neutron Reflectometry – an *in operando* sample environment for active polymer interface studies

Steven C. DeCaluwe, Colorado School of Mines Mechanical Engineering

Program Scope

Functional, ion-conducting polymers play critical roles in numerous emergent electrochemical energy devices, including polymer electrolyte membrane fuel cells (PEMFCs), Li-O_2 batteries, and solid-state batteries. Improving polymer and electrode design are necessary to commercialize these devices, e.g. for electric vehicles, but progress is hindered by poor fundamental understanding of coupled transport and chemical processes in functional polymers during device operation. This program's aim is to develop a novel *operando* sample environment for neutron reflectometry (NR) of non-equilibrated thin film polymer samples in the presence of species fluxes.

NR is a powerful technique for thin film analysis, but *operando* measurements are impeded by the need for very flat samples. Because PEMFCs and batteries require stable material interfaces with fast interfacial reactions and species transport, measurement of *active* interfaces with species fluxes is essential. This work will enable first-of-their-kind "flow-through" NR measurements of non-equilibrated samples, for fundamental structure-property relationships for conductive polymers in PEMFCs and batteries. Device simulations validated against the measurements serve as a framework for correlating and interpreting the results for a mechanistic description of device function and a scientifically guided, validated design tool for advanced electrochemical devices.

Recent Progress

Research activities have followed four tracks: (*i*) develop and verify the *operando* sample environment; (*ii*) standard, "baseline" NR of Nafion on relevant PEMFC substrates (e.g. carbon); (*iii*) develop complementary *operando* characterization techniques, and (*iv*) device simulations to demonstrate the impact of accurate structure-property information in functional polymers.

Sample environment: The sample environment has two novel features: (*i*) a sample chamber that allows two gas feeds (one for either side of the sample) and precise temperature and relative humidity control, and (*ii*) a porous sample support that provides gas/liquid access to both sides of the sample. The sample chamber has been designed and is currently being fabricated (Figure 1) for delivery before year's end. The sample support (Figure 2) consists of a 300 mm thick Si wafer, made porous via deep reactive ion etching, coupled with a microporous spin on

glass. The support has been fabricated and verified by NR measurements on the Liquids Reflectometer at the SNS, and indeed provides a porous but flat support for high-quality NR data.

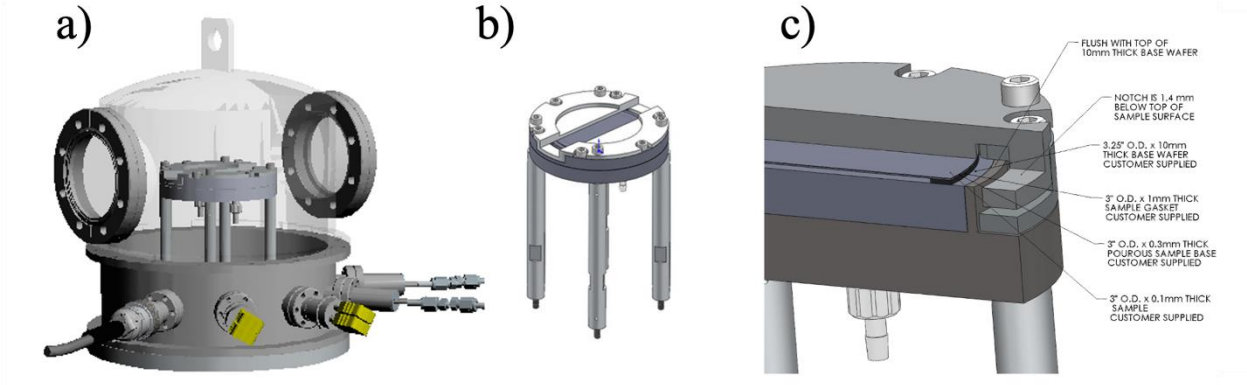

Figure 1. Operando "flow through" NR sample environment design. a) sample chamber, held at constant T, with two gas and electrochemical feedthroughs. b) Sample pedestal allowing for NR measurement of a porous sample held between two separate gas environments. c) Close up of sample pedestal details.

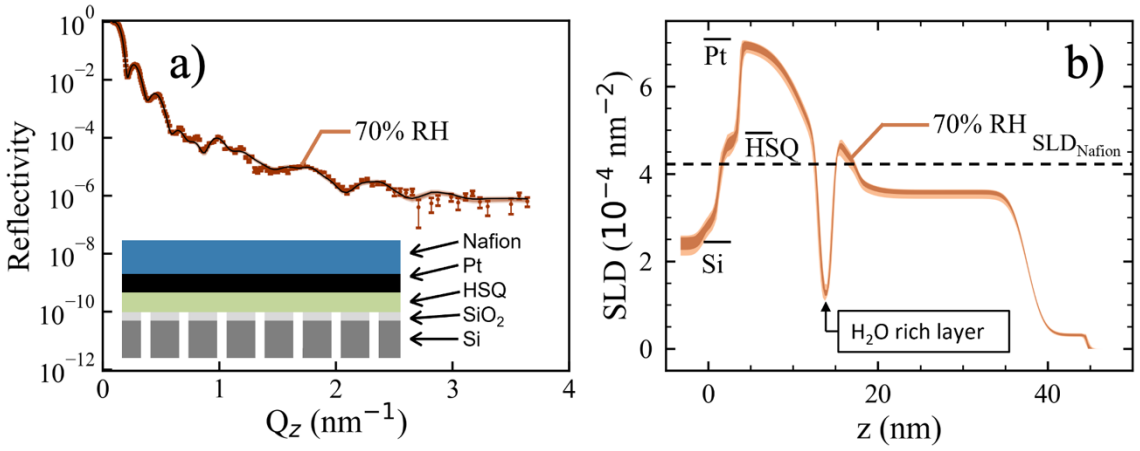

Figure 2. Porous sample support with Pt-Nafion sample a) Sample schematic and NR data, demonstrating low surface roughness (good reflectivity out to Q = 3.5 nm^{-1}). b) Fitted SLD profile shows details of Nafion-Pt interfacial structure.

Equilibrium NR: While the sample environment is fabricated, we have filled gaps in existing literature for NR on PEMFC-relevant materials (e.g. Carbon), using standard (equlibrium) NR approaches. We have conducted a survey of NR on various carbon surfaces, to understand the range of interfacial structures and water uptake in Nafion thin films. Results show an array of possible structures, which depend on both the carbon morphology, surface chemistry, and sample roughness (Figure 3). These results are in preparation for publication by year's end.

Complementary techniques: we have developed a sample environment for precise, time-resolved mass uptake measurements in Nafion thin films via quartz crystal microbalance (QCM),

to quantify time-varying surface chemistry and transport rates. These will serve as an important complement to the steady-state non-equilibrium NR. Data collection is currently underway.

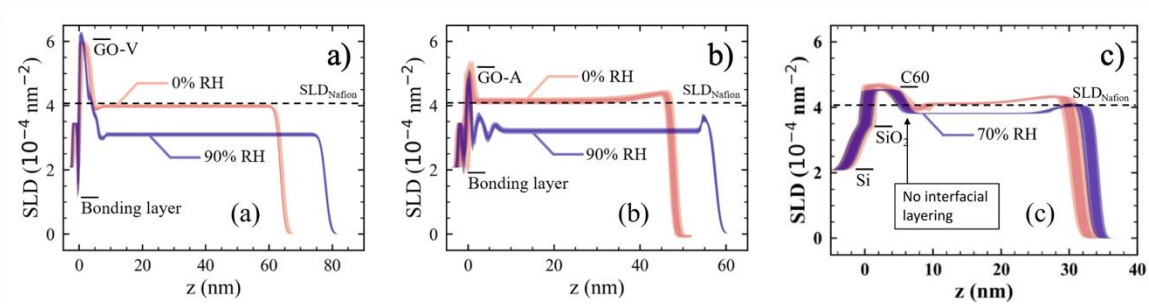

Figure 3. SLD profiles for Nafion thin films on varying carbon substrates. a) graphene oxide, annealed in vacuum; b) graphene oxide, annealed in argon; c) C60 fullerenes. The resulting Nafion interfacial structures varying according to the substrate roughness and hydrophobicity.

Numerical simulations: numerical simulation tools have been developed to incorporate detailed structure-property relationships from NR measurements in predictions of PEMFC performance. Results (Figure 4) show that the performance predictions are sensitive to the Nafion structure-property model used, demonstrating the need for accurate property measurements. Moreover, incorporating accurate structure-property relationships for Nafion thin films can uncover new design rules to increase maximum power density by up to 40%, compared to catalyst layers where Pt and Nafion are uniformly distributed (Figure 5).

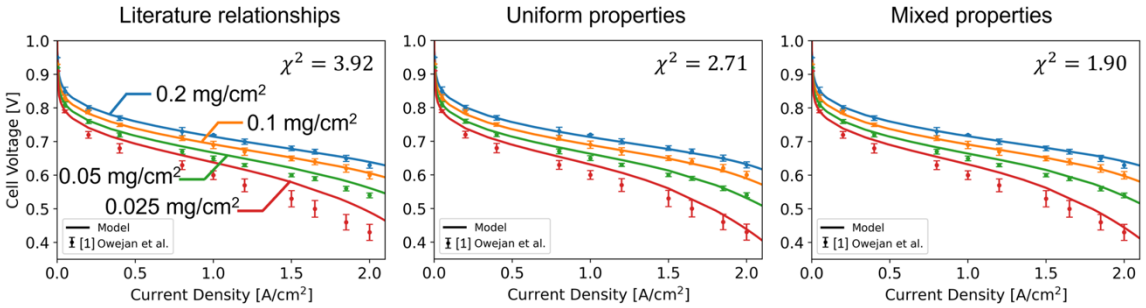

Figure 4. Predicted and measured PEMFC performance under varying platinum loading (0.025 – 0.2 mg of Pt per cm^2 of fuel cell area). Catalyst layer Nafion ionic conductivity derived from a) literature values for thick membranes; b) NR-derived thin film conductivities that ignore interfacial structures; c) fully accurate structure-property relationships derived from NR. Results show that accurate structure-property relationships, as measured in this study, are required to understand limits under low Pt loading.

Numerical simulations: numerical simulation tools have been developed to incorporate detailed structure-property relationships from NR measurements in predictions of PEMFC performance. Results (Figure 4) show that the performance predictions are sensitive to the Nafion structure-property model used, demonstrating the need for accurate property measurements. Moreover, incorporating accurate structure-property relationships for Nafion thin films can

uncover new design rules to increase maximum power density by up to 40%, compared to catalyst layers where Pt and Nafion are uniformly distributed (Figure 5).

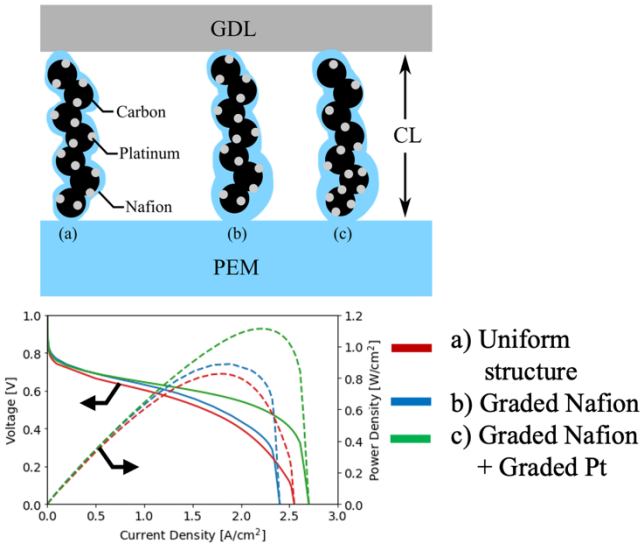

Figure 5. Electrode design with accurate structure property relationships. Upper pane: three possible Nafion and Pt distributions. Lower pane: predicted PEMFC performance for each. With accurate Nafion structure-property relationships, we can uncover new designs to improve PEMFC power density by as much as 40%.

Future Plans

The remaining tasks involve utilizing the operando platform for simultaneous measurement of Nafion SLD profiles and species fluxes across the sample. By measuring the SLD gradients and how they change as a function of the gas phase boundary conditions on either side of the thin film, we can quantify reaction rate and species transport parameters as a function of Nafion thickness, ambient gas-phase conditions, and substrate material properties. There are a wide range of experiments enabled by the measurement platform to yield direct insights into limiting phenomena in PEMFC electrodes. These results will be correlated with time resolved QCM and conductivity measurements to improve the multi-scale simulation tool, for a scientifically guided electrode design tool.

Publications

Randall, C.R.; DeCaluwe, S.C. "Physically Based Modeling of PEMFC Cathode Catalyst Layers: Effective Microstructure and Ionomer Structure-Property Relationship Impacts." *J. Electrochem. Energy. Conv. Storage: 2020 Emerging Investigators Special Issue*, **17**(4), 2020, 041104 – 041113.

Neutron scattering studies of phonon anharmonicity and coupling with spin and charge degrees of freedom

Olivier Delaire, Duke University

Program Scope

Understanding the microscopic processes involved in the transport and conversion of energy from the atomic scale to the mesoscale is critical for the development of next-generation materials for energy sustainability and quantum information sciences. The fundamental underpinnings of thermal transport in crystalline insulators and semiconductors reside in the propagation of phonon quasiparticles through the lattice. These phonon vibrations also critically modulate the interactions between orbitals and spins providing material functionalities. Significant progress has enabled a nanoscale understanding of heat transfer based on novel experimental techniques and first-principles modeling of Boltzmann transport for phonons. Yet, regimes of strong anharmonicity close to lattice instabilities reside beyond perturbation theories currently used to investigate phonon-phonon scattering rates. Further, the impacts of strong electron-phonon coupling and spin-phonon coupling on phase stability and transport phenomena remain insufficiently understood. Simultaneously, quantum effects involving coupled degrees-of-freedom may impact the properties of materials over wide ranges of compositions and temperatures. This project investigates phonon anharmonicity and phonon interactions with other degrees of freedom, using a combination of neutron scattering, thermal and transport characterization, and first-principles simulations. In particular, we investigate spin-phonon coupling and anharmonic effects near phase transitions, for example in ferroelectrics and multiferroics, with the aim of better understanding their thermodynamics and transport properties, as well as the role of quantum fluctuations. The key role of soft phonon modes or hybrid-improper mechanisms involving multiple coupled modes is investigated in both canonical and novel materials, taking advantage of single-crystal measurements to map extended regions in wave-vector space.

Recent Progress

2D fluctuations and phonon breakdown near structural transitions in $CsPbBr_3$ [Nature Materials 20, 977–983 (2021)]

Understanding the atomic structure and dynamics of lead-halide perovskites (LHPs) is critical to rationalize their performance in photovoltaic, radiation detection and thermoelectric applications [1,2]. LHPs exhibit structural instabilities and large atomic fluctuations thought to impact their optical and thermal properties, yet the structural and temporal correlations of their atomic motions have remained poorly understood. We resolved these correlations in $CsPbBr_3$ using neutron and x-ray scattering as a function of temperature, complemented with first-principles simulations [pub1]. We performed single-crystal time-of-flight inelastic neutron scattering (INS)

with the CNCS and ARCS spectrometers at the Spallation Neutron Source and the SPINS three-axis spectrometer at the NIST Center for Neutron Research. We probed phonons across large swaths of 4D (Q;E) space in all three phases (orthorhombic, tetragonal, cubic). Further, x-ray diffuse scattering was performed at the Advanced Photon Source by our collaborators (R. Osborn and S. Rosenkranz, Argonne Nat. Lab.). Strong temperature-dependent diffuse rods were observed along Brillouin zone (BZ) boundaries in both x-ray and neutron measurements. INS revealed striking extended over-damped phonon modes forming a quasielastic continuum across the BZ edges. The unusual atomic dynamics revealed by INS reflect extended two-dimensional fluctuating sheets of collective $PbBr_6$ octahedra rotations. We also performed anharmonic fist-principles phonon simulations based on ab-initio molecular dynamics (AIMD), which captured the neutron/x-ray observations and revealed their primary origin in the weak and anharmonic interatomic potential connecting Br atoms across $PbBr_6$ octahedra. Further, the overdamped phonon modes identified here strongly modulate the electronic band edge states and bandgap. These results provide key insights to understand the origin of both the ultralow thermal conductivity and the large amplitude vibrations coupling to the electronic structure in LHPs.

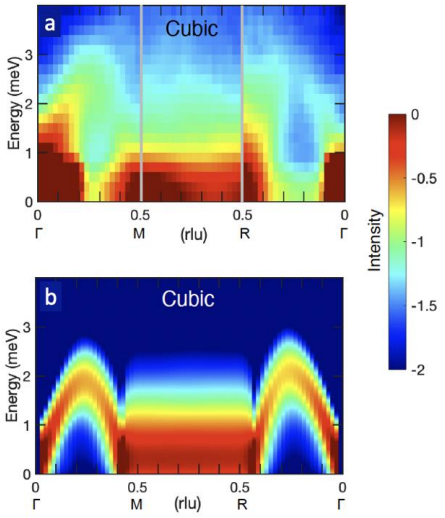

Figure 1 Overdamped phonons along M-R in the cubic phase of CsPbBr3. (a) INS measurements (b) first-principles simulations of anharmonic spectral functions.

Magnetically driven phonon instability and metal–insulator transition in h-FeS [Nature Physics 16, 669–675 (2020)]:

Hexagonal iron-sulfide (*h*-FeS) exhibits intimately coexisting magnetic, structural, and metal-insulator transitions in a simple stoichiometry, and was recently proposed to also harbor magnetoelectric coupling [3]. Yet its microscopic degrees-of-freedom have remained little explored and a solid understanding of the metal-insulator transition (MIT) had been lacking, with in particular several conflicting theoretical scenarios. Recent studies predicted that *h*-FeS (troilite phase) exhibits magneto-electric (ME) properties emerging at ~415 K, at the onset of a structural phase transitions (SPT). Prior theoretical work proposed that the SPT is driven by zone-boundary phonon instabilities coupled to a non-polar zone-center mode [3].

We used neutron and x-ray scattering measurements, together with first-principles simulations and thermodynamic analysis, to determine the sequence of microscopic couplings triggering the MIT, revealing a new and important connection between magnetic ordering and phonon instabilities [pub2]. The AFM ordering enables the emergence of two zone-boundary soft phonons, whose condensation couples to a zone-center mode, with the resulting lattice distortion opening the electronic band gap. Simultaneously, spin-lattice coupling opens a gap in the magnon spectrum that impacts the entropy and thermodynamics of the MIT.

We observed two magnetic transitions with neutron diffraction, one between 440 and 500 K (AFM ordering, spins pointing along c-axis) and another spin-reorientation transition between 580 and 700 K (AFM, spins pointing in-plane). Above 700 K, FeS is a non-magnetic metal. We measured the phonon dispersions and DOS of FeS using both INS and IXS. Our IXS measurements revealed the instability of the H_1 distortion (Fig. 2 right). The phonon at ~5 meV in the metallic phase condenses at the SPT to form a Bragg peak at (4,0,3). A similar behavior is observed for the K_5 distortion. Further, we performed finite-temperature phonon simulations, explicitly including anharmonicity. Our simulations reproduced the measurements (Fig. 2). Beyond resolving the mechanism of the MIT in h-FeS, our study highlights the importance of controlling anharmonic lattice instabilities through magnetic interactions, a new direction to tune material response [pub2].

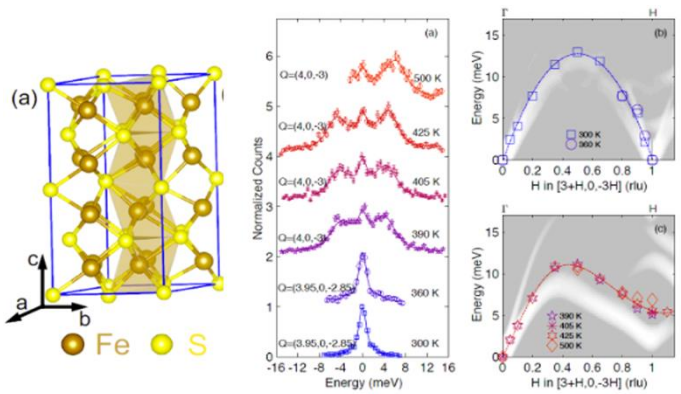

Figure 2 (left) Structure of FeS below Tc, showing tilts and rotations of FeS_6 polyhedra and displacement of Fe atoms along c-axis. (right) Dynamics of primary lattice instability (H1) across the MIT. (a) Constant-Q scans near (4,0,-3) Bragg peaks at various temperatures fitted with the damped harmonic oscillator profile. (b,c) phonon dispersions measured below (blue) and above (red) the metal-insulator transition in FeS, and S(Q,E) calculated from first-principles for both phase (gray scale).

<u>Anharmonic Eigenvectors and Acoustic Phonon Disappearance in Quantum Paraelectric SrTiO3 [Physical Review Letters 124, 145901 (2020)]</u>

$SrTiO_3$ is an incipient ferroelectric perovskite, undergoing an antiferrodistortive (AFD) transition (cubic to tetragonal) at Tc=105K, through the softening of the R_{25} phonon mode at the R-point [4,5,6]. While the zone-center TO mode also softens on cooling, the ferroelectric transition is suppressed by quantum fluctuations. In addition, theoretical studies of the dynamics of $SrTiO_3$ have emphasized the competition between FE and AFD instabilities.

Pronounced anomalies in the SrTiO3 dynamical structure factor, S(**Q**,E), including the disappearance of acoustic phonon branches at low temperatures, were uncovered with INS and simulations [pub3]. Through combined experimental studies with inelastic neutron scattering on single-crystals at the SNS and HFIR at ORNL, as well as first-principles lattice dynamics simulations explicitly taking into account anharmonicity, we have rationalized the observation of the disappearance of transverse acoustic modes at low temperatures on approaching the quantum critical point. The striking effect reflects anharmonic couplings between acoustic and optic phonons and the incipient ferroelectric instability near the quantum critical point. It is rationalized using a first-principles renormalized anharmonic phonon approach, pointing to nonlinear Ti-O hybridization causing unusual changes in real-space phonon eigenvectors, frequencies, group velocities, and scattering phase space. Our method is general and establishes how T dependences beyond the harmonic regime, assessed by INS mapping of large reciprocal-space volumes, provide real-space insights into anharmonic atomic dynamics near phase transitions [pub3].

Our results on $SrTiO_3$ establish how a strong T dependence of phonon intensities beyond the harmonic model can be quantitatively measured with INS by mapping large S(**Q**, E). volumes, providing direct insights into the anharmonic behavior of phonon eigenvectors, and also show how first-principles simulations including anharmonic effects can reproduce and rationalize such effects. The identified T dependence of force constants and dispersions is important to quantitatively rationalize unusual thermal transport in $SrTiO_3$. Our methods directly carry over to the study of other anharmonic materials.

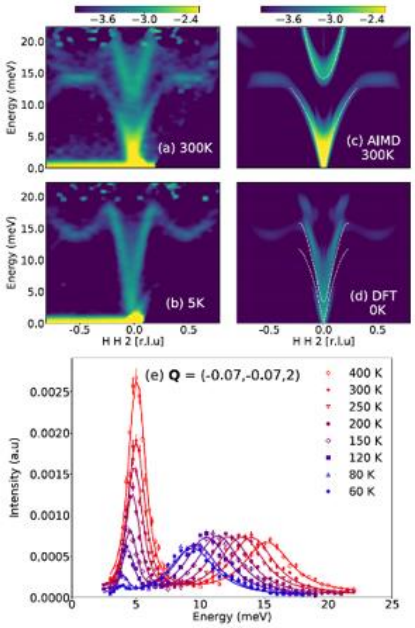

Figure 3 T-dependent S(**Q**, E) in $SrTiO_3$ showing disappearance of the TA branch at low T. (top) INS data from HYSPEC; and simulations. (bottom) HB-3 spectra at Q =(−0.07,−0.07, 2) at different temperatures (markers), and fitted curves.

Future Plans

Building on our recent success at rationalizing anharmonic phonons in the quantum paralectric SrTiO3, we will investigate phonons near the QCP in KTaO3 and doped compounds $K(Ta,Nb)O_3$ (KTN), using INS and anharmonic phonon simulations. We have large single-crystals available and plan to measure these at SNS and HFIR. First-principles simulations (DFT and AIMD) will be performed at NERSC. Additional diffuse scattering measurements will be performed with CORELLI. The zone-center soft mode in $SrTiO_3$ was previously found to be sensitive to an external electric field. We plan to investigate the field dependence of anharmonic phonons in both STO and KTN.

We have recently performed measurements of phonon linewidths and shifts with micro-eV resolution using neutron-resonant spin-echo (NRSE) TAS at HFIR in collaboration with Fankang Li. We plan to continue our studies of anharmonic phonon scattering with high resolution to help rationalize scattering processes at low temperature in the quantum regime.

References

[1] Huang, J., Yuan, Y., Shao, Y. & Yan, Y. Nat. Rev. Mater. 2, 17042 (2017).

[2] Lee, W. et al. Proc. Natl Acad. Sci. USA 114, 8693–8697 (2017).

[3] Ricci, F. & Bousquet, E. Phys. Rev. Lett. 116, 227601 (2016).

[4] Cowley, R. A., Buyers, W. J. L. & Dolling, G., Solid St. Commun. 7, 181 (1969)

[5] G. Shirane and Y. Yamada, Phys. Rev. 177, 858 (1969)

[6] S. M. Shapiro, J. D. Axe, G. Shirane, and T. Riste, Phys. Rev. B 6, 4332–4341 (1972).

Publications

- [pub1] T. Lanigan-Atkins*, X. He*, M. J. Krogstad, D. M. Pajerowski, D. L. Abernathy, Guangyong NMN Xu, Zhijun Xu, D.-Y. Chung, M. G. Kanatzidis, S. Rosenkranz, R. Osborn, and O. Delaire, "Two-dimensional overdamped fluctuations of soft perovskite lattice in $CsPbBr_3$", **Nature Materials** 20, 977–983 (2021). https://doi.org/10.1038/s41563-021-00947-y

- [pub2] D. Bansal, J. L. Niedziela, S. Calder, T. Lanigan-Atkins, R. Rawl, A.H. Said, D.L. Abernathy, A.I. Kolesnikov, H. Zhou, and O. Delaire, "Magnetically-driven phonon instability enables the metal-insulator transition in h-FeS", **Nature Physics** 16, 669-675, (2020). DOI: https://doi.org/10.1038/s41567-020-0857-1

- [pub3] Xing He, Dipanshu Bansal, Barry Winn, Songxue Chi, Lynn Boatner, and Olivier Delaire, "Anharmonic Eigenvectors and Acoustic Phonon Disappearance in Quantum Paraelectric $SrTiO_3$", **Physical Review Letters** 124, 145901 (2020). https://doi.org/10.1103/PhysRevLett.124.145901

- [pub4] Jennifer Neu, Kaya Wei, Xing He, Olivier Delaire, Ryan Baumbach, Zhenzhen Feng, Yuhao Fu, Yongsheng Zhang, David J. Singh, and Theo Siegrist, "Orthorhombic to monoclinic phase transition in $NbNiTe_2$", **Phys. Rev. B** 100, 144102 (2019).

- [pub5] Mayanak K Gupta, Jingxuan Ding, Naresh C Osti, Douglas L. Abernathy, William Arnold, Hui Wang, Zachary Hood and Olivier Delaire, "Fast Na Diffusion and Anharmonic Phonon Dynamics in Superionic Na_3PS_4", **Energy Environ. Sci.** (2021), DOI:10.1039/D1EE01509E.

- [pub6] Yijing Huang, Shan Yang, Samuel Teitelbaum, Gilberto De la Pena, Takahiro Sato, Matthieu Chollet, Diling Zhu, Jennifer L. Niedziela, Dipanshu Bansal, Andrew P. May, Aaron M.Lindenberg, Olivier Delaire, David A.Reis, Mariano Trigo, "Photoinduced Lattice Instability in SnSe", under review in PRX (2021) – resubmitted

- [pub7] Junjie Li, Lijun Wu, Shan Yang, Xilian Jin, Wei Wang, Jing Tao, Lynn Boatner, Marcus Babzien, Mikhail Fedurin, Mark Palmer, Weiguo Yin, Olivier Delaire, and Yimei Zhu, "Direct detection of V-V atom dimerization and rotation dynamic pathways upon ultrafast photoexcitation in VO_2", under review in PRX (2021) – resubmitted

- [pub8] Lebing Chen, Chengjie Mao, Jae-Ho Chung, Matthew B. Stone, Alexander I. Kolesnikov, Xiaoping Wang, Kenji Nakajima, Seiko Ohira-Kawamura, Bin Gao, Olivier Delaire and Pengcheng Dai, "Anisotropic magnon damping by zero-temperature quantum fluctuations of the Cr atom in ferromagnetic $CrGeTe_3$", submitted (under review, Nature Communications).

Equilibrium and Non-Equilibrium Vortex and Skyrmion Lattices

Morten R. Eskildsen, University of Notre Dame

Program Scope

The program is focused on the small-angle neutron scattering (SANS) studies of mesoscopic magnetic structures, specifically the vortex lattice (VL) in type-II superconductors and the skyrmion lattice (SkL) in chiral magnets in nonequilibrium conditions. The vortex studies have a dual focus: (i) Using the VL as a probe of the superconducting state in unconventional superconductors, and (ii) Studies of the structural transition kinetics and activated behavior in vortex matter. Similarly, the SkL studies has a dual objective: (i) Determination of the activation barrier for skyrmion formation/annihilation from hysteresis measurements, and (ii) using transport currents to access and manipulate metastable or out-of-equilibrium SkL configurations. Both the VL and SkL studies are complemented by molecular dynamics (MD) simulations.

Recent Progress

Skyrmion stability and manipulation. Our initial studies of the SkL focused on the topological protection of the individual skyrmions, using SANS measurements of the field-hysteresis of the SkL phase in combination with a minimum-energy path analysis based on atomistic spin simulations [1]. This showed that the SkL in MnSi forms from the conical phase progressively in small domains, each of which consisting of hundreds of skyrmions, and with an activation barrier of several eV per skyrmion. The activation barrier is independent of temperatures, as expected if this is topological in nature.

More recently, we have begun studies of the SkL under the influence of electric and thermal currents, which both are known to cause skyrmion motion [2-3]. To resolve the SkL motion by SANS we have adapted a Corbino geometry with a radial current flow. Here, the inhomogeneous current gives rise to a torque on the SkL and hence a rotation directly visible by SANS. Our initial measurements showed a non-monotonic response, with the SkL rotating in one direction for low

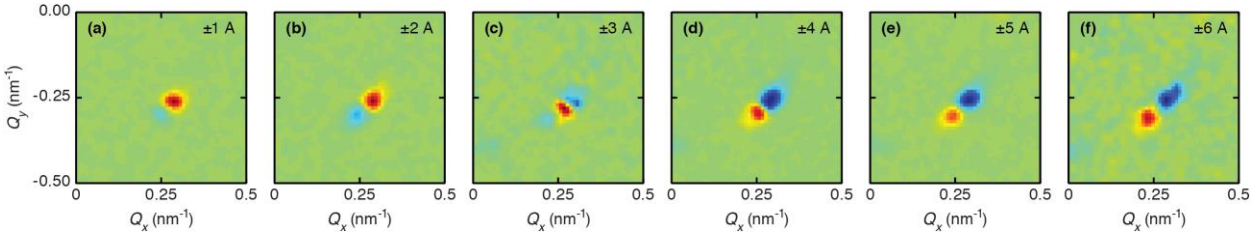

Fig. 1 Difference between SkL diffraction patterns obtained at positive and negative currents of the same magnitude. An intensity "dipole" is visible at all currents, except at the inflection point at ±3 A where it switches polarity. Only one of the six SkL Bragg peaks is visible in the region of reciprocal space shown.

currents and in the opposite direction for high currents, as shown in Fig. 1. We understand this switching to be due to a competition between the electrical current and the accompanying thermal current in the sample. Experimentally, the two effects can be separated by having the two currents flowing in the same or opposite directions. Modelling of the data, including a finite element analysis of the sample current and temperature profiles, is in progress.

Reversible ordering and disordering of the vortex lattice in UPt_3. We have demonstrated a novel approach to structural studies of vortex matter whereby reversible quenched disorder can be introduced locally in superconducting UPt_3 [4]. In this material, the VL undergoes a gradual disordering on a time scale of tens of minutes when subjected to a beam of cold neutrons, as shown in Fig. 2. The disordering is due to local heating events caused by neutron induced fission of ^{235}U, which leaves an increasing fraction of the sample in a vortex glass state. The VL does not spontaneously re-order once the local heating has been dissipated, but can be re-annealed by the application of a damped field oscillation. Fission induced VL disordering will also be a factor in potential SANS studies of other U-based superconductors such as UTe_2.

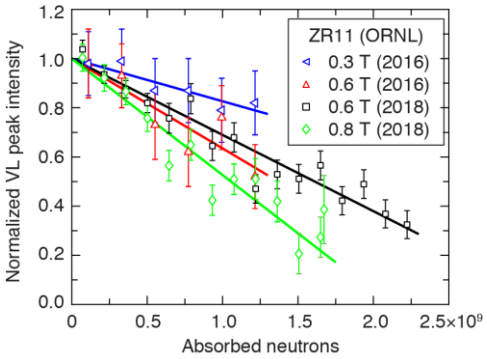

Fig. 2 VL scattering rate vs absorbed neutrons per area transmitted through the sample for different fields. Intensities are normalized such that linear fits extrapolate to unity for the pristine VL.

Field angle dependent vortex lattice phase diagram in MgB_2. The VL in MgB_2 has been used as a model system for studies of kinetics and activated behavior in connection with the transition from metastable to equilibrium states [5]. Rotation the applied field about the crystalline *a*-axis and towards the basal plane in this material, is found to suppress the intermediate VL phase which exists between end states aligned with two high-symmetry directions in the hexagonal basal plane for $\boldsymbol{H} \parallel \boldsymbol{c}$ [6]. Above a critical angle, the intermediate state disappears entirely and the previously continuous transition becomes discontinuous, as shown in Fig. 3. The ability to tune the VL phase diagram makes opens up possible studies of the transition kinetics associated with a first order VL reorientation transition, complementing our previous work.

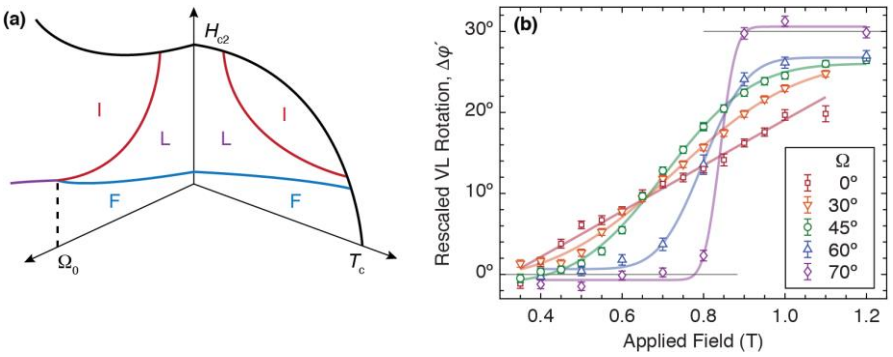

Fig. 3 (a) Qualitative MgB_2 VL phase diagram in the *H*-*T* and *H*-Ω planes. (b) Evolution of the VL rotation transition versus applied field for increasing field angle, Ω. At Ω = 70° the transition becomes essentially discontinuous (first order).

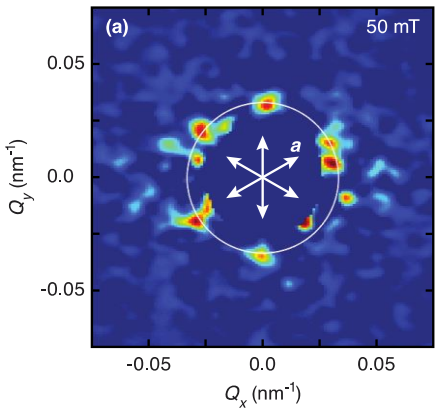

Fig. 4 VL diffraction pattern obtained on CsV_3Sb_5 at 50 mT and 35 mK. Arrows indicate the crystal-line *a*-axes, and the circle shows the magnitude of the scattering vector expected for a triangular VL.

Exploratory VL studies in CsV_3Sb_5. Superconductivity in the V-based materials AV_3Sb_5 (A = K, Rb, Cs) have attracted great attention since the initial discovery by Ortiz *et al*. [1]. These materials represent a rare example of an intrinsically superconducting layered kagome metal, and the additional discovery that CsV_3Sb_5 is a topologically nontrivial $\mathbb{Z}_2$ metal makes unconventional superconductivity in these materials likely [1]. We performed an exploratory SANS experiment on this material to determine if VL studies are feasible. As shown in Fig. 4, scattering from the VL is visible although very faint. This is as expected in a material with a long penetration depth, which we estimate as $\lambda \sim 600$ nm from our measurements.

Molecular dynamics simulations of particle-based systems with anisotropic interactions. Both skyrmions and vortices exist within materials which invariable possess a degree of anisotropy. This gives rise to an alignment of the SkL or VL relative to the crystalline axes of the host, and can result in domain formation, as seen in MgB_2 [6] and UPt_3 [8]. To properly model such systems we have, as the first, implemented anisotropic interactions in MD simulations to provide information about individual skyrmions/vortices in real space as a complement to our SANS studies [9]. In contract to simulations with isotropic interactions, dislocations and defects emerge spontaneously in our studies, either in isolation or stringed together in domain walls as shown in Fig. 5.

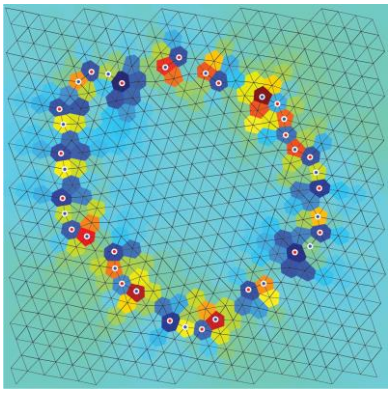

Fig. 5 VL grain boundary observed by MD. For simplicity, only five- and sevenfold coordinated vortices along with their sixfold coordinated neighbors are shown. The vortices are overlaid on a heatmap indicating their relative energy.

Future Plans

Skyrmion manipulation in conducting and insulating chiral magnets. The SkL studies under the influence of a radial current in MnSi will be continued. These will include high precision measurements, both in terms of the current and the location within the sample. In the initial data, a distinct azimuthal broadening of the Bragg peaks was observed as electric current was increased, indicating that the SkL breaks into domains. Measurements on a smaller region of the sample will reduce this effect, greatly simplifying the modeling and interpretation of the data. Furthermore, measurements along the radial direction will also be carried out as both Magnus and drag forces will decay with distance from the center.

To complement the studies under the influence of both an electrical and thermal current, measurements will also be carried out on the insulating skyrmion-hosting material Cu_2OSeO_3. This will allow studies under the influence of a purely thermal current.

Spatially resolved SANS measurements. This is both related to the SkL measurements discussed above, and for the study of VL domain formation in MgB_2. In the latter we have studied metastable VL phases and demonstrated a new kind of collective vortex behavior governed by nucleation and growth of equilibrium VL domains rather than conventional vortex pinning [10]. We will also complete studies of VL metastability and transition kinetics in this material, with the magnetic field has rotated away from the *c*-axis to render the transition discontinuous.

SANS studies under strain. Strain has emerged as a powerful method for manipulating the Fermi surface of materials and thereby their electronic properties. A prominent example is Sr_2RuO_4 where recent μSR measurements showed a splitting between the superconducting critical temperature and the onset of time-reversal symmetry breaking [11]. We have performed initial SANS experiments on in niobium which clearly showed that the VL in niobium is affected by strain, and that it can thus be used to explore the effects on the superconducting state. These measurements will be continued.

Molecular dynamics simulations of skyrmions and vortices. MD simulations will continue, carried out by Notre Dame undergraduate students. We are currently the only group to perform such studies for systems with anisotropic interactions, necessary to model real materials. This presents us with a vast range of interesting problems for skyrmions, vortices and beyond. Currently simulations are underway to study VL transitions between metastable and equilibrium states as well as the formation of smectic phases in systems with a two-fold anisotropy.

References

1. A. W. D. Leishman *et al*., Phys. Rev. B **103**, 094516 (2021).
2. F. Jonietz *et al*., Science **330**, 1648–1651 (2010)
3. X. Yu *et al*., Nat. Commun. **12**, 5079 (2021).
4. K. E. Avers *et al*., arXiv:2103.09843.
5. E. R. Louden *et al*., Phys. Rev. B **99**, 060502(R) (2019); *ibid* **99**, 144515 (2019).
6. A. W. D. Leishman *et al*., Phys. Rev. B **103**, 094516 (2021).
7. B. R. Ortiz *et al*., Phys. Rev. Lett. **125**, 247002 (2020).
8. K. E. Avers *et al*., Nat. Phys. **16**, 531-535 (2020).
9. M. W. Olszewski *et al*., New. J. Phys. **20**, 023005 (2018); Phys. Rev. B **101**, 224504 (2020).
10. E. R. Louden *et al*., New J. Phys. **21**, 063003 (2019).
11. V. Grinenko *et al*., Nat. Phys. **17**, 748-754 (2021).

Publications

1. K. E. Avers, W. J. Gannon, S. J. Kuhn, W. P. Halperin, J. A. Sauls, L. DeBeer-Schmitt, C. D. Dewhurst, J. Gavilano, G. Nagy, U. Gasser, and M. R. Eskildsen, *Broken time-reversal symmetry in the topological superconductor UPt_3*, Nat. Phys. **16**, 531-535 (2020).
2. M. W. Olszewski, M. R. Eskildsen, C. Reichhardt, and C. J. O. Reichhardt, *Rotational transition, dislocations and domain formation in vortex systems with combined sixfold and twelve anisotropic interactions*, Phys. Rev. B **101**, 224504 (2020).
3. A. W. D. Leishman, R. M. Menezes, G. Longbons, E. D. Bauer, M. Janoschek, D. Honecker, L. DeBeer-Schmitt, J. S. White, A. Sokolova, M. V. Milošević, and M. R. Eskildsen, *Topological energy barrier for skyrmion lattice formation in MnSi*, Phys. Rev. B **102**, 104416 (2020).
4. A. W. D. Leishman, A. Sokolova, M. Bleuel, N. D. Zhigadlo, and M. R. Eskildsen, *Field-angle dependent vortex lattice phase diagram in MgB_2*, Phys. Rev. B **103**, 094516 (2021).
5. K. E. Avers, S. J. Kuhn, A. W. D. Leishman, L. DeBeer-Schmitt, C. D. Dewhurst, D. Honecker, R. Cubitt, W. P. Halperin and M. R. Eskildsen, *Reversible ordering and disordering of the vortex lattice in UPt_3*, arXiv:2103.09843.

Probing Short-Range Structure and Magnetism in Next-Generation Energy Conversion Materials

Benjamin Frandsen, Department of Physics and Astronomy, Brigham Young University

Program Scope

This project employs advanced neutron scattering methods and other complementary techniques to study three classes of materials with significant technological potential for energy conversion applications: magnetic thermoelectrics, magnetocalorics, and multiferroics. Given that the properties of functional materials often depend sensitively on the details of *local* structural and magnetic correlations, i.e. correlations that are well defined on length scales up to several unit cells but that average to zero on longer length scales, we utilize atomic and magnetic pair distribution function (PDF) analysis of neutron scattering data. The PDF data reveal the local pairwise correlations directly in real space, providing an intuitive view of the relevant short-range correlations and allowing for quantitative refinements of models of the local structure. In addition to atomic and magnetic PDF analysis of neutron scattering data, we also utilize inelastic neutron scattering, x-ray total scattering, and muon spin relaxation (μSR) experiments to gain a comprehensive understanding of the local structure and dynamics of relevant materials.

Specific material systems under investigation include MnTe and related antiferromagnetic semiconductors for potential thermoelectric applications, Mn-based ferromagnets such as $(Mn,Fe)_2(P,Si)$ for exhibiting large magnetocaloric responses, and representative multiferroics such as $(Sr,Ba)MnO_3$ and hexagonal rare-earth manganites. In addition to establishing the influence of local atomic and magnetic correlations in these materials on their technologically relevant properties, this project aims to develop magnetic PDF methods further, from new experimental approaches (e.g. with polarized neutrons) to user-friendly software infrastructure with novel data visualization and modeling capabilities.

Recent Progress

MnTe: The hexagonal antiferromagnetic semiconductor MnTe is a potential high-performance thermoelectric material when doped with small amounts of Li or Na [1]. Remarkably, short-range magnetic correlations that persist above the Neel temperature (T_N = 307 K) appear to play a key role in enhancing the thermoelectric figure of merit zT through a phenomenon known as paramagnon drag [2]. A major focus of this project has been to study the nature of these short-range magnetic correlations using magnetic PDF methods. We have performed several neutron scattering experiments on this material, including comprehensive atomic and magnetic PDF measurements on powder samples of pure MnTe and Na-doped MnTe on the NOMAD

instrument, single-crystal neutron diffraction experiments on CORELLI for three-dimensional magnetic PDF (3D-mPDF), and inelastic neutron scattering on ARCS. We have also conducted x-ray PDF and μSR experiments on MnTe. The powder and single-crystal magnetic PDF results have revealed robust antiferromagnetic correlations on the nanometer scale that persist up to at least 500 K. As seen in Fig. 1, these short-range correlations are spatially anisotropic, with a significantly longer correlation length along the *c* axis than within the *ab* plane. The x-ray PDF experiments have revealed an unusually large and anisotropic spontaneous magnetostriction across the Neel transition, along with a very localized distortion of nearest neighbor Mn-Te pairs that is still under investigation. The μSR results are fairly blind to the short-range magnetic correlations at high temperature, indicating they are mostly dynamical correlations on a time scale that is too fast for muons. However, an unexpected low-temperature dynamical feature is evident around 80 K in the μSR data but does not show up in the ARCS data, suggesting the characteristic energy scale is too small for ARCS. Work to understand these details is ongoing.

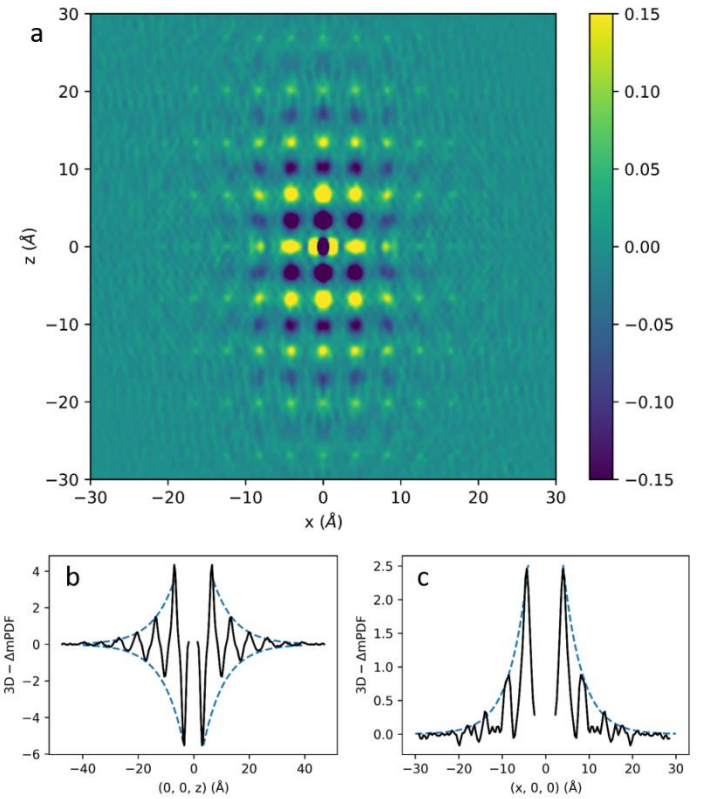

Fig. 1. Three-dimensional magnetic PDF results on MnTe at 340 K. (a) Slice in the *xz* plane showing antiferromagnetic correlations along *z* and ferromagnetic correlations along *x*. (b, c) Line cuts through the data showing the significantly longer correlation length along *z* than within the *xy* plane.

(Sr,Ba)MnO_3: We have performed neutron and x-ray PDF experiments on four compositions of the multiferroic system (Sr,Ba)MnO_3, which exhibits systematic changes in the ferroelectric transition temperature and the Neel ordering temperature as a function of Ba content [3]. We have also performed μSR experiments on two of these samples. The PDF analysis reveals a local enhancement of the ferroelectric distortion that persists over ~2 nm both above and below the ferroelectric transition, suggesting an order-disorder transition mechanism in this material (see Fig. 2). This also suggests that the average ferroelectric moment is not fully saturated and could potentially be increased further if the locally enhanced distortion could be transferred into the long-range structure. We are currently investigating how the magnetic dynamics revealed by μSR relates to the observed properties of the local structure.

Technique Development: We have recently conducted polarized neutron scattering measurements of MnTe on HYSPEC with the intent of performing high-resolution magnetic PDF analysis on the data. Polarization analysis allows us to cleanly separate the magnetic scattering from the nuclear scattering, and characteristics of HYSPEC provide meaningful data up to 6 $Å^{-1}$, sufficient for Fourier transformation into real space to yield the magnetic PDF. With the magnetic scattering successfully isolated, we can generate a higher resolution magnetic PDF pattern by applying additional normalizations that are not possible when the magnetic scattering is mixed in with the nuclear scattering. We are currently developing best practices for obtaining this higher resolution magnetic PDF pattern. We are also actively developing open-source software capabilities for magnetic PDF analysis. We have written code to generate 3D-mPDF patterns from magnetic models, developed more effective algorithms for combined atomic and magnetic PDF fits, introduced a hybrid small-box/big-box modeling approach for complex magnetic correlations, and started developing a graphical user interface for magnetic PDF analysis.

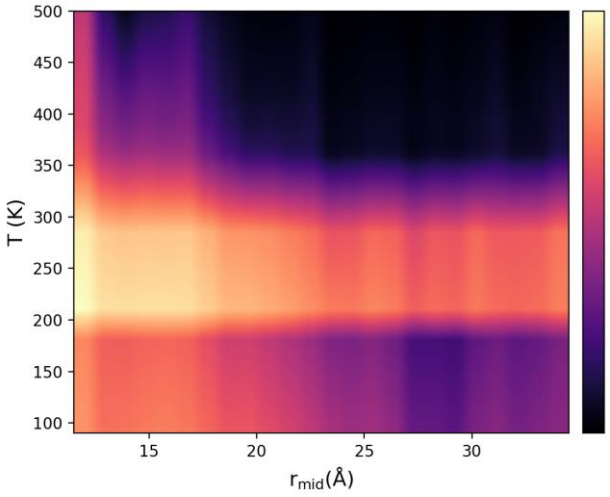

Fig. 2. Magnitude of the ferroelectric distortion in $Sr_{0.45}Ba_{0.55}MnO_3$ as revealed by PDF boxcar fits as a function of temperature. The horizontal axis is the midpoint of the fitting range for the refinement.

Future Plans

Having successfully characterized the short-range magnetic correlations that enhance the thermoelectric properties of MnTe, we plan to perform similar magnetic PDF investigations of related compounds, including the MnSb-CrSb solid solution and the classic antiferromagnet MnF_2. The MnSb-CrSb solid solution is intriguing because it switches from ferromagnetic (MnSb) to antiferromagnetic (CrSb) while maintaining the same hexagonal structure, and it has also been shown to exhibit paramagnon drag [4]. MnSb has also been identified for potential magnetocaloric applications. MnF_2 will allow us to revisit a classic antiferromagnet using modern characterization techniques that are especially well suited for short-range correlations, providing fresh insight into the conditions that give rise to robust short-range magnetism such as those resulting in paramagnon drag in MnTe.

The observation of significant local enhancement of the ferroelectric distortion in (Sr,Ba)MnO_3 invites investigation of other multiferroic systems. We plan to study the classic Type-I multiferroics of the hexagonal rare-earth manganite family *R*MnO_3. We will begin with neutron and x-ray PDF studies of powder samples, followed by a polarized neutron study on HYSPEC to perform detailed magnetic PDF analysis. The goal is to determine how short-range atomic and

magnetic correlations interact with each other and influence the intertwined magnetoelectric phases in multiferroic materials.

We also plan to study the giant magnetocaloric system $(Mn,Fe)_2(P,Si)$ using atomic and magnetic PDF analysis. The objective is to determine how the local structure dictates the behavior across the first-order magnetostructural/magnetoelastic transitions in this system. Initial efforts to study this system have been on hold due to Covid-related delays, but we hope this will be resolved soon.

References

[1] Y. Xu et al, "Performance optimization and single parabolic band behavior of thermoelectric MnTe", *J. Mater. Chem. A* **5** 19143 (2017).
[2] Y. Zheng et al, "Paramagnon drag in the high thermoelectric figure of merit Li-doped MnTe", *Sci. Adv.* **5** eaat9461 (2019).
[3] Kamal Chapagain et al., "Tunable multiferroic order parameters in $Sr_{1-x}Ba_xMn_{1-y}Ti_yO_3$." *Phys. Rev. Materials* **3**, 084401 (2019).
[4] Polash et al., "Magnon-drag thermopower in antiferromagnets versus ferromagnets." *J. Mater. Chem. C* **8**, 4049-4057 (2020).

Publications

1. Zhiling Dun, Marcus Daum, Raju Baral, Henry E. Fischer, Huibo Cao, Yaohua Liu, Matthew B. Stone, Jose A. Rodriguez-Rivera, Eun Sang Choi, Qing Huang, Haidong Zhou, Martin Mourigal, and Benjamin A. Frandsen. "Neutron scattering investigation of proposed Kosterlitz-Thouless transitions in the triangular-lattice Ising antiferromagnet $TmMgGaO_4$". *Phys. Rev. B* **103**, 064424 (2021)

2. Pietro Bonfa, Muhammad Maikudi Isah, Benjamin A. Frandsen, Ethan J. Gibson, Ekkes Brück, Ifeanyi John Onuorah, Roberto De Renzi, and Giuseppe Allodi. "*Ab initio* modeling and experimental investigation of Fe_2P by DFT and spin spectroscopies". *Phys. Rev. Mater.* **5**, 044411 (2021).

3. Ethan R. A. Fletcher, Kentaro Higashi, Yoav Kalcheim, Hiroshi Kageyama, and Benjamin A. Frandsen. "Uniform structural phase transition in V_2O_3 without short-range distortions of the local structure". In press at *Physical Review B*.

Inelastic Neutron Scattering Studies of Quantum Anharmonicity and Nonlinear Phonons

Brent Fultz, Dept. Applied Physics and Materials Science, California Institute of Technology, Pasadena, CA 91125

Program Scope

Entropy is the central concept of thermodynamics, a subject that underlies the structure and properties of materials. Atom vibrations are the primary source of entropy in materials, and inelastic neutron scattering (INS) can measure the vibrational modes in detail. We use INS to understand the main part of the entropy of phase transitions and thermophysical properties of materials.

In crystals at high temperatures, the normal modes of vibration begin to interact with each other and lose independence. This is "anharmonicity," which alters, and can dominate, the thermo-physical properties of thermal expansion, thermal conductivity, and the temperature dependence of elastic constants. Some of these anharmonic effects that be best understood with the efficient inelastic neutron instruments at the SNS.

Many-body theory, as developed with perturbation theory [1], is useful for analyzing phonon shifts and lifetimes for small departures from harmonic behavior, but modern computational methods are applicable to large anharmonicities, and give the vibrational spectra that can be compared to INS data. Our focus is on anharmonic effects that require approaches beyond many-body theory. Some can be measured only with the instruments at the SNS. Here ideas from the fields of quantum optics and nonlinear dynamics help interpret strong anharmonicity in materials, making phonon physics a richer field.

Recent Progress

With single crystal methods for chopper spectrometers such as ARCS, it is possible to measure simultaneously the energies and lineshapes of numerous phonons. We are exploiting this new opportunity to analyze all phonons in the first Brillouin zone that account for thermophysical properties such as thermal expansion or the temperature dependence of elastic constants. We have found some unexpected results in the origin of thermophysical properties from phonon physics, such as persistent failures of the popular quasiharmonic approximation to predict thermal trends of measured phonons. Weak effects that were beneath the "noise" in the past are appearing now, sometime giving fundamental surprises. We have discovered three new types of nonlinear vibrations in crystals of NaBr and Cu_2O.

The first is the generation of a pair of "intermodulation phonon sidebands" from strong anharmonic interactions of two phonon modes. (These sidebands are conceptually similar to intermodulation distortion in nonlinear amplifiers.) In a crystal of NaBr, the lower sideband is an intrinsic localized mode (ILM), which was observed previously by Mike Manley. Our finding of a partner upper sideband completes the picture, and allows a new explanation of the shapes and intensities of phonon intermodulation sidebands by adapting the theory of sidebands from the input-output theory of quantum optics [2]. The sideband excitations may be new quasiparticles like those from the coupling between a laser and a mode of vibration of a cavity. We replaced the noiseless laser with a thermally excited phonon, and solved the Heisenberg-Langevin equations of motion to obtain susceptibility functions for inelastic neutron scattering. The spectral weight was in good agreement with the experimental intensities, as shown in Fig. 1.

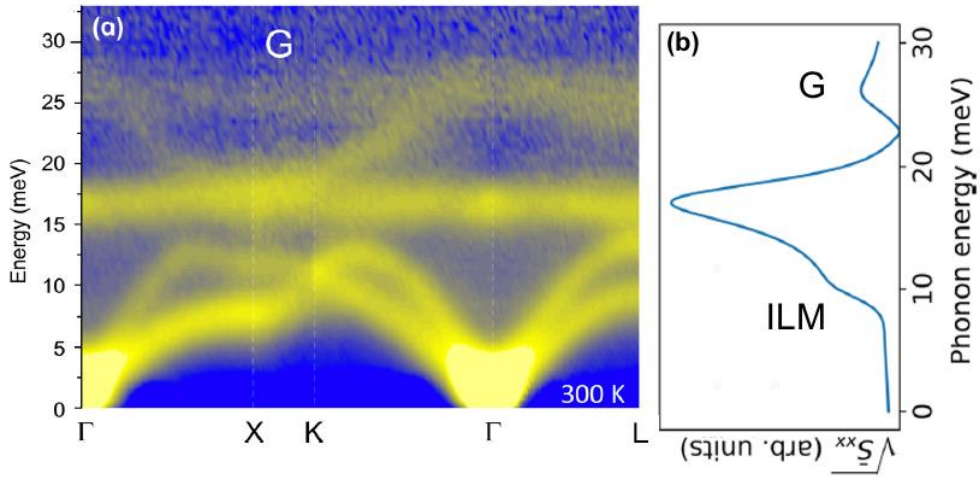

Fig. 1. (a) Experimental phonon dispersions from ARCS at 300 K, 50 meV incident energy. Data were corrected for multiphonon scattering, background, and folded into first Brillouin zone.
(b) Intensity calculated with input-output theory [2] for two anharmonic phonons TA and TO in the medium coupling regime, assumed dispersionless.

We found another new nonlinear behavior in a single crystal of cuprite, Cu_2O. Its phonon dispersions are crisp and clear at 10 K, but Fig. 2 shows a broad, diffuse inelastic intensity at 300 K, and at 700 K there are no longer distinct dispersions, only the diffuse inelastic intensity. Our interpretation is evolving, but it has been possible to obtain some of this diffuse intensity in molecular dynamics simulations. Our picture is that for the most part, the oxygen and copper atoms vibrate independently. The mean frequency for O atoms is 6 times higher than Cu. Nevertheless, with movement of the Cu atoms around an O atom, the O atom oscillations are disturbed. The O atoms undergo shifts in the phase of their oscillation cycles that occur at approximately the frequency of Cu atom vibrations. This "phase noise" has a time-time correlation function that gives a diffuse inelastic intensity as shown at the top of Fig. 2. Small changes in the phase uncertainty spread, γ, give a wide range of spectral shapes, as shown in the top figure.

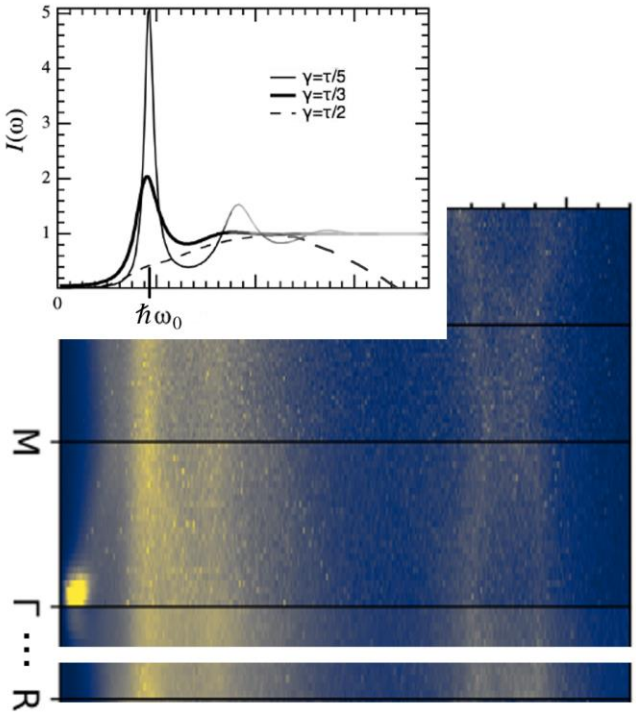

Fig. 2. Top: Shapes of intensity profiles for flat dispersions altered by a "phase noise" in oxygen atom oscillations, caused by copper atom oscillations at ω_0. Bottom: experimental phonon dispersions from cuprite at 300 K.

Future Plans

After we better understand the highly nonlinear phonon effects in cuprite and NaBr, our plan is to identify such effects in other crystals. An efficient approach may be to perform INS on powders, and identify high-energy upper intermodulation sidebands in the phonon density of states. Particular emphasis will be on (electronically) nonlinear optical materials that might be able to encode phonon information after light scattering.

The nature of the intermodulation phonon sidebands is being investigated with a colleague at Caltech who has developed an ultrafast pump-probe infrared laser system. The experiment will test how long the energy resides in the sideband before it decays. If there is a reasonable lifetime for sideband excitations, they may be treated as quasiparticles for purposes of thermal physics.

Finally, we are working to identifying phonon contributions to the latent heat of the glass transition [3]. Results on a Pt-based metallic glass are nearly complete.

References

[1] A.A. Maradudin and A.E. Fein, "Scattering of Neutrons by an Anharmonic Crystal," Phys. Rev. 128, 2589 (1962).

[2] C.W. Gardiner and M.J. Collett, "Input and Output in Damped Quantum-Systems -- Quantum Stochastic Differential-Equations and the Master Equation," Phys. Rev. A 31, 3761 (1985).

[3] H.L. Smith, et al., "Separating the Configurational and Vibrational Entropy Contributions in Metallic Glasses," Nature Physics 13, 900 (2017).

Publications

Y. Shen, C.N. Saunders, C.M. Bernal, D.L. Abernathy, M.E. Manley, B. Fultz, "The Anharmonic Origin of the Large Thermal Expansion of NaBr," Phys. Rev. Lett. 125, 085504 (2020). DOI: 10.1103/PhysRevLett.125.085504.

Fred C-R. Yang, O. Hellman, and B. Fultz, "Temperature dependence of electron-phonon interactions in vanadium," Phys. Rev. B, 101, 094305 (2020).

J.E. Herriman and B. Fultz, "Phonon thermodynamics and elastic behavior of GaAs at high temperatures and pressures," Phys. Rev. B 101, 214108 (2020).

S.H. Lohaus, M.B. Johnson, P.F. Ahnn, C.N. Saunders, H.L. Smith, M.A. White and B. Fultz, "Thermodynamic stability and contributions to the Gibbs free energy of nanocrystalline Ni_3Fe," Phys. Rev. Mater 4, 086002 (2020).

D.S. Kim, O. Hellman, N. Shulumba, C.N. Saunders, J.Y.Y. Lin, H.L. Smith, J.E. Herriman, J.L. Niedziela, D.L. Abernathy, C.W. Li, and B. Fultz, "Temperature-dependent phonon lifetimes and thermal conductivity of silicon by inelastic neutron scattering and ab initio calculations," Phys. Rev. B 102, 174311 (2020).

Y. Shen, C.N. Saunders, C.M. Bernal, D.L. Abernathy, M.E. Manley, and B. Fultz, "Quantum anharmonicity and intermodulation phonon sidebands in NaBr," Phys. Rev. B 103, 134302 (2021). DOI: 10.1103/PhysRevB.103.134302.

C.N. Saunders, D.S. Kim, O. Hellman, H.L. Smith, C.M. Bernal, N.J. Weadock, S.T. Omelchenko, G.E. Granroth, D.L. Abernathy, and B. Fultz, "Anharmonic Phonons in Cu_2O and Thermal Expansion: A Computational and Experimental Study" Phys. Rev. B, submitted.

Jane Elizabeth Herriman, “Phonon thermodynamics and elastic behavior of GaN and GaAs at high temperatures and pressures,” Ph.D. thesis in Materials Science, Feb. 14, 2020. presently: Lawrence Livermore National Laboratory.

Yang Shen, “Phonon Anharmonicity at the Limits of Perturbation Theory,” Ph.D. thesis in Applied Physics, May 27, 2020.

Exotic Uses of Neutrons and X-rays as Probes for Chiral Magnets

Dustin A. Gilbert, Materials Science and Engineering, University of Tennessee, Knoxville

Program Scope

The current program proposes to use neutron and X-rays in creative ways to investigate chiral and non-colinear magnetic materials. The scope includes fabricating thin-films and heterostructures and performing magnetic, electronic and high-frequency measurements in our lab. Informed by these measurements, appropriate neutron and X-ray experiment are designed to investigate specific details of these systems. These measurements include polarized neutron reflectometry (PNR) to access magnetic structures at interfaces, and small angle neutron scattering (SANS) to identify mesoscopic structures. In both cases, the novelty of the measurement is a product of the experimental design and the use of unique sample environments. The current proposal included several projects: high-frequency skyrmion dynamics probed with SANS,[1] low-frequency skyrmion lattice formation[2] probed with tine-resolved TSANS, 3D structure of magnetic skyrmions[3] probed with grazing-incidence GISANS, measuring *in-situ* skyrmion kinetics[4] with SANS, commensurate-locking of skyrmions with superconductors[5] with GISANS or off-specular PNR, and imprint antiferromagnetic skyrmions[6] by proximity effects.

Recent Progress

The unforeseen shutdown of HFIR and then NCNR – which is still shut down until April 2022 – and the pandemic shuttering many other user facilities, has had the potentially to significantly impact the proposed projects. Part of the project, for example, was supposed to station a student at NCNR for a year, but this is currently in jeopardy. However, we have made some progress on many of these projects and they are all moving forward in some way.

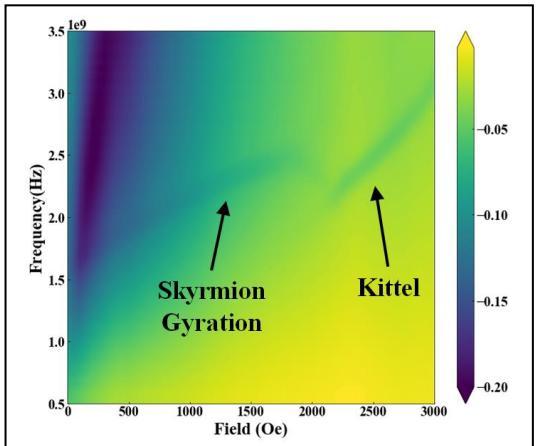

Figure 1 2D FMR data showing the skyrmion gyration mode and saturated Kittel resonance

The high-frequency dynamics in-particular has been very successful. This experiment was performed on dipole-stabilized hybrid skyrmions in Gd/Fe multilayers.[7] These films were made by our collaborators E.E. Fullerton and S. Montoya. These structures are comprised of three stacked skyrmions, with Néel-type skyrmions at the film surfaces and Bloch-type skyrmions in the middle of the film thickness. We used a ferromagnetic resonance (FMR) setup to apply an in-plane RF field, and out-of-plane static field; the FMR system was designed and built within our lab to fit into a PPMS as part of this project. This configuration excites the skyrmion gyration mode. The 2D FMR data is shown in Figure 1, with the skyrmion gyration mode and saturated Kittel mode clearly resolved. We then took this system to NCNR and prepared the same setup on VSANS: an in-plane RF field, and out-of-plane static field, with the neutron beam along the static (out-of-plane) direction. To our knowledge, this is the only system to have seen the characteristic 6-fold skyrmion diffraction pattern in thin-films with SANS, and again we were successful. VSANS or GPSANS is necessary because the skyrmions in these

systems are very large (210 nm periodicity; q=0.003 $Å^{-1}$). Initial considerations would suggest that the signal should not change, that simple translations of the skyrmion lattice under periodic gyration would be removed in the Fourier transform. However, it was observed that, approaching resonance, the background and low-q scattering increases significantly, and wanes at frequencies above the resonance. The experiment was also performed fixing the frequency and increasing the magnetic field, again passing through resonance. This became a highly-charged result because the total scattering increased by >5× at resonance, which our team could not explain. We repeated the experiment at GPSANS, and had similar results, shown in Figure 2. With the GPSANS data, the additional scattering could be modeled by an exponential decay function, and in doing so, it is revealed that the signal from the skyrmion-derived hexagonal pattern does not change. Since most scattering follows a power-law like fall-off, we propose that this is not traditional scattering. Our current theory is that this is inelastic scattering between the neutron and moving skyrmion. What makes this possible is that the measurements were performed with long wavelengths (14 Å) and so were moving very slowly – comparable to the speed of the skyrmion. One could consider a thermodynamic argument about the probability of a transiting neutron absorbing a small amount of energy as it passes through the film. We are currently working on completing this argument and will publish soon. These results may present an opportunity for new SANS measurement capabilities of other high-frequency systems.

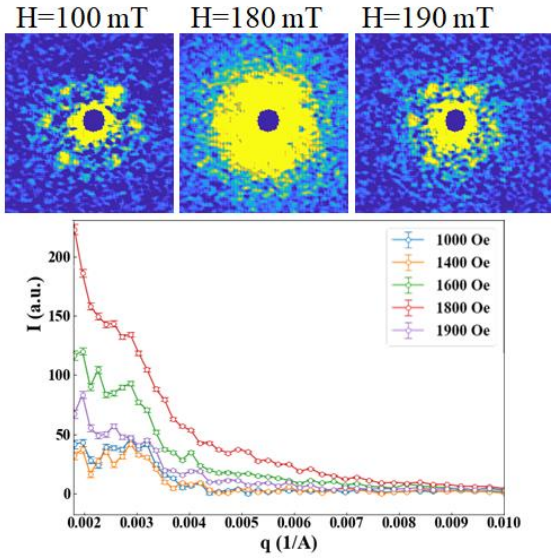

Figure 2 2D SANS data (left) below, (center) at, and (right) above the resonant condition. Data is shown on the same scale. (below) Intensity versus q plots of the 2D data.

We have also had good success performing GISANS on our skyrmion films, with the target of resolving the 3D structure. These measurements were again performed on Gd/Fe thin-films hosing hybrid skyrmions. Preliminary specular measurements were performed at NCNR on the MAGIK reflectometer by Lizabeth Quigley, who was a SURF student at the time, and is now in a Ph.D. program at Purdue. The PNR results were expected to show nothing, since the depth-resolved average of the magnetic moment in a skyrmion is zero. However, features were observed, with a net magnetization throughout the thickness, with increased magnetization at the surfaces. We can attribute these features to two factors: (1) the measurements were performed with an out-of-plane magnetic field, meaning all magnetic scattering contributes together in the spin-flip channel, and (2) the neutron coherence length covers a relatively small number of skyrmions. As a result of these factors, a net magnetization is captured in the diffraction pattern. A measurement was also taken at saturation. The PNR results were fitted with Refl1D, providing the

magnetic and nuclear scattering length density (SLD) profile. Next, transmission and GISANS measurements were performed on the same sample on the VSANS instrument, and later on GPSANS (ORNL). Transmission SANS measurements confirmed the hexagonal skyrmion ordering. The GISANS measurements, shown in Figure 3, include the specular peak and flanking off-specular peaks, from the in-plane skyrmion lattice. Note again, this is data from a single thin-film, ≈100 nm thick. Measuring the intensity-versus sample angle traces a path through (q_x, q_z) space which simultaneously encodes the in-plane and out-of-plane structure. To analyze the data, a micromagnetic model was generated using the results from the PNR measurements. This model generates a magnetic skyrmion lattice representative of our experimental system and grounded in the relavent underlying physics. Using a custom Born-approximation Python code, the GISANS pattern is tabulated and compared to the experimental results. By iteratively changing the model parameters and comparing to the experimental results, we arrive at a 3D structure which accurately reproduces the experimental results. We are currently writing this up and will publish the results soon. The 3D structure of hybrid skyrmions is critical to understanding their robust stability. This was the first GISANS experiment on GPSANS, and one of the few GISANS measurements performed on a magnetic system. The Python code developed in this project has subsequently been used to interpret the SANS results from other magnetic systems.

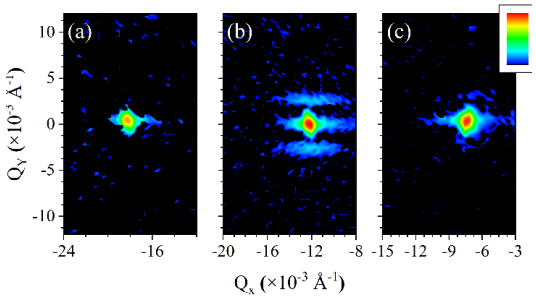

Figure 3 GISANS data from (a) the saturated state, (b) strip state, (c) skyrmion state.

Progress has also been made on the lattice formation dynamics experiment. In these experiments, transmission SANS measurements were made on bulk B20 materials as the applied magnetic field is changed in a stepwise manner. The field step changes the system from the skyrmion stability regime to the conical or helical state, and back. Using the time-resolving feature, the diffraction-pattern is measured as the skyrmion lattice is generated or destroyed. On NG7SANS, this feature is developed and provided promising data, showing that it takes several 10's of milliseconds to create or destroy the lattice. This result was exciting because magnetic dynamics is typically much faster than this (typically nanoseconds). However, this data faced an issue that the magnetic field was poorly defined due to slow changes in the ferrous cores of the electromagnet. We designed and fabricated a pair of water-cooled Helmholtz coils which were designed to fit into MAG-H at GPSANS. The experiment was repeated and appears to show comparable results. Current efforts are underway to apply the time-parsing functionality of the GPSANS data.

Part of our program included performing these measurements on B20 materials. We have recently been working to prepare thin-films of these B20 materials. First, using molecular beam epitaxy (MBE) we are able to heat our Si(111) substrates, achieving the 7x7 surface reconstruction necessary to prepare the B20 structure. The Mn source is prepared and we recently were able to evaporate Si from the e-beam evaporator source. We view this progress as getting close. We also

recently received a DOE surplus sputtering source, specific for preparing oxides. The system was re-assembled and tested, generating an RF plasma in the magnetron sputtering source. Current plans are to prepare a Cu_2O+SeO_3 sintered/pressed composite target and grow Cu_2OSeO_3 skyrmion films.

With NCNR being down, HFIR being consequentially oversubscribed, and the pandemic blanketing everything, the supported students had the opportunity to contribute to other projects, particularly on non-colinear magnetic systems. These have included the magnetism in bilayer films with orthogonal coupling using PNR, magnetism and magnetic dynamics in alloyed and phase separated magnetic nanoparticles, antiferromagnetism in alloys of immiscible FM/noble metal systems, magnetostriction in CoTb systems and PDF measurements of high-entropy oxides.

Future Plans

We have current efforts to prepare the (Gd/Fe)/Nb system to demonstrate skyrmion/vortex locking. Our preliminary measurements on this system with full-scale films yielded no identifiable coupling. After discussion with collaborators who have worked on similar coupled-vortex systems, we concluded that the system needed to be patterned to a dogbone structure, increasing the current density. As noted above, we are also on the cusp of preparing B20 MnSi and Cu_2OSeO_3 by MBE and sputtering, respectively. Once these films are prepared, FMR measurements will be performed to identify the resonance, then we will perform the SANS and GISANS measurements, elucidating the role of DMI in determining the dynamics and structure.

References

[1] R. Tomasello, L. Sánchez-Tejerina, M. Carpentieri. 7 - Dynamics of magnetic skyrmions. In: *Magnetic Skyrmions and Their Applications*. Woodhead Publishing (2021).

[2] L. J. Bannenberg, F. Qian, R. M. Dalgliesh, N. Martin, G. Chaboussant, M. Schmidt, D. L. Schlagel, T. A. Lograsso, H. Wilhelm, C. Pappas. Reorientations, relaxations, metastabilities, and multidomains of skyrmion lattices. *Physical Review B* **96**, 184416 (2017).

[3] H. S. Park, X. Yu, S. Aizawa, T. Tanigaki, T. Akashi, Y. Takahashi, T. Matsuda, N. Kanazawa, Y. Onose, D. Shindo, A. Tonomura, Y. Tokura. Observation of the magnetic flux and three-dimensional structure of skyrmion lattices by electron holography. *Nature Nanotechnology* **9**, 337-342 (2014).

[4] A. Fert, V. Cros, J. Sampaio. Skyrmions on the track. *Nature Nanotechnology* **8**, 152-156 (2013).

[5] A. Gomez, D. A. Gilbert, E. M. Gonzalez, K. Liu, J. L. Vicent. Control of dissipation in superconducting films by magnetic stray fields. *Applied Physics Letters* **102**, 052601 (2013).

[6] J. Wu, D. Carlton, J. S. Park, Y. Meng, E. Arenholz, A. Doran, A. T. Young, A. Scholl, C. Hwang, H. W. Zhao, J. Bokor, Z. Q. Qiu. Direct observation of imprinted antiferromagnetic vortex states in CoO/Fe/Ag(001) discs. *Nature Physics* **7**, 303-306 (2011).

[7] R. D. Desautels, L. Debeer-Schmitt, S. A. Montoya, J. A. Borchers, S.-G. Je, N. Tang, M.-Y. Im, M. R. Fitzsimmons, E. E. Fullerton, D. A. Gilbert. Realization of ordered magnetic skyrmions in thin films at ambient conditions. *Physical Review Materials* **3**, 104406 (2019).

Publications

1. Walker L. Boldman, David Garfinkel, Robyn Collette, Cameron S. Jorgenson, Dhiren K. Pradhan, Dustin A. Gilbert, Philip D. Rack "Exploring the composition and phase separation and structure of AgFe alloys for magneto-optical applications" *Materials Science & Engineering B* **266**, 115044 (2021)

2. Colin R. Rementer, Michelle E. Jamer, Dustin A. Gilbert, K. Fitzell, Julie A. Borchers, Brian J. Kirby, Gregory P. Carman, and Jane P. Chang, "Determining reversal mechanisms in FeGa/FeNi Heterostructures on Silicon" *Appl. Phys. Lett.* **118**, 212405 (2021).

3. Brandon Wilfong, WLNC Liyanage, Jared Naphy, Dustin A. Gilbert, Steve P. Bennett, and Michelle E. Jamer "Using methodical compositional tuning to optimize Co_xTb_{1-x} structural and magnetic properties" *Appl. Phys. Lett.* **118**, 212405 (2021).

4. Wolfgang Kreuzpaintner, Andreas Schmehl, Alexander Book, Thomas Mairoser, Jingfan Ye, Birgit Wiedemann, Sina Mayr, Jean-François Moulin, Jochen Stahn, Dustin A. Gilbert, Henrik Gabold, Zahra Inanloo-Maranloo, Michael Heigl, Sergey Masalovich, Robert Georgii, Manfred Albrecht, Jochen Mannhart, Peter Böni "Reflectometry with Polarized Neutrons on In Situ Grown Thin Films" *Physica Status Solidi B (2021).*

5. Dhiren K. Pradhan, Hari Sankar Mohanty, Shalini Kumari, Krishnamayee Bhoi, Nan Tang, Ravikant, M. M. Rahaman, Dillip K. Pradhan, Ashok Kumar, Dustin A. Gilbert, Philip D. Rack "Phase Transitions and Magnetoelectric Coupling in Cobalt doped $BaTiO_3$", *J. Mater. Chem. C* **9**, 12694 (2021).

6. Palani Raja Jothi, Namila Liyanage, Daniel Olds, Dustin Gilbert, and Katharine Page "Robust structure and frustrated magnetism in high entropy rare-earth zirconates" **In Press, Small**

7. David A. Garfinkel, Nan Tang, Grace Pakeltis, Reece Emory, Ilia N. Ivanov, Dustin A. Gilbert, Philip D. Rack "Magneto-Optical Properties of Au-Co Solid Solution and Phase Separated Thin Films and Nanoparticles" **Under Review**

8. Nan Tang, Sergio Montoya, W.L.N.C. Liyanage, Sheena Patel, Lizabeth J. Quigley, Alexander J. Grutter, Michael R. Fitzsimmons, Sunil Sinha, Julie A. Borchers, Eric Fullerton, Lisa Debeer-Schmitt, Dustin A. Gilbert "In-situ GHz Dynamics of Skyrmions Probed with SANS" **In Preparation**

University of Minnesota Center for Quantum Materials (CQM)

Turan Birol[1], Rafael Fernandes[2], Martin Greven (PI)[2], Bharat Jalan[1], Chris Leighton[1]

[1]Department of Chemical Engineering and Materials Science, University of Minnesota

[2]School of Physics and Astronomy, University of Minnesota

Program Scope

The University of Minnesota Center for Quantum Materials (CQM), founded in 2016, is comprised of an inter-disciplinary team of five faculty and more than a dozen Ph.D. students and post-docs. The team investigates the structural and electronic properties of select quantum materials, particularly complex oxides. These embody many of the most fundamental questions regarding quantum behavior of interacting electrons, and are relevant to important technologies, including data storage, spintronics, catalysis, and fuel cells. In these quantum materials, the interplay between electronic kinetic energy and interactions gives rise to myriad quantum states and complex phase diagrams, which can, in principle, be controlled. *The overarching CQM vision is to substantially advance the understanding of quantum electronic phases and phase transitions in these materials, thereby addressing multiple BES grand challenges. This is achieved through the synthesis of exceptional quality model materials in bulk and thin-film form, the application of cutting-edge neutron, x-ray, and other probes, the exploration of novel materials control paradigms, and tight coupling to first-principles and analytical theory.*

Recent Progress

Field-leading synthesis efforts, broad application of state-of-the-art neutron and x-ray techniques, and the pursuit of new opportunities such as elastic and plastic deformation control, have enabled significant recent CQM advances [1-45]. This has been accompanied by rapidly increasing synergy among the CQM investigators, despite COVID-19-related challenges, generating substantial increases in all aspects of center research output.

Examples of recent CQM progress – strain tuning and strain engineering. The high level of synergy within the CQM is exemplified by recent advances in strain-tuning and strain-engineering (Fig. 1), such as pioneering work on enhanced superconductivity and ferroelectricity in *plastically*-deformed strontium titanate [35]. This breakthrough result involves three senior CQM investigators (*Fernandes, Greven, Leighton*), state-of-the-art diffuse neutron and x-ray scattering at ORNL and ANL, and uniaxial pressure techniques, which induce novel self-organization of dislocation structures. A related recent example is the demonstration of strain-tuned Curie temperature, understood at a deep theoretical level, in rare-earth titanate crystals (*Birol, Fernandes, Greven*) [37]. Another example is the demonstration of strain-induced majority carrier inversion in heteroepitaxial thin films of ferromagnetic $LaCoO_3$, again involving three senior CQM investigators (*Birol, Greven, Leighton*) [2].

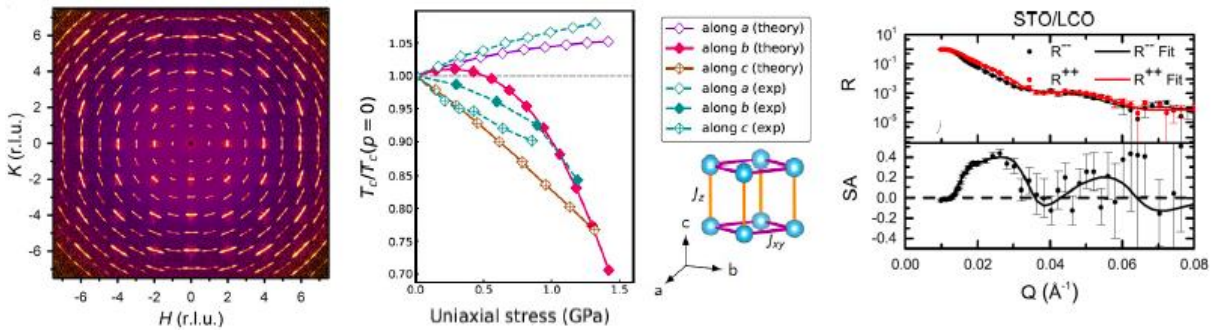

Figure 1: Left: Diffuse neutron scattering (CORELLI, SNS) for lightly-doped $SrTiO_3$, *plastically* deformed by 4.5% along [010]. The response is arc-like, with a fine pattern indicative of periodic dislocation walls, near which superconductivity and ferroelectricity are substantially enhanced [35]. Middle: Comparison of *elastic* stress dependence of Curie temperature of $YTiO_3$ from ac susceptibility with mean-field results from DFT [37]. Right: Neutron reflectivity (R) and spin asymmetry (SA) *vs* scattering vector at 5 K in a 30 kOe in-plane magnetic field for a 200-Å-thick $LaCoO_{3-\delta}$ film on $SrTiO_3$ (Polarized Beam Reflectometer, NCNR) [2].

Examples of recent CQM progress – rare-earth titanates. The rare-earth (RE) titanates $RETiO_3$ are a major CQM focus due to fascinating Mott-insulating states, non-trivial magnetic transitions/crossovers, and lattice/charge/spin/orbital coupling [6,16,22,26,27,37,39,42]. *Jalan* and *Greven* completed a study of $YTiO_3$ (YTO) films and crystals that revealed the role played by small polarons in this, and related Mott insulators [16], also obtaining fresh insight into the growth of La- and Ca-substituted YTO, and enabling the first inelastic neutron scattering (INS) measurements of spin-waves [42]. A comprehensive study by *Greven* and *Leighton* of La-substituted YTO ($Y_{1-x}La_xTiO_3$), including neutron diffraction, SANS, and XAS/XMCD, revealed that the ferromagnetic (FM) to antiferromagnetic (AF) transition is first-order, settling a long debate [26]. Detailed subsequent INS measurements of spin-wave spectra in $Y_{1-x}La_xTiO_3$ by *Greven* appear to defy theoretical predictions of changes in exchange across the FM-AFM transition. This motivated *Fernandes* to develop a model that considers a local distribution of exchange couplings induced by bond-disorder due to La-substitution, capturing experimental observations; a manuscript (*Fernandes* and *Greven*) is in preparation. Going beyond $Y_{1-x}La_xTiO_3$, and employing group theory, phenomenology, and first-principles calculations, *Fernandes* and *Birol* then developed a general model for the FM-AFM crossover as a function of RE radius [39], leading to a prediction of a possible quantum critical endpoint tuned by strain. *Greven* and *Birol* also completed a combined XAS, transport, and DFT+U study of the insulator-metal transition in $Y_{1-y}Ca_yTiO_3$ at $y \sim 0.35$ [27]; electronic phase separation into hole-rich metallic regions and hole-poor Mott-insulating regions was revealed. *Greven* is currently working on a comprehensive manuscript on neutron diffraction and muon spin rotation (with Y. Uemura, Columbia), revealing strong suppression of local ordered moments, with volume-wise phase separation into FM and paramagnetic phases at $y \sim 0.2$. This points to a first-order phase transition, highly complementary to the work by *Greven* and *Birol* [27]. As a whole, these efforts with $RETiO_3$ compounds have employed both bulk and film samples, multiple neutron methods combined with other probes, and have greatly advanced both experimental and theoretical understanding.

Examples of recent CQM progress – strontium titanate. In addition to the plastic deformation work described above [35] (Fig. 1), work on $SrTiO_3$ included a comprehensive analysis of the superconducting and transport properties of Nd-doped epitaxial thin films over a wide electron concentration range. Specifically, in a joint theoretical-experimental collaboration, *Jalan* and *Fernandes* showed [43] that the changes in the residual resistivity and superconducting transition temperature across the second Lifshitz transition agree with a model in which intra-band scattering dominates over inter-band scattering. This is in contrast to what is expected to occur at the first Lifshitz transition. This work also revealed direct manifestations of the antiferrodistortive transition on the behavior of the Hall carrier density. Related to the above, *Leighton* and *Jalan* completed a detailed study of structure-property relationships and mobility in the wide-gap oxide $BaSnO_3$, resulting in ~100 $cm^2V^{-1}s^{-1}$ room temperature mobility in *sputtered* films.

Examples of recent CQM progress – cobaltites. *Leighton*'s data on bulk perovskite cobaltites were interpreted in terms of a theoretical model previously developed by *Fernandes* in which magnetic *frustration* plays a key, previously unconsidered role in shaping the phase diagrams of these materials [40]. Magnetic frustration delays the onset of ferromagnetism relative to the percolation of spin-state polarons, resolving a troubling inconsistency in these model systems. As noted above, *Leighton*, *Greven* and *Birol* also extended their heteroepitaxial strain tuning of $LaCoO_3$ and $La_{1-x}Sr_xCoO_{3-\delta}$ films [2,14]. This included strain-tuning of the majority carrier type in $LaCoO_3$, revealing that the extraordinary ferromagnetism under tensile strain is intimately linked to *n*-type transport. Related efforts with $La_{1-x}Sr_xCoO_{3-\delta}$ led to the discovery of a giant form of anisotropic magnetoresistance [14], likely the largest reported in the 150-year history of this phenomenon in ferromagnets, driven by strain-induced oxygen vacancy ordering.

Examples of recent CQM progress – cuprates. *Greven* made considerable advances with cuprates [5,7,8,13,15,19,23,32,36,38], in part due to the nearly unique capability to grow high-quality crystals of the model system $HgBa_2CuO_{4+\delta}$. In collaboration with D. Reznik (U. Colorado), new insights into the phonon spectrum were obtained *via* INS (ARCS, SNS) and data mining of many Brillouin zones [5]. Inelastic x-ray scattering provided evidence of dynamic charge correlations at the superconducting pairing scale [7], whereas resonant x-ray diffraction and Raman scattering (with *Greven's* former student Y. Li, Peking U., China) revealed phonon anomalies for $HgBa_2CuO_{4+\delta}$ and double-layer $HgBa_2Cu_2CaO_{6+\delta}$, which precede the static charge correlations at low temperatures. This indicates that charge order is an emergent phenomenon. Detailed transport results for $HgBa_2CuO_{4+\delta}$ enabled an important test of a phenomenological model for the cuprates that *Greven* had previously developed [13] and led to new insight into the transport phase diagram [38]. Neutron (CORELLI, SNS) and x-ray (6-ID-D, APS) diffuse scattering (with R. Osborn, ANL) for two other cuprates revealed deep insight into unusual 'hidden' structural correlations and their connection with superconducting correlations [36]. Further results include collaborative photoemission work with I. Vishik (UC Davis) [15] and second-harmonic generation measurements with D. Hsieh (Caltech) [23].

Examples of recent CQM progress – ruthenates. *Fernandes* advanced the theoretical proposal that the debated experimental evidence for time-reversal-symmetry breaking in Sr_2RuO_4 is associated with extended defects (dislocations) [28]. In joint theory-experimental work, *Fernandes* demonstrated that the unusual emergence of superconductivity, observed by *Greven* in nonlinear magnetic response measurements of Sr_2RuO_4 (and other oxide superconductors), cannot be captured with a simple model of inhomogeneity, instead pointing to possible rare-region or phase fluctuation effects [30]. *Jalan* demonstrated growth of epitaxial RuO_2 films by a novel solid-source metal-organic MBE approach [34], paving the way for controlled synthesis of many other challenging complex oxides.

Examples of recent CQM progress – review papers and other projects. Important additional efforts include review papers on superconductivity in dilute $SrTiO_3$ (*Fernandes*) [3] and MBE of complex oxide semiconductors (*Jalan*) [33], in addition to various exploratory and collaborative projects. The latter encompass transition metal sulfides [10,20,44], which pose many challenges and opportunities related to oxides in the realm of quantum materials, complex magnetic alloys [25] that are a natural extension of CQM work on electronic phase competition, and extension of neutron methods previously applied to oxides to nanoparticle systems [12].

Future Plans

Building on the success of our synergistic approach, we plan to advance the understanding of exemplary quantum materials (the above, plus some new oxide systems) in three primary ways: through entirely new experimental approaches, particularly around elastic and plastic strain control; through further expansion of CQM activities in neutron scattering; and through yet stronger emphasis on synthesis and processing of quantum materials. Pivotal to much of this will be recent CQM successes with the development and use of unique, high-force strain cells, and close coupling to theory [35,37]. For example, we plan to advance our work on plastic-[35] and elastic-[37] deformation control of quantum materials through *in situ* tunable stress experiments at DOE neutron (HFIR, SNS) and x-ray (APS) facilities, including INS. We also plan to combine discrete heteroepitaxial strain with continuously tunable external compressive strain, dramatically enhancing a widely adopted strategy in thin-film quantum materials, potentially opening up new vistas on quantum critical behavior. We also plan to combine synthesis and stress control by using stress applied at high temperatures to create bulk materials in non-equilibrium conditions. This has the potential to enable tuning and selection of novel crystalline states of matter. We will additionally continue to provide leadership in the application of emerging neutron techniques, including diffuse scattering and Δ-PDF methods, polarized SANS, and white-beam PNR.

Publications

1. "*Kohn-Luttinger correction to T_c in a phonon superconductor*," D. Phan and **A. V. Chubukov**, Phys. Rev. B **101**, 024503 (2020).
2. *"Strain-induced majority carrier inversion in ferromagnetic epitaxial $LaCoO_{3-\delta}$ thin films,"* V. Chaturvedi, J. Walter, A. Paul, A. Grutter, B. Kirby, J. S. Joeng, H. Zhou, Z. Zhang, B. Yu, **M. Greven**, A. Mkhoyan, **T. Birol**, and **C. Leighton**, Phys. Rev. Mater. **4**, 034403 (2020).
3. *"Superconductivity in dilute $SrTiO_3$: a review,"* M. N. Gastiasoro, J. Ruhman, and **R. M. Fernandes**, Annals of Physics **417**, 168107 (2020).
4. *"Anisotropic superconductivity mediated by ferroelectric fluctuations in cubic systems with spin-orbit coupling,"* M. N. Gastiasoro, T. V. Trevisan, **R. M. Fernandes**, Phys. Rev. B **101**, 174501 (2020).
5. *"Phonon Spectrum of underdoped $HgBa_2CuO_{4+\delta}$ investigated by neutron scattering,"* I. Ahamadova, T.C. Sterling, A. C. Sokolik, D. L. Abernathy, **M. Greven**, and D. Reznik, Phys. Rev. B **101**, 184508 (2020).
6. *"Multiferroic behaviour in $EuTiO_3$ films constrained by symmetry,"* P. J. Ryan, G. E. Sterbinsky, Y. Choi, J. C. Woicik, L. Zhu, J. S. Jiang, J.-H. Lee, D. G. Schlom, **T. Birol**, S. D. Brown, P. B. J. Thompson, P. S. Normile, J. Lang, and J.-W. Kim, Phys. Rev. B **101**, 180409(R) (2020).
7. *"Unusual dynamic charge correlations in $HgBa_2CuO_{4+\delta}$,"* B. Yu, W. Tabis, I. Bialo, F. Yakhou, N. B. Brookes, Z. Anderson, Y. Tang, G. Yu, and **M. Greven**, Phys. Rev. X **10**, 021059 (2020).
8. *"Doping-dependent phonon anomaly and charge-ordering phenomena in $HgBa_2CuO_{4+\delta}$ and $HgBa_2CaCu_2O_{6+\delta}$ superconductors,"* L. Wang, B. Yu, R. Jing, X. Luo, J. Zheng, J. Li, I. Bialo, M. Bluschke, Y. Tang, J. Freyermuth, G. Yu, R. Sutarto, F. He, E. Weschke, W. Tabis, **M. Greven**, and Y. Li, Phys. Rev. B **101**, 220509R (2020).
9. *"Effects of paramagnetic pair-breaking and spin-orbital coupling on multi-band superconductivity,"* Y. Ayino, J. Yue, T. Wang**, B. Jalan** and V. Pribiag, J. Phys.: Condens. Matter. **32**, 38LT02 (2020).
10. *"Observation of an internal p-n junction in pyrite FeS_2 single crystals: potential origin of the low open circuit voltage in pyrite solar cells,"* B. Voigt, W. Moore, M. Maiti, J. Walter, B. Das, M. Manno, **C. Leighton** and E.S. Aydil, ACS Materials Lett. **2**, 861-868 (2020).
11. *"Coexistence and interaction of spinons and magnons in an antiferromagnet with alternating antiferromagnetic and ferromagnetic quantum spin chains,"* H. Zhang, Z. Zhao, D. Gautreau, M. Raczkowski, A. Saha, V.O. Garlea, H. Cao, T. Hong, H. O. Jeschke, Subhendra D. Mahanti, **T. Birol**, F. F. Assaad, and X. Ke, Phys. Rev. Lett. **125**, 037204 (2020).
12. *"Quantitative understanding of superparamagnetic blocking in thoroughly characterized Ni nanoparticle assemblies,"* J. Batley, M.Nguyen, I. Kamboj, C. Korostynski, E.S. Aydil and **C. Leighton**, Chem. Mater. **32**, 6494-6506 (2020).
13. *"Resistivity phase diagram of cuprates revisited,"* D. Pelc, M. J. Veit, C. Dorow, Y. Ge, N. Barišić, and **M. Greven**, Phys. Rev. B **102**, 075114 (2020)
14. *"Giant anisotropic magnetoresistance in oxygen-vacancy-ordered epitaxial $La_{0.5}Sr_{0.5}CoO_{3-\delta}$ films,"* J. Walter, S. Bose, M. Cabero, M. Varela, and **C. Leighton**, Phys. Rev. Mater. **4**, 091401(R) (2020).

15. *"Three interaction energy scales in single-layer high T_c cuprate $HgBa_2CuO_{4+\delta}$,"* S. A. Sreedhar, A. Rossi, J. Nayak, Z. W. Anderson, Y. Tang, B. Gregory, M. Hashimoto, D. -H. Lu, E. Rotenberg, R. J. Birgeneau, **M. Greven**, M. Yi, and I. M. Vishik, Phys. Rev. B **102**, 205109 (2020).
16. *"Electronic Structure and Small Hole Polarons in $YTiO_3$,"* J. Yue, N. F. Quackenbush, I. Laraib, H. Carfagno, S. Hameed, A. Prakash, L. R. Thoutam, J. M. Ablett, T. Lee, **M. Greven**, M. F. Doty, A. Janotti, and **B. Jalan**, Phys. Rev. Mater. **4**, 112001(R) (2020).
17. *"Electronic correlations in the semiconducting half-Heusler compound FeVSb,"* E. H. Shourov, P. J. Strohbeen, D. Du, A. Sharan, F. C. de Lima, F. Rodolakis, J. L. McChesney, V. Yannello, A. Janotti, **T. Birol**, and J. K. Kawasaki, Phys. Rev. B **103**, 045134 (2021).
18. *"First-principles characterization of the magnetic properties of $Cu_2(OH)_3Br$,"* D. M. Gautreau, A. Saha, and **T. Birol**, Phys. Rev. Mater. **5**, 024407 (2021).
19. *"Post-growth annealing effects on charge and spin excitations in $Nd_{2-x}Ce_xCuO_4$,"* K. Ishii, S. Asano, M. Ashida, M. Fujita, B. Yu, **M. Greven**, J. Okamoto, D.-J. Huang, and J. Mizuki, Phys. Rev. Mater. **5**, 024803 (2021).
20. *"Mitigation of the internal p-n junction in CoS_2-contacted FeS_2 single crystals: Accessing bulk semiconducting transport,"* B. Voigt, B. Das, D. M. Carr, D. Ray, M. Maiti, W. Moore, M. Manno, J. Walter, E. S. Aydil, and **C. Leighton**, Phys. Rev. Mater. **5**, 025405 (2021).
21. *"Meron, skyrmion, and vortex crystals in centrosymmetric tetragonal magnets,"* Z. Wang, Y. Su, S.-Z. Lin, and C. D. Batista, Phys. Rev. B **103**, 104408 (2021).
22. *"From Weak Antilocalization to Kondo Scattering in a Magnetic Complex Oxide Interface,"* X. Cai, J. Yue, P. Xu, **B. Jalan**, and V. S. Pribiag, Phys. Rev. B **103**, 115434 (2021).
23. *"Mirror symmetry breaking in a model insulating cuprate $Sr_2CuO_2Cl_2$,"* A. de la Torre, K. L Seyler, L. Zhao, S. Di Matteo, M. S. Scheurer, Y. Li, B. Yu, **M. Greven**, S. Sachdev, M. R. Norman and D. Hsieh, Nat. Phys. **17**, 777 (2021).
24. *"Structure-property relationships and mobility optimization in sputtered La-doped $BaSnO_3$ films: Toward 100 $cm^2V^{-1}s^{-1}$ mobility,"* W. M. Postiglione, K. Ganguly, H. Yun, J.S. Jeong, A. Jacobson, L. Borgeson, **B. Jalan**, K.A. Mkhoyan and **C. Leighton**, Phys. Rev. Mater. **5**, 044604 (2021).
25. *"Understanding Magnetic Phase Coexistence in $Ru_2Mn_{1-x}Fe_xSn$ Heusler Alloys: A Neutron Scattering, Thermodynamic, and Phenomenological Analysis,"* E. McCalla, E. E. Levin, J. E. Douglas, J. G. Barker, M. Frontzek, W. Tian, **R. M. Fernandes**, R. Seshadri, and **C. Leighton**, Phys. Rev. Mater. **5**, 064417 (2021).
26. *"Nature of the ferromagnetic-antiferromagnetic transition in $Y_{1-x}La_xTiO_3$,"* S. Hameed, S. El-Khatib, K. P. Olson, B. Yu, T. J. Williams, T. Hong, Q. Sheng, K. Yamakawa, J. Zang, Y. J. Uemura, G. Q. Zhao, C. Q. Jin, L. Fu, Y. Gu, F. Ning, Y. Cai, K. M. Kojima, J. W. Freeland, M. Matsuda, **C. Leighton**, and **M. Greven**, Phys. Rev. B **104**, 024410 (2021). Selected as an Editors' Suggestion.
27. *"Two-component electronic phase separation in the doped Mott insulator $Y_{1-x}Ca_xTiO_3$,"* S. Hameed, J. Joe, D. Gautreau, J. Freeland, **T. Birol** and **M. Greven**, Phys. Rev. B **104**, 045112 (2021). (Selected as an Editors' Suggestion).
28. *"Inhomogeneous time-reversal symmetry breaking in Sr_2RuO_4,"* R. Willa, M. Hecker, **R. M. Fernandes**, and J. Schmalian, Phys. Rev. B **104**, 024511 (2021). (Selected as an Editors' Suggestion).

29. *"A Quantitative Method for In-Situ Pump-Beam Metrology in Ultrafast Electron Microscopy,"* J. Chen, **C. Leighton**, and D. Flannigan, Cambridge University Press (2021).
30. *"Phenomenological model of the third-harmonic response due to superconducting fluctuations: application to Sr_2RuO_4,"* F. Chen, D. Pelc, **M. Greven**, and **R. M. Fernandes**, Phys. Rev. B **104**, 064502 (2021).
31. *"Novel Synthesis Approach for 'Stubborn' Metals and Metal Oxides,"* W. Nunn, A. K. Manjeshwar, J. Yue, A. Rajapitamahuni, T. K. Truttmann and **B. Jalan**, Proc. Nat. Acad. Sci. **118**, 32 e2105713118 (2021).
32. *"Anisotropic time-domain electronic response in cuprates driven by midinfrared pulses,"* F. Giusti, A. Montanaro, A. Marciniak, F. Randi, F. Boschini, F. Glerean, G. Jarc, H. Eisaki, **M. Greven**, A. Damascelli, A. Avella, and D. Fausti, Phys. Rev. B **104**, 125121 (2021).
33. *"A review of molecular-beam epitaxy of wide bandgap complex oxide semiconductors,"* W. Nunn, T. K. Truttmann, and **B. Jalan**, J. Mater. Res. (2021).
    https://doi.org/10.1557/s43578-021-00377-1
34. *"Solid-source metal-organic molecular beam epitaxy of epitaxial RuO_2,"* W. Nunn, S. Nair, H. Yun, A. K. Manjeshwar, A. Rajapitamahuni, D. Lee, K. A. Mkhoyan, and **B. Jalan**, APL Materials **9**, 091112 (2021). (Editor's Pick) (featured on the journal cover).
35. *"Enhanced superconductivity and ferroelectric quantum criticality in plastically deformed strontium titanate,"* S. Hameed, D. Pelc, Z. W. Anderson, A. Klein, R. J. Spieker, L. Yue, B. Das, J. Ramberger, M. Lukas, Y. Liu, M. J. Krogstad, R. Osborn, Y. Li, **C. Leighton**, **R. M. Fernandes**, and **M. Greven**, Nat. Mater. (2021).
    https://doi.org/10.1038/s41563-021-01102-3
36. *"Unconventional short-range structural fluctuations in cuprate high-T_c superconductors,"* D. Pelc, R. J. Spieker, Z. W. Anderson, M. J. Krogstad, N. Biniskos, N. G. Bielinski, B. Yu, T. Sasagawa, L. Chauviere, P. Dosanjh, R. Liang, D. A. Bonn, A. Damascelli, Y. Liu, R. Osborn, and **M. Greven**, submitted (2021), (arXiv:2103.05482).
37. *"Uniaxial strain control of bulk ferromagnetism in rare-earth titanates,"* A. Najev, S. Hameed, D. Gautreau, Z. Wang, J. Joe, M. Požek, **T. Birol**, **R. M. Fernandes**, **M. Greven**, and D. Pelc, submitted (2021), (arXiv:2105.06695).
38. *"Arc-to-pocket transition and quantitative understanding of transport properties in cuprate superconductors,"* W. Tabis, P. Popčević, B. Klebel-Knobloch, I. Bialo, C. M. N. Kumar, B. Vignolle, **M. Greven**, and N. Barišić, submitted (2021), (arXiv:2106.07457).
39. *"Strain-tunable metamagnetic critical end-point in Mott insulating rare-earth titanates,"* Z. Wang, D. Gautreau, **T. Birol**, and **R. M. Fernandes**, submitted (2021), (arXiv:2105.01559).
40. *"The essential role of magnetic frustration in the phase diagrams of doped cobaltites,"* P. Orth, D. Phelan, J. Zhao, H. Zheng, J. F. Mitchell, **C. Leighton**, and R. M. Fernandes, submitted (2021), (arXiv:2105.06402).
41. *"Coherent phonon disruption and lock-in during a photoinduced charge-density-wave phase transition,"* S. A. Reisbick, Y. Zhang, J. Chen, P. E. Engen, and D. J. Flannigan, in press, J. Phys. Chem. Lett. (2021), (chemrxiv.14357342).
42. *"Growth and characterization of large (Y,La)TiO_3 and (Y,Ca)TiO_3 single crystals,"* S. Hameed, J. Joe, L. R. Thoutam, J. Garcia-Barriocanal, B. Yu, G. Yu, S. Chi, T. Hong, T. J. Williams, J. W. Freeland, P. M. Gehring, Z. Xu, M. Matsuda, **B. Jalan**, and **M. Greven**, submitted (2021), (arXiv:2106.10253).

43. *"Anomalous transport in high-mobility superconducting $SrTiO_3$ thin films,"* J. Yue, Y. Ayino, T. K. Truttmann, M. N. Gastiasoro, E. Persky, A. Khanukov, D. Lee, L. R. Thoutam, B. Kalisky, **R. M. Fernandes**, V. S. Pribiag, and **B. Jalan**, submitted (2021), (arXiv:2107.10904).
44. "*Conduction via surface states in antiferromagnetic Mott-Insulating NiS_2 single crystals*", S. El-Khatib, B. Voigt, B. Das, A. Stahl, W. Moore, M. Maiti and **C. Leighton**, submitted (2021).
45. "*Synergetic ferroelectricity and superconductivity in zero-density Direac semimetals near quantum criticality*", V. Kozii, A. Klein, **R. M. Fernandes**, and J. Ruhman, submitted (2021), (arXiv:2110.09530).

Precise chain conformation and dynamics control for conjugated polymers in organic electronic thin film devices

Xiaodan Gu, School of Polymer Science and Engineering, The University of Southern Mississippi

Program Scope

The aim of this early-career project is to provide fundamental knowledge to bridge the gap between solution state polymer conformations and deposited solid-state morphology, thus enabling robust structure and property relationship correlation for organic electronic devices. Filling this gap will help guide the rational design of proper processing parameters for controlling microstructures for solution process electronic devices and promoting device performance. To achieve the above goal, this proposal utilizes various DOE neutron and X-ray sources to probe the chain conformation and dynamics in both the solution and solid-state. This project will also utilize high-throughput instrumentation and machine learning to mine out key processing parameters that influence final device morphology and performance. We propose the following aims: 1) harness non-covalent interactions to pre-set CPs into preferred chain conformations; 2) utilize high throughput robotic processing and machine learning methodology to mine out key determining factors for obtaining highly ideal chain morphology; 3) develop grazing incidence scattering techniques and use ex situ neutron scattering and deuterium labeling to study chain conformation in solid-state bulk and thin films; 4) study heterogeneity of chain dynamics in bulk and thin film, and investigate the impact of chain dynamics on CPs' optoelectronic property.

Recent Progress

This early-career project started in Sept 2021, for the past two months, the team has been focusing on the synthesis of deuterated conjugated donor-acceptor polymers, as well as perform solution scattering.

Synthesis of deuterated DPP polymers with different deuterated sidechains.

We have synthesized a series of DPP polymers with different side-chain structures (Fig. 1). A wide variety of polymers with both protonated and deuterated sidechains were synthesized. The synthesis schematic is shown in Figure 1. The deuterated sidechains were synthesized at the CNMS through an accepted user proposal using a hydrogen-deuterium exchange reaction[1]. After successful deuteration sidechain synthesis was verified by NMR spectroscopy. Different alkyl sidechains have been installed into the conjugated polymer backbone and then polymerized through cross-coupling reactions[2]. Currently, four out of eight proposed DPP polymers with different side chains were synthesized. We plan to study the effect of alkyl sidechain length on the backbone rigidity and dynamics for CPs in the condensed solid-state, in contrast to our previous focus on the solution state. We secured some SANS neutron beamtime for the next cycle. We plan to blend protonated polymers into the deuterated polymer matrix, then perform transmission SANS above the melting point of the conjugated polymers[3]. The scattering data will be analyzed and compared to solution scattering for a single chain. Additionally, QENS experiments are also planned for spring, 2022 at SNS.

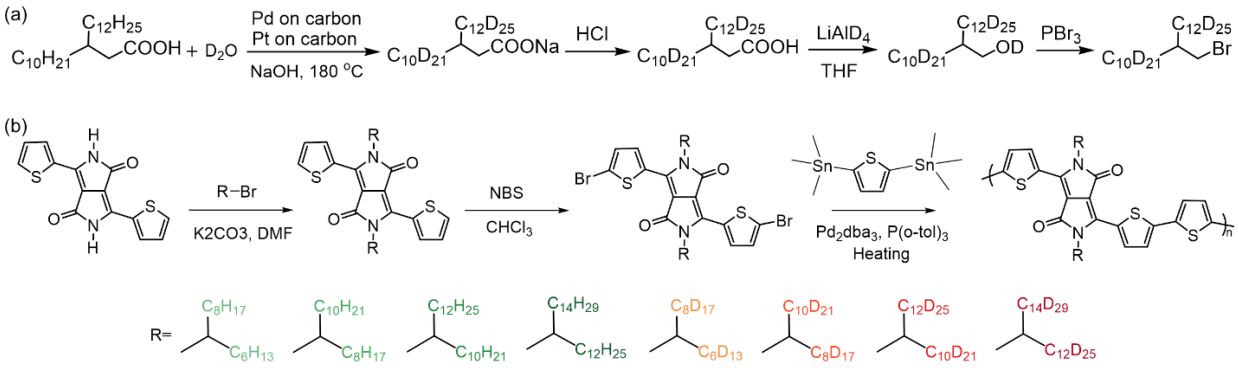

Figure 1. (a) Synthetic route of deuterated branched long alkyl sidechains. (b) Synthetic route of conjugated polymers with protonated and deuterated branched alkyl sidechains.

Synthesis of DPP polymers with non-covalent sidechain to lock chain conformation.

In order to achieve more precise control of polymer chain conformation, non-covalent interactions can be used to modulate the dihedral angle between different building blocks along the polymer backbone[4]. In order to demonstrate this is feasible, we proposed two different DPP polymers with different non-covalent interactions along its backbone. We have synthesized those two DPP-based polymers, incorporating either pyrazine or benzene moieties flanked by thiophenes with pendant amide side chains. Using either pyrazine or benzene moieties in the polymer's π-conjugated backbone, control over the orientation and type of H-bonds is possible[5]. When pyrazine is used, intramolecular H-bonds are promoted in the polymer, while benzene only allows for intermolecular noncovalent interactions between the amide side chains. The intramolecular locking effect is expected to have a vital influence on backbone planarity and rigidity. To investigate this effect, small-angle neutron scattering (SANS) was performed on diluted solutions of the polymer solubilized in a deuterated solvent and thereby isolating the effect of the lock on the rigidity of single polymer chains. Using the flexible cylinder model, results obtained from SANS in solution revealed that P1 has a persistence length (Lp) of 13.5 nm, while P2 has a shorter Lp of 6.6 nm. The intramolecular H-bonding inter-actions along the conjugated backbone of P1 enhance chain rigidity by bringing the backbone into greater planarity, resulting in greater chain rigidity and longer Lp. Currently, we are also exploring using MD simulation to further rationalize our findings, as well as planning other non-covalent interaction functional groups to deepen our understanding here.

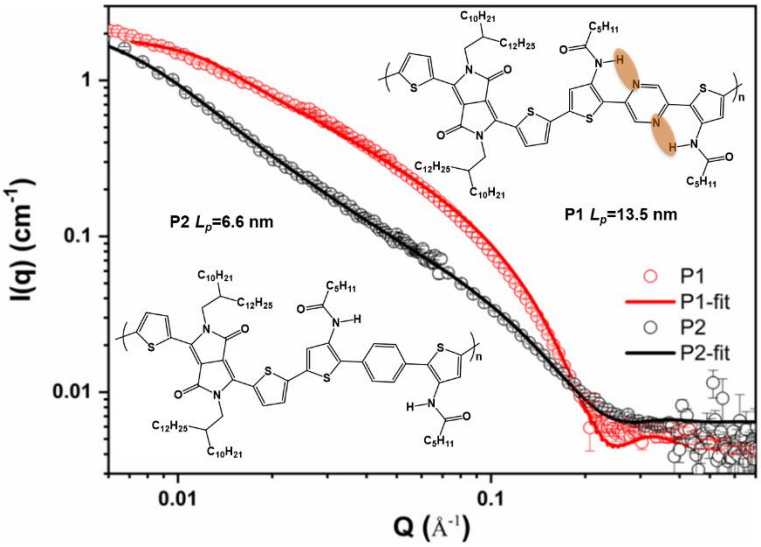

Figure 2. Small angle neutron scattering raw curve (dots) and fitted curve (solid lines) for P1 (red) and P2 (black).

Future Plans

1) We plan to perform a molecular dynamics simulation to develop an in-depth understanding of the impact of non-covalent interactions on polymer chain conformation. After that, we will plan to develop different non-covalent interactions to further modulate the solution chain conformation. Different non-covalent interactions will be engineered into conjugated polymer backbones and use this interaction to promote chain rigidity and planarity.

2) Previously, our group have successfully investigated the solution assembly of conjugated polymers and a few design rules were elucidated to control chain rigidity. As we discussed in recent progress, we plan to use the unique capabilities of neutron and deuteration chemistry to facilitate the study of the chain conformation for conjugated polymer in the solid states, either bulk or thin film. We will study the chain conformation for polymer in the melt state for obtaining a single chain conformation and compare it with the property in the solution state. We have finished the initial synthesis, so additional synthesis and then scattering experiments will be planned to execute this task. Our goal is to find a rational method to process the polymer to further control the chain conformation in the solid state.

3) We plan to study the dynamics of the conjugated polymers using a suite of quasi-elastic neutron scattering and neutron spin-echo methods. The ultimate goal for us is to understand the dynamics of the polymer chain at different temperatures. The neutron experiment will be complemented by ellipsometry, vibronic spectroscopy, and UV-vis spectroscopy characterization. Additionally, the experimental finding will be compliment with molecular dynamics simulation to understand the mean square displacement for our polymer. We hope to understand the role of chain dynamics on the optoelectronic property, especially when operated at an elevated temperature.

References

(1) Li, L.; Jakowski, J.; Do, C.; Hong, K. Deuteration and Polymers: Rich History with Great Potential. *Macromolecules* **2021**, *54* (8), 3555–3584.

https://doi.org/10.1021/acs.macromol.0c02284.
(2) Nielsen, C. B.; Turbiez, M.; McCulloch, I. Recent Advances in the Development of Semiconducting DPP-Containing Polymers for Transistor Applications. *Advanced Materials*. 2013. https://doi.org/10.1002/adma.201201795.
(3) Jones, R. L.; Kumar, S. K.; Ho, D. L.; Briber, R. M.; Russell, T. P. Chain Conformation in Ultrathin Polymer Films. *Nature* **1999**, *400* (6740), 146–149. https://doi.org/10.1038/22080.
(4) Oh, J. Y.; Rondeau-Gagné, S.; Chiu, Y.-C.; Chortos, A.; Lissel, F.; Wang, G.-J. N.; Schroeder, B. C.; Kurosawa, T.; Lopez, J.; Katsumata, T.; Xu, J.; Zhu, C.; Gu, X.; Bae, W.-G.; Kim, Y.; Jin, L.; Chung, J. W.; Tok, J. B.-H.; Bao, Z. Intrinsically Stretchable and Healable Semiconducting Polymer for Organic Transistors. *Nature* **2016**, *539* (7629), 411–415. https://doi.org/10.1038/nature20102.
(5) Jackson, N. E.; Savoie, B. M.; Kohlstedt, K. L.; Olvera de la Cruz, M.; Schatz, G. C.; Chen, L. X.; Ratner, M. A. Controlling Conformations of Conjugated Polymers and Small Molecules: The Role of Nonbonding Interactions. *J. Am. Chem. Soc.* **2013**, *135* (28), 10475–10483. https://doi.org/10.1021/ja403667s.

Publications

We do not have publications to report. The project initiated three months ago.

Understanding the Structure and Dynamics of Conjugated Polymers by Advancing Deuteration Chemistry and Neutron Scattering

Xiaodan Gu and Jason Azoulay, School of Polymer Science and Engineering, The University of Southern Mississippi

Program Scope

This program aims to understand the structure and dynamics of conjugated polymers (CPs) by new click based deuteration chemistry and neutron scattering. This project aims to: i) develop new methodologies to efficiently deuterate sidechains of CPs; ii) understand the role of dynamic and static disorder of the sidechains on backbone rigidity and how this impacts optical, mechanical and electronic properties; and iii) formulate design principles for next-generation CPs that are resilient to disorder through precise control of electronic structure through manipulating backbone and side chain structure. This project will provide new methodologies to quantitatively measure chain conformation of CPs, which is vital for further advancements, understanding underlying structure-function relationships that lead to emerging CPs, discovering new phenomena, improving device performance, and creating new energy-related technologies.

Recent Progress

In this second report, we performed an in-depth study of the conjugated polymer chain conformation by combining synthesis, characterization, and modeling. Despite the COVID situation, the team made the following progress regarding the development of CPs with deuterated sidechains and characterization of conjugated polymer's chain conformation or assembly by solution neutron scattering. Our progress can be viewed in detail in our publications, which includes ten major publications that benefited from this grant primary funding sources and another eighteen associated publications with partial support. Here are five highlights of our progress.

Probe conjugated polymers backbone conformation by neutron scattering in contrast varied solvents. [1] Although considerable progress has been made to optimize the optoelectronic properties of CPs, the rational design of CPs with tailored physical properties for end-use applications remains a significant challenge. Specifically, experimental characterization of conjugated polymer backbone conformations remains underexplored due to limited techniques that are capable of distinguishing the backbone and side-chain structures at nanoscopic resolution. Thus, relating the electronically functional backbone conformation to the material's macroscopic optoelectronic property is an ongoing challenge. We performed small-angle neutron scattering techniques (SANS) with contrast-variation (CV) experiments on poly(3-alkylthiophenes) (P3ATs) with both deuterated and protonated side chains in a mixture of protonated and deuterated solvents to decouple the backbone and side-chain scattering signals. We obtained the form factor of P3ATs' backbone, side chains, and cross-scattering term by deconvoluting their respective scattering signals. Poly(3-decylthiophene) shows a persistence length of 1.05 ± 0.1 nm for the conjugated polymer

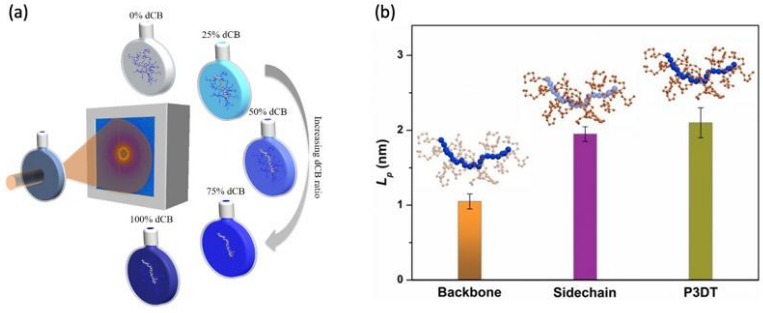

Figure 1: (a) Contrast matching experiments for polymer in contrast varied solvents. (b) The persistence length for P3AT polymers with scattering from its backbone, sidechain, and overall chain.

backbone and 2.10 ± 0.2 nm for the entire chain. The strong scattering signal from long and flexible alkyl side chains leads to a seemingly more rigid conjugated polymer, which is further revealed by coarse-grained molecular dynamics (CG-MD) simulations. This work offers a methodology to decouple the scattering contribution from the CPs' backbone and side chains, thus elucidating the inherent conformation of the electronically active conjugated backbone, which provides guidance for the rational design of next-generation polymeric semiconductors.

Effective of chemical building blocks backbone and sidechains on conjugated polymer. The less studied chain conformation of donor-accepter conjugated polymers (D-A CPs) hinders the fundamental understanding on their optical and electronic properties. Here, we explore the effect of sidechains and backbones on chain conformation experimentally as well as computationally and optoelectronic properties of diketopyrrolopyrrole (DPP) and isoindigo (IID) based polymers. Using small-angle neutron scattering (SANS) measurements, we find that for DPP-based polymers with the same side chains the chain rigidity significantly decreases from 18.5 nm for DPP-T-C2C10C12 to 10.0 nm for DPP-T3-C2C10C12 as the number of thiophene increases. Chain rigidity of DPP-based polymers increases with side-chain length, from 15.7 nm for DPP-T-C2C6C8 to 20.5 nm for DPP-T-C2C12C14. The chain rigidity of IID-based polymers increases when moving the branch position farther away to the backbone, from 15.8 nm for IID-C2C10C10 to 18.6 nm for IID-C5C10C10. Using atomistic molecular dynamics (MD), we further validated the experimental results. This work fills the fundamental gaps in our knowledge of the most basic relationships between polymer structure and chain conformation.

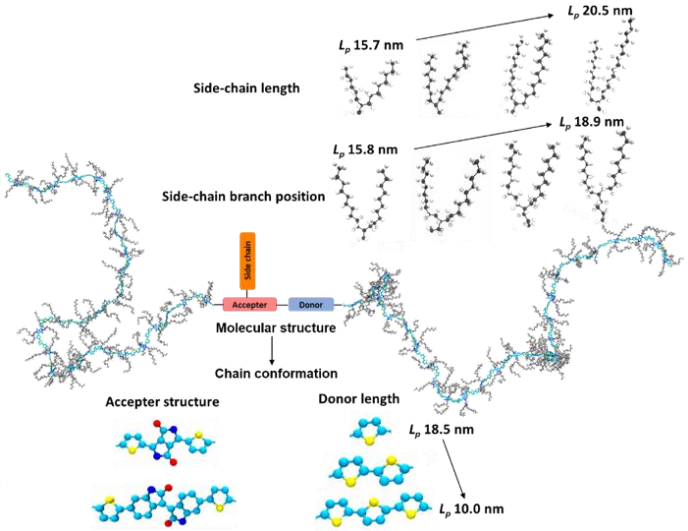

Figure 2: Combing SANS and MD to study the effect backbone and sidechain structures on chain conformation.

Effect of molecular weight on the chain conformation and conjugation length. [2]The molecular weight effect on chain conformation was also systematically evaluated here. There is a knowledge gap about how the semi-rigid polymer molecular weight impacts material properties. Here, a discrete and monodisperse oligomer series and conjugated polymers were synthesized by C–H-activated cross-coupling. This series reveals a rod-to-coil transition at n = 15 and coil formation at polymer length scales of ~28 units via solution SANS characterization. The oxidation states are deciphered via cyclic voltammetry, differential pulse voltammetry, spectroelectrochemistry, and

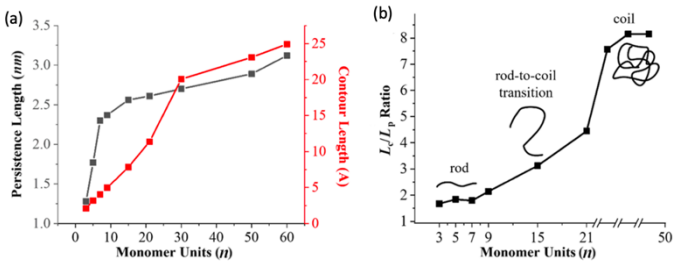

Figure 3: (a) Persistence length of conjugate polymer oligomers and polymer with different numbers of repeating units fitted by a flexible cylinder model. (b) Contour length (LC)/persistence length (LP) change with repeat units.

density functional theory calculations. Oligomers 3–9 undergo successive one-electron oxidation steps, while 15 and higher undergo multielectron oxidations per step. Furthermore, oxidized 15 has a lower electronic transition energy compared to its polymer homologue, as shown by spectroelectrochemistry, revealing a synergy between the chain length and the oxidation state properties. This study proves that the convergence limit between small molecule and polymer behavior occurs at approximately 15 units and highlights the property transitions that occur as a function of chain length for a DA CPs.

Influence of the backbone rigidity on the physical property of CPs.[3] For the past two years, the research team also performed in depth understanding of the backbone rigidity on a wide range of materials property. Specifically, our recent work provide the first holistic approach to understand the fundamental influence of backbone rigidity on an n-type naphthalene diimide-based conjugated polymer, through the insertion of a flexible conjugation break spacer (CBS). Solution SANS and oscillatory shear rheometry were employed to provide the first quantitative evidence of conjugation break spacer influence over conjugated polymer chain rigidity and entanglement molecular weight, demonstrating a reduction in the Kuhn length from 521 to 36 Å for fully conjugated PNDI-C0 and PNDI-C6, respectively. Thermomechanical properties, such as elastic modulus and glass-transition temperature, were shown to decrease with an increasing length of conjugation break spacer. An extraordinary ductility, upwards of 400% tensile strain before fracture, was observed for high-molecular-weight PNDI-C4. Overall, this work sheds light on the important role of backbone rigidity in designing flexible and stretchable conjugated polymers.

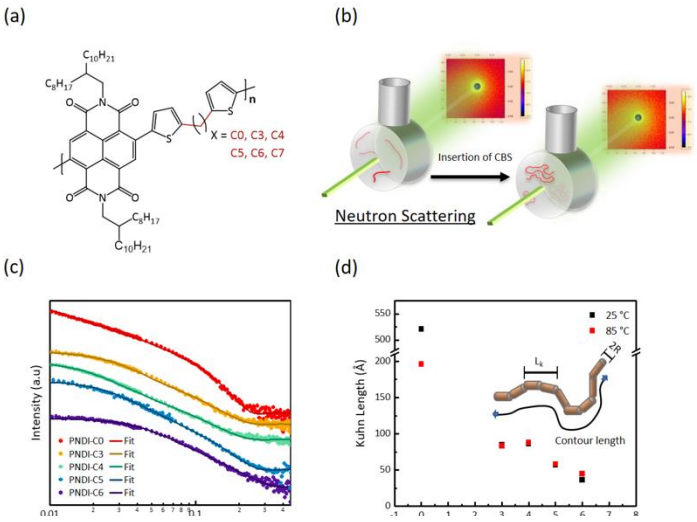

Figure 4: (a) PNDI-Cx polymers structure. (b) Illustration of solution SANS upon insertion of CBS. (c) 1D scattering profile obtained at 25 ˚C in deuterated chlorobenzene. (d) Kuhn length dependence on conjugation breaker spacer length as fitted using the flexible cylinder model.

Effect of the water/polymer interface on thin film mechanics. Additionally, the research program assisted in the develop a new thin-film tensile tool that is capable of measuring the thin film mechanic of sub-10nm polymeric thin film. This work has been granted a US Patent. This technique is reviewed in our recent review article[4]. We first discussed the progression of thin-film mechanical testing methods based on the supporting substrate: film-on-solid substrate method, film-on-water tensile tests, and water-assisted free-standing tensile tests. By comparing past studies on a model polymer, polystyrene, the effect of different substrates and confinement effect on the thin-film mechanics is evaluated. These techniques have generated fruitful scientific knowledge in the field of organic semiconductors for the understanding of structure–mechanical property relationships. More recently, we present the shear motion-assisted robust transfer technique (SMART) for fabricating free-standing sub-100 nm films and measuring their inherent structural–mechanical properties[5]. This unique tool allowed us to compare thin-film mechanics for freestanding film and water-supported film, exploring two phenomena: 1) The influence of

confinement on mechanics and 2) the role of water on the mechanical properties of hydrophobic films. Upon confinement, polymer thin films exhibit increased strain at failure, and reduced yield stress, while modulus is reduced only for the thinnest 19 nm film. Water measurements demonstrate subtle differences in mechanics which we elucidate using neutron reflectometry.

Overall, our work demonstrated that the backbone of the conjugated polymers plays an important role in their physical and optoelectronic property. We propose additional works to further our understanding and control the conjugated polymer's backbone rigidity to further enhance optoelectronic properties.

Future Plans

1) We plan to use non-covalent interactions to impose additional chain conformational constraints to promote rigid and torsion-free backbone conformation. This will be achieved through new material synthesis, solution-phase neutron scattering, and molecular dynamics simulation to understand, predict, and control chain conformation for single-chain CPs. This aim is built upon our previous work toward understanding backbone rigidity for D-A CPs in the solution state. In our previous program, we systematically investigated the influence of backbone moieties and sidechain length on the chain rigidity of P3ATs and D-A CPs. The next step is to utilize the non-covalent interactions to further modulate the solution chain conformation. Different non-covalent interactions will be engineered into conjugated polymer backbones and use this interaction to promote chain rigidity and planarity.

2) We will also study the effect of the rigidity of polymer backbones on their physical, optical, and electronic property. We plan to perform solution-based spectroscopy (UV-vis and fluorescence spectroscopy) on previous synthesis CPs with or without deuterated sidechains. We expect the rigidity of the polymer backbone would have an impact on their conjugated length and optical property. We will study the temperature-dependent chain conformation to understand the ability to make polymers that are robust to thermal disorder. One interesting question we had is how does deuteration impact the physical property of conjugated polymers.

3) Understanding the correlation between the solution phase and solid film is critical for material development and processing and has excited great interest in the organic electronic community. Along this line, we have successfully investigated the solution assembly of conjugated polymers. Moving forward, we plan to use the unique capabilities of neutron and deuteration chemistry to facilitate the study of the structure and dynamics of CPs in the solid bulk states. We will study the chain conformation for polymer in the melt state for obtaining a single chain conformation and compare it with the property in solution state.

References

(1) Cao, Z.; Li, Z.; Zhang, S.; Galuska, L.; Li, T.; Do, C.; Xia, W.; Hong, K.; Gu, X. *Macromolecules* **2020**, *53* (24), 11142–11152.

(2) Chaudhry, S.; Wu, Y.; Cao, Z.; Li, S.; Canada, J. L.; Gu, X.; Risko, C.; Mei, J. *Macromolecules* **2021**, acs.macromol.1c00963.

(3) Galuska, L. A.; McNutt, W. W.; Qian, Z.; Zhang, S.; Weller, D. W.; Dhakal, S.; King, E. R.; Morgan, S. E.; Azoulay, J. D.; Mei, J.; Gu, X. *Macromolecules* **2020**, *53* (14), 6032–6042.

(4) Zhang, S.; Galuska, L. A.; Gu, X. *J. Polym. Sci.* **2021**, No. April, pol.20210281.

(5) Galuska, L. A.; Muckley, E. S.; Cao, Z.; Ehlenberg, D. F.; Qian, Z.; Zhang, S.; Rondeau-Gagné, S.; Phan, M. D.; Ankner, J. F.; Ivanov, I. N.; Gu, X. *Nat. Commun.* **2021**, *12* (1), 2347.

Publications

Publications with majority support from this award [from Jun 2019 to Oct 2021]

(1) Qian, Z.; Galuska, L.; McNutt, W. W.; Ocheje, M. U.; He, Y.; Cao, Z.; Zhang, S.; Xu, J.; Hong, K.; Goodman, R. B.; et al. Challenge and Solution of Characterizing Glass Transition Temperature for Conjugated Polymers by Differential Scanning Calorimetry. *J. Polym. Sci. Part B Polym. Phys.* **2019**, *57* (23), 1635–1644. https://doi.org/10.1002/polb.24889.

(2) Galuska, L. A.; McNutt, W. W.; Qian, Z.; Zhang, S.; Weller, D. W.; Dhakal, S.; King, E. R.; Morgan, S. E.; Azoulay, J. D.; Mei, J.; et al. Impact of Backbone Rigidity on the Thermomechanical Properties of Semiconducting Polymers with Conjugation Break Spacers. *Macromolecules* **2020**, *53* (14), 6032–6042. https://doi.org/10.1021/acs.macromol.0c00889.

(3) Cao, Z.; Galuska, L.; Qian, Z.; Zhang, S.; Huang, L.; Prine, N.; Li, T.; He, Y.; Hong, K.; Gu, X. The Effect of Side-Chain Branch Position on the Thermal Properties of Poly(3-Alkylthiophenes). *Polym. Chem.* **2020**, *11* (2), 517–526. https://doi.org/10.1039/C9PY01026B.

(4) Cao, Z.; Li, Z.; Zhang, S.; Galuska, L.; Li, T.; Do, C.; Xia, W.; Hong, K.; Gu, X. Decoupling Poly(3-Alkylthiophenes)' Backbone and Side-Chain Conformation by Selective Deuteration and Neutron Scattering. *Macromolecules* **2020**, *53* (24), 11142–11152. https://doi.org/10.1021/acs.macromol.0c02086.

(5) Zhang, S.; Alesadi, A.; Mason, G. T.; Chen, K.-L.; Freychet, G.; Galuska, L.; Cheng, Y.-H.; St. Onge, P. B. J.; Ocheje, M. U.; Ma, G.; et al. Molecular Origin of Strain-Induced Chain Alignment in PDPP-Based Semiconducting Polymeric Thin Films. *Adv. Funct. Mater.* **2021**, *31* (21), 2100161. https://doi.org/10.1002/adfm.202100161.

(6) Zhang, S.; Galuska, L. A.; Gu, X. Water-assisted Mechanical Testing of Polymeric Thin-films. *J. Polym. Sci.* **2021**, No. April, pol.20210281. https://doi.org/10.1002/pol.20210281.

(7) Yan, X.; Xiong, M.; Deng, X.; Liu, K.; Li, J.; Wang, X.-Q.; Zhang, S.; Prine, N.; Zhang, Z.; Huang, W.; et al. Approaching Disorder-Tolerant Semiconducting Polymers. *Nat. Commun.* **2021**, *12* (1), 5723. https://doi.org/10.1038/s41467-021-26043-y.

(8) Chaudhry, S.; Wu, Y.; Cao, Z.; Li, S.; Canada, J. L.; Gu, X.; Risko, C.; Mei, J. Evolution of Chain Dynamics and Oxidation States with Increasing Chain Length for a Donor–Acceptor-Conjugated Oligomer Series. *Macromolecules* **2021**, acs.macromol.1c00963. https://doi.org/10.1021/acs.macromol.1c00963.

(9) Galuska, L. A.; Muckley, E. S.; Cao, Z.; Ehlenberg, D. F.; Qian, Z.; Zhang, S.; Rondeau-Gagné, S.; Phan, M. D.; Ankner, J. F.; Ivanov, I. N.; et al. SMART Transfer Method to Directly Compare the Mechanical Response of Water-Supported and Free-Standing Ultrathin Polymeric Films. *Nat. Commun.* **2021**, *12* (1), 2347. https://doi.org/10.1038/s41467-021-22473-w.

(10) Xiong, M.; Yan, X.; Li, J. T.; Zhang, S.; Cao, Z.; Prine, N.; Lu, Y.; Wang, J. Y.; Gu, X.; Lei, T. Efficient N-Doping of Polymeric Semiconductors through Controlling the Dynamics of Solution-State Polymer Aggregates. *Angew. Chemie - Int. Ed.* **2021**, *60* (15), 8189–8197. https://doi.org/10.1002/anie.202015216.

Other Publications benefited from this grant [from Jun 2019 to Oct 2021]

Partially supported due to morphology characterization by scattering technique

(11) Yan, X.; Xiong, M.; Li, J.-T.; Zhang, S.; Ahmad, Z.; Lu, Y.; Wang, Z.-Y.; Yao, Z.-F.; Wang, J.-Y.; Gu, X.; et al. Pyrazine-Flanked Diketopyrrolopyrrole (DPP): A New Polymer Building Block for High-Performance n-Type Organic Thermoelectrics. *J. Am. Chem. Soc.* **2019**, *141* (51), 20215–20221. https://doi.org/10.1021/jacs.9b10107.

(12) Savikhin, V.; Shapiro, D. A.; Gu, X.; Oosterhout, S. D.; Toney, M. F. Ptychography of Organic Thin Films at Soft X-Ray Energies. *Chem. Mater.* **2019**, *31* (13), 4913–4918. https://doi.org/10.1021/acs.chemmater.9b01690.

(13) Huang, L.; Eedugurala, N.; Benasco, A.; Zhang, S.; Mayer, K. S.; Adams, D. J.; Fowler, B.; Lockart, M. M.; Saghayezhian, M.; Tahir, H.; et al. Open-Shell Donor–Acceptor Conjugated Polymers with High Electrical Conductivity. *Adv. Funct. Mater.* **2020**, *1909805*, 1909805. https://doi.org/10.1002/adfm.201909805.

(14) Li, Q.-Y.; Yao, Z.-F.; Lu, Y.; Zhang, S.; Ahmad, Z.; Wang, J.-Y.; Gu, X.; Pei, J. Achieving High Alignment of Conjugated Polymers by Controlled Dip-Coating. *Adv. Electron. Mater.* **2020**, *2000080*, 2000080. https://doi.org/10.1002/aelm.202000080.

(15) Pang, S.; Zhou, X.; Zhang, S.; Tang, H.; Dhakal, S.; Gu, X.; Duan, C.; Huang, F.; Cao, Y. Nonfused Nonfullerene Acceptors with an A–D–A′–D–A Framework and a Benzothiadiazole Core for High-Performance Organic Solar Cells. *ACS Appl. Mater. Interfaces* **2020**, *12* (14), 16531–16540. https://doi.org/10.1021/acsami.0c01850.

(16) Mooney, M.; Wang, Y.; Nyayachavadi, A.; Zhang, S.; Gu, X.; Rondeau-Gagné, S. Enhancing the Solubility of Semiconducting Polymers in Eco-Friendly Solvents with Carbohydrate-Containing Side Chains. *ACS Appl. Mater. Interfaces* **2021**, *13* (21), 25175–25185. https://doi.org/10.1021/acsami.1c02860.

(17) Jia, H.; Huang, Z.; Li, P.; Zhang, S.; Wang, Y.; Wang, J.-Y.; Gu, X.; Lei, T. Engineering Donor–Acceptor Conjugated Polymers for High-Performance and Fast-Response Organic Electrochemical Transistors. *J. Mater. Chem. C* **2021**, *9* (14), 4927–4934. https://doi.org/10.1039/D1TC00440A.

(18) Mayer, K. S.; Adams, D. J.; Eedugurala, N.; Lockart, M. M.; Mahalingavelar, P.; Huang, L.; Galuska, L. A.; King, E. R.; Gu, X.; Bowman, M. K.; et al. Topology and Ground State Control in Open-Shell Donor-Acceptor Conjugated Polymers. *Cell Reports Phys. Sci.* **2021**, *2* (6), 100467. https://doi.org/10.1016/j.xcrp.2021.100467.

(19) Luo, S.; Li, N.; Zhang, S.; Zhang, C.; Qu, T.; Ocheje, M. U.; Xue, G.; Gu, X.; Rondeau-Gagné, S.; Hu, W.; et al. Observation of Stepwise Ultrafast Crystallization Kinetics of Donor–Acceptor Conjugated Polymers and Correlation with Field Effect Mobility. *Chem. Mater.* **2021**, acs.chemmater.0c03854. https://doi.org/10.1021/acs.chemmater.0c03854.

(20) Li, N.; Dai, Y.; Li, Y.; Dai, S.; Strzalka, J.; Su, Q.; De Oliveira, N.; Zhang, Q.; St. Onge, P. B. J.; Rondeau-Gagné, S.; et al. A Universal and Facile Approach for Building Multifunctional Conjugated Polymers for Human-Integrated Electronics. *Matter* **2021**, *4* (9), 3015–3029. https://doi.org/10.1016/j.matt.2021.07.013.

(21) Li, B.; Zhang, Q.; Zhang, S.; Ahmad, Z.; Chidanguro, T.; Hunter Davis, A.; Simon, Y. C.; Gu, X.; Zheng, W.; Pradhan, N.; et al. Spontaneously Supersaturated Nucleation Strategy for High Reproducible and Efficient Perovskite Solar Cells. *Chem. Eng. J.* **2021**, *405*, 126998. https://doi.org/10.1016/j.cej.2020.126998.

(22) Mooney, M.; Wang, Y.; Nyayachavadi, A.; Zhang, S.; Gu, X.; Rondeau-Gagné, S. Enhancing the Solubility of Semiconducting Polymers in Eco-Friendly Solvents with Carbohydrate-Containing Side Chains. *ACS Appl. Mater. Interfaces* **2021**. https://doi.org/10.1021/acsami.1c02860.

(23) Zhao, Y.; Liu, T.; Wu, B.; Zhang, S.; Prine, N.; Zhang, L.; Pang, S.; Yin, B.; Ye, L.; Gu, X.; et al. High-Performance All-Polymer Solar Cells and Photodetectors Enabled by a High-Mobility n-Type Polymer and Optimized Bulk-Heterojunction Morphology. *Chem. Mater.* **2021**. https://doi.org/10.1021/acs.chemmater.1c00825.

Partially supported due to thin film tensile technique developed in this work

(24) Zheng, Y.; Wang, G. N.; Kang, J.; Nikolka, M.; Wu, H.; Tran, H.; Zhang, S.; Yan, H.; Chen, H.; Yuen, P. Y.; et al. An Intrinsically Stretchable High-Performance Polymer Semiconductor with Low Crystallinity. *Adv. Funct. Mater.* **2019**, *29* (46), 1905340. https://doi.org/10.1002/adfm.201905340.

(25) Luo, S.; Wang, T.; Ocheje, M. U.; Zhang, S.; Xu, J.; Qian, Z.; Gu, X.; Xue, G.; Rondeau-Gagné, S.; Jiang, J.; et al. Multiamorphous Phases in Diketopyrrolopyrrole-Based Conjugated Polymers: From Bulk to Ultrathin Films. *Macromolecules* **2020**, *53* (11), 4480–4489. https://doi.org/10.1021/acs.macromol.9b02738.

(26) Zhang, S.; Cheng, Y.; Galuska, L.; Roy, A.; Lorenz, M.; Chen, B.; Luo, S.; Li, Y.; Hung, C.; Qian, Z.; et al. Tacky Elastomers to Enable Tear-Resistant and Autonomous Self-Healing Semiconductor Composites. *Adv. Funct. Mater.* **2020**, *2000663*, 2000663. https://doi.org/10.1002/adfm.202000663.

(27) Pignanelli, J.; Qian, Z.; Gu, X.; Ahamed, M. J.; Rondeau-Gagné, S. Modulating the Thermomechanical Properties and Self-Healing Efficiency of Siloxane-Based Soft Polymers through Metal–Ligand Coordination. *New J. Chem.* **2020**. https://doi.org/10.1039/D0NJ01119C.

(28) Weller, D. W.; Ma, G.; Galuska, L. A.; Zhang, S.; Stringer, M.; Aracri, S.; Wang, W.; Hong, K.; Gu, X. Strain-Induced Nanocavitation in Block Copolymer Thin Films for High Performance Filtration Membranes. *ACS Appl. Polym. Mater.* **2021**, acsapm.1c00963. https://doi.org/10.1021/acsapm.1c00963.

Understanding the role of polymer topology on molecular deformation and scission under extreme shear using *in situ* neutron scattering

Matthew E. Helgeson, Dept. of Chem. Eng., UC Santa Barbara
Patrick T. Underhill, Dept. of Chem. And Biol. Eng., Rensselaer Polytechnic Institute

Program Scope

Engineered polymers for energy production, efficiency, and recycling/upcycling can experience extreme deformation rates that break chemical bonds along the polymer backbone, leading to mechanical degradation and compromised performance. Modern approaches to engineer this behavior involve the design of topologically complex polymers including branched and star-like architectures. However, previously established relationships between topology and extreme shear rheology of polymers have remained largely empirical due to a lack of methods to characterize fluid and molecular microstructure in extreme flows. The proposed research aims to fill this gap by developing mechanistic, molecular-scale understanding for how topology affects polymer deformation at very high shear rates, and how this deformation drives the breakage of chemical bonds along the polymer. This will be achieved through *in situ* small angle neutron scattering (SANS) measurements and parameter-matched molecular simulations and scattering models that can resolve single-molecule deformations of polymers at extreme shear rates, which will be applied to families of topologically complex polymers where synthetic control will be used to understand how the type and degree of branching on a polymer influence the distribution of molecular deformation and tension at extreme shear rates. Results will be combined with theories for the chemical kinetics of chemical bond scission under tension to generate an *in silico* model to predict the mechanical degradation of polymers observed in *ex situ* experiments. Ultimately, these studies will provide guidelines for engineering polymers to enhance mechanical stability, or conversely to engineer flows that direct the mechanical degradation of polymers for targeted materials properties and applications. This project critically leverages a recently developed *in situ* neutron scattering technique for SANS in high shear rate flows, called capillary rheo-SANS, which will be disseminated to the national neutron scattering community through established collaborations with beam scientists at neutron sources.

Recent Progress

In the previous reporting period, we developed expertise with *in situ* characterization of polymer deformation by leveraging a novel capillary device developed by scientists at NCNR to perform rheo-SANS experiments at shear rates of 10^6 s^{-1} and higher.[1] Experiments to investigate the role of topology at fixed polymer relaxation time are planned, but have been postponed due to delayed re-establishment of in-person experiments at ORNL (due to the COVID-19 pandemic) and NCNR (due to the fuel leak in early 2021). As a result, we have redirected efforts in the current period toward simulation and modeling of scattering from deformed polymers in shear flow in order to have a validated modeling workflow in place for capillary rheo-SANS experiments when they become available.

Adapting and optimizing molecular simulations of polymers at high deformation rates for comparison to scattering measurements. We have implemented Brownian dynamics (BD) simulations to compute the conformations and dynamics in flow of (initially linear) deformed polymers. The model takes the form of a coarse-grained bead-spring chain in which only a few locations on the polymer are explicitly tracked (**Figure 1a**). The solvent is treated implicitly in terms of the impact on the polymer conformations in flow, as well as through excluded volume interactions (EV). Validations of the simulation have been performed. The two most important features for connection with experimental measurements are the nonlinear elasticity due to finite

extensibility (FENE) of the polymers and hydrodynamic interactions (HI) between polymer segments through the suspending solvent. Both of these effects cause the behavior to deviate from simple analytical (Gaussian) approximations.

Using these simulations we have computed how polymer conformations are distorted at high shear rates (**Figure 1b**). We have done this at a range of levels of coarse-graining, i.e. how much detail is explicitly tracked versus averaged. This allows us to determine the optimal balance between speed and accuracy of the simulations. In analyzing the conformations, we have focused on understanding when the assumptions used in interpreting scattering experiments are valid and when the assumptions are not. The output of the simulations include measurement of the probability distribution function (PDF) of displacements between beads *i* and *j*, $\langle \psi_{ij}(\boldsymbol{r}) \rangle$. In this way, the simulations can be used as inputs to a forward scattering analysis and as a way of testing inverse scattering analysis.

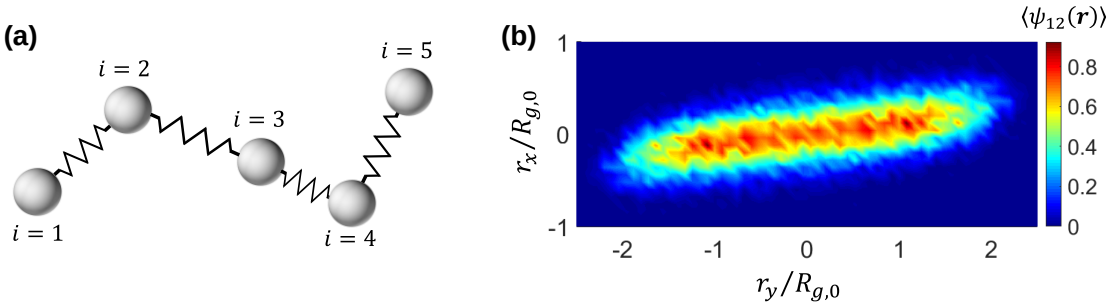

Figure 1. (a) Cartoon of a FENE bead-spring chain with N = 5 beads. **(b)** Representative result for the 2-bead PDF of a FENE chain with $N = 5$ beads including EV and HI at $Wi = 10$, projected into the x-y (flow-gradient) plane. The shape of the PDF indicates that the chain is highly stretched in the flow-direction.

Developing model-independent forward and inverse scattering analysis to extract measures of polymer deformation in flow. The BD simulations were used to develop and validate a model-independent tool to obtain molecular descriptors of deformed polymers in flow from rheo-SANS data. Such an approach is valuable for our purposes, as it is agnostic to the topology of the polymer chain. Previous model-free approaches to analyze scattering from deformed polymers, such as the spherical harmonics approach,[2] assume that deformed chains remain Gaussian in conformation; this assumption is invalid for high shear rate flows of non-Hookean chains. Our analysis aims to overcome this limitation by analyzing scattering from the entire segment density distribution. The analysis scheme has two parts: a forward problem, in which two-dimensional SANS patterns are predicted from a known ensemble of molecular configurations (from simulation); and an inverse problem, in which various parameterizations of the PDF are extracted from a 2D scattering pattern, such as components of the gyration tensor, $\boldsymbol{Q} = \langle \boldsymbol{R_g R_g} \rangle$.

The forward scheme was implemented for calculating SANS patterns either from the full, discretized PDF of bead separations, or from the ensemble-averaged gyration tensor components (depending on the simulation output), and was validated comparisons between simulations on an $N = 5$ bead-spring Hookean chain and the corresponding analytical result for a Gaussian chain at equilibrium. The inverse scheme was validated for estimation of gyration tensor components for a number of simulated chains in flow, including Hookean chains, FENE chains w/o HI, and FENE w/ HI with $N = 2$ and 5, at Weissenberg numbers ranging from near equilibrium (Wi = 0.1) to strongly deformed (Wi = 10). Analysis of the predicted scattering in the q_x-q_y (flow-gradient) plane (**Figure 2a**). Validation was achieved by comparing estimations of the non-zero components of the gyration tensor (Q_{xx}, Q_{yy}, Q_{zz}, Q_{xy}) extracted via the inverse method in the low-q limit with those obtained directly from simulation, which produces quantitative agreement to within numerical precision (**Figure 2b**). Importantly, the non-Gaussian nature of the bead PDF is evident for sufficiently high Wi due to the non-Gaussian signatures of the FENE springs, highlighting the need for an approach that directly expresses the scattering in terms of the PDF. Ongoing efforts are focused on extending the inverse method to extract higher-order moments of the PDF from higher-q scattering data, as will be described below.

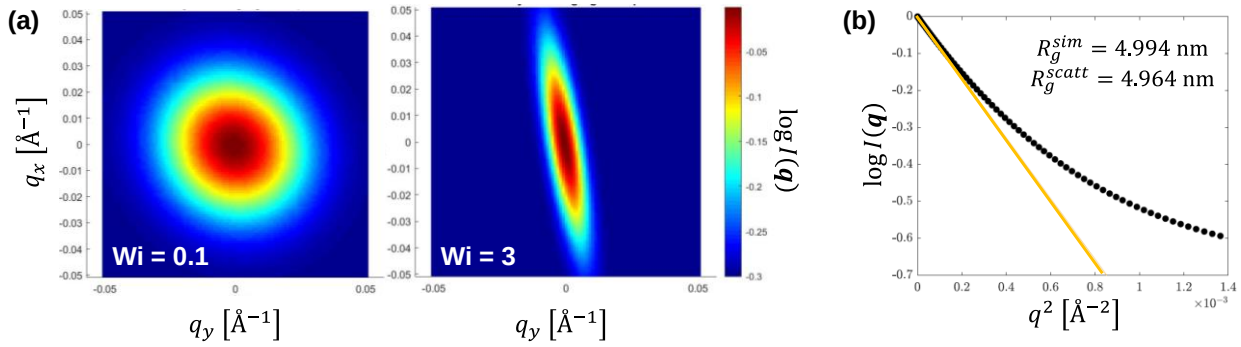

Figure 2. (a) 2D SANS patterns in the flow (y)-gradient (x) plane calculated using $\langle \psi_{ij}(\boldsymbol{r}) \rangle$ of polymers in flow for Wi = 0.1 (left) and Wi = 3 (right). **(b)** Guinier plot for Wi = 0.1. Inset demonstrates quantitative agreement between the radius of gyration obtained directly from the BD simulations (R_g^{sim}) and from the calculated scattering (R_g^{scatt}).

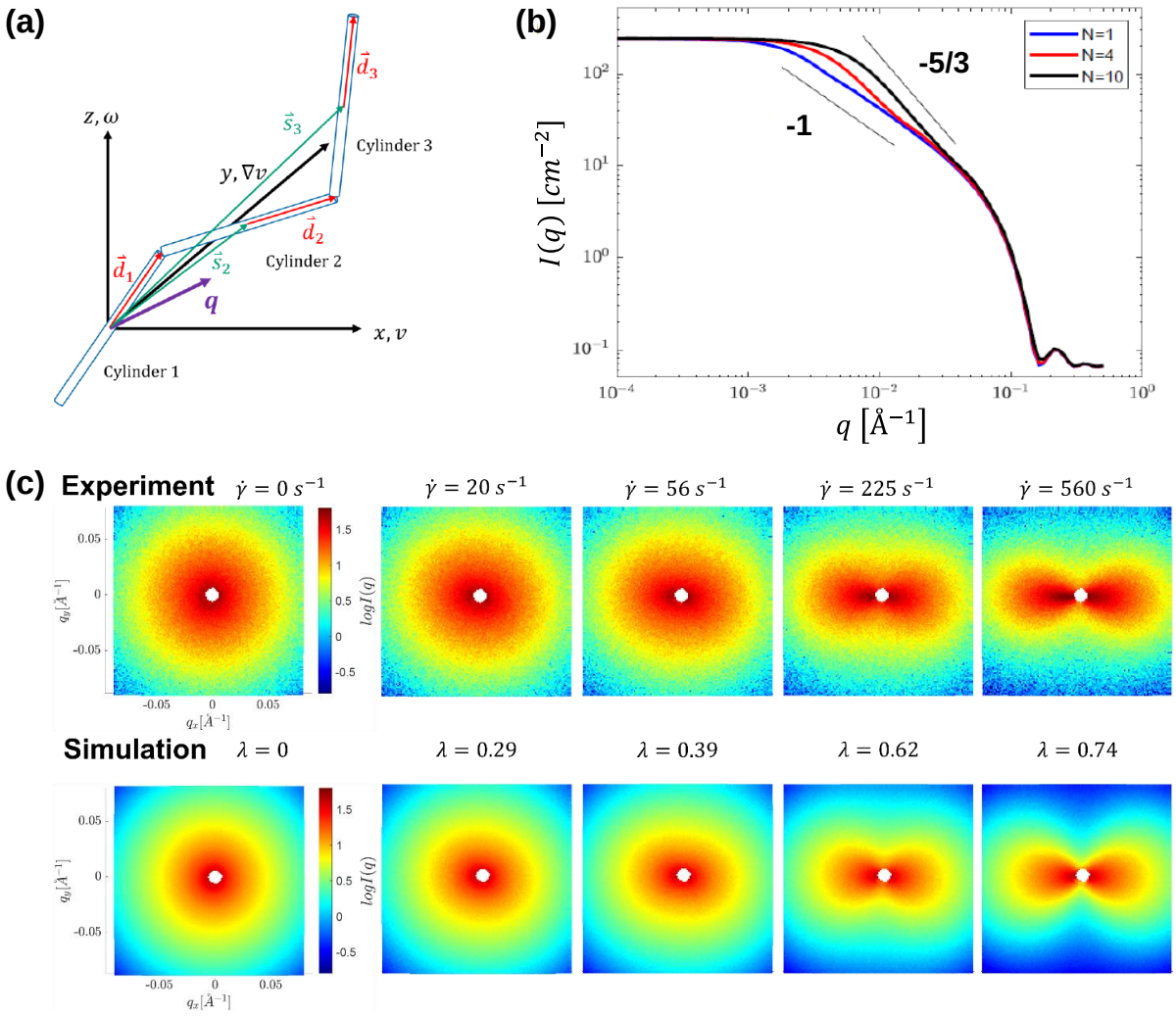

Figure 3. (a) Schematic diagram of the TCCR model for scattering of polymers in flow. **(b)** 1D SANS predictions of the TCCR model at equilibrium (λ = 0) for chains with increasing number of rods, N. Power law slopes of -1 and -5/3 represent those predicted for rigid rods and excluded volume chains, respectively. (c) 2D SANS patterns for wormlike micelles measured using rheo-SANS experiments (top) and predicted by a form of the TCCR model with polydisperse chain length (bottom) for the best-fit values of λ indicated.

Developing a connected-rod scattering model for (semi)flexible polymers in flow. Our first attempts at t modeling the higher-q scattering of deformed chains have involved a thermodynamically-consistent connected rod (TCCR) scattering model for flexible and semi-flexible chains. The initial model formulation involves predictions of the scattering from a linear chain of N (**Figure 3a**). Importantly, although the primitive chain is assumed to be freely-jointed (i.e., no orientational correlations between adjacent rods), the orientation distribution of rods is chosen such that the propagation of orientation along the connected rod-chain is consistent with the overall stretch and orientation of the end-to-end vector of the chain. To achieve this, we incorporated an approach previously developed by Underhill and co-workers,[3] in which the segment orientation distribution is subject to an effective force, whose magnitude is chosen to be thermodynamically consistent with the force required to stretch the contour of the chain using a Boltzmann inversion scheme. The advantages of using a thermodynamically-consistent formulation of the model are that it automatically produces the correct components of $\boldsymbol{Q}$, and that the non-equilibrium configuration of the chain is described by a adjustable parameter, the fractional chain extension λ; as such, the TCCR model can be integrated seamlessly with molecular simulation and the model-independent scattering analyses just presented.

The TCCR model was validated through comparison to both analytical theory and experimental data. In the former case, equilibrium predictions of the TCCR model at equilibrium ($\lambda = 0$) were compared to analytical results for the scattering of various chain models (**Figure 3b**) depending on the relative magnitudes of the persistence length, l_p, and the contour length, L_c. We find that, as N is increased, the predicted shape of the scattering changes from that expected for a rigid rod, to a semi-flexible chain with $2l_p / L_c < N$, and ultimately to a flexible excluded volume chain with $2l_p / L_c << N$ ($N > 10$). In the latter case, anisotropic scattering predictions of the TCCR model in flow were validated by comparing a formulation of the model with polydisperse chain length to experimental rheo-SANS data on a model wormlike micellar surfactant solution whose equilibrium structure was previously characterized,[4] such that all model parameters were independently measured and held fixed except for λ, which was allowed to vary to fit the observed scattering anisotropy. The results of the model (**Figure 3c**) show near quantitative agreement with the measured scattering, with a shear-rate dependence of λ that is consistent with previous observations on semi-flexible polymers in shear flow.

Future Plans

With the various pieces of the combined molecular simulation/scattering modeling framework in place, we will work to integrate these pieces into a fully functioning tool for forward and inverse scattering from across the entire q-range. To achieve this will require mapping of the BD simulation parameters onto the parameters of the TCCR model, as well as integration of the TCCR model of our recently-developed Bayesian approach to the inverse problem, maximum a posteriori scattering inference (MAPSI),[5] in order to extract chain configuration parameters from scattering data In anticipation of the re-establishment of in-person user experiments at ORNL and NCNR in the coming year, we have submitted user proposals for SANS experiments with the capillary rheo-SANS device aimed at validating our new modeling framework on a series of high-molecular weight linear polymers. This will complete the studies described above, and the results will provide, to our knowledge, the first complete integration of experiment, molecular simulation and scattering models to describe the deformation of flowing polymers.

We will then extend this integrated approach to the study of high-shear deformation of nonlinear chain topologies. In experiment, this will be achieved by synthesis and capillary rheo-SANS experiments on a library of topology-defined polymers with equivalent longest relaxation time to probe influence of nonlinear topology on global/local chain deformation at equivalent Wi. In simulation and scattering modeling, this will require extension of the BD simulations and the TCCR model to nonlinear topologies, resulting in a framework that allows branching to be incorporated into the description of the chain and its various parameterizations under deformation.

References

[1] R.P. Murphy, Z.W. Riedel, M.A. Nakatani, P.F. Salipante, J.S. Weston, S.D. Hudson and K.M. Weigandt (2020). Capillary RheoSANS: measuring the rheology and nanostructure of complex fluids at high shear rates. *Soft Matter, 16*(27), 6285-6293.

[2] Z. Wang, C.N. Lam, W.R. Chen, W. Wang, J. Liu, Y. Liu, ... and Y. Wang (2017). Fingerprinting molecular relaxation in deformed polymers. Physical Review X, 7(3), 031003.

[3] H. Pandey and P.T. Underhill (2015). Coarse-grained model of conformation-dependent electrophoretic mobility and its influence on DNA dynamics. Physical Review E, 92(5), 052301.

[4] M.E. Helgeson, T.K. Hodgdon, E.W. Kaler and N.J. Wagner (2010). A systematic study of equilibrium structure, thermodynamics, and rheology of aqueous CTAB/NaNO3 wormlike micelles. Journal of colloid and interface science, 349(1), 1-12.

[5] P.T. Corona, P. T., K.S. Silmore, R. Adkins, C. Lang, M.P. Lettinga, J.W. Swan, L.G. Leal and M.E. Helgeson (2021). Bayesian estimations of orientation distribution functions from small-angle scattering enable direct prediction of mechanical stress in anisotropic materials. Physical Review Materials, 5(6), 065601.

Publications

L.T. Andriano, N. Ruocco, J.D. Peterson, D.P. Olds, S. Costanzo, D. Vlassopoulos, M.E. Helgeson, K. Ntetsikas, N. Hadjichristidis, L.G. Leal, "Microstructural characterization of a star-linear polymer blend under shear flow by using rheo-SANS", *Journal of Rheology*, 2020, 64:663. [DOI: 10.1122/1.5121317]

C.J. Dahlman, N.R. Venkatesan, P.T. Corona, R.M. Kennard, L. Mao, N. Smith, J. Zhang, R. Seshadri, M.E. Helgeson and M.L. Chabinyc, "Structural Evolution of Layered Hybrid Lead Iodide Perovskites – Colloidal Nanocrystals or Ruddlesden-Popper Phases?", *ACS Nano*, 2020, 14(9): 11294-11308. [DOI: 10.1021/acsnano.0c03219]

P.T. Corona, K.S. Silmore, C. Lang, P. Lettinga, J.W. Swan, L.G. Leal and M.E. Helgeson, "Bayesian estimations of orientation distribution functions from small-angle scattering enable direct prediction of mechanical stress in anisotropic materials", *Physical Review Materials*, 2021, 5(6): 065601. [DOI: 10.1103/PhysRevMaterials.5.065601]

J. Zhang, A. Jurzyk, M.E. Helgeson and L.G. Leal, "Modeling Orthogonal Superposition Rheometry to Probe Nonequilibrium Dynamics of Entangled Polymers", *Journal of Rheology*, 2021, 65(5): 983-998. [DOI: 10.1122/8.0000272]

P.T. Corona, B. Berke, M. Guizar-Sicairos, L.G. Leal, M. Liebi and M.E. Helgeson, "Fingerprinting soft material nanostructure response to complex flow histories", Submitted.

J. Zhang, G.S. Smith, P.T. Corona, L.G. Leal and M.E. Helgeson, "A thermodynamically-consistent connected rod model for small angle scattering of polymers in flow", Submitted.

Novel quantum phenomena in geometrically frustrated magnets near the metal-insulator phase boundary

Xianglin Ke, Department of Physics and Astronomy, Michigan State University, MI 48824

Program Scope

Geometric frustration, which arises from the competing interactions between magnetic ions placed on regular lattice sites, can often lead to a large degeneracy of spin states, giving rise to a rich variety of unconventional magnetic phases. To date, most of the research on frustrated magnets has focused on insulating materials, whose ground state properties are mainly determined by short-range interactions between localized spins. In contrast, fewer studies have been performed on metallic frustrated magnets, particularly on geometrically frustrated magnets in close proximity to a metal-insulator transition, i.e., proximate itinerant frustrated magnets. The primary objective of this proposal is to study novel quantum phenomena in geometrically frustrated magnets near the metal-insulator phase boundary and understand how the interplay and cooperation between electron itinerancy and magnetic frustration determines materials' physical properties.

Recent Progress

Since this program was awarded in September 2018, we have been investigating various frustrated magnetic systems as described below.

A. Ruthenates and other frustrated magnets. The electron and magnetic correlation of d and f electrons has been a core research topic in condensed matter physics. In ruthenates, ruthenium ions possess extended 4d orbitals with reduced electron Coulomb repulsion energy and enhanced orbital hybridization, providing a character intermediate between localized and itinerant orbitals. This, combined with the large crystal electric field, strong spin-lattice coupling, and the non-negligible spin-orbit coupling of ruthenium ions, enables ruthenates to display a multitude of interesting electronic and magnetic properties. We have demonstrated complex magnetism in $Ba_5Ru_3O_{12}$, a compound consisting of isolated Ru_3O_{12} trimers [1]. We showed that this system develops long-range antiferromagnetic ordering at T_N ~ 60 K without structural distortion or metal-insulator transition, which is in sharp contrast to other Barium Ruthenate trimer systems such as 9R-$BaRuO_3$ and $Ba_4Ru_3O_{10}$. A complex magnetic structure was revealed which was attributed to different degree of hybridization (localization) of Ru-atoms and strong spin-frustration in this system. We have also studied the important role of interactions between 4d and 4f electrons of Ru ions and rare earth ions (R) in $Ba_3RRu_2O_9$ system which exhibits large magnetodielectric coupling [2]. In particular, we showed that the strong Ru(4d) - Ho(4f) coupling leads to cooperative magnetic ordering in multiferroic $Ba_3HoRu_2O_9$. At low

temperature a phase coexistence was observed and a complex spin structure was solved that may be responsible for the ferroelectric polarization observed in this system [3].

We have also studied the magnetic competition in $GeNi_2O_4$ [4] and γ-Fe_2WO_6 [5] systems. $GeNi_2O_4$ is a spinel compound where the magnetic Ni ions occupy on a pyrochlore lattice and give rise to strong magnetic frustration. We have established a *T-H* phase diagram where a new magnetic phase is revealed in the presence of magnetic field applied along the [111] direction. This new phase is associated with field-induced spin-reorientation, resulting from the synergetic effect of magnetic anisotropy, Zeeman interaction, and competing exchange interactions. And Fe_2WO_6 has been of significant interest recently for its photocatalytic activity and possible uses in photoelectrochemical devices. We found that the magnetic ground state of γ-Fe_2WO_6 exhibits two coexisting phases which are sensitive to the structural distortion. Furthermore, our first-principles calculations showed that these two magnetic phases are correlated with electronic properties, with one being insulating and the other being metallic. These features suggest that γ-Fe_2WO_6 exhibits competing energetic states in which spin, charge, and lattice degrees of freedom are strongly coupled to each other.

B. Quasi-1D spin chains. We have a unique quasi-1D compound $Cu_2(OH)_3Br$ in which Cu^{2+} ions with S = 1/2 form a quasi-2D distorted triangular lattice. Despite the quasi-2D triangular lattice of Cu^{2+} ions, very interestingly we find that the local coordinates of Cu ions relative to Br ions, combined with the magnetic frustration resulting from the triangular lattice geometry, leads to quasi-1D nature of magnetic exchange interaction between Cu ions. In another words, this system can be effectively treated as a unique quantum antiferromagnet consisting of weakly coupled, alternating ferromagnetic and antiferromagnetic S = 1/2 chains, as illustrated in Fig 1(a). As a result, this system exhibits the coexistence of two different magnetic quasi-particles, i.e., magons and spinons associated with ferromagnetic chains and antiferromagnetic chains respectively. These two magnetic quasi-particles interact with each other via the weak interchain coupling, opening spin gaps and inducing spectral asymmetry in the magnetic excitations (Fig. 1(b)). This study presents a new toy model which opens an unexplored paradigm where one can study the interaction between two different types of magnetic quasiparticles, magnons and spinons [6].

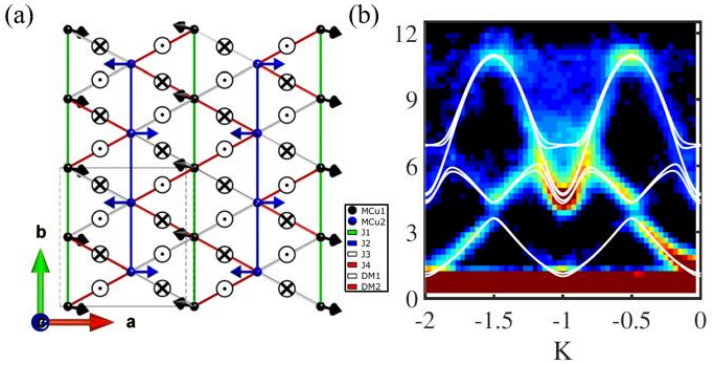

Figure 1. (a) Schematics of spin structure of Cu^{2+} ions and the relevant exchange interactions in the system, showing alternating ferromagnetic and antiferromagnetic quasi-1D chains. (b) Magnetic excitation spectra of $Cu_2(OH)_3Br$ and the comparison to linear spin-wave calculations. The lower-energy branches are associated with wave fittings. ferromagnetic chains (denoted by green line) while the higher-energy branches are associated with antiferromagnetic chains (blue lines). The white curves are linear spin

C. Topological properties in metallic frustrated systems. We have extended our research to metallic frustrated systems, in which the integration of magnetism and nontrivial band topology (induced by the lattice geometry) can lead to exotic quantum phenomena. Rare earth half-Heuslers LnPtBi have been proposed to be candidates of topological materials. We show that DyPtBi hosts a delicate balance between two different magnetic ground states, which can be controlled by a moderate magnetic field [7]. Furthermore, it exhibits giant anomalous Hall effect ($\sigma^A = 1540\ \Omega^{-1}\ cm^{-1}, \theta_{AHE} = 24\ \%$) in a field-induced Type-I spin structure (Figure 2), presumably attributed to the enhanced Berry curvature associated with avoided band-crossings near the Fermi energy and / or non-zero spin chirality. The latter mechanism points DyPtBi towards a rare potential realization of anomalous Hall effect in an antiferromagnet with face-center-cubic lattice.

We have also investigated magnetic and electronic properties of metallic systems with Kagome lattice, including Fe_3Sn_2 [8] and YMn_6Sn_6 [9]. In addition to the potential magnetic frustration associated with the Kagome lattice structure, the intrinsic spin-orbit coupling associated with the lattice gives rise to artificial magnetic flux and opens the bandgap on the Dirac points, resulting in nontrivial electronic bands. For instance, we have showed that the magnetic ground state of $YMn_6Sn_{6-x}Ga_x$ ($0 \le x \le 0.61$) evolves from incommensurate antiferromagnet to ferromagnet with increasing Ga substitution x, a feature which is accompanied by the decrease in magnetoresistance. Furthermore, the topological Hall effect observed in the pristine compound is absent in the Ga-substituted ones; instead, the anomalous Hall effect persists which may be associated with the Berry curvature of gapped Dirac bands near the Fermi energy. These results suggest strong correlation between electronic properties and magnetism in this topological magnet that can be readily tuned via Ga substitution.

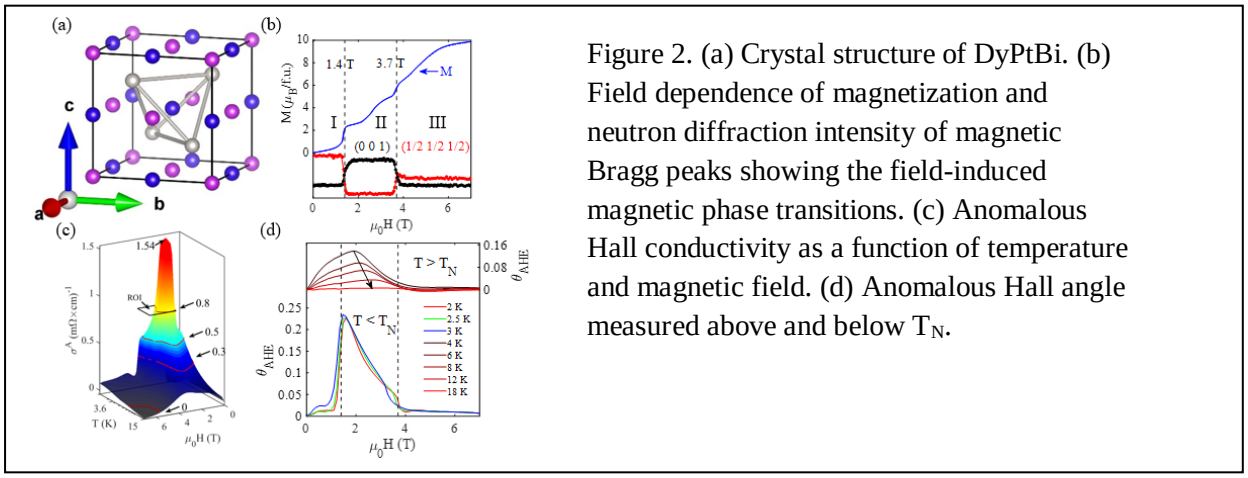

Figure 2. (a) Crystal structure of DyPtBi. (b) Field dependence of magnetization and neutron diffraction intensity of magnetic Bragg peaks showing the field-induced magnetic phase transitions. (c) Anomalous Hall conductivity as a function of temperature and magnetic field. (d) Anomalous Hall angle measured above and below T_N.

Future Plans

Our initial studies of metallic frustrated systems discussed above have shown that magnetism and topological electronic properties intertwine each other. In the future we will study the effect of lattice geometry on magnetism and topological electronic properties and the application of topological concept to magnetism.

References

Publications

1. T. Basu, F. Y. Wei, Q. Zhang, Y. Fang, and **X. Ke**, "*Complex magnetic structure in $Ba_5Ru_3O_{12}$ with isolated Ru_3O_{12} trimer*", Phys. Rev. Materials **4**, 114401 (2020).
2. T. Basu, V. Caignaert, S. Ghara, **X. Ke**, A. Pautrat, S. Krohns, A. Loidl, and B. Raveau, "*Enhancement of magnetodielectric coupling in 6H-perovskites $Ba_3RRu_2O_9$ for behavior rare-earth cations (R=Ho, Tb)*", Phys. Rev. Materials **3**, 114401 (2019).
3. T Basu, V Caignaert, F Damay, TW Heitmann, B Raveau, and **X Ke**, "*Cooperative Ru(4d)-Ho(4f) magnetic ordering and phase coexistence in the 6H perovskite multiferroic $Ba_3HoRu_2O_9$*", Phys. Rev. B **102**, 020409 (R) (2020).
4. T. Basu, T. Zou, Z. Dun, C.R. Dela Cruz, Tao Hong, H.B. Cao, K.M. Taddei, H.D. Zhou, and **X. Ke**, "*Magnetic field induced phase transition in spinel $GeNi_2O_4$*", Phys. Rev. B, **102**, 134421(2020).
5. M. Sretenovic, S. Okamoto, G. Peiker, T. X. Tang, H. Zhang, C.Q. Xu, T. W. Heitmann, Q. Zhang, C. R. dela Cruz, and **X. Ke**, "*Competing energetic states in γ-Fe_2WO_6 with strong spin-charge-lattice coupling*", Phys. Rev. B **104**, 134413 (2021).
6. H. Zhang, Z. Zhao, D. Gautreau, M. Raczkowski, A. Saha, V.O. Garlea, H. Cao, T. Hong, H. O. Jeschke, Subhendra D. Mahanti, T. Birol, F. F. Assaad, and **X. Ke**, "*Coexistence and interaction of spinons and magnons in anantiferromagnetwith alternating antiferromagnetic and ferromagnetic quantum spin chains*", Phys. Rev. Lett. **125**, 037204 (2020).
7. H. Zhang, Y. L. Zhu, Y. Qiu, W. Tian, H. B. Cao, Z. Q. Mao, and **X. Ke**, "*Field-induced magnetic phase transitions and the resultant giant anomalous Hall effect in antiferromagnetic half-Heusler DyPtBi*", Phys. Rev. B **102**, 094424 (2020).
8. H. Zhang, C.Q. Xu, and **X. Ke**, "*Topological Nernst effect, anomalous Nernst effect, and anomalous thermal Hall effect in Dirac semimetal Fe_3Sn_2*", Phys. Rev. B **103**, L201101 (2021).
9. C.Q. Xu, T. W. Heitmann, H. Zhang, Xiaofeng Xu, and **X. Ke**, "*Magnetic phase transition, magnetoresistance, and anomalous Hall effect in Ga-substituted YMn_6Sn_6 with a ferromagnetic kagome lattice*", Phys. Rev. B **104**, 024413 (2021)

Role of Organic Cations in Organic-Inorganic Perovskite Solar Cells

Seung-Hun Lee (PI) and Joshua J. Choi (Co-PI)

University of Virginia

Program Scope

Hybrid organic-inorganic perovskites (HOIPs) are among the most promising next generation solar cell materials.[1, 2] HOIPs are unique in that they combine low-cost solution processability with superb electronic quality that is comparable to, or surpasses, that of the state-of-the-art epitaxial grown semiconductors. Moreover, the crystal structure and optoelectronic properties of HOIPs are widely tunable by using different organic molecules and inorganic components.[3, 4]

In this program, the structure and properties of HOIPs are investigated at multiple length scales to achieve a full understanding of the microscopic mechanism of the photovoltaic effect. Specifically, this research program is testing the hypothesis that the structure and dynamics of organic cations and their associated electric multipoles cause screening and protection of charge carriers which results in long carrier lifetime and high solar cell efficiency. The experimental approach is to employ several complimentary techniques that can probe from atomic to macroscopic properties: molecular structure and dynamics at the microscopic level, charge recombination at the mesoscopic level, and the solar cell efficiency at the macroscopic level. Neutron diffraction and time-of-flight neutron scattering spectroscopy are used to characterize the structure and rotational and vibrational dynamics. Optical spectroscopy, electrical transport measurements and solar cell fabrication and testing are employed to determine the impact of organic cations on the bulk properties and photovoltaic performance of the three- and two-dimensional HOIPs.

Recent Progress

We performed time-of-flight (TOF) inelastic neutron scattering (INS) experiments and first-principles density-functional theory (DFT) calculations to investigate the lattice vibrations in three-dimensional $MAPbI_3$ (methylammonium lead iodide, $MA^+ = CH_3NH_3^+$) and two-dimensional $(BA)_2PbI_4$ (butylammonium lead iodide, $BA^+ = CH_3(CH_2)_3NH_3^+$). The detailed results, such as their time-of-flight neutron scattering data, vibrational energy fractions, and energies and animations of phonon modes, are available for researchers in our website: https://discovery.phys.virginia.edu/research/groups/nextlab/research.html

Our TOF neutron data as a function of temperature indicate that optical phonons lose temporal coherence gradually with increasing temperature in both three-dimensional and two-dimensional systems, which is due to the fact that they are ionic crystals. We have also performed low energy TOF neutron scattering experiments on $(BA)_2PbI_4$ to investigate the rotational dynamics of BA molecule as a function of temperature. Our detailed analysis on vibrational and rotational dynamics

in $(BA)_2PbI_4$ indicates that the temperature dependence of either inorganic phonon modes or hybrid phonon modes does not show predominant correlations with its photoluminescence properties. On the other hand, the rotational dynamics of organic BA molecule dominates the intensity of photoluminescence.

To verify our conclusion with other local probe, we have collaborated a muon group in Japan (Dr. Kadono's group) to perform muon scattering experiments on $MAPbI_3$. Our muon data also supported our conclusion that the rotational dynamics of organic molecules dominates the optoelectronic performance of 3D and 2D HOIPs.

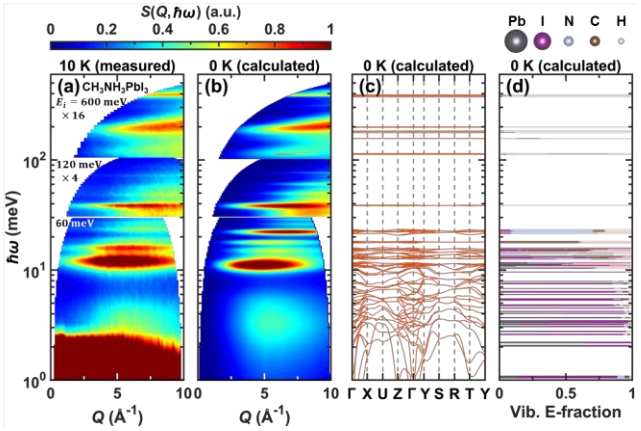

Fig. 1. Phonon spectra of $MAPbI_3$. ((a) and (b)) Color contour maps of the experimental (a) and calculated (b) phonon spectra $S(Q, \hbar\omega)$. (c) DFT phonon band structure of orthorhombic $MAPbI_3$ along high-symmetry Q points. (d) Vibrational energy fractions (Vib. E-fraction) at the Γ point for each phonon mode.

Future Plans

In order to investigate the relationship between the rotational dynamics of organic molecule and photoelectronic properties, we plan to study two-dimensional (2D) HOIPs with different organic molecules, such as $(PEA)_2PbI_4$ (phenethyl-ammonium lead iodide, $PEA^+ = C_6H_5(CH_2)_2NH_3^+$). PEA molecule has a benzene at one end, and thus its rotational dynamics is expected to be very limited, compared to $(BA)_2PbI_4$ that does not have benzene. By analyzing vibrational as well as rotational dynamics in detail using neutron scattering, DFT calculations, and point group theory analysis, we will determine the rotational and vibrational contributions in the neutron signal, and compare them with the photoelectronic properties of $(PEA)_2PbI_4$. We will also perform muon scattering measurements on both $(PEA)_2PbI_4$ and $(PEA)_2PbI_4$.

References

1. E. H. Jung *et al.*, Efficient, stable and scalable perovskite solar cells using poly (3-hexylthiophene). *Nature* **567**, 511 (2019)
2. Brenner, T. M., Egger, D. A., Kronik, L., Hodes, G. and Cahen, D. Hybrid organic—inorganic perovskites: low-cost semiconductors with intriguing charge-transport properties. *Nature Reviews Materials* **1**, 15007 (2016).
3. Chen, T., Chen, W.-L., Foley, B. J., Lee, J., Ruff, J. P. C., Ko, J. Y. P., Brown, C. M., Harriger, L. W., Zhang, D., Park, C., Yoon, M., Chang, Y.-M., Choi, J. J. and Lee, S.-H. Origin of long lifetime of band-edge charge carriers in organic–inorganic lead iodide perovskites. *PNAS* **114**, 7519-7524 (2017).

4. Chen, T., Foley, B. J., Park, C., Brown, C. M., Harriger, L. W., Lee, J., Ruff, J., Yoon, M., Choi, J. J. and Lee, S.-H. Entropy-driven structural transition and kinetic trapping in formamidinium lead iodide perovskite. *Science Advances* **2**, e1601650 (2016)

Publications

1. *Organic Molecular Dynamics and Charge-carrier Lifetime in Lead Iodide Perovskite $MAPbI_3$*, A. Koda, H. Okabe, M. Hiraishi, R. Kadono, K. A. Dagnall, J. J. Choi , S.-H. Lee, Proc. Natl. Acad. Sci., under revision (2021).
2. *Freezing of a disorder induced spin liquid with strong quantum fluctuations*, X. Hu, D. M. Pajerowski, D. Zhang, A. A. Podlesnyak, Y. Qiu, Q. Huang, H. Zhou, I. Klich, A. I. Kolesnikov, M. B. Stone, S.-H. Lee, Phys. Rev. Lett. **127**, 017201 (2021).
3. *Temporally decoherent and spatially coherent vibrations in metal halide perovskites*, D. Zhang, M. Kofu, W.-L. Chen, A. Z. Chen, M. Yoon, C. M. Raghavan, T.-P. Chen, D. L. Abernathy, B. J. Foley, C. M. Brown, G. Xu, L. W. Harriger, R. Kajimoto, M. Nakamura, S. Ohira-Kawamura, C.-W. Chen, Y.-M. Chang, J. J. Choi, S.-H. Lee, Phys. Rev. B **102**, 224310 (2020).
4. *Ultralow thermal conductivity of two-dimensional metal halide perovskites*, A. Giri, A. Z. Chen, A. Mattoni, K. Aryana, D. Zhang, X. Hu, S.-H. Lee, J. J. Choi, and P. Hopkins, Nano Letters **20**, 3331-3337 (2020).
5. *Relationship between the Nature of Monovalent Cations and Charge Recombination in Metal Halide Perovskites*, K. A. Dagnall, B. J. Foley, S. A. Cuthriell, M. R. Alpert, X. Deng, A. Z. Chen, Z. Sun, M. C. Gupta, K. Xiao, S.-H. Lee, Y.-Z. Ma, J. J. Choi, ACS Applied Energy Materials **3**, 1298-1304 (2020).
6. *Crystal structure and rotational dynamics of a two-dimensional metal halide perovskite $(OA)_2PbI_4$*, X. Hu, D. Zhang, A. Z. Chen, E. N. Holmgren, Q. Zhang, D. M. Pajerowski, M. Yoon, G. Xu, J. J. Choi, S.-H. Lee, J. Chem. Phys. **152**, 014703 (2020).

Scattering and Spectroscopic Studies of Quantum Materials

Young Lee (Stanford University and SLAC National Accelerator Laboratory)

Hongchen Jiang (SLAC National Accelerator Laboratory

Jiajia Wen (SLAC National Accelerator Laboratory)

Program Scope

We focus on studying quantum materials with a comprehensive effort involving crystal growth, sample characterization, neutron and x-ray scattering, and theory. A primary goal is to synthesize and measure materials with unusual quantum properties, such as quantum spin liquids which have highly entangled ground states. Such states may be relevant to our understanding of high-temperature superconductivity and has possible applications in quantum information. New synthesis techniques for growing high quality single crystals are developed, and the unique crystals serve as the basis for detailed inelastic neutron scattering and resonant x-ray scattering experiments of the excitation spectrum. We aim to expand the base of spin liquid compounds and associated experimental signatures and compare with theoretical predictions based on realistic Hamiltonians. In addition, we will study the effects of disorder on the quantum ground states, including intertwined spin and charge order in unconventional superconductors and quantum spin liquids.

Recent Progress

We performed comprehensive studies of several quantum spin liquid compounds, involving both experiment and theory. In barlowite (the parent compound of the Zn-barowite QSL), magnetic neutron scattering indicates a magnetically ordered ground state, and our numerical studies show the stability of a nearby valence bond crystal state that is competitive in energy.[1] The barlowite family appears to intertwine aspects of both valence bond crystal order and spin order, indicating that these states are closely competitive with the quantum spin liquid phase, see Figure 1. Surprisingly, even with only 50% Zn-substitution, the compound exhibits spin liquid behavior, attesting to the robustness of the QSL on the kagome layers. Moreover, we performed the first resonant inelastic x-ray scattering (RIXS) measurements on new quantum spin liquid (QSL) materials.[2] Using single crystal samples of Zn-barlowite and barlowite, we measured spin excitations which persist to energies as high as 14 times the magnetic exchange energy scale. This is the first indication of significant scattering from multiple pairs of spinons (or spinon-antispinon) in the kagome QSL. The high energy spectrum in barlowite is found to have similar features as that in Zn-barlowite indicating that spinon-based scattering can dominate at high energies even if magnetic order occurs at low temperatures.

We developed a new method to grow large single crystals of Zn-barlowite, which is significant since hydrothermal-zone crystal growth of materials containing highly reactive F ions has not been previously achieved. Furthermore, our experiments and analysis show that the effects of disorder (an important issue) are less significant in Zn-barlowite compared to herbertsmithite. This effort involved a variety of synchrotron x-ray measurements (scattering and spectroscopy) probing multiple length scales, as well as complementary first-principles calculations. [3] We precisely determined the population of and the structural environment around the impurities, which is crucial information to interpret the low energy physics of the ground state. With this structural information, we can better understand the magnetic properties. We investigated how the spin-gaps in the kagome QSL materials Zn-barlowite and herbertsmithite are formed upon cooling into the ground state.[4] Using NMR techniques, we discovered that the spin gap is spatially inhomogeneous, likely a result of the small number of excess Cu impurities in between the kagome layers. The evidence confirming a spin gap in the bulk material is key in classifying the QSL ground state.

	Barlowite 1	Barlowite 2	$Zn_{0.56}$	$Zn_{0.95}$
Formula	$Cu_4(OH)_6FBr$	$Cu_4(OH)_6FBr$	$Cu_{3.44}Zn_{0.56}(OH)_6FBr$	$Cu_{3.05}Zn_{0.95}(OH)_6FBr$
Form	Powder + small crystals	Crystals	Crystals	Powder + small crystals
Kagome Triangles	All distorted	¼ equilateral, ¾ distorted	All equilateral	All equilateral
Symmetry @ T = 100 K	Orthorhombic, *Pnma*	Hexagonal, $P6_3/m$	Hexagonal, $P6_3/mmc$	Hexagonal, $P6_3/mmc$
Structural Bond Pattern in the Kagome Layer	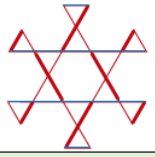	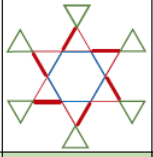		
Kagome Magnetism	Magnetic order with orthorhombic symmetry	Predicted VBC / Induced pinwheel $q=0$ order	Quantum spin liquid	Quantum spin liquid

Figure 1. Quantum ground states stabilized by modulations of the kagome lattice. Structural and magnetic characteristics are tabulated. The second to last row shows the magnetic interactions on the kagome planes of barlowite 1, barlowite 2, and Zn-substituted barlowite. The thickness of the line indicates bond strength as expressed through its Cu–O–Cu bond angle. In Zn0.56 and Zn0.95, the kagome motif consists only of equilateral triangles (green); however, in barlowite 2 the kagome motif is expanded due to a mix of equilateral (green) and distorted (red/blue) triangles. Taken from Ref [1].

We performed neutron scattering measurements of the spin correlations in superconducting $La_{1.88}Sr_{0.12}CuO_4$. We determined that both the static and dynamic stripes are tilted by about 3 degrees with respect to the underlying crystallographic axes. We simultaneously performed density matrix renormalization group (DMRG) calculations which show that the anisotopy of the hopping term t' is important to describe the stripe state in this high-T_C superconductor. [5] We have also used x-ray scattering measurements to better understand the charge density wave (CDW) order in $La_{2-x}Sr_xCuO_4$ superconductors. This involved measurements at the LCLS using a high-field pulsed magnet. These results suggest the simultaneous presence of two types of CDW in the samples, on strongly intertwined with the superconductivity and one strongly intertwined with the spin density waves. We find that short-range CDW correlations are compatible with local superconducting pairing.

We studied the lightly doped Kitaev QSL on the honeycomb lattice within the t-J_K model using DMRG. Upon light doping, we find that the ground state of the system has quasi-long-range

charge-density-wave correlations coexisting with superconducting correlations which oscillate in sign. [6] Although these correlations fall rapidly at long distances, this is never-the-less the first example where a pair-density wave is the leading instability in the pairing channel on the honeycomb lattice. Our results may be relevant to Na_2IrO_3 and α-$RuCl_3$ upon doping. We have also performed DMRG studies of square lattice t−J model with small hole doping. We include frustration in the form of a second-neighbor exchange coupling such that the undoped parent state is a QSL. In contrast to the relatively short-range superconducting correlations that have been observed in the absence of frustration, the doped QSL has stronger power-law SC correlations. [7] Additionally we addressed the nature of an enigmatic gapless paramagnetic phase in the antiferromagnetic Kitaev model, under an intermediate magnetic field perpendicular to the plane. Combining theoretical and numerical efforts, we identify this gapless phase as a U(1) quantum spin liquid with spinon Fermi surfaces. [8] We also revealed the nature of continuous quantum phase transitions involving this U(1) quantum spin liquid, and obtain a phase diagram of the Kitaev model as a function of bond anisotropy and perpendicular magnetic field.

Future Plans

We will investigate the spin excitations in the kagome QSL materials (including our new Zn-barlowite single crystals) with neutron scattering in high magnetic fields (up to 14 Tesla). We will focus on changes to the low-energy kagome spin fluctuations as the spin-gap is closed with fields above ~10 Tesla, which is indicative of a quantum phase transition. We will perform DMRG calculations of the spin Hamiltonian in high fields to support the analysis of the data. We will also perform DMRG calculations on the QSL states found on the triangular lattice and the honeycomb lattice (Kitaev model). In these cases, we will investigate how longer-range magnetic or hopping interactions affect the QSL, and whether doping with holes can give rise to superconducting correlations.

We try to better understand the nematic phase transition in $Tm_{1-x}Y_xVO_4$ using neutron scattering data. We will investigate whether the doped system shows stronger effects of quantum critical fluctuations near the critical point, and we will model the diffuse scattering. We will further investigate the charge density wave (CDW) correlations in the cuprate superconductors in high magnetic fields, using pulsed fields at the LCLS. We will compare samples which have the low temperature orthorhombic and the low temperature tetragonal structures to better understand the intriguing relationship between the CDW and the superconductivity. In parallel, DMRG calculations in high fields will be performed to compare with the experiments.

References

1. **Materializing rival ground states in the barlowite family of kagome magnets: quantum spin liquid, spin ordered, and valence bond crystal states**, R. W. Smaha, W. He, J. M. Jiang, J. Wen, Y.-F. Jiang, J. P. Sheckelton, C. J. Titus, S. G. Wang, Y.-S. Chen, S. J. Teat, A. A. Aczel, Y. Zhao, G. Xu, J. W. Lynn, H.-C. Jiang, Y.S. Lee, npj Quantum Mater., 5, 23 (2020).

2. **High energy spin excitations in the quantum spin liquid candidate Zn-barlowite probed by resonant inelastic x-ray scattering**, Rebecca W. Smaha, Jonathan Pelliciari, Ignace Jarrige, Valentina Bisogni, Aaron T. Breidenbach, Jack Mingde Jiang, Jiajia Wen, Hong-Chen Jiang, and Young S. Lee, arXiv:2108.11506, **submitted.**
3. **Site-specific structure at multiple length scales in kagome quantum spin liquid candidates,** R.W. Smaha, I. Boukahil, C. J. Titus, J. M. Jiang, J. P. Sheckelton, W. He, J.-J. Wen, J. Vinson, S. G. Wang, Y.-S. Chen, S. J. Teat, T. P. Devereaux, C. D. Pemmaraju, and Y. S. Lee, Phys. Rev. Materials, 4, 124406 (2020).
4. **Emergence of spin singlets with inhomogeneous gaps in the kagome lattice Heisenberg antiferromagnets Zn-barlowite and herbertsmithite**, Jiaming Wang, Weishi Yuan, Philip M. Singer, Rebecca W. Smaha, Wei He, Jiajia Wen, Young S. Lee, and Takashi Imai, Nature Physics (2021), https://doi.org/10.1038/s41567-021-01310-3.
5. **Prevalence of tilted stripes in $La_{1.88}Sr0.12CuO_4$ and the importance of *t*' in the Hamiltonian**, W. He, J.-J. Wen, H.-C. Jiang G. Xu, W. Tian, T. Taniguchi, Y. Ikeda, M. Fujita, and Y. S. Lee, arXiv:2107.10264, **submitted.**
6. **Precursor of pair-density wave in doping Kitaev spin liquid on the honeycomb lattice,** Cheng Peng, Yi-Fan Jiang, Thomas P. Devereaux, Hong-Chen Jiang, *npj Quantum Mater.* **6,** 64 (2021).
7. **High Temperature Superconductivity in a Lightly Doped Quantum Spin Liquid,** Hong-Chen Jiang and Steven A. Kivelson, Phys. Rev. Lett. 127, 097002 (2021).
8. **Field-induced quantum spin liquid in the Kitaev-Heisenberg model and its relation to α-$RuCl_3$**, Yi-Fan Jiang, Thomas P. Devereaux, Hong-Chen Jiang, Phys. Rev. B **100**, 165123 (2019).

Publications

1. **Observation of two types of charge-density-wave orders in superconducting $La_{2-x}Sr_xCuO_4$,** J.J. Wen, H. Huang, S.-J. Lee, H. Jang, J. Knight, Y. S. Lee, M. Fujita, K. M. Suzuki, S. Asano, S. A. Kivelson, C.-C. Kao, J.-S. Lee, Nature Communications 10, 3269 (2019).
2. **Field-induced quantum spin liquid in the Kitaev-Heisenberg model and its relation to α-$RuCl_3$**, Yi-Fan Jiang, Thomas P. Devereaux, Hong-Chen Jiang, Phys. Rev. B **100**, 165123 (2019).
3. **Materializing rival ground states in the barlowite family of kagome magnets: quantum spin liquid, spin ordered, and valence bond crystal states**, R. W. Smaha, W. He, J. M. Jiang, J. Wen, Y.-F. Jiang, J. P. Sheckelton, C. J. Titus, S. G. Wang, Y.-S. Chen, S. J. Teat, A. A. Aczel, Y. Zhao, G. Xu, J. W. Lynn, H.-C. Jiang, Y.S. Lee, npj Quantum Mater., 5, 23 (2020).
4. **Site-specific structure at multiple length scales in kagome quantum spin liquid candidates,** R.W. Smaha, I. Boukahil, C. J. Titus, J. M. Jiang, J. P. Sheckelton, W. He, J.-J.

Wen, J. Vinson, S. G. Wang, Y.-S. Chen, S. J. Teat, T. P. Devereaux, C. D. Pemmaraju, and Y. S. Lee, Phys. Rev. Materials, 4, 124406 (2020).

5. **Doping Quantum Spin Liquids on the Kagome Lattice,** Cheng Peng, Yi-Fan Jiang, Dong-Ning Sheng, and Hong-Chen Jiang, Adv. Quantum Technol. 2000126 (2021).
6. **Precursor of pair-density wave in doping Kitaev spin liquid on the honeycomb lattice,** Cheng Peng, Yi-Fan Jiang, Thomas P. Devereaux, Hong-Chen Jiang, *npj Quantum Mater.* **6,** 64 (2021).
7. **Emergence of spin singlets with inhomogeneous gaps in the kagome lattice Heisenberg antiferromagnets Zn-barlowite and herbertsmithite**, Jiaming Wang, Weishi Yuan, Philip M. Singer, Rebecca W. Smaha, Wei He, Jiajia Wen, Young S. Lee, and Takashi Imai, Nature Physics (2021), https://doi.org/10.1038/s41567-021-01310-3.
8. **High Temperature Superconductivity in a Lightly Doped Quantum Spin Liquid,** Hong-Chen Jiang and Steven A. Kivelson, Phys. Rev. Lett. 127, 097002 (2021).
9. **Superconductivity in the doped Hubbard model and its interplay with next-nearest hopping *t′***, Hong-Chen Jiang and Thomas Devereaux. Science 365, 1424-1428 (2019).
10. **Kondo physics in antiferromagnetic Weyl semimetal $Mn_{3+x}Sn_{1-x}$ films**, Durga Khadka, T. R. Thapaliya, Sebastian Hurtado Parra, Xingyue Han, Jiajia Wen, Ryan F. Need, Pravin Khanal, Weigang Wang, Jiadong Zang, James M. Kikkawa, Liang Wu and, S. X. Huang, *Sci. Adv.* 2020; **6, 35,** eabc1977 Aug. 28 (2020).
11. **Anomalous Hall and Nernst effects in epitaxial films of topological kagome magnet Fe_3Sn_2**, Durga Khadka, T. R. Thapaliya, Sebastian Hurtado Parra, Jiajia Wen, Ryan Need, James M. Kikkawa, and S. X. Huang, Phys. Rev. Materials **4**, 084203 (2020).
12. **High quality epitaxial thin films and exchange bias of antiferromagnetic Dirac semimetal FeSn**, Durga Khadka, T. R. Thapaliya, Jiajia Wen, Ryan F. Need, and S. X. Huang, Appl. Phys. Lett. 117, 032403 (2020).
13. **Ground state phase diagram of the doped Hubbard model on the four-leg cylinders**, Yi-Fan Jiang, Jan Zaanen, Thomas P. Devereaux, Hong-Chen Jiang, Phys. Rev. Research **2**, 033073(2020).
14. **Topological superconductivity in the doped chiral spin liquid on the triangular lattice,** Yi-Fan Jiang, Hong-Chen Jiang, Phys. Rev. Lett. 125, 157002 (2020).
15. **Orbital Chern Insulator and Quantum Phase Diagram of a Kagome Electron System with Half-Filled Flat Bands**, Yafei Ren, Hong-Chen Jiang, Zhenhua Qiao, D. N. Sheng, Phys. Rev. Lett. 126, 117602 (2021).
16. **Alloying a single and a double perovskite: a $Cu^{+/2+}$ mixed-valence layered halide perovskite with strong optical absorption**, Bridget A. Connor, Rebecca W. Smaha, Jiayi Li, Aryeh Gold-Parker, Alexander J. Heyer, Michael F. Toney, Young S. Lee and Hemamala I. Karunadasa. Chem. Sci., 2021, 12, 8689.

Tracing the Topological Fingerprint of Weyl Semimetals Using Neutron Probes

Mingda Li, Massachusetts Institute of Technology

Program Scope

This program aims to use neutron scattering to investigate the fundamental physical properties in a class of emergent quantum materials called topological Weyl semimetals (WSMs). WSMs have attracted wide recent research attention, due to exotic fundamental aspects of the topological singularity of Weyl points, surface Fermi arcs, and chiral anomaly[1], and vast applications ranging from high-speed electronics to high-efficient energy harvesting[2], from broadband photodetectors[3] to qubits for quantum computing. However, conventional probes detecting WSMs face a series of limitations. Since a WSM has nontrivial bulk singularity, it can induce giant observable effects on its bulk structural, magnetic, and excitation properties, thus enables the exploration through elastic, magnetic, and inelastic neutron scattering. A number of exotic effects are expected to be directly probed with neutrons, such as the pseudo-scalar phonon induced by Adler-Bell-Jackiw chiral anomaly, which can hardly be examined by any other means. High quality, large-size single crystalline WSMs are synthesized PI's lab, ensuring the steady sample supply. The neutron scattering observations will further be supported by combined efforts including electrical and thermal transport measurements, theoretical models, and first-principles calculations. Since the neutron scattering studies on topological materials are scarce, this proposal may unveil many fundamental discoveries in WSMs, and promote the neutron scattering utilization to the topological materials research in general.

Recent Progress

In the past 2 years, with the powerful techniques of neutron and synchrotron X-ray scattering, supported by theories and other measurements, we have made a few fundamental breakthroughs of topological materials and scattering, including

a) Discovery of topological Chiral Kohn anomaly in topological Weyl semimetal (inelastic scattering, *Phys. Rev. Lett.* 2020 with Editors Suggestion; **Fig. 1a, b**)[4].
b) Discovery of "quantized thermoelectric Hall effect" and shows a 10-fold power factor enhancement comparing to best-reported value in Weyl semimetal (inelastic scattering, *Nat. Commun.* 2020, **Fig. 1c**).
c) Demonstrate exotic many-body localization (MBL) in disordered superlattices, as the first demo of MBL in solid-state systems (grazing incidence inelastic X-ray scattering, *Nano Lett.* 2021, **Fig. 1d**)[5].
d) Develop a machine-learning model that can rapidly predict phonon density-of-states using atomic coordinates, which has open-source codes, and has been implemented in ORNL vibrational beamline and supporting their LDRD effort (*Adv. Sci.* 2021, **Fig. 1e**)[6].
e) Discovery of the extended Kohler rule in Wayl semimetal (*Phys. Rev. X 2021,* **Fig. 1f**)[7].

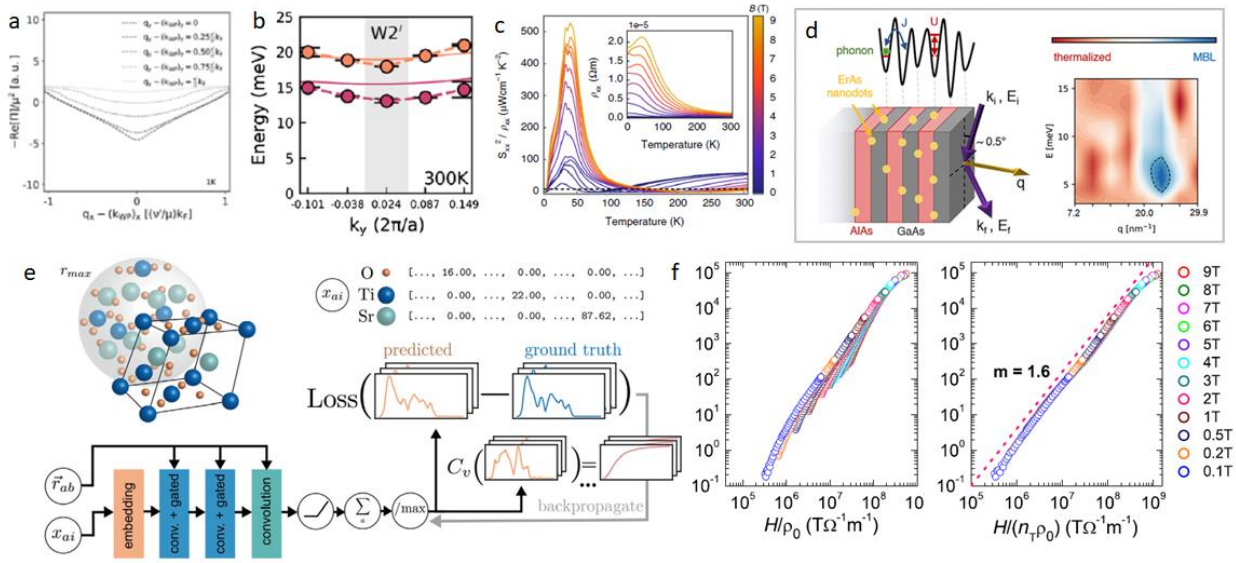

Fig. 1. Theoretical prediction (a) and experimental phonon softening (b) in Weyl semimetal TaP. (c) Enhancement of the thermoelectric power factor. (d) The mechanism and results on the possible many-body localization phase. (e) The neural network architecture for phonon density-of-states prediction. (f) The conventional Kohler rule for magnetoresistance (left) and the extended Kohler's rule (right) where all curves collapse into one curve.

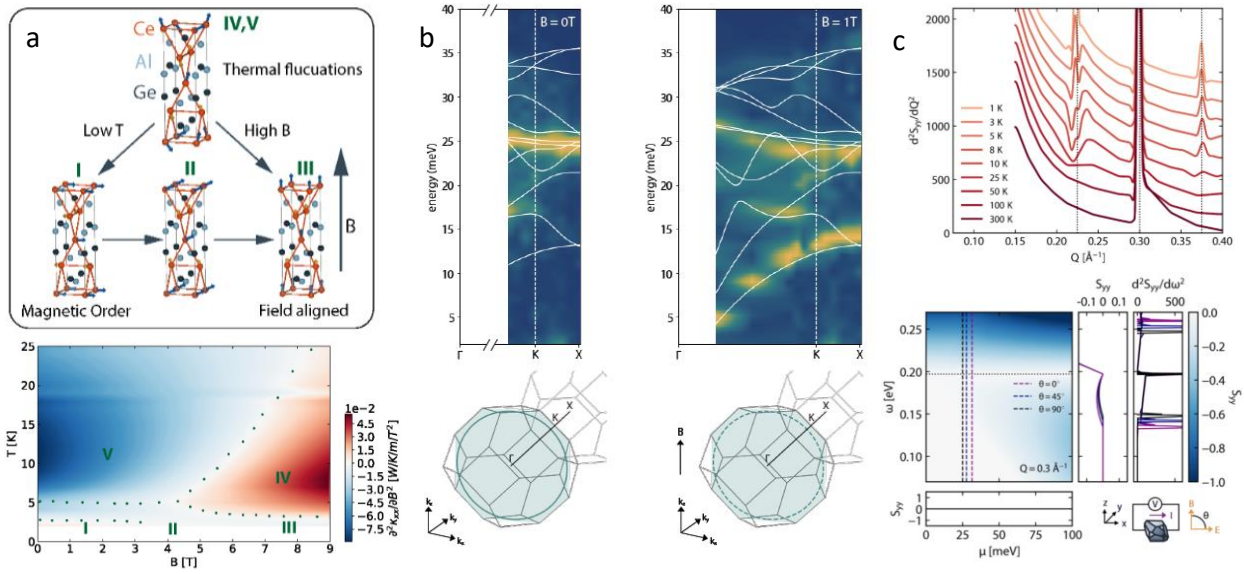

Fig. 2. (a) Fluctuation-driven ordering in magnetic Weyl semimetal. (b) The exotic phonon behavior showing possible chiral anomaly. (c) The structure factor demonstrating the effects from Weyl nodes.

Besides, we are actively making progresses for the following milestone projects:

f) Discovery of exotic quantum ordering *above* magnetic transition, originated from the coupling between topological Weyl fermion and magnetic *fluctuations* (neutron diffraction, field-dependent inelastic scattering, under review, **Fig. 2a**).
Significance: First work showing we show novel phases can be created when topology couples with *symmetry-restoring* magnetic fluctuations.

g) Discovery of phonon chiral anomaly and PT-symmetric non-Hermitian physics in Weyl semimetals (field-dependent inelastic scattering, **Fig. 2b**, to submit).

   Significance: First time we were able to show the phonon signature of chiral anomaly, and non-Hermitian physics in solid-state material.

h) Derivation of a comprehensive theoretical framework showing the strong neutron signal for Weyl semimetals when passing through a current (**Fig. 2c**, under review).

Future Plans

Future plan will be focused on topological materials with 4 Thrusts, including topological flatbands, topological quantum criticality, topological superconductors and detection of long-range entanglement.

Thrust 1. Colossal electron-phonon interactions in topological flat-band materials. Thrust 1 aims to achieve giant electron-phonon interaction phenomena caused by dual topological flat-electron-band flat-phonon-band coupling. Our preliminary heat capacity results show an anomalously large magnetic-field-tuning even without magnetic ordering and our preliminary inelastic scattering results show the flat band phononsError! Reference source not found.. In particular, we plan to synthesize the single crystals of a few non-magnetic and magnetic flat-band materials using recent database (Task 1.1), and perform field-dependent elastic and inelastic scattering to determine their phonon structures and flat band evolution (Task 1.2), and perform inelastic spin-echo measurements for high-precision linewidth determination (Task 1.3).

Significance: The success of Thrust 1 could lead to the *largest electron-phonon interaction strength* ever reported, and enable the electrical tuning of phonon properties with order-of-magnitudes enhancement.

Thrust 2. Discovery the topology driven quantum criticality.

The goal of Thrust 2 is to demonstrate the exotic quantum orderings through the coupling of topological states and heavy 4*f* electrons. In particular, from the recent database[1], we have identified a few Nd-based compounds that contain both nontrivial band topology, heavy fermion behaviors and magnetic orderings, such as NdCoSi, $Nd_3Ru_4Al_{12}$, Nd_5Si_4, and NdZn. We will synthesize the Nd-based compounds and perform doping with La, Ce, and Pr atoms (Task 2.1), and perform in-house electrical, thermal transport to reveal the quantum criticality (Task 2.2), and send the co-aligned crystals to perform elastic, diffuse and inelastic scattering near the quantum critical regime to measure the correlation properties and clarify the role of topology in neutron scattering (Task 3.3).

Significance: The Thrust 2 could lead to fundamental discoveries of new universal classes of quantum critical behaviors, and enter into a no-man's land to study topological states near quantum critical regime.

Thrust 3. Three-dimensional profile mapping of topological superconductors.

Thrust 3 aims to design a new methodology based on dual analysis of grazing-incidence small-angle neutron scattering (SANS) and polarized neutron reflectometry (PNR) to reliably recover the neutron signature of topological superconductivity through neutron spectra. The preliminary results show the feasibility (Error! Reference source not found.**d, e)**. We plan to complete the theoretical ground (Task 3.1), and to study thin film topological superconductor samples such as $FeSe_{0.5}Te_{0.5}$ and 2M-WS2 grown by molecular beam epitaxy and perform the PNR (Task 3.2) and SANS measurements in (*B, T*) space (Task 3.3), which can directly be used to characterize the spatial profile of the Majorana fermions.

Significance: Thrust 3 will enable an alternative probing route of topological superconductivity, which largely complements the current probes such as STM, which are local and surface-sensitive.

Thrust 4. Design a new architecture to identify the long-range entangled states.

Long-range entangled states such as quantum spin liquid are technologically important for potential quantum computing applications. However, current thermal transport measurements often give inconclusive results, and inelastic scattering does not have any excitation feature. We propose to use *entangled neutrons* to measure the materials. Our preliminary results show promising outcome that can conclusively distinguish a long-range entangled toric code to a short-range Heisenberg model (Error! Reference source not found.**f**). The work may have far-reaching impact.

References

1 Armitage, N. P., Mele, E. J. & Vishwanath, A. Weyl and Dirac semimetals in three-dimensional solids. *Rev Mod Phys* **90**, 015001, doi:10.1103/RevModPhys.90.015001 (2018).

2 Skinner, B. & Fu, L. Large, nonsaturating thermopower in a quantizing magnetic field. *Science Advances* **4**, eaat2621, doi:ARTN eaat2621.10.1126/sciadv.aat2621 (2018).

3 Liu, J., Xia, F., Xiao, D., Garcia de Abajo, F. J. & Sun, D. Semimetals for high-performance photodetection. *Nat Mater* **19**, 830-837, doi:10.1038/s41563-020-0715-7 (2020).

4 Nguyen, T. *et al.* Topological Singularity Induced Chiral Kohn Anomaly in a Weyl Semimetal. *Phys Rev Lett* **124**, 236401, doi:10.1103/PhysRevLett.124.236401 (2020).

5 Nguyen, T. *et al.* Signature of Many-Body Localization of Phonons in Strongly Disordered Superlattices. *Nano Lett* **21**, 7419-7425, doi:10.1021/acs.nanolett.1c01905 (2021).

6 Chen, Z. *et al.* Direct Prediction of Phonon Density of States With Euclidean Neural Networks. *Advanced Science*, doi:10.1002/advs.202004214 (2021).

7 Xu, J. *et al.* Extended Kohler's Rule of Magnetoresistance. *Physical Review X* **11**, doi:10.1103/PhysRevX.11.041029 (2021).

Publications

* denote corresponding author(s)

01. T. Nguyen, F. Han, N. Andrejevic, R. Pablo-Pedro† A. Apte, Y. Tsurimaki, Z. Ding, K. Zhang, A. Alatas, E. E. Alp, S. Chi, J. Fernandez-Baca, M. Matsuda, D.A. Tennant, Y. Zhao, Z. Xu, J.W. Lynn, S. Huang and **M. Li***, "Topological Singularity Induced Chiral Kohn Anomaly in a Weyl Semimetal", Phys. Rev. Lett. **124**, 236401 (2020).
02. F. Han*, N. Andrejevic, T. Nguyen, V. Kozii, Q. Nguyen, T. Hogan, Z. Ding, R. Pablo-Pedro, S. Parjan, B. Skinner, A. Alatas, E. Alp, S. Chi, J. Fernandez-Baca, S. Huang, L. Fu* and **M. Li***, "Quantized Thermoelectric Hall Effect Induces Giant Power Factor in a Topological Semimetal", *Nature Communications*, **11**, 6167 (2020).
03. K. Zhang, T. Wang, X. Pang, F. Han, S-L Shang, N.T. Hung, A.R.T. Nugraha, Z-K Liu, **M Li***, R. Saito* and S Huang*, "Anisotropic Fano resonance in a Weyl semimetal candidate LaAlSi", *Phys. Rev. B* **102**, 235162 (2020).
04. Z. Chen, N. Andrejevic, T. Smidt, Z. Ding, Y-T Chi, Q. Nguyen, A. Alatas, J. Kong and **M. Li***, "Direct prediction of phonon density of states with Euclidean neural networks", DOI:10.1002/advs.202004214, Advanced Science (2021).
05. T. Nguyen, N. Andrejevic, H. C. Po, Y. Tsurimaki, N. Drucker, A. Alatas, E. E. Alp, B. M. Leu, A. Cunsolo, Y. Cai, L. Wu, J. A. Garlow, Y. Zhu, A. C. Gossard, S. Huang* and **M. Li***, "Signature of Many-Body Localization of Phonons in Strongly Disordered Superlattices", *Nano Lett.* **21**, 7419 (2021).
06. J. Xu, F. Han, T-T Wang, LR Thoutam, SE Pate, **M. Li***, X. Zhang, Y-L Wang*, R. Fotovat, U. Welp, X. Zhou, W-K Kwok, DY Chung, MG Kanatzidis, and Z-L Xiao*, "Extended Kohler's Rule of Magnetoresistance", *Phys. Rev. X*. **11**, 041029 (2021).
07. Z. Chen, N. Andrejevic, N. C. Drucker, T. Nguyen, R.P. Xian, T. Smidt, Y. Wang, R. Ernstorfer, A. Tennant, M. Chan, and **M. Li***, "Material Learning on Neutron and X-Ray Scattering", Chem. Phys. Rev **2**, 031301 (2021)

Machine Learning-Augmented Multimodal Neutron Scattering for Emergent Topological Materials

Mingda Li, Massachusetts Institute of Technology

Program Scope

The goal of this project is to test our overarching hypothesis that neutron scattering augmented by new machine learning architectures can be employed to 1) measure the topological properties of materials that are difficult or impossible to assess using current methods; and 2) measure topological properties of materials under multimodal sample environments, such as gate voltages, and external electrical and magnetic fields; and 3) enable massive searches for materials with desirable phonon states. This research will focus on three classes of topological materials: topological insulators (TIs), materials with topological magnetism (TMs), and materials with topological phonons (TPhs). We will implement and design novel machine learning architectures applied to ¬in-situ multimodal measurements. Machine learning will enable the direct extraction of materials information without the need for fitting models. The multimodality will provide new neutron scattering parameter spaces to be compared with theory. This project is organized around three thrusts, focused on TIs, TMs and TPhs, respectively.

Recent Progress

In the past 4 months since the start of the Project in July 2021, by combining the neutron scattering and machine learning, we have completed the following two works:

a) Construct a machine-learning-based framework that can resolve the small signals for polarized neutron reflectometry (PNR, **Fig. 1**)[1]. We have built a conditioned variational autoencoder framework that can bring down the spatial resolution of PNR to ~0.5nm, almost half comparing to the current resolution limit from manual analysis. Moreover, we have made the codes publicly available in GitHub[2]. Using this framework, we were able to conclusively resolve the elusive magnetic proximity effect in a topological insulator heterostructure, which is The work is currently being reviewed under a high-impact journal.

b) Develop a machine-learning based framework that can enable the classification of magnetic order, including ternary classification of ferromagnetism, anti-ferromagnetism, and non-magnetism, and also the magnetic propagation vector with zero and non-zero propagation vector (**Fig. 2**). The main results are shown in **Fig. 3**, where an 80% accuracy on magnetic order prediction and a 72% accuracy on propagation vector prediction is achieved.

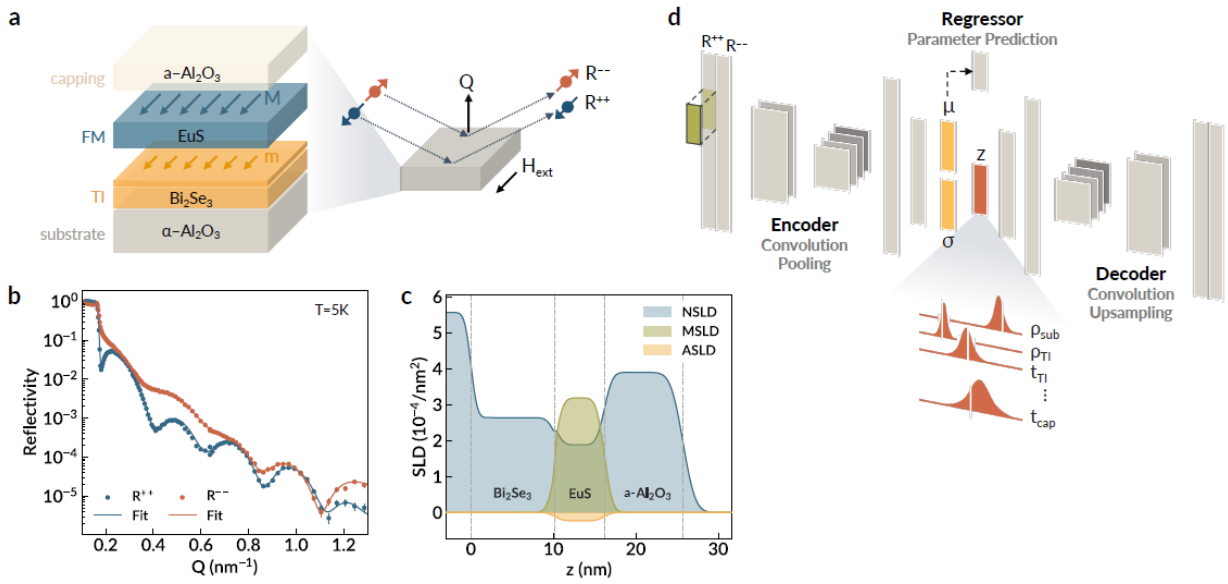

Fig. 1. Machine-learning analysis of PNR. (a) A topological insulator heterostructure sample being studied by PNR. (b) The PNR spectra and the (c) scattering length densities fitting. (d) Variational autoencoder structure showing the machine-learning based fitting procedure.

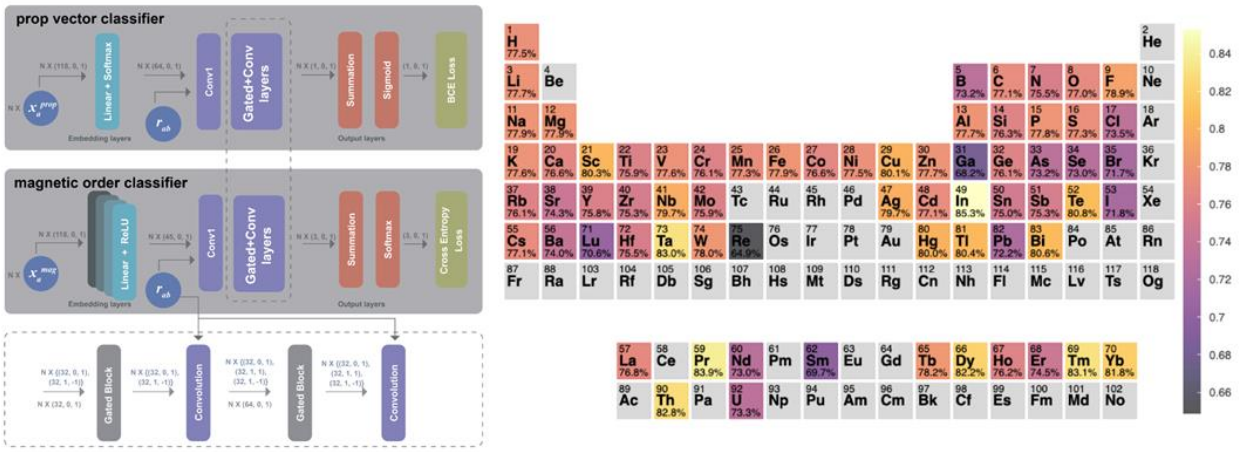

Fig. 2. (Left) the architecture of the magnetism classifier and the corresponding element-wise accuracy of the classifier.

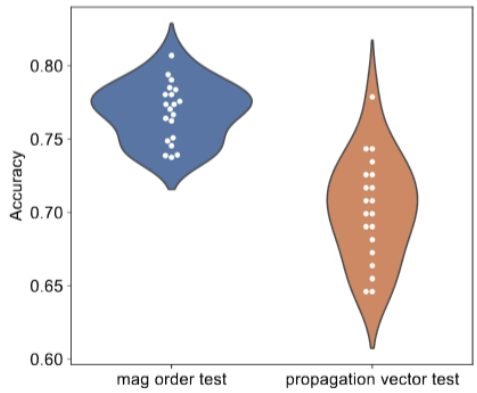

class	precision	recall	f1-score
NM	0.93	0.93	0.93
AFM	0.72	0.69	0.71
FM	0.74	0.77	0.75

Table 1: Metrics of a representative magnetic order classification model.

class	precision	recall	f1-score
Zero	0.66	0.79	0.72
Non-zero	0.78	0.66	0.71

Table 2: Metrics of a representative propagation vector classifier.

Fig. 3. Summarized results in the magnetic classifier.

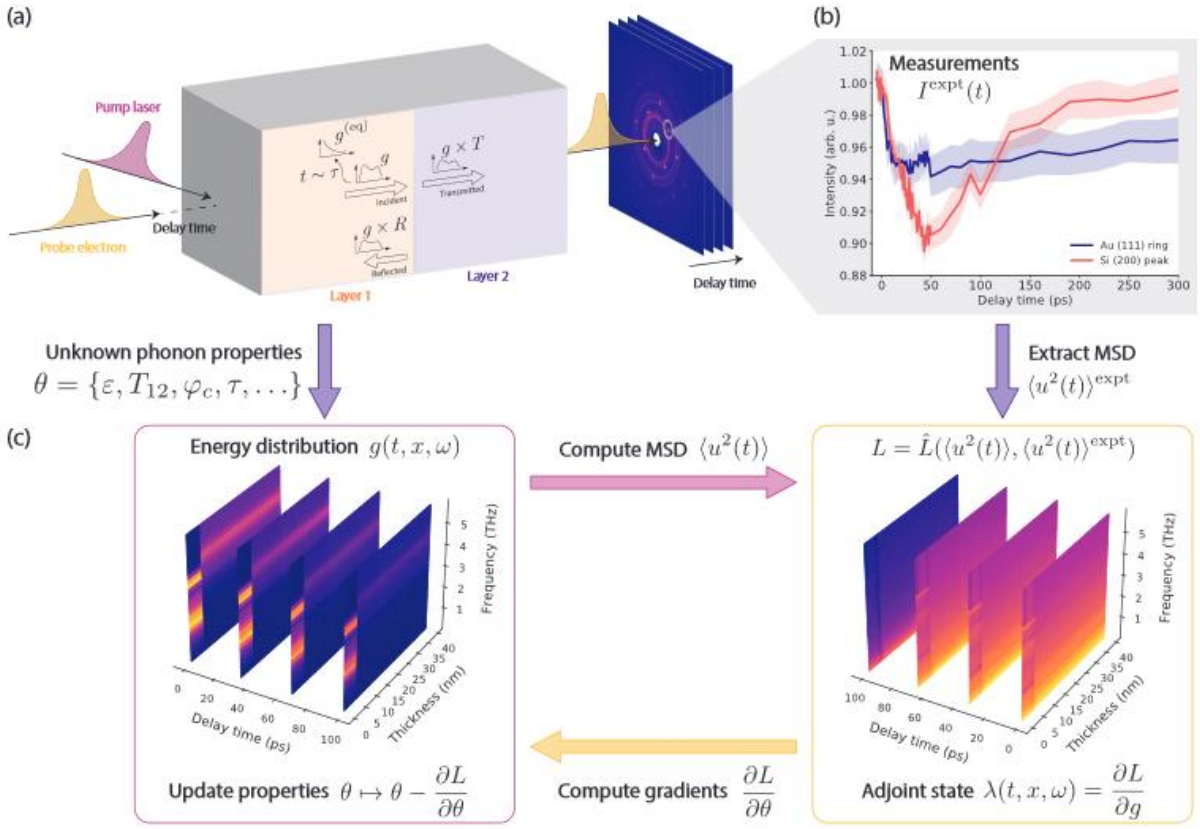

Fig. 4. Ongoing research machine-learning ultrafast diffraction .

Besides, we are actively making progresses for the following milestone project:

c) Construction of a machine-learning framework that leads to a comprehensive phonon transport mapping from time-resolved diffraction (**Fig. 4**).

Future Plans

Future plan will be focused on machine-learning for topological insulators, topological magnetism, and topological phonons.

In Thrust 1, we aim to test our hypothesis, supported by preliminary results, that the effect on polarized neutron reflectometry (PNR) spectra of the magnetic proximity effect in TIs can be captured by well-designed convolutional neural network architectures that correlate and amplify small spectral features, even under a noisy environment. We will design a true fitting-parameter-free, autoencoder-based predictive model to analyze the proximity effect in TI thin films based on PNR spectra in the presence of noise. Such a model will be further applied to PNR measurements on multilayer axion insulator heterostructures at various gate voltages.

In Thrust 2, we aim to test our hypothesis that machine-learning architectures, when applied to 2D small-angle neutron scattering (SANS) data, can be used to directly determine magnetic phases and extract microscopic interaction parameters in topological magnetism such as skyrmions with improved reliability. Our preliminary results demonstrated the capability to perform magnetic structure and SANS pattern calculations from microscopic parameters. We will further apply Koopman operator formalism for dynamic systems to study magnetic dynamics, and carry out SANS under multimodal magnetic fields in Kagome Weyl semimetals, which may host both momentum-space and real-space topology.

In Thrust 3, we will build a symmetry-imposed graphic neural network model that directly predicts phonon dispersion from atomic coordinates, which incurs small computational costs but accuracy comparable to ab initio calculations. Our recent work on phonon density-of-states predictions demonstrates the feasibility of this approach. We will carry out a massive materials search for topological phonon systems with low-energy band-crossings, and perform strain-dependent inelastic neutron scattering to test our predictions on the evolution of topological bands, which are inaccessible with current methods.

References

1 Andrejevic, N. *et al.* Elucidating proximity magnetism through polarized neutron reflectometry and machine learning. arXiv:2109.08005 (2021). <https://ui.adsabs.harvard.edu/abs/2021arXiv210908005A>.

2 Code Repository for "Elucidating proximity magnetism through polarized neutron reflectometry and machine learning" https://github.com/ninarina12/ML_PNR (2021).

Publications

N/A.

Structure and Dynamics of Ion-Containing Nanostructured Ternary Polymer Blend

Timothy P. Lodge and Frank S. Bates, University of Minnesota

Program Scope

A central challenge in next-generation materials is to develop a broadly applicable strategy to systematically tailor nanostructure, in order to simultaneously optimize two (or more) orthogonal properties. A prime example of this competition is to prepare polymeric membranes that exhibit both (a) high transport for selected small molecules or ions, while (b) concurrently exhibiting superior mechanical, thermal and chemical robustness. For a single component polymeric material, any strategy to improve mechanical strength will impede molecular motion. The key to achieving this goal is to prepare a co-continuous nanostructure, in which one domain is responsible for molecular or ionic transport, while the other imparts mechanical strength. Systems containing at least two polymeric components are therefore required, and their attributes and the mixture composition must be designed to impart co-continuity. We have shown that ternary blends comprising A and B homopolymers, plus an A-B block copolymer surfactant, present a broadly tunable and widely applicable strategy to accessing functional co-continuous nanostructures, especially the polymeric bicontinuous microemulsion (BuE),[1] in systems with both added salt[2] and with an ionic polymer component.[3] The focus for this project is to build on these discoveries by expanding both the range of molecular variables and the range of the ternary phase prisms to be explored. Our experimental approach relies on synthesis of model polymers with well-controlled molar mass, composition, architecture, and charge density. Phase behavior is examined by a powerful combination of small-angle X-ray scattering (SAXS) and small-angle neutron scattering (SANS), bolstered by optical transmission and electron microscopy. Model systems will be selectively crosslinked, in order to achieve exceptional combinations of mechanical and conductivity properties.

Recent Progress

Fig. 1. C15 Laves phase in a salt-doped ternary blend.

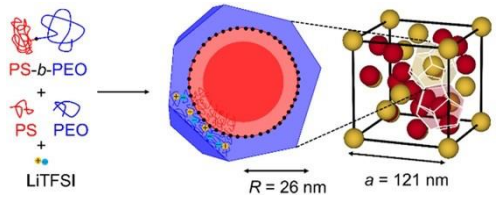

In the context of ternary blends with added salt, we have explored the system polystyrene (S), polyethylene oxide (O) and added salts such as LiTFSI. We showed that this system can exhibit the BuE along the volumetrically symmetric isopleth (equal amounts of S and O homopolymer, with a symmetric SO diblock).[2] We have extended this study to the full isothermal phase triangle; remarkably, we uncovered a C15 Laves phase over a significant region of the phase diagram, and rationalized its appearance as a joint effect of increasing segregation strength and differential wet-brush to dry-brush transitions in the S and O domains (Fig. 1).[4] Interestingly, this structure has a unit cell parameter of 120 nm, almost in the photonic

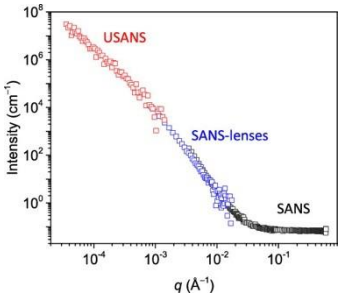

Fig. 2 SANS from dPEO (40 kDa) with added LiTFSI (r = 1/64) with three different instruments.

regime, even though the largest component molecule is only 2-3 nm is size. Using deuterium labeling, we conducted an in-depth SANS analysis of chain locations within the BuE,[5] and also of salt effects on the conformations of the O chains.[6] This latter study also exposed a recalcitrant problem in isotope labeled polymers, a substantial low-q coherent component in the pure polymer, which is attributable to microvoids (see Fig. 2). In particular, measurements at NIST and at ORNL were consistent, as were measurements on different configurations, eliminating instrumental issues as the cause. Using SANS and different contrast conditions, we were able to quantify the intermingling of S homopolymer and SO diblocks within the BuE; an example of the relevant SANS profiles are shown in Fig. 3.

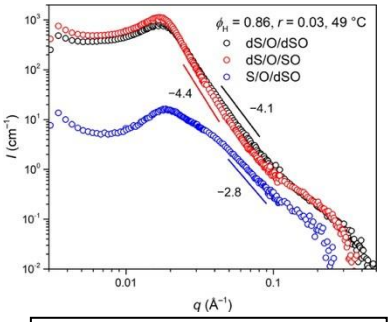

Fig. 3 SANS for dS/O/dSO, dS/O/SO, and S/O/dSO with ϕ_H = 0.86, r = 0.03 at 49 °C.

We have developed convenient synthetic routes to several new block copolymer systems with charged ("single-ion-conductor") blocks (Fig. 4), and are exploring the phase behavior both as pure copolymers, and in ternary blends. In all cases the length and dispersity of each block can be carefully controlled, and the fraction of charge-bearing groups can be tuned continuously.

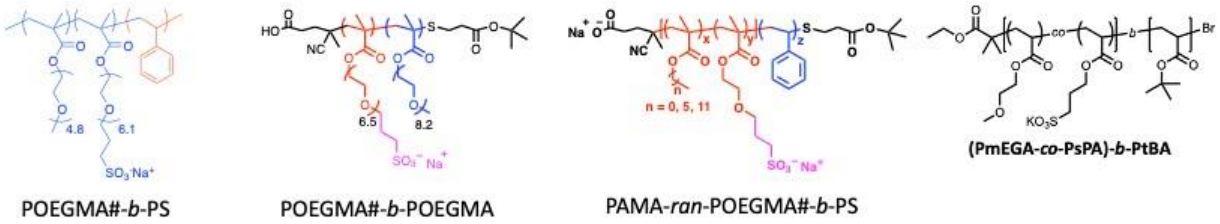

Fig. 4. Four new model charge-bearing block copolymer systems under study; # denotes fraction of charged monomers.

We previously showed that pure POEGMA#-PS can form a novel superlattice structure,[7] and also that it could form the BuE along the symmetric isopleth.[8] We have now extended this study to the full phase prism by SAXS; an example is shown in Figure 5. The region labeled "disordered" is likely includes a BuE, but we await access to SANS to confirm this. The system is remarkably symmetric, given the strong charge interactions. Another interesting feature in this system is that the domain spacing along the isopleth increases very steeply with added homopolymer, suggestive of the same dry-drush phenomenon that drives C15 formation in salt-doped blends.

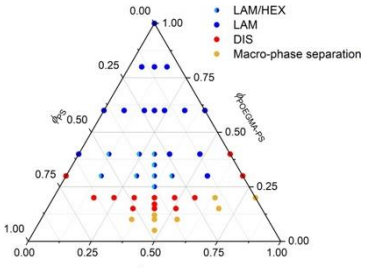

Fig. 5. Phase diagram POEGMA#15 / PS /POEGMA#15-PS at 120 °C.

An interesting theatrical prediction in the literature is that in charge-neutral diblocks, the phase diagram can become extremely asymmetric with only modest amounts of charge. We

explored this idea in detail with a series of POEGMA#-PS diblocks of varying molecular weight and charge density. Interestingly, in all cases the samples remained lamellar, and the phase diagram could be anticipated on the basis of a "mean-field" idea, that added charge simply increases the effective interaction parameter, as shown in Fig. 6.[9] In the figure the experimental phase diagrams are shown, along with the mean-field correlation for the order-disorder transition (ODT). The important conclusion from this study is that when the dielectric constant mismatch between the two blocks is large, the counterions never leave the corresponding domains (due to the huge differential in Born solvation energy). To try and overcome this, we have developed the second and third systems shown in Fig. 4, which we are now exploring.

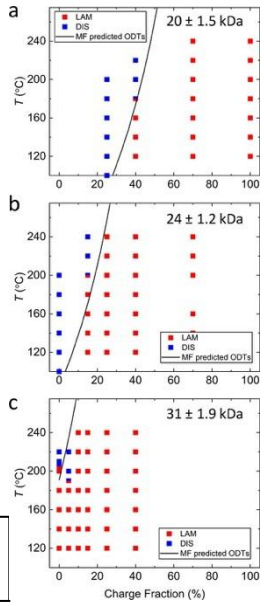

Fig. 6. Phase portraits as a function of charge fraction for polymers with the indicated molecular weights.

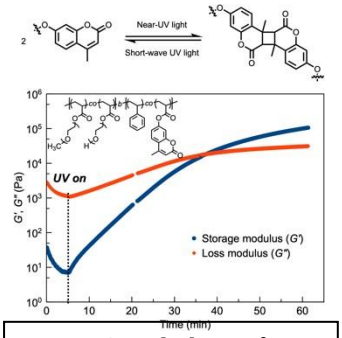

Fig. 7. Crosslinking of a model coumarin-containing block polymer under long-wave UV

In addition to these studies of phase behavior, we have begun developing effective strategies to crosslink the insulating domains, to afford robust bicontinuous materials. This goal is not straightforward to achieve, as changes in volume and molecular weight with crosslinking can disrupt the delicate thermodynamic balance required for a BuE, leading to unwanted changes in nanostructure. We have devised a photoactivated approach through coumarin dimerization (Fig. 7), using the fourth polymer system identified in Fig. 4. As a promising first test, the rheological properties of a coumarin-labeled diblock show a clear gelation transition on steady illumination.

Future Plans

We will characterize the phase behavior of these newly synthesized polymers and will construct phase diagrams as a function of volume fraction, charge fraction, and alkyl chain length of the charged block. To investigate the potential of these systems as polymer electrolytes, conductivity will be measured for different morphologies as a function of temperature. The transference number of cations will also be determined and compared with previous reports. We then intend to incorporate different ions into the conductive domains, in order to study how molecular parameters affect material properties. We will extend the coumarin-based photocrosslinking to selected BuE blends, and use SANS to verify the preservation of nanostructure during solidification.

References

[1] "Phase behavior of diblock copolymer-homopolymer ternary blends with a compositionally asymmetric diblock copolymer", B. Zhang, S. Xie, T. P. Lodge, F. S. Bates, *Macromolecules*, 54, 460-472, **2021**. 10.1021/acs.macromol.0c01745

[2] "Structure and properties of bicontinuous microemulsions from salt-doped ternary polymer blends." Xie, S. Y.; Meyer, D. J.; Wang, E.; Bates, F. S.; Lodge, T. P. *Macromolecules*, 52, 9693-9702, **2019**. 10.1021/acs.macromol.9b01963

[3] "Bicontinuous Microemulsions in Partially Charged Ternary Polymer Blends", J. Shim, F.S. Bates, and T.P. Lodge, *ACS Macro Lett.*, 8, 1166-1171, **2019**. 10.1021/acsmacrolett.9b00554

[4] "Formation of a C15 Laves Phase in Salt-Doped A/B/AB Ternary Polymer Blends", S. Xie, A. P. Lindsay, F.S. Bates, and T. P. Lodge, *ACS Nano*, 14, 13754-13764, **2020**. 10.1021/acsnano.0c06071

[5] "Phase Behavior of Salt-Doped A/B/AB Ternary Polymer Blends: The Role of Homopolymer Distribution", S. Xie, B. Zhang, F. S. Bates, T. P. Lodge, *Macromolecules*, 54, 6990-7002, **2021**. 10.1021/acs.macromol.1c00928

[6] "Influence of Added Salt on Chain Conformations in Poly(ethylene oxide) Melts: SANS Analysis with Complications", S. Xie, B. Zhang, Y. Mao, L. He, K. Hong, F. S. Bates, and T. P. Lodge, *Macromolecules*, 53, 7141-7149, **2020**. 10.1021/acs.macromol.0c01194

[7] "Superlattice by Charged Block Copolymer Self-Assembly", J. Shim, F. S. Bates, and T. P. Lodge, *Nature Commun.*, 10, **2019**. 10.1038/s41467-019-10141-z

[8] "Bicontinuous Microemulsions in Partially Charged Ternary Polymer Blends", J. Shim, F.S. Bates, and T.P. Lodge, *ACS Macro Lett.*, 8, 1166-1171, **2019**. 10.1021/acsmacrolett.9b00554

[9] "Phase Behavior of Symmetric Single-Ion Conducting Diblock Copolymers", B. Zhang, C. Zheng, M. B. Sims, F. S. Bates, T. P. Lodge, *ACS Macro Lett*., 10, 1035-1040, **2021**. 10.1021/acsmacrolett.1c00393

Publications

"Phase Behavior of Symmetric Single-Ion Conducting Diblock Copolymers", B. Zhang, C. Zheng, M. B. Sims, F. S. Bates, T. P. Lodge, *ACS Macro Lett.*, 10, 1035-1040, **2021**. 10.1021/acsmacrolett.1c00393

"Phase Behavior of Salt-Doped A/B/AB Ternary Polymer Blends: The Role of Homopolymer Distribution", S. Xie, B. Zhang, F. S. Bates, T. P. Lodge, *Macromolecules*, 54, 6990-7002, **2021**. 10.1021/acs.macromol.1c00928

"Phase behavior of diblock copolymer-homopolymer ternary blends with a compositionally asymmetric diblock copolymer", B. Zhang, S. Xie, T. P. Lodge, F. S. Bates, *Macromolecules*, 54, 460-472, **2021**. 10.1021/acs.macromol.0c01745

"Formation of a C15 Laves Phase in Salt-Doped A/B/AB Ternary Polymer Blends", S. Xie, A. P. Lindsay, F.S. Bates, and T. P. Lodge, *ACS Nano*, 14, 13754-13764, **2020**. 10.1021/acsnano.0c06071

"Influence of Added Salt on Chain Conformations in Poly(ethylene oxide) Melts: SANS Analysis with Complications", S. Xie, B. Zhang, Y. Mao, L. He, K. Hong, F. S. Bates, and T. P. Lodge, *Macromolecules*, 53, 7141-7149, **2020**. 10.1021/acs.macromol.0c01194

"Bicontinuous Microemulsions in Partially Charged Ternary Polymer Blends", J. Shim, F.S. Bates, and T.P. Lodge, *ACS Macro Lett.*, 8, 1166-1171, **2019**. 10.1021/acsmacrolett.9b00554

"Structure and properties of bicontinuous microemulsions from salt-doped ternary polymer blends." Xie, S. Y.; Meyer, D. J.; Wang, E.; Bates, F. S.; Lodge, T. P. *Macromolecules*, 52, 9693-9702, **2019**. 10.1021/acs.macromol.9b01963

"Superlattice by Charged Block Copolymer Self-Assembly", J. Shim, F. S. Bates, and T. P. Lodge, *Nature Commun.*, 10, **2019**. 10.1038/s41467-019-10141-z

Quantum Materials with non-trivial Electronic Topologies and Flat Bands Studied via Neutron Scattering

Despina Louca, University of Virginia

Program Scope

The scope of this program is to investigate the nature of electron-lattice interactions and quantum fluctuations in the presence of flat bands, by probing materials with broken time-reversal symmetry (TRS), as in the Van der Waals layered kagome lattices of FeSn, Fe_3Sn_2, and Mn_3Sn and the honeycomb lattice of $CrCl_3$. We seek to obtain a fundamental understanding of flat band-enabled electron localization by focusing on its real-space features to deduce lattice distortions and local interactions. We further seek to explore defect-enabled electron localization in the presence of broken spatial inversion, P, and TRS in Na_xMnBi_y by focusing on charge modulations and magnetic fluctuations and their resultant effects in momentum-space. A central knowledge gap is what happens to topological signatures when translational symmetry is broken due to distortions and momentum conservation is compromised. At present, there are no experimental studies that systematically examine the effects of localization and interactions in these classes of materials.

It is expected that interactions modify the electronic states within the flat band manifold and these can best be visualized in real-space by local probes such as the Pair Density Function analysis technique. This work seeks to delineate the role played by electron correlation effects due to electron-lattice and electro-magnetic interactions in the emergence of excitations. Specific objectives are: (1) focus on the tunability of the 3D topological materials and their protected surface states where strong localization is expected due to the presence of flat bands. This will be achieved by tuning the selected topological flat band materials by modulating spin-orbit coupling (SOC) through doping/substitution and changing the interlayer interactions, and applications of electric, magnetic and strain fields; (2) perform a systematic investigation of the static and dynamic structures via neutron scattering and make connections with quantum behaviors and identify relevant quantum characteristics; (3) understand the persistence of gapless phases in disordered solids and identify key topological signatures; (4) characterize atomistic traits of unconventional topological phases that become stable (or get destroyed) in the presence of strong localization. This work seeks to elucidate the topological structures in real-space rather than in momentum space because of the spatially localized character of the states in the flat bands.

This project involves neutron scattering studies on novel topological insulators and semiconductors that have been identified as promising candidates for the development of the next generation spintronic and optoelectronic devices. Knowledge obtained and transferred from our studies on layer stacking faults, lattice defects and the effects of disorder will feed into identifying key components to modulating the Van der Waals interactions across layers in the kagome and honeycomb structures which will in turn control interactions. It may also lead to an understanding

of the origin of charge modulations and large magnetoresistance (MR) in antiferromagnetic spintronic materials such as NaMnBi.

Successful completion of this project will elucidate the relation between short-range coherence of lattice signatures and the mechanism(s) giving rise to topological features in disordered/flat band topological phases. Importantly, we will be positioned to answer *what happens to the flat band topology when long-range coherence is suppressed.* In an extension to the findings from the current grant, to predict and control topological phase transitions in the presence of disorder, the proposed project will focus on disorder-induced flat bands and on flat band induced disorder. The proposed program integrates synthesis, physical properties characterization and neutron scattering to resolve the atomic structures and dynamical properties as they evolve with strain, magnetic and electric fields and tuning of SOC. The experimental output can be fed directly into theoretical modeling that can help improve the predictive capabilities of the next generation of materials. If successful, this research could pave the way to new emerging fields of semiconductors and their applications.

Publications

1. "*Bismuth kagome sublattice distortions by quenching and flux pinning in superconducting $RbBi_2$*", Sharon S. Philip, Junjie Yang, Despina Louca, P. F. S. Rosa, J. D. Thompson, and K. L. Page, Phys. Rev. B **104**, 104503 (2021).
2. "G*apless Dirac magnons in $CrCl_3$*", J. A. Schneeloch, Y. Tao, Y. Cheng, L. Daemen, G. Xu, Q. Zhang, and D. Louca, submitted (2021).
3. "*Weak trimeriazation in the frustrated 2D triangular Heisenberg antiferromagnetc $Lu_yY_{1-y}MnO_3$*", S. Yano, C.-W. Wang, J. S. Gardner, W. T. Chen, K. Iida, R. A. Mole, D. H. Yu, and D. Louca, submitted to Phys. Rev. B (2021).
4. "*Out-of-plane sulfur distortions in the $Bi_4O_4S_3$ superconductor*", S. S. Philip, A. Athauda, D. Louca, Y. Mizuguchi and Y. Goto, accepted Quantum Complex Matter (2021).
5. "*Lattice and magnetic dynamics studied by neutron scattering in perovskite YVO_3 Mott insulator*", Yu Tao, Douglas L. Abernathy, Jiaqiang Yan, Tianran Chen, Taner Yildirim, Jianshi Zhou, John B. Goodenough, and Despina Louca, submitted to Phys. Rev. B (2021).
6. "*Phonons in $MoTe_2$*", J. Schneeloch, Y. Tao, D. Louca, submitted to Phys. Rev. B (2021).
7. **"***Charge-ordered state satisfying the Anderson condition in LiRh2O4 arising from local dimer order*", M. Shiomi, K. Kojima, N. Katayama, S. Maeda, J. Schneeloch, D. Louca, Y. Okamoto, and H. Sawa, submitted to Phys. Rev. Lett. (2021).
8. "*Metal-insulator transition and doping-induced phase change in $Ge_2Sb_2Se_{5x}Te_{5-5x}$*", Z. Xu, K. Park, J. A. Schneeloch, and D. Louca, Applied Physics Letters **117**, 193503 (2020).
9. "*Evidence for pseudo–Jahn-Teller distortions in the charge density wave phase of 1T-$TiSe_2$*", A. Wegner, J. Zhao, J. Li, J. Yang, A. A. Anikin, G. Karapetrov, K. Esfarjani, D. Louca, U. Chatterjee", Phys. Rev. B **101**, 195145 (2020).
10. "*Charge Density Modulation and Defect Ordering in NaMnBi magnetic semimetal",* A. Wegner, D. Louca, K. Taddei, J. Neuefeind, D. Louca, Phys. Rev. B **102**, 020403(R) (2020).

11. "*Evolution of the structural transition in $Mo_{1-x}W_xTe_2$*", J. A. Schneeloch, Y. Tao, C. Duan, M. Matsuda, A. A. Aczel, J. A. Fernandez-Baca, G. Xu, J. C. Neuefeind, J. Yang and D. Louca, Phys. Rev. B **102**, 054105, (2020).
12. *"T_d to 1T' structural phase transition in WTe_2 Weyl semimetal"*, Y. Tao, J. A. Schneeloch, A. A. Aczel, and D. Louca, Phys. Rev. B 102, 060103(R) (2020).
13. *"*Electric control of the magnetic transition in multiferroic $LuMnO_3$*", C. Duan, J. Yang, L. Harriger, and D. Louca, under review in J. Phys. Soc. JPN (2019).*
14. *"Emergence of topologically protected states in $MoTe_2$ Weyl semimetal with layer stacking order",* J. A. Schneeloch, C. Duan, J. Yang, J. Liu, X. Wang, and D. Louca, Phys. Rev. B. **99**, 161105(R) (2019).
15. *"Appearance of a T_d* phase across the Td-1T' phase boundary in Weyl semimetal $Mo_{1-x}W_xTe_2$",* Y. Tao, J. A. Schneeloch, C. Duan, M. Matsuda, S. E. Dissanayake, A. Aczel, J. A. Fernandez-Baca, and D. Louca, Physical Review B **100** (10), 100101(R) (2019).
16. *"Electronic band tuning under pressure in $MoTe_2$ Weyl semimetal",* S. Dissanayake, C. Duan, J. Yang, J. Liu, M. Matsuda, C. Yue, J. A. Schneeloch, J. C. Y. Teo, and D. Louca, to NPJ Quantum Materials **4**, 45 (2019).
17. **"***Local trigonal modes and the suppression of the charge density wave in $TiSe_{2-x}Te_x$",* A. Wegner, D. Louca, and J. Yang, Physical Review B **99** (20), 205110 (2019).

Quantification of Dynamic Disorder in Electronic and Excitonic Organic Materials

Adam J. Moulé
University of California, Davis
Department of Chemical Engineering

Program Scope: The long-term goal of this project is to gain a comprehensive understanding of and the ability to predict optoelectronic and excitonic materials properties of organic semiconductors. Our central hypothesis is that the use of electronic (DFT) and molecular dynamics (MD) modeling methods validated by neutron scattering data will yield new understanding of the relationship between structural heterogeneity and charge delocalization, charge transport, exciton transport, dopant site choice, and dopant transport. To fully explore and develop this research area, we proposed three specific hypothesis driven aims:

(1) **Quantify effects of inter- and intramolecular dynamic disorder on charge transport:** We studied molecular crystals to determine which dynamic modes affect charge transport.
(2) **Develop modeling methods to interpret INS data from non-**crystalline samples: We developed DFTB and MD methods to interpret INS data and systematically tested the accuracy, computational expense, and transferability of the models.
(3) **Develop new optical excitation sample environment at VISION beamline:** We hired and trained the student that will carry out this project, but we could not start due to COVID-19 travel restrictions.

In addition to these proposed aims, we had two backlogged projects from before 2019 and one new side project that produced interesting neutron science but was not part of our main program.

Recent Progress: We have made significant progress on our research goals, resulting in six published and one in progress new peer reviewed publications in the last 2 years. The progress and challenges in each sub project are described below.

Developing Low-Cost methods to Simulate INS spectra: In our past work, we showed that the INS can directly measure the dynamic disorder in crystalline OE materials. The dynamic disorder coupled to a charge transport model yields accurate quantitative prediction of the charge mobility in OE crystals for the first time.[1] However, most OE materials are not crystalline. Even samples with strong diffraction patterns have high levels of internal disorder (para-crystallinity). The simulation method to determine the phonon spectrum accurately depends on DFT, which is computationally expensive and scales with the atom number (N) to the third power, thus a doubling of the system size results in an eight times increase in computational expense.

We proposed to separately develop MD and density functional tight binding (DFTB) methods to simulate INS spectra and to compare the methods to determine which yields the best combination of accuracy and reduced computational expense.

Publication 1: In this paper we develop a series of simulation steps that enables the use of DFTB to simulate INS spectra. We found that DFTB approximates the INS spectrum much less well than DFT because the DFTB does not simulate repulsive van der Waals forces as well as DFT. We can make this assignment because intramolecular phonons are simulated accurately whereas intermolecular phonons fit poorly. We improve the fit to DFTB using ChIMES, which is an empirical machine learning potential that corrects the repulsive potentials. We showed that using the combination of DFTB and ChIMES yielded an accurate simulation of measured INS data. We also showed that the ChIMES potential was transferrable to other similar OE crystals, which an important demonstration of model transferability.[2]

Publication 2: In this paper we develop a method to simulate INS spectra from MD trajectories. We choose the polymer P3HT as our sample because we had previously attempted to simulate P3HT and found that we could get a good fit to intramolecular phonons (>700 cm^{-1}) but could not accurately simulate intermolecular phonon modes. Our new method used a fourier transform of the velocity autocorrelation function to solve the spectrum. We also developed a method to fit the overtone spectra from a classical method (classical codes only have 0-1 harmonic transitions). Using this method we showed a better fit to the low energy part of the P3HT INS spectrum than using DFT.[3] The method we developed is nearly identical to that of (Chen/Ramirez 2020). More on the differences in results below.

Publication 3: The goal in this publication was to compare the methods developed in Pub1 and Pub2 to see which is more accurate and has lower computational cost. This study was exhaustive and took very very very much effort. We studied the crystalline material Rubrene (highest mobility recorded). We compared DFT, DFTB, DFTB/ChIMES, MD, Machine Learning (many version of our own code), and Machine Learning (ANI-1). The figure below shows the comparison between spectra. DFT fits the best followed closely by DFTB/ChIMES.[4] The MD fits very poorly, whereas the MD fit well in (Chen/Ramirez 2020). The difference is because we studied large non-polar molecules that are heavily influenced by dispersion forces. In comparison (Chen/Ramirez 2020) studied simple materials (glass, ice) with strong bonds. MD forces are well developed for covalent/ionic bonds but poorly describe dispersion forces – thus only samples with really excellent MD forces can be accurately simulated using MD. DFTB and DFTB/ChIMES were each ~1000x less expensive that DFT. Interestingly, since MD and ML methods needed to converge but the dispersion forces are very week the potential energy surface being fit is fairly flat. As a result the training times are extremely high for ML and MD methods, making them also less computationally efficient that DFTB. Also, ML and MD forces are specific to one molecule, but ChIMES potentials can be transferred between molecules.

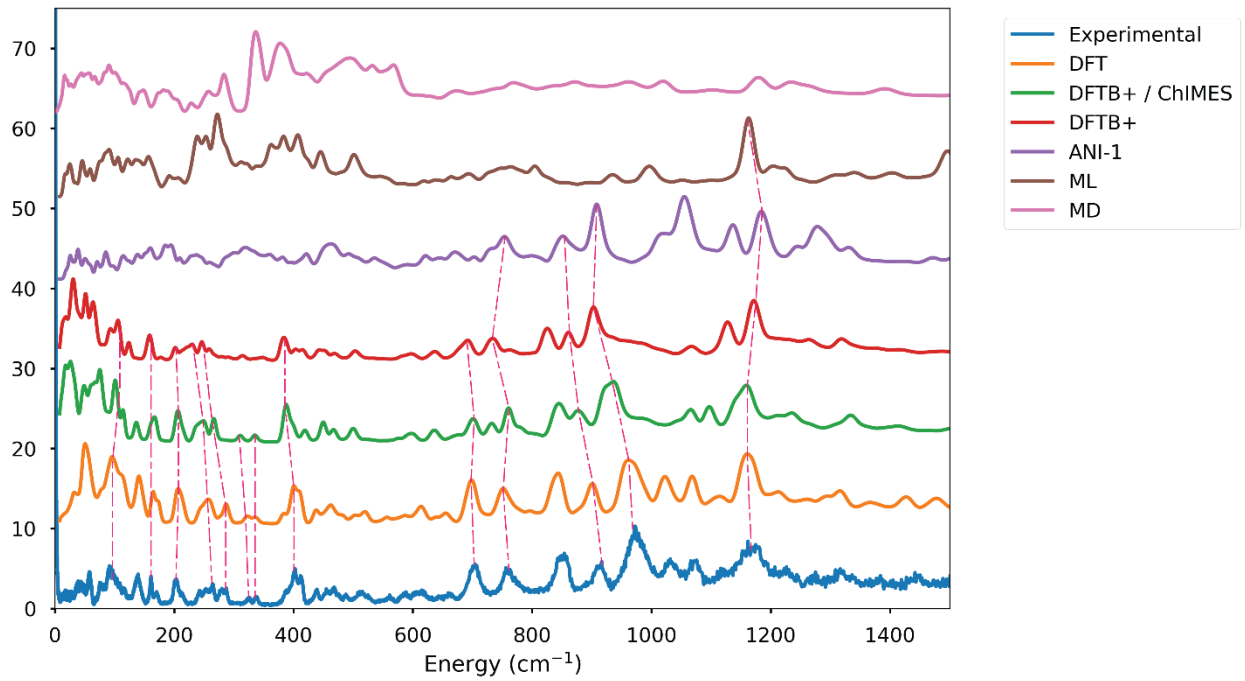

Publication 4: The process for simulating INS spectra using DFTB / ChIMES involves multiple different simulation codes that all have different input requirements. In general we had to (1) relax the structure using DFTB, (2) train ChIMES forces by comparing DFTB and DFT simulations, (3) calculate restoring forces using Phonopy, and (4) the load forces into the ORNL program OCLIMAX to simulate the INS spectrum. We took all of these steps and made a single useful workflow. We published this workflow as a GITHUB site so that it is freely available to the Neutron community and simulation community (https://gitlab.com/lucassamir1/DCS-Flow). We put considerable effort into bug-checking DCS-Flow and making an instruction manual and examples for how to use DCS-Flow efficiently (https://dcs-flow.readthedocs.io/en/latest/index.html). We also published DCS-Discover, an online searchable database of INS spectra would DFT, DFTB, and DFTB/ChIMES fits to the data (https://dcsdiscover.org/) The research article demonstrated that the ChIMES potential could be fit from small molecule samples, for example toluene, and still yield an accurate fit to large molecules. The training molecule must have all relevant bonds. Toluene has SP2 and SP3 hybridized C-C and C-H bonds, so the ChIMES model is valid for samples with these bond types. This transferability is critical if we ever want to simulate polymers accurately.[5]

Publication 5: Is an examination of which phonon modes contribute to the dynamic disorder and how should they be simulated. The Moule group published that all of the modes contribute to dynamic disorder and that the full Brillouin zone (FBZ) needs to be sampled in the DFT to accurately reproduce an INS spectrum and thus to validate the simulation. A competitor from Cambridge published a competing idea that Γ-point simulations are sufficient and that only one "killer" long axis phonon mode is responsible for the majority of the dynamic disorder. The appeal of the "killer mode" model is that it yields a synthetic design criteria. We compared Γ-point and FBZ simulations and showed that Γ-point underestimates dynamic disorder by 20-30%. In

addition, we show that simulation assuming only a single mode results in almost 300% underestimate of dynamic disorder. This paper is in review for the 3rd time.[6]

Publication 6: In this article we studied a mixture of small molecule donor and acceptor molecules for organic PV applications. The donor are merocyanines that had previously not shown good PV properties due to a tendency to phase separate from the fullerene. We studied the mixtures using SANS and GISANS (GI data did not work out). Our measurements allowed us to determine the mixing ratios in the two phases as a function of the side chain length. This is a nice materials study. The SANS study was pretty standard.

Publication 7: This study started in 2014. We had accidentally shown that we could optically pattern conjugated polymers but had no clue what the mechanism was. My undergrads developed a simple optical model based on shadow mask experiments. We submitted in 2015 but the paper was rejected. So, we got more data – the undergrad left – the project floundered. More recently we completed the paper on NSF funding and published in ACS Nano. The work in the first 4 figures is from the DOE work in 2014.[7]

Future Plans: We made an enormous investment in improved and lower cost methods to simulate INS spectra, specifically of OE materials for which intermolecular forces are mostly weak van der Waals forces. Next, we will use our recently developed methods to improve our ability to simulate structural disorder. One new possibility for gaining better insight to which atoms contribute to each dynamic mode is a new method to produce single atom INS spectra. We recently realized that we can create a separate spectrum for each atom (not just each proton) and we can use correlation methods to determine which atoms do and do not participate in correlated modes. We plan to apply this new method to the study of ever more complex OE samples.

A second goal is to simulate disorder. With MD the force field is poor and with DFTB we require repeating boundary conditions. We will work on a method to implement repeating supercells that contain disordered molecular geometries. Also we will develop a method to calculate restoring forces (the phonon energy) in non-relaxed molecular geometries. We plan to use differences in the peak widths and the single atom spectra method to fingerprint which parts of the sample are more and less ordered. The long-term goal behind all of these steps is to achieve high accuracy simulation of INS spectra for semi-crystalline and amorphous samples.

We will design and submit plans for a optical excitation sample environment on the VISION beamline. Daniel Vong is a 4th year PhD student from my group that received a SCGSR fellowship to work at SNS to design this sample environment. He will start in January 2022. The current best design uses a fiber optic to illuminate a powder sample that will be agitated or stirred to constantly mix the powder. Our goal is to achieve high density of excited states so that the INS spectrum of excited state sites can be detected and compared to the neutral sites. We believe that we can determine the triplet state transport rate in relation to excited state dynamic disorder using this measurement.

References

(1) Harrelson, T. F.; Dantanarayana, V.; Xie, X.; Koshnick, C.; Nai, D.; Fair, R.; Nunez, S. A.; Thomas, A. K.; Murrey, T. L.; Mickner, M. A.; Grey, J. K.; Anthony, J. E.; Gomez, E. D.; Troisi, A.; Faller, R.; Moule, A. J. Direct probe of the nuclear modes limiting charge mobility in molecular semiconductors. *Material Horizons* **2019**, *6*, 182-191.

(2) Dantanarayana, V.; Nematiaram, T.; Vong, D.; Cong, K. N.; Anthony, J. E.; Troisi, A.; Goldman, N.; Faller, R.; Moule, A. J. Predictive model of charge mobilities in organic semiconductor small molecules with force-match potentials. *Journal of Chemical Theory and Computation* **2020**, *16*, 3494-3503.

(3) Harrelson, T. F.; Dettmann, M. A.; Scherer, C.; Andrienko, D.; Moule, A. J.; Faller, R. Computing Inelastic Neutron Scattering Spectra from Molecular Dynamics Trajectories. *Scientific Reports* **2021**, *11*, 7938.

(4) Dettmann, M. A.; Cavalcante, L. S. R.; Magdaleno, C.; Masalkovait\'e, K.; Vong, D.; Dull, J. T.; Rand, B. P.; Daemen, L. L.; Goldman, N.; Faller, R.; Moule, A. J. Comparing the expense and accuracy of methods to simulate phonon modes in Rubrene. *Journal of Chemical Theory and Computation (in press)* **2021**.

(5) Cavalcante, L. S. R.; Daemen, L. L.; Goldman, N.; Moulé, A. J. Davis Computational Spectroscopy Workflow—From Structure to Spectra. *Journal of Chemical Information and Modeling* **2021**, *61*, 4486-4496.

(6) Vong, D.; Dettmann, M. A.; Murrey, T. L.; Gurses, S. M.; Nematiaram, T.; Radhakrishnan, D.; Daemen, L. L.; Anthony, J. E.; Koski, K. J.; Troisi, A.; Kronawitter, C. X.; Moule, A. J. Quantitative Hole Mobility Simulation andValidation in Substituted Acenes. *Journal of Physical Chemistry Letters (submitted)* **2022**.

(7) Jacobs, I. E.; Bedolla-Valdez, Z. I.; Rotondo, B. T.; Bilski, D. J.; Lewis, R.; Oviedo, A. N. A.; Gonel, G.; Armitage, J.; Li, J.; Moule, A. J. Super-Resolution Photothermal Patterning in Conductive Polymers Enabled by Thermally Activated Solubility. *ACS Nano* **2021**, *15*, 7006-7020.

Quantum multipolar fluctuations in spin-orbit magnets

Martin Mourigal, Georgia Institute of Technology, Atlanta, GA

Cristian Batista, University of Tennessee, Knoxville, TN

Program Scope

Insulating quantum magnets, where correlated magnetic moments reside at the vertices of a periodic lattice, are a central experimental and theoretical platform to understand the fundamental behavior of quantum materials. Quantum magnets are interacting quantum systems with the potential to host topological states that may form the bedrock of future energy and quantum technologies. The search for such topologically ordered states of matter, dominated by long-range quantum entanglement between spins rather than conventional magnetic order, is one of the grand challenges in contemporary material science [1]. Several controllable materials components are known to enhance quantum over classical correlations in spin-1/2 magnets: low lattice dimensionality as for chain- and ladder-based quantum liquids, geometrical frustration as for kagome, and pyrochlore lattice quantum spin-liquids, and exchange frustration as for the Kitaev honeycomb model. Although it is widely appreciated that higher spin-S systems (such as those comprising spin-1 moments) can realize unusual quantum states, for example, the Haldane and Affleck-Kennedy-Lieb-Tasaki chains, higher-spin systems have not been investigated for their quantum properties as thoroughly as their spin-1/2 counterparts.

The scope of this program is to explore a different class of quantum magnetic systems comprising spin-1 magnetic moments. The first objective of this program is to demonstrate that despite apparent conventional magnetic ordering at low temperature, the excitations of these compounds are highly unusual in that they carry multipolar moments with purely quantum dynamics (vanishing in the limit $\hbar = 0$). By using external material control tools such as magnetic-field, chemical substitution, and pressure, a second objective is to drive these quantum excitations to become the lowest-energy fluctuations in the systems under study. As a result, an outcome of this program is the emulation and understanding of magnetic materials proximate to quantum melting points and the development of tools and concepts to certify the existence of topological quantum states in materials.

This program combines expertise in materials science and neutron scattering at Georgia Tech and theory at the University of Tennessee to achieve its goals. A distinctive aspect of this program is the complete integration of experimental and theoretical efforts through the high-fidelity modeling of magnetic excitations measured on high-quality single-crystalline materials by time-of-flight inelastic neutron scattering. Materials growth is performed in-house or through collaborations with the Platform for the Accelerated Realization, Analysis, and Discovery of

Interface Materials (PARADIM). Neutron scattering experiments are performed at the Spallation Neutron Source (SNS) at Oak Ridge National Laboratory (ORNL) with a strong engagement of the researchers in forward-looking activities developing next-generation instrumentation for the High Flux Isotope Reactor and the Second Target Station of the SNS. Experimental neutron scattering data modeling is achieved by developing efficient spin dynamics simulations codes to tackle the direct and inverse problems for generalized magnetic Hamiltonians, including higher spin systems, anisotropic exchange, and dipolar interactions. These open-source resources are co-designed with a broader community of researchers at Los Alamos National Laboratory, University of Tennessee, and ORNL with broad expertise in computer simulations, quantum physics, magnetic materials, and scattering.

Recent Progress

- *Identification of FeI_2 as a model spin-1 system to understand quadrupolar excitations*

One of the achievements of this program is to have identified Ferrous Iodide (FeI_2) as a realization of the spin-1 antiferromagnet with hybridized dipolar and quadrupolar spin fluctuations. FeI_2 crystallizes in a trigonal space group with Fe^{2+} ions forming layers of perfect triangular lattice with strong single-ion anisotropy along the *c*-axis [**Fig 1a**]. In zero magnetic field, an antiferromagnetic ordered phase (AF) develops below $T = 9.3$ K and the magnetic structure features alternating stripes of up-up and down-down spins in the triangular plane. Two-magnon bound states (TMBS) were observed in this compound as early as the 1970's in this compound by far-infrared spectroscopy, triple-axis neutron scattering, Raman scattering and electron-spin resonance. The TMBS excitation in FeI_2 is unusual and corresponds to a $\Delta S^z = \pm 2$ transition. The bound-state is formed in a single site by flipping a spin twice from $S^z = +1$ to $S^z = -1$. Because this violates the dipolar selection rule, TMBS excitations have a quadrupolar character. We have uncovered the precise mechanism that makes such TMBS visible to various experimental techniques by measuring the entire momentum dependence of both single-magnon and TMBS branches in FeI_2 using SEQUOIA at ORNL. Spin-orbital coupling and local crystal field environment give rise to a triplet ground state with a large gap (>30meV) to higher multiplets. At low energy, FeI_2 can be described by a S_{eff}=1 model with a large uniaxial anisotropy. The key to the resolution of the apparent violation of the selection rule is to go beyond a simple Heisenberg exchange model and include anisotropic exchange interactions allowed by

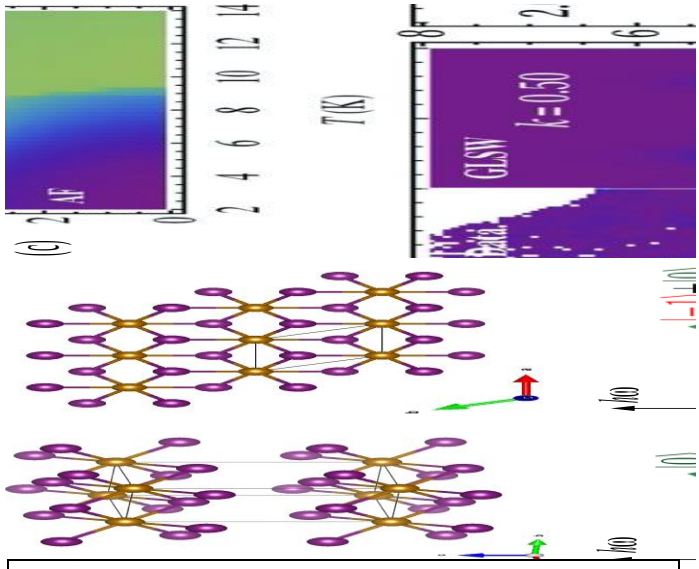

Fig. 1 (a) Crystal structure of FeI_2 (purple spheres: Fe, orange spheres): I; (b) mechanism of hybridization between dipolar and quadrupolar excitations through symmetric off-diagonal exchange interactions in FeI_2.

symmetry. In FeI_2, the off-diagonal exchange interaction $J^{z\pm}$ term is unusually large and dominates other exchanges. The $J^{z\pm}$ term leads to an hybridization between single-magnon and two-magnon bound-state bands, that accidentally overlap in zero field, hence making two-magnon states visible to neutron scattering and various other probes [**Fig. 1b**]. Using a generalized spin-wave theory (GLSW) approach for SU(3) spins explains all details of the zero-field data when including up to third-neighbor interactions in the triangular planes and between those planes [See publication **8** below].

- *Magnon pairing and decay of excitations in FeI_2*

Given the presence of significant off-diagonal exchange interactions, parameterized by exchange interactions $J^{z\pm}$ and $J^{\pm\pm}$, new forms of spontaneous (zero-temperature) magnon decays are possible in FeI_2. Using neutron scattering in an applied magnetic field on the HYSPEC spectrometer, this program observed these instabilities [**Fig. 2a**], which correspond to a new mechanism for spontaneous decay between conventional and heavy magnons (TMBS). We also observed the recombination of these quasiparticles into a super-heavy bound state. Akin to other contemporary problems in quantum materials, the microscopic origin for new physics in FeI_2 is the quasi-flat nature of excitation bands and the presence of Kitaev-like anisotropic magnetic exchange interactions. What is truly remarkable is to observe such purely quantum phenomena in a well-ordered magnet [See publication **4** below].

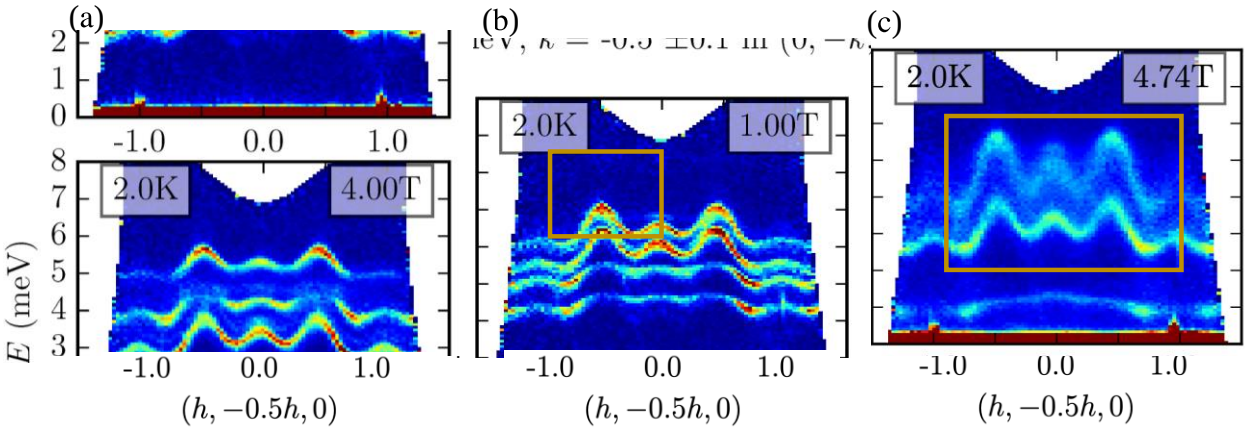

Fig. 2 Excitations of FeI_2 measured at 1 T on HYSPEC revealing the Zeeman splitting of zero-field excitations. (b) Excitations at 4 T evidencing the finite lifetime of one of the excitation branches (orange square). (c) Excitations at 4.74 T evidencing a dramatic broadening of the entire excitation spectrum when one of the two-magnon bound-state excitations approaches the elastic line and gets thermally populated.

- *Finite-temperature dynamics of SU(N) magnets*

When a large magnetic field is applied to FeI_2, a series of high-field meta-magnetic phases occur. In proximity to the transition, thermal fluctuations are important as shown by our neutron results [**Fig. 2b**]. It is an open theoretical question to understand how quantum and classical spin dynamics differ in the proximity to such transition, when the individual degrees of freedoms are spin-S and

not spin-1/2. To understand this problem this program introduced a classical limit of the dynamics of quantum spin systems based on coherent states of SU(*N*), where N is the dimension of the local Hilbert space. This approach, that generalizes the well-known Landau-Lifshitz dynamics from SU(2) to SU(N), provides a better approximation to the exact quantum dynamics for a large class of realistic spin Hamiltonians, including systems with large single-ion anisotropy [See publication **6** below]. This idea was illustrated by comparing the spin structure factors of a single-ion *S*=1 model that are obtained with the SU(2) and SU(3) classical spin dynamics against the exact solution. These results pave the way to generalized approach to deal with finite temperature, finite magnetic field spin dynamics for S≥1 systems such as FeI_2.

Future Work

- *High-field extraction of accurate spin Hamiltonians for FeI_2 and $FeBr_2$*

Combining these theoretical and experimental developments, our future work involves modeling the excitations of FeI_2 over its entire temperature-magnetic-field phase diagram. Doing so requires understanding the spin Hamiltonian in detail. Using the new high-magnetic field capabilities at ORNL, we have measured [**Fig. 3**] the saturated dispersion of magnons in FeI_2 at 14T and related material $FeBr_2$ at 3T to extract model Hamiltonians and understand the role of ligand spin-orbit coupling in this class of magnetic systems. The future work is to implement an inverse modeling technique to extract the many-parameters Hamiltonian from data at zero and high fields.

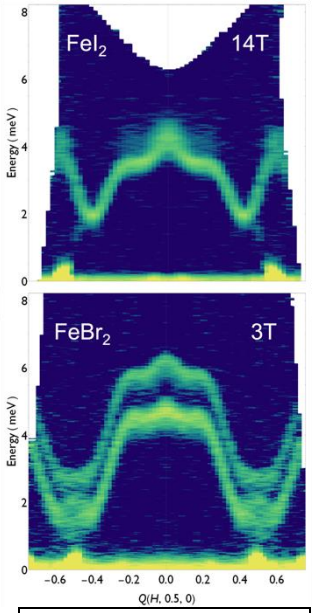

Fig. 3. Comparison of saturated magnetic field excitations for FeI_2 at 14T and $FeBr_2$ at 3T.

- *Modeling exotic meta-magnetic phases and near-magnon condensation in FeI_2*

With accurately determined Hamiltonians at hand, future work will measure and model the spin dynamics in the meta-magnetic phases of FeI_2 and $FeBr_2$ to understand excitations in multipolar spin systems proximate to quantum melting points.

- *Development of community-led open-source spin dynamics simulation codes*

The above activities will rely on the on-going development and acceleration of computer codes to simulate the spin dynamics of generalized SU(*N*) Hamiltonians including complete treatment of bilinear spin interactions (off diagonal, and dipolar). Future work involves participating in the community development of a Julia-based code "Su(N)ny": https://github.com/MagSims/Sunny.jl

References

[1] C. Broholm, R. J. Cava, S. A. Kivelson, D. G. Nocera, M. R. Norman, T. Senthil, Quantum Spin Liquids, Science 367, 263 (2020) https://doi.org/10.1126/science.aay0668

Publications (November 2019 to November 2021)

9. Anaëlle Legros, Shang-Shun Zhang, Xiaojian Bai, Hao Zhang, Zhiling Dun, W. Adam Phelan, Cristian D. Batista, Martin Mourigal, N. P. Armitage, *Observation of 4- and 6-magnon bound-states in the spin-anisotropic frustrated antiferromagnet FeI_2*, Submitted. https://arxiv.org/abs/2012.04205

8. Xiaojian Bai, Shang-Shun Zhang, Hao Zhang, Zhiling Dun, W. Adam Phelan, V. Ovidiu Garlea, Martin Mourigal, Cristian D. Batista, *Instabilities of heavy magnons in an anisotropic magnet*, Submitted. https://arxiv.org/abs/2107.05694

7. Jingyue Wang, Yuxuan Jiang, Tianhao Zhao, Zhiling Dun, Anna L. Miettinen, Xiaosong Wu, Martin Mourigal, Haidong Zhou, Wei Pan, Dmitry Smirnov, Zhigang Jiang, *Magneto-transport evidence for strong topological insulator phase in $ZrTe_5$*, Nature Communications (In Press), (2021-11-02). https://arxiv.org/abs/2111.01451

6. Hao Zhang, Cristian D. Batista, *Classical spin dynamics based on SU(N) coherent states*, Phys. Rev. B **104**, 104409 (2021-09-07). https://doi.org/10.1103/PhysRevB.104.104409

5. Zhiling Dun, Xiaojian Bai, Matthew B. Stone, Haidong Zhou, and Martin Mourigal, *Effective point-charge analysis of crystal fields: Application to rare-earth pyrochlores and tripod kagome magnets $R_3Mg_2Sb_3O_{14}$*, Phys. Rev. Research **3**, 023012 (2021-04-02). https://doi.org/10.1103/PhysRevResearch.3.023012

4. Xiaojian Bai, Shang-Shun Zhang, Zhiling Dun, Hao Zhang, Qing Huang, Haidong Zhou, Matthew B. Stone, Alexander I. Kolesnikov, Feng Ye, Cristian D. Batista, and Martin Mourigal, *Hybridized quadrupolar excitations in the spin-anisotropic frustrated magnet FeI_2*, Nature Physics **17**, 467–472 (2021-01-04). https://doi.org/10.1038/s41567-020-01110-1

3. Zhiling Dun, Xiaojian Bai, Joseph A. M. Paddison, Emily Hollingworth, Nicholas P. Butch, Clarina D. Cruz, Matthew B. Stone, Tao Hong, Franz Demmel, Martin Mourigal, and Haidong Zhou, *Quantum Versus Classical Spin Fragmentation in Dipolar Kagome Ice $Ho_3Mg_2Sb_3O_{14}$*, Phys. Rev. X **10**, 031069 (2020-09-29). https://doi.org/10.1103/PhysRevX.10.031069

2. Y. Jiang, J. Wang, T. Zhao, Z. L. Dun, Q. Huang, X. S. Wu, M. Mourigal, H. D. Zhou, W. Pan, M. Ozerov, D. Smirnov, and Z. Jiang, *Unraveling the Topological Phase of $ZrTe_5$ via Magnetoinfrared Spectroscopy*, Phys. Rev. Lett. **125**, 046403 (2020-07-24). https://doi.org/10.1103/PhysRevLett.125.046403

1. X. Bai, *Neutron Scattering and Quantitative Modeling of Magnetic Excitations In Frustrated Magnets*, PhD Thesis, Georgia Institute of Technology (2019-11-06). http://hdl.handle.net/1853/64040.

Encoding Material Structure Into the Primary Sequence of Polymers

Bradley Olsen, Department of Chemical Engineering, Massachusetts Institute of Technology

Program Scope

One of the largest research challenges in soft materials is using chemistry to design molecules where the arrangement of atoms encodes for the formation of exquisite, hierarchically structured materials that can approach the complex and highly functional systems made in biology, variants of which have been identified in several key DOE-BES reports as priority research directions. The problem of encoding material structure using primary sequence for linear chains requires the ability to construct a polymer with a given function, f(s) where s is the path length variable along the backbone of the polymer chain and f is a vector of relevant properties along the length of the chain such as hydrophobicity, polarity, presence of specific hydrogen bonding groups, charge, or aromatic groups. Second, one must learn the translation function by which a chain with a given f(s) forms a specific nanostructure, such that one can solve the problem of designing an f(s) in order to achieve a given nanostructure. This problem has been approached with great success for several decades using relatively simple f(s); for example, step functions characterize diblock copolymers and monotonically increasing or decreasing curves characterize gradient or tapered copolymers. There is potential for further transformative advance if we could design polymers with arbitrary f(s) because it would enable us to potentially discover new phases and material structures and to more carefully encode the free energy surface and consequently non-equilibrium behavior of the material in a way that could enable us to exquisitely tune the phase formed based on the processing pathway utilized. Synthesis of an arbitrary f(s) is easily achieved today using biological synthesis of elastin-like proteins (ELPs), enabling the preparation of long macromolecules in comparatively high yield. In this proposal, we will therefore exploit biological sequence-controlled polymerization as a well-established tool to specifically encode material structure and free energy surfaces, developing new paradigms for designing equilibrium and far from equilibrium structures. To enable these scientific developments, we will also develop new methods of experimentation and data analysis, particularly related to the use of neutron scattering techniques, that facilitate the characterization of equilibrium and non-equilibrium structure and the dynamics of these materials.

Recent Progress

Development of a Model for Sequence-Defined Self-Assembly. A novel formalism for self-consistent field theory (SCFT) was developed allowing fast and simple simulation of the ordered

phases formed by sequence-defined polymers. Within the sequence-defined view enabled by this formalism, the chemical identities and interactions between dissimilar monomers found in polymers formed from two or more monomer are encapsulated via a set of interaction functions. These chain functions ***f(s)*** are defined along the polymer backbone (denoted with contour variable *s*). Classical SCFT was extended to enable the use of this continuous backbone function via the introduction of four-dimensional fields (defined within the three direct space dimensions and the contour dimension) and a scalar pairwise interaction model. Figure 1 shows a schematic of how this novel SCFT method (sequence-SCFT) operates. The Hamiltonian term which is minimized in SCFT under the sequence-SCFT formalism is shown. Numerical solution of this novel formalism was performed using a custom code. By pseudospectrally solving the SCFT propagator equations and using basis functions reflecting the space group symmetries of the self-assembled structures, sequence-SCFT has successfully been (1) validated against the classical diblock phases (lamellar, hexagonally packed cylinders, and body-centered cubic), and (2) used to recreate structures formed by more complex sequences such as those of triblocks and inverse tapers.

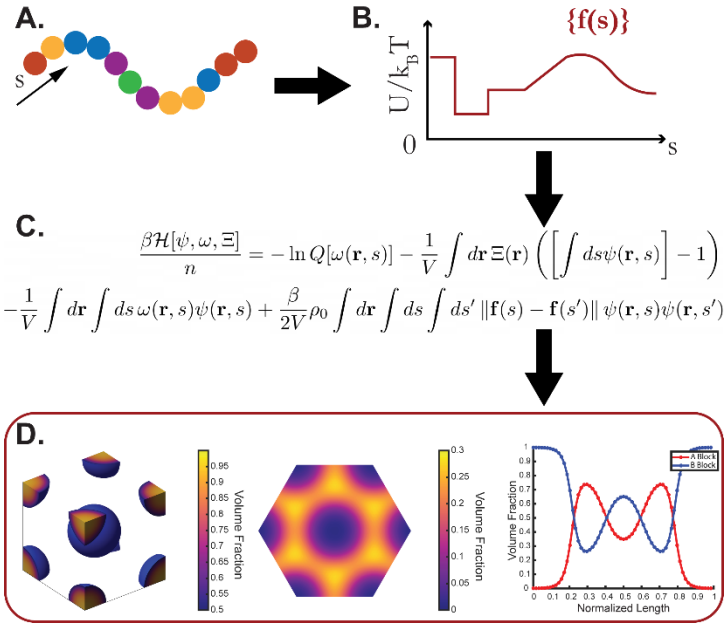

Figure 1: (A) Sequence-defined polymers can be represented by a set of interaction functions of any form (B). (C) The novel SCFT formalism we developed to handle sequence-defined polymers has a Hamiltonian containing fields defined in four dimensions (direct and contour space). (D) Using this formalism, we have successfully validated our SCFT results with those of classic diblock structures (left), and simulated the ordered phases of more complex polymers such as triblocks (center – shown is the minority block), and inverse tapers (right).

Design and Synthesis of Sequence-Defined ELPs. As a basis for sequence-controlled design, we must connect the sequence functions used in theory to specific identities of ELP repeats. To do this, we designed and synthesized a set of seven different ELPs with guest residues V, I, K, D, N, G, and S, spanning the majority of the different chemical functionalities accessible using amino acids. To parameterize the interactions of these materials, we are measuring their thermal transition temperatures under a variety of salt and cononsolvent conditions, providing detailed maps of their interactions. The cononsolvency effect in ELPs itself is a very new phenomenon in protein materials that has not yet been thoroughly explored, and this ongoing study will represent the first work systematically exploring residue substitution and its effect on cononsolvency.

These interactions measured during this fundamental study will then be used as the basis for the design of micellar self-assembled materials with novel structural transitions governed by their kinetic assembly pathway. To prepare for these studies, we are developing both a custom dialysis holder for SANS as well as new analysis methods that will enable us to speed up data acquisition to capture more of the kinetics of structural transitions. Our technique for higher speed data acquisition will rely on using parameter estimation errors to systematically shorten data acquisition times without compromising data quality, as illustrated in Figure 2.

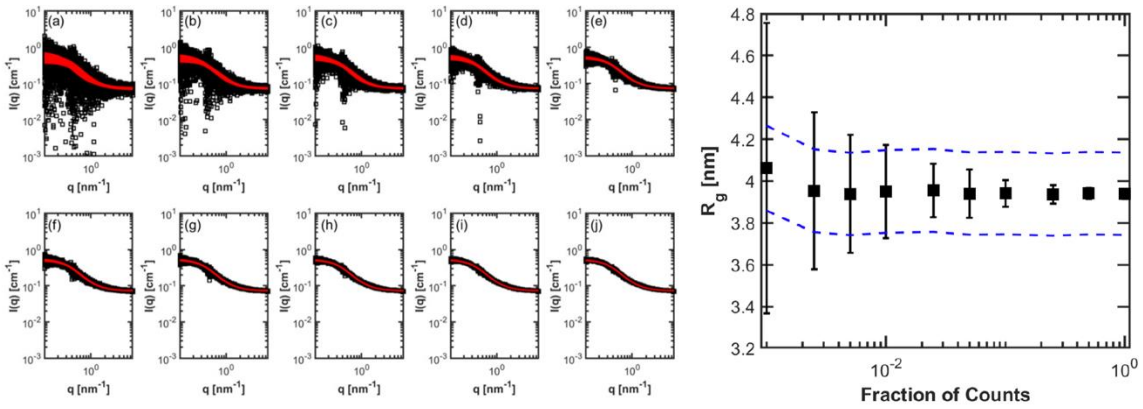

Figure 2. (Left) Bootstrapped SANS intensity curves with predicted uncertainties from reducing the number of total counts. The data were simulated for fractions of the total counts collected from 0.001 to 1. The red lines illustrate the fit of each bootstrapped dataset to the Debye form factor. (Right) Radius of gyration of PNIPAM in 100% D2O as a function of the number of neutron counts, estimated as a fraction of the total number of counts collected from a SANS experiment. The error bars are 1 standard deviation calculated from bootstrapped replicates. The blue lines represent a 5% error tolerance.

Quantification of Bound Water in Concentrated Systems. A key aspect of understanding the self-assembly of sequence-defined proteins is the way that these systems interact with water. Therefore, we have developed tools for quantifying bound hydration water that can be applied to these systems. While this challenge has been extensively addressed in dilute solution, moving to concentrated systems relevant to self-assembly (micellar cores, bulk nanostructured phases) presents a novel challenge. To address this issue, we have applied existing dilute solution methods for hydration number estimation and developed several new methods that generalize to high concentration for a total of six different fitting methods. We have then performed detailed SANS contrast matching experiments for three different

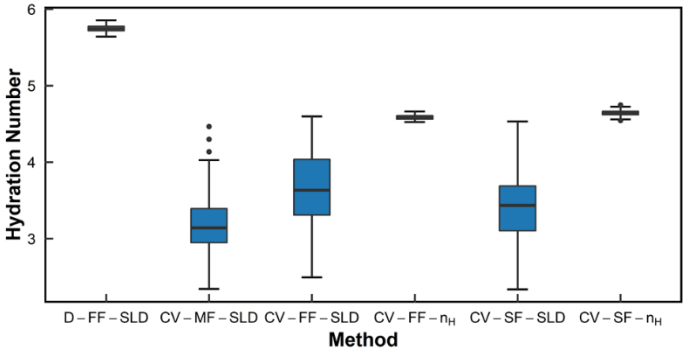

Figure 3. Six different fitting methods for dilute (13.75 mg/mL PNIPAM solutions.

water-soluble polymers, and the data was modeled using each of the six different approaches to explore both the stability of fitting and the values of hydration number they produced. Error was estimated with a novel bootstrapping technique that we find produces significantly more representative errors for SANS parameter extraction tasks (Figure 3). The most robust fitting workflow for dilute solutions was found to be form factor fitting without CV-SANS (i.e. polymer in 100% D_2O). For semidilute and concentrated solutions, structure-factor based approaches were found to be most successful. The measured hydration numbers were consistent with the number of tightly bound water molecules associated with each monomer unit, and the concentration dependence of the hydration number was largely governed by the chemistry-specific interactions between water and polymer. Polymers with weaker water-polymer interactions (i.e. those with fewer hydration water molecules) were found to have more bound water at higher concentrations than those with stronger water-polymer interactions due to the increase in the number of forced water-polymer contacts in the concentrated system.

Future Plans

Now that we have developed the underlying SCFT to serve as a structure prediction and design engine, we will make the next step in development of this theory by imposing specific lattice symmetries and then solving for chain functions f(s) which are predicted to preferentially self-assemble into those symmetries. A straightforward approach to finding such functions is to explore f(s) space with a given set of symmetry-adapted basis functions that represent the lattice symmetry we are targeting, identifying functions that yield a minimum free energy. The functions that lead to local minima must then be screened in other lattice symmetries to compare phases and determine that the target phase is in fact the lowest free energy. Using the phase diagram studies of ELPs that are currently underway, we will then parameterize thermodynamic models for polymer solutions that will then serve as the basis for translating different sequence functions into specific chemical manifestations which we will express and use to evaluate the overall predictive workflow developed here. In addition, these interactions determined from cononsolvency studies will be used in the design of micellar systems with triggered transitions as described in our original proposal.

Using elastin-like polypeptides (ELP), we have designed domains capable of forming dynamic interactions that can produce kinetically controlled phases. These dynamic interactions will be used as orthogonal levers in conjunction with global thermodynamic variables such as temperature or salt concentration to control the assembly pathway of ordered phases in ELP and to investigate nonequilibrium structure. Ordered micelles are formed from these ELP due to the difference in coil-globule transition between the endblocks in triblocks and in one of the two blocks in diblocks. The percentage and distribution of histidine (f_{His}) in the midblock region was varied to investigate the use of histidine-metal coordination bonds as an additional dimension of control over self-assembly, and the distance between pairs of cysteines (l_{Cys})—staples—was varied to control the degree of single-chain "stapling". Material synthesis is currently underway.

Publications

1. “SANS Quantification of Bound Water in Water-Soluble Polymers Across Multiple Hydration Regimes.” H. Yao and B.D. Olsen. *Soft Matter* **2021**, *21,* 5303-5318.

2. “Effect of Protein Surface Charge Distribution on Protein-Polyelectrolyte Complexation.” S. Kim, H.V. Sureka, A.B. Kayitmazer, G. Wang, J.W. Swan, and B.D. Olsen. *Biomacromolecules* **2020,** *21*, 3026-3037.

3. “Polymer Domains Control Diffusion in Protein-Polymer Conjugate Biosensors.” J. Paloni and B.D. Olsen. *ACS Applied Polymer Materials* **2020**, *2,* 4481-4492.

4. “Coiled-Coil Domains for Self-Assembly and Sensitivity Enhancement of Protein-Polymer Conjugate Biosensors.” J. Paloni and B.D. Olsen. *ACS Applied Polymer Materials* **2020**, *2,* 1114-1123.

5. “Secondary Structure Drives Self-Assembly in Weakly Segregated Globular Protein-Rod Block Copolymers.” H. Yao, K. Sheng, J. Sun, S. Yan, Y. Hou, H. Lu, and B.D. Olsen. *Polymer Chemistry* **2020**, *11*, 3032-3045.

6. “Bridging Dynamic Regimes of Segmental Relaxation and Center-of-Mass Diffusion in Associative Protein Hydrogels.” A. Rao, H. Yao, and B.D. Olsen. *Physical Review Materials,* **2020,** 043369.

7. “SANS Partial Structure Factor Analysis for Determining Protein-Polymer Interactions in Semidilute Solution.” A. Huang, H. Yao, and B.D. Olsen. *Soft Matter* **2019**, *15,* 7350-7359.

Ionic Polymers Under Dynamic Conditions
Dvora Perahia, Clemson University

Program Scope

The program aims to resolve the structure and dynamics of ionic polymers under fields using neutron scattering and computational tools. In their many applications, [1-3] such as clean energy, water purification, protective layers, memory shape material and a large variety of biotechnologies, ionic polymers function under external fields such as shear, elongation flow, and electrical fields. In the quiescent state the segregation between ionic and non-ionic domains enables their function and stability. [4, 5]

Even though the quiescent state has been thoroughly interrogated, the fundamentals that correlate the ionic assemblies characteristics with the dynamics of the polymers that ultimately affect their function is yet to be achieved. The current program focuses on probing the inter relation between ionic clusters and inherent dynamics through the study of the polymer response to shear and flow fields. Detailed neutron scattering studies including in situ measurements under fields, coupled with molecular dynamics simulations, are used to derive quantitative structure-dynamics-forces correlations in model ionic polymers.[6-8] Polystyrene sulfonate was chosen as a model polymer for this study. This polymer either by itself or as a block in a structured polymer has been thoroughly studied, allowing us to focus on understanding the relation between the characteristics of the ionizable domains, the inherent dynamics and shear response. The research consists of two main efforts: a) resolving structure and dynamics of quiescent ionic polymers as the cohesiveness of ionic clusters is tuned, b) resolving effects of shear and flow fields on the ionic clusters.

In situ neutron scattering techniques are in a unique position to capture detailed structure and dynamics in ionizable polymers on the nanometer length scale. Computational studies are used to provide molecular insight into the systems studied by neutron scattering and tether measurements from different length and time scales. The structures obtained from atomistic molecular dynamics simulations provide detailed insight into assemblies that cannot be captured directly by scattering techniques. Neutron scattering together with computational studies provide the insight needed to capture the inherent dynamic processes and those that take place under applied fields.

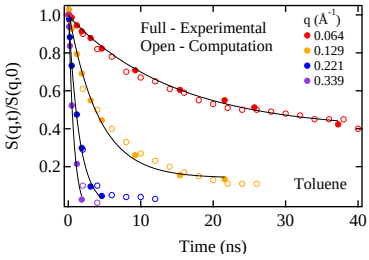

Figure 1. Experimental and computational neutron spin echo results for a 3% sulfonated polystyrene sulfonate in a 10Wt% solution of polymer in toluene at room temperature.

Finally, through bridging across length, time and energy scales, transformative fundamental knowledge that underline dynamic ionic assemblies under fields are probed. The excellent match between neutron scattering and molecular dynamics (MD) simulations demonstrated in Figure 1 for NSE of PSS in toluene, provide a first of a kind insight into the structure and dynamics of ionizable polymers.[9, 10] The fundamental insight attained by neutron techniques and MD simulations provide a critical insight for the design of new ionic polymers with controlled properties.

Recent Progress

The interrelation between neutron scattering and computational studies provide molecular insight to the ensemble averaging attained by neutron techniques. Here we will discuss the molecular insight attained into SANS, QENS and NSE coupled with MD simulations, followed by MD studies of response of melts and dense slurries to shear and elongational flows. These MD studies are carried out along the research plans with neutron studies awaiting beam time allocation.

I-Cluster Characteristics Effects on Inherent Structure and Dynamics of Polystyrene Sulfonate Solutions.

Polystyrene sulfonate solutions in toluene were studied by SANS, QENS and NSE. The ionic assemblies were modified by controlling the degree of sulfonation, varying the concentration of the polymer, as the ionic groups are formed and addition of aliquots of polar solvents that affect the polarity of the solvent. The excellent match of the experimental and computational SANS patterns is shown in Figure 2-a and the impact of addition of a polar solvent is depicted in Figure 2-b. Large domains, attributed to concentration fluctuations, are evident at low q, independent of the polymer concentration. In the middle q range, a characteristic Gaussian chain form factor is observed in low concentrations and low sulfonation fractions and transform to a signature of an ionic domain with increasing concentrations. These data were analyzed in terms of a Bacauge model. When alcohol is added the solutions, the solution become significantly more homogenous and the signature at low concentrations disappears. In parallel to this experimental study, S(q) was calculated and analyzed. Due to computational limitations, S(q) captures only the intermendiate q range. The conjunction of both techniques clearly show that both concentrations and polar solvents directly influence the packing of the ionizable groups within the ionic domains. While polar solvents affect the correlations between the ionic groups, they do not desocciate the clusters.

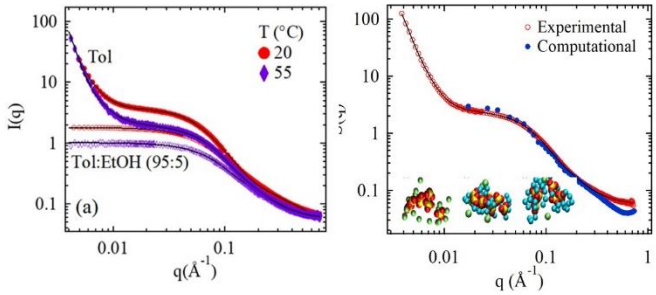

Figure 2. SANS results for a 10Wt% PSS in toluene with a 3% sulfonation a) in toluene and as ethanol is added, and b- experimental I(q) and calculated S(q) for the toluene solution together with visualization of the clusters with different ethanol fractions with the following color key. Yellow- Sulfur, Red- Oxygen, Blue- EtOH Oxygen atom, Green- Toluene CH_3 C atom. Note that the backbone is not shown.

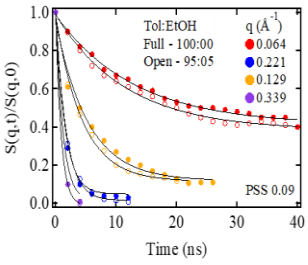

Figure 3. NSE data of the PSS in toluene and toluene-ethanol.

The packing of the ionic groups however affects the chain dynamics as observed in both NSE, shown in Figure 1 and in QENS. Using NSE we were able to attain the motion of ionomer networks on the length scale of propagation of electrostatic interactions and that of the ionic clusters. The

data were analyzed by a sum of two exponentials resulting in an excellent fit. We were able to distinguish two characteristic environments, confined to the ionic clusters and the ionic region. Further we were able to show that the presence of polar solvents affects the packing of the ionic groups and accelerate dynamics, as shown in Figure 3. The excellent match between the experimental data and the simulations has allowed us to identify the motion of the polymer on different time and length scales moving from general models traditionally used to analyze NSE results to a comprehensive insight into dynamics.

QENS measurements of the same polymer were then carried out in cyclohexane (to avoid overlapping signals from the polymer and the solvent). The samples were heated to ensure that the backbone of the polymer is in good solvent. The scattering patterns were analyzed by Kohlrausch-Williams-Watts (KWW) to extract characteristic relaxation times. Here we show for the first time that in hydrophobic solvents, the segmental dynamics, which is relatively fast, is constrained in solutions on the length scale of smallest rigid segment. Addition of small amounts of ethanol enhances dynamics across the entire q range measured, however, the effects become larger for larger q values, demonstrating the coupling of length scales. Here we show that both ionic clusters and ionic clouds affect segmental motion on multiple length scales even though the ionic clusters are only slightly modified.

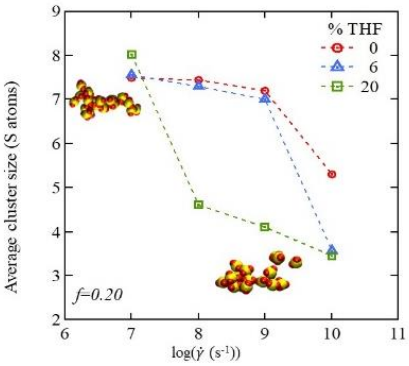

Figure 4. Average cluster size for PSS with 20% sulfonation as a function of shear rate at T = 500 K for the neat melt and swollen with THF.

The results attained from simulations are marked by an extraordinary matching between neutron scattering results and those obtained by computations, opening the way to new neutrons-computational insight into polymers for the energy water nexus.

II-Viscoelastic Response of Ionizable Polymer Melts and Dense Slurries Following the understanding of inherent dynamics the interrelation between ionic clusters and ionizable polymers response to shear has been probed by non-equilibrium MD simualtions of PSS melts and dense slurries, as a model polymer. Initially, the melts were prepared and slightly swollen with THF. THF that is a non-solvent for PSS, thus swells the ionic clusters and affect their cohesion without plasticizing the PS backbone. S(q) and S(q,t) were calculated. With increasing THF concentration, the melts are dominated by finite size ionic clusters. While these melts are locked in by the clusters, as observed by mean square displacement measurement, S(q,t) was able to depict segmental dynamics on a nanometer and bond length scales.

The response of these melts to shear was then probed. Cluster size as a function of shear rates is shown in Figure 4 and the shear viscosity as a function of time is depict in Figure 5. We find that the shear response strongly depends on cluster size and shape which is also affected by the interrelation with the degree of swelling.

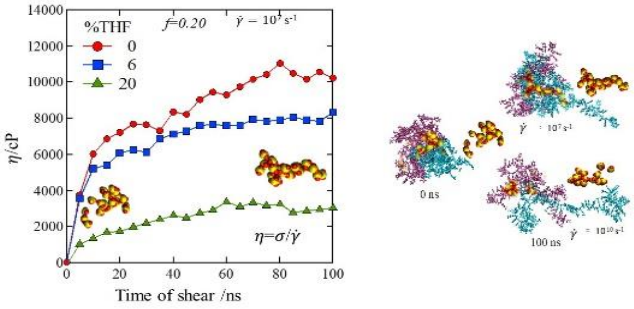

Figure 5. Shear viscosity for polystyrene sulfonate as a function of shear rates at the indicated THF concentrations as time elapses. The right panel visualized one representative cluster.

Finally, the response to elongational flows was measured and the viscosity was correlated with chain conformation and the ionic cluster characteristics. We find that with extensional flow, the ionic clusters are dynamic, rapidly breaking and reforming. For low sulfonation fractions, the chains are stretched while at higher sulfonation fractions a very broad distribution of end-to-end distances of the chains is observed.

The experimental part is awaiting beam time.

Future Plans

With our neutron studies fully coupled to molecular dynamics simulations, we were able to achieve for the first time an in-depth insight into the correlation of cluster cohesion and dynamics of ionic polymers. Selected neutron experiments are planned to study the structure evolution of polystyrene sulfonate as shear and elongational flow are applied.

References

1. Rajangam, P., Hydrogen Fuel Cells as Green Energy. In *Cases on Green Energy and Sustainable Development*, IGI Global: 2020; pp 291-323.
2. Li, D.; Park, E. J.; Zhu, W.; Shi, Q.; Zhou, Y.; Tian, H.; Lin, Y.; Serov, A.; Zulevi, B.; Baca, E. D., Highly quaternized polystyrene ionomers for high performance anion exchange membrane water electrolysers. *Nature Energy* **2020**, 1-8.
3. Adhikari, S.; Pagels, M. K.; Jeon, J. Y.; Bae, C., Ionomers for Electrochemical Energy Conversion & Storage Technologies. *Polymer* **2020**, 123080.
4. Bostwick, J. E.; Zanelotti, C. J.; Iacob, C.; Korovich, A. G.; Madsen, L. A.; Colby, R. H., Ion Transport and Mechanical Properties of Non-Crystallizable Molecular Ionic Composite Electrolytes. *Macromolecules* **2020,** *53* (4), 1405-1414.
5. Wang, Y.; Diaz, D. F. R.; Chen, K. S.; Wang, Z.; Adroher, X. C., Materials, technological status, and fundamentals of PEM fuel cells–a review. *Materials Today* **2020,** *32*, 178-203.
6. Richards, J. J.; Riley, J. K., Dielectric RheoSANS: A Mutual Electrical and Rheological Characterization Technique using Small Angle Neutron Scattering. *Current Opinion in Colloid & Interface Science* **2019**.
7. De Luca, E.; Waigh, T. A.; Monkenbusch, M.; Kim, J. S.; Jeon, H. S., Neutron spin echo study of the dynamics of micellar solutions of randomly sulphonated polystyrene. *Polymer* **2007,** *48* (14), 3930-3934.
8. Earnest Jr, T.; Higgins, J.; Handlin, D.; MacKnight, W., Small-angle neutron scattering from sulfonate ionomers. *Macromolecules* **1981,** *14* (1), 192-196.
9. Senanayake, M.; Aryal, D.; Grest, G. S.; Perahia, D., Interfacial Response and Structural Adaptation of Structured Polyelectrolyte Thin Films. *Macromolecules* **2021,** *54* (6), 2892-2898.

Manuscripts Currently Published and In-Preparation.

1. Invited Book Chapter: *Neutron tools: probing structure and dynamics of light weight, ionizable polymers for energy generation and storage*, Editor S. Greenbaum, in Analytical Tools for Energy Applications. Springer. Dvora Perahia (In press)

2. *Effects of interaction strength of associating groups on linear and star polymer dynamics,* M. Senanayake, D. Perahia, and G. S. Grest, 2021, The Journal of Chemical Physics 154, 074903. *This paper was selected as an Editor's Pick.*

3. *Effects of Nonlinear Elongation Flows of Associating Polymer Melts,* Supun S. Mohottalalage, Manjula Senanayake, Dvora Perahia, Gary S. Grest, and Thomas O'Connor, in Review, PRX.

4. *Response of Sulfonated Polystyrene Ionomers to Extensional flow,* Supun S. Mohottalalage, Chathurika Kosgallana, Shalika D. K. Meedin, Dvora Perahia, Gary S. Grest, and Thomas O'Connor, *In preparation to Soft Matter.*

5. Effects of Ion Group Distribution on the Structure and Dynamics of Amorphous Ionomers Supun S. Mohottalalage, Dipak Aryal, Bryce Thurston, Gary S. Grest, and Dvora Perahia *In review, Macromolecules.*

6. *Effects of ionic clusters size and distribution on the structure of polystyrene sulfonate solutions: SANS and Computational Insight.* Chathurika Kosgallana, Supun S. Mohottalage, Manjua Senanayake, Lilin He, Gary S. Grest, and Dvora Perahia, *In preparation to PRL*

7. Effect of Cluster Formation on Dynamics of Ionic Polymers in Solutions: Molecular Dynamics Simulations Studies Chathurika Kosgallana. Supun S. Mohottalalage, Gary S. Grest Dvora Perahia, *In preparation to J. Chem. Phys.*

8. *Segmental Dynamics of Lightly Sulfonated Polystyrene Ionomers in Solutions: Quasi Elastic Neutron Scattering Study*, Supun S. Mohottalalage, Manjula Senanayake, Naresh Osti, Lilin He, Dvora Perahia, *In Preparation JACS.*

9. Solvent effects on Dynamics of polystyrene sulfonate solutions NSE insight Sidath Wijesinghe, Chathurika Kosgallana, Manjula Senanayake, Michael Ole, Piotre Zolnierczuk , Gary S. Grest, Dvora Perahia. *In Preparation to PRL*

10. Sulfonated Polystyrene Melts and Dense Suspension: Ionomer Regime, Chathurika Kosgallana, Gary S. Grest, Dvora Perahia. *In Preparation to Macromolecules*

11. NMR Study of Solvent Effects on Diffusion of Polystyrene sulfonate in solutions Shaika Meedin, Chathrika Kosgallana, Supun S. Mohottalalage, and Dvora Perahia *In preparation to JMR or Macromolecules*

12. Sulfonated Polystyrene Melts and Dense Suspension: Polyelectrolyte Regime Shalika Meedin, Gary S. Grest, Dvora Perahia *In Preparation to Macromolecules*

13. Unlocking Ionic Polymer Melts through Solvents and Shear: Molecular Dynamics Simulations Study, Shalika D. K. Meedin, Chathurika Kosgallana, Supun S. Mohottalalage, Dvora Perahia, and Gary S. Grest, *In Preparation to Journal of Rheology*

Deciphering Low Energy Spin and Orbital Dynamics in Frustrated Quantum Magnets

Kemp Plumb, Brown University, Department of Physics, Providence, RI 02912

Program Scope

Quantum spin liquids are novel states of matter that exist in magnetic materials near absolute zero and are defined by the presence of long-range entanglement. They are of fundamental interest because they defy the conventional paradigm of symmetry breaking and local order parameters, while at the same time have great practical significance for future quantum information applications. These quantum states are predicted to appear in frustrated magnetic materials where magnetic interactions compete to destabilize classical magnetic ordering. Typically, these phases emerge in materials with many closely competing electronic energy scales, but they are notoriously difficult to predict. Tantamount to this theoretical challenge is the experimental task of identifying such quantum states of matter.

The overarching goal is to obtain a detailed quantitative understanding of the interplay between spin, orbital, and lattice energy scales in materials where strong spin-orbit coupling and strong electronic correlations compete to determine the ground state. We employ a suite of inelastic and elastic neutron scattering techniques to uncover the order and collective excitations that characterize quantum ground states in model materials. Particular emphasis is placed on materials with strong-spin orbit coupling and orbital degeneracy. In this case, spin orbit coupling can overcome the tendency towards degeneracy breaking Jahn-Teller distortions and quantum fluctuations between the spin+orbital configurations can dominate the ground state giving rise to multipolar orderings and quantum spin-orbital liquids [1, 2] .

Recent Progress

Spin+orbital magnets: In $GaTa_4Se_8$ a single unpaired electron occupies the highest molecular orbital of tetrahedral clusters. The molecular orbital wavefunctions maintain the character of the d-orbitals and strong spin-orbit coupling results in the formation of highly quantum $j_{eff}=3/2$ molecular orbitals. [1,2] Exchange interactions between the spin-orbital entangled $j_{eff}=3/2$ states can potentially stabilize multipolar ordering and/or a spin orbital liquid phase on the FCC lattice of $GaTa_4Se_8$. On the other hand, depending on the balance of energy scales, Jahn-Teller instabilities can also act to locally remove the orbital degeneracy and stabilize a classical Neel state. We have completed a detailed investigation of the lattice dynamics around a spin-orbital singlet transition in the lacunar spinel GaTa4Se8 and find evidence for the formation of a spin-orbital singlet phase mediated by inter-cluster orbital exchange interaction.

Using single crystal diffraction, we have found that $GaTa_4Se_8$ undergoes a unit cell doubling structural transition concomitant with the formation of magnetic singles between Ta_4 clusters. Neutron pair distribution (PDF) measurements shown in Figure 1 reveal that local distortions of Ta_4 clusters are present at all temperatures and the structural transition corresponds to an orientational ordering of the distorted clusters, not involving any atomic translations within the unit cell. Neutron phonon density of states measurements reveal an anomalous phonon mode above the structural transition that is forbidden by the symmetry of the cubic structure, but allowed in the tetragonal one. Through DFT modeling we have found that this anomalous mode modulates inter Ta_4 cluster bond geometries and may potentially mediated orbital exchange. Owing to the large magnetic exchange energy scales, and the expected reduction in on-site Jahn-Teller coupling for heavy transition metals [3], we believe the orientational symmetry breaking and dimer singlet formation is driven by this intercluster orbital exchange.

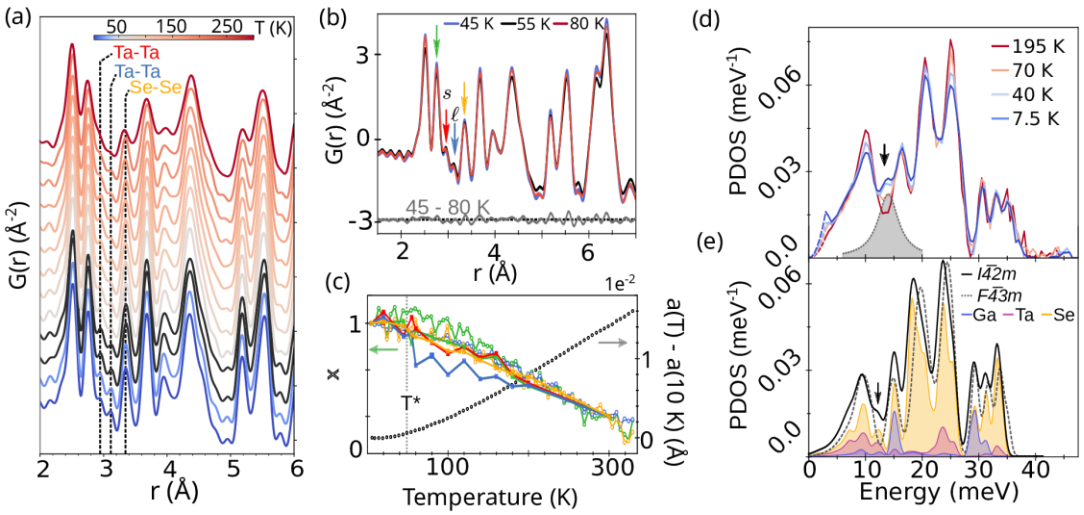

Figure 1: (a) Temperature dependent neutron PDF measurements in GaTa4Se8. (b) Detailed view of the local structure showing the absence of an redistribution in atomic pair spacing across the dimer singlet transition. (c) Temperature dependence of normalized PDF intensities showing that the local structure is not sensitive to the dimer singlet transition at 50 K. (d) Measured and (e) calculated neutron weighted phonon density of states for the high temperature cubic and low temperature tetragonal phase. The anomalous phonon mode appears at 13 meV.

These measurements reveal that when spin orbit coupling is strong, inter-site orbital exchange can dominate over on-site Jahn-Teller instabilities and act to generate magnetic phases with fluctuating spin and orbital degrees of freedom.

Highly frustrated magnets with anisotropic exchange: We have completed measurements of the spin wave spectra in the frustrated FCC iridate K_2IrCl_6. This compound harbors both strong nearest neighbor Kitaev interactions as well as strong next nearest neighbor Heisenberg exchange resulting in a high degree of magnetic frustration. We found a complex magnon spectrum that is consistent with strong magnetic anisotropy and Kitaev interactions, but not consistent with model Hamiltonian's previously deduced by other groups from thermodynamic data. We have also found evidence for magnon decay and excitation continua over large portions of the Brillouin zone. Analysis of the neutron data should allow us to constrain a microscopic mechanism for the decay. In turn, our measurements will provide a more detailed understanding of how excitation continua arise in frustrated magnets with strong anisotropic interactions, when there is no fractionalization of magnon quasiparticles.

Future Plans

We have recently succeeded in preparing single crystals of $GaTa_4Se_8$ suitable for inelastic neutron scattering experiments and plan to carry out a full investigation of the magnetic excitations emerging from the spin-orbital singlet phase using the MACS spectrometer at NCNR.

Following our successful program investigating the lattice and orbital dynamics in $GaTa_4Se_8$, we are aiming to develop a systematic understanding of the relative influence of spin-orbit coupling and Jahn-Teller instabilities in orbitaly degenerate systems, since the balance of these energy scales is tuned by chemical composition. We plan to take advantage of this and carry out an investigation of the lattice dynamics across the family of lacunar spines GaM_4X_8, M=(V, Nb, Ta), X=(S, Se) , where atomic spin orbit coupling can be systematically varied by changing the transition metal site from V to Ta, and ligand hybridization varied by changing from S to Se. We have completed phonon DOS measurements and plan to carry total scattering measurements across this series.

We are also exploring the possibility to use hydrostatic pressure to tune the magnetism in the FCC Kitaev irridates. Proof of principle experiments are planned for January 2022 and if successful, we aim to test the possibility of stabilizing quantum fluctuating magnetic states in this highly frustrated magnet.

References

1. G. Chen et al., Phys. Rev. B, 82, 74440 (2010).
2. W. M. H. Natori, M. Daghofer, and R. G. Pereira, Phys. Rev. B, 96, 125109, (2017).
3. H. S. Kim et al., Nat. Comms. 5, 952-958 (2014).
4. M. Y. Jeong et al., Nat. Comms. 8, 782 (2017).
5. S. V. Streltsov and D. I. Khomskii, *Phys. Rev. X* **10**, 031043 (2020).

Publications

This is a new program (September 2020), we have two publications in preparation.

Neutron Analysis of Structure-Property Relationships in Conductive Polymer Plastic Composites

Prof. Lilo D. Pozzo, Department of Chemical Engineering, Department of Materials Science and Engineering. Prof. Christine Luscombe, Department of Materials Science and Engineering. University of Washington Seattle

Program Scope

Organic electronics, including photovoltaics, wearable electronics, and field-effect transistors, are low-cost, flexible, and lightweight alternatives to inorganic devices. They are enabled by semi-conducting, or electronically conjugated, polymers (CPs) found in the active layers of the device architecture. However, CPs have poor mechanical integrity, are prone to cracking and have low environmental stability when compared to commodity polymers such as polystyrene, polyethylene and synthetic rubbers. A promising solution to achieving balanced properties is to use blends of conjugated and commodity polymers, resulting in mechanically and environmentally robust composite films with minimal impact on device performance, even at CP concentrations as low as 1 wt%.[1] In spite of the success that has been demonstrated, there is much that is left to learn about conjugated polymer plastic composite (CPPC) blends and about how fundamental interactions between conjugated and commodity polymers enable optimization of morphology and performance metrics. This project uses small angle neutron scattering (SANS) to improve our understanding of how CPPC conformation, self-assembly and electronic performance are affected by composition, processing, and mechanical deformation.

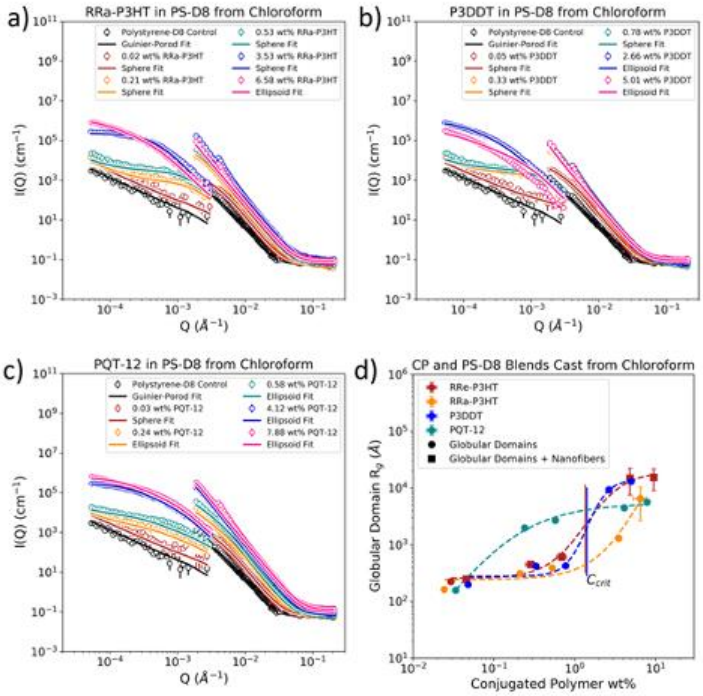

Figure 1: a-c) USANS and SANS data for CCPC blends from various variants of polythiophene and d-Polystyrene. d) Phase separation domain size as a function of concentration and molecular architecture showing a critical point.

Recent Progress

<u>Multi-Scale Structural Analysis of Polythiophene – Polystyrene Blends:</u> Recent work focused on systematically evaluating the effects of solvent and CPPC blend composition (i.e. conjugated polymer concentration and molecular architecture) on the multi-scale structure in model blends of polythiophenes and polystyrene. We characterized blend structures over a wide range of length

scales via contrast variation small-angle and ultra-small-angle neutron scattering (SANS and USANS). For this, deuterated polystyrene (D-PS) and conjugated polymers of variable molecular architecture (e.g. regio-regularity, side-chain identity) were mixed in solvents of variable thermophysical properties and heat processed to produce solid blends. We further employed analytical fits as well as Porod analyses to SANS and USANS data to demonstrate that there is a critical point (**Figure 1**) associated to the large-scale phase-separation in CPPCs and that this point is sensitive to the molecular architecture of the CP. Wide-angle X-ray scattering (WAXS) was also used to assess the local crystallinity of the CP components and these morphological features were related to bulk conductivity tests.[2]

Induced Assembly of Conjugated Polymers in Solutions with Non-Interacting Polymers: Most CPPCs are produced by co-dissolution of CP and commodity polymers in a common solvent followed by coating and drying during processing. Contrast variation SANS experiments were performed to analyze the influence of increased osmotic pressure, due to the presence of non-interacting d-PS, on the association of CPs in solution prior to coating. CV-SANS demonstrates that addition of d-PS, even in very good solvents, results in an increased driving force for assembly of CPs in solution. This suggests a potential mechanism to understand how 'ink' formulation parameters (e.g. molecular weight, concentration, solvent) influences the resulting CPPC morphology and performance metrics. Here, CV-SANS is essential to demonstrating that self-association of the CP component is occurring in mixtures with high concentrations of the commodity polymer, where it would otherwise dominate the scattering intensity.

Templated Conjugated Polymers in Thermoplastic Elastomer Lamellar Phases: CPPCs produced from thermoplastic elastomers, such as polystyrene-polyisoprene-polystyrene (SIS) and polystyrene-polybutadiene-polystyrene (SBDS) triblock copolymers, are of particular technological importance because their high elasticity enables uses in electronic skin, haptics and wearable device applications.[3] Ongoing work also focuses on scattering analysis of P3HT-SIS and P3HT-SBDS CPPCs to characterize multi-scale morphological transitions. High-throughput remote SAXS and USAXS experiments were performed at APS, during COVID lockdowns, to evaluate the influence of the CP additive on the structure of the lamellar morphology of the triblock matrix. Results show that significant loadings (~ 5wt%) of CP can be incorporated into structured mesophases without negatively impacting organization and preservation of the template. WAXS experiments also demonstrate that CPs crystallize within the CPPC, which is important for sustaining electronic conduction. Swelling of the lamellar periodicity also suggests that the CP is incorporated into the mesophase and that this strategy produces structured CPPCs with long range order. Ongoing experiments will correlate their morphology to electronic conduction.

Organic Mixed Ionic Electronic Conductors (OMIEC) from Structured Blends with Conjugated Polymers: CPPCs were also produced from blends of ionic conducting polymers and CPs. Here, triblock copolymers containing polyethylene oxide (PEO) blocks were used as a structured template for co-assembly of the polar conjugated polymer poly-3-potassium-butanoate-thiophene (PPBT). Such composite materials conduct both ionic (PEO) and electronic charges (PPBT),

which results in an organic mixed ionic electronic conductor (OMIEC) complex with long range structural order. OMIECs have recently received significant attention due to their potential use in neuromorphic computing applications where strong electronic-ionic coupling, fast switching between states and temporal stability are key metrics.[4] Remote high-throughput SAXS experiments were again performed at APS to identify the influence of adding a CP additive on the self-assembly of the triblock copolymer matrix (PEO-PPO-PEO). Nearly 500 composite OMIEC samples were prepared using laboratory robotic automation to map the compositional parameter space. **Figure 2** demonstrates that the addition of CP to the triblock mesophase, up to a critical loading concentration, results in structured composites with long range order. Beyond this critical concentration, the CP additive will negatively impact the organization of the mesophase leading to disorder.

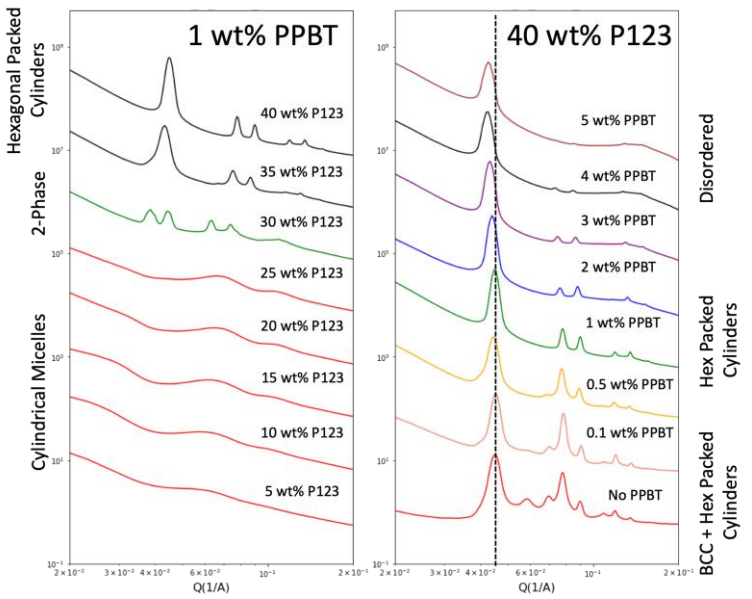

Figure 2: (left) When mixed with 1wt% PPBT, cylindrical micelle structures are formed at low concentrations of Pluronic P123 and hexagonally packed arrays of cylinders (HPC) result at high concentrations. In the absence of the CP, the triblock-copolymer forms spherical micelles at low concentrations and a 2-phase mixture of body-centered cubic and HCP mesophases at higher loadings. (right) Increased loading of PPBT to P123 mesophase results in pure HCP phase up to ~1 wt%, followed by significant swelling of the lattice and the loss of long-range order.

Future Plans

In the following years, we will continue to perform electrochemical and mechanical characterization of CPPC samples to enable drawing direct links between multi-scale morphology and material properties. Electrochemical impedance spectroscopy (EIS) and organic electrochemical transistors (OECTs) will be used to measure conductivity in electronically conductive CPPCs and transistor switching performance in structured OMIECs. Rheological measurements are also planned for OMIEC blends and tensile tests for elastomeric CPPCs. In addition to this, we aim to continue to develop tools to enable more efficient analysis of the complex multi-variate design spaces in CCPCs and OMIECs (e.g. concentration, MWs, molecular architecture, solvent, processing, dopants). In the next phase of this project, we plan to further explore integration of laboratory automation, advanced sampling (Bayesian) and classification analysis for accelerated mapping of phase space in structured OMIEC materials with neutron scattering. During the COVID19 lockdown, our team produced hardware and software tools to

increase efficiency of scattering experiments, via integration of automation and data-driven design of experiment practices, that also enabled remote execution with higher beamtime-utilization efficiency than ever. These will be now applied to the analysis and optimization of these complex class of materials.

References

1-"Multicomponent semiconducting polymer systems with low crystallization-induced percolation threshold." Goffri, S.; Muller, C.; Stingelin-Stutzmann, N.; Breiby, D. W.; Radano, C. P.; Andreasen, J. W.; Thompson, R.; Janssen, R. A. J.; Nielsen, M. M.; Smith, P.; Sirringhaus, H., Nature Materials, 5 (12), 950-956 (2006).

2-"Blend Morphology in Polythiophene–Polystyrene Composites from Neutron and X-Ray Scattering." Wolf, C. M.; Guio, L.; Scheiwiller, S. C.; O'Hara, R. P.; Luscombe, C. K.; Pozzo, L. D. Macromolecules, 54(6), 2960-2978 (2021).

3-"Beyond Stretchability: Strength, Toughness, and Elastic Range in Semiconducting Polymers" Chen, A. X., Kleinschmidt, A. T., Choudhary, K. & Lipomi, D. J. Chemistry of Materials 32, 7582–7601 (2020).

4- " Organic Mixed Ionic–Electronic Conductors", Paulsen, B. D.; Tybrandt, K.; Stavrinidou, E.; Rivnay, J. Nature Materials., 19 (1), 13–26. (2020)

Publications (last 2 years)

"Assessment of Molecular Dynamics Simulations for Amorphous Poly (3-Hexylthiophene) Using Neutron and X-Ray Scattering Experiments." Wolf, C.; Kanekal, K.; Yimer, Y.; Tyagi, M.; Omar-Diallo, S.; Pakhnyuk, V.; Luscombe, C.; Pfaendtner, J.; Pozzo, L. D. Soft Matter, 15(25), 5067-5083 (2019).

"Blend Morphology in Polythiophene–Polystyrene Composites from Neutron and X-Ray Scattering." Wolf, C. M.; Guio, L.; Scheiwiller, S. C.; O'Hara, R. P.; Luscombe, C. K.; Pozzo, L. D. Macromolecules, 54(6), 2960-2978 (2021).

"Strategies for the development of conjugated polymer molecular dynamics force fields validated with neutron and X-ray scattering", C. Wolf, L. Guio, S. Scheiwiller, V. Pakhnyuk, C. Luscombe, L.D. Pozzo, ACS Polymers Au, (2021) doi.org/10.1021/acspolymersau.1c00027

"Dual-Stimuli Responsive Single-Chain Polymer Folding via Intrachain Complexation of Tetramethoxyazobenzene and β-Cyclodextrin" D.C. Lee, K.N. Guye, R.K. Paranji, K. Lachowski, L.D. Pozzo, D.S. Ginger, S.H. Pun, Langmuir, 37(33), 10126-10134 (2021)

Inelastic Neutron and X-ray Scattering Investigation of Electron-Phonon Effects in Quantum Materials

Dmitry Reznik, University of Colorado-Boulder

Program Scope

This program combines scattering experiments with first principles (Density functional theory, DFT and molecular dynamics, MD) calculations to gain insights into **electron-phonon interactions that lead to charge localization and delocalization, phonon damping, thermal conductivity and electrical current-driven structural defect generation via phonons**. We are also developing, upgrading, and training users in Phonon Explorer software, which is a great productivity tool with an order of magnitude improvement of the speed with which time-of-flight neutron scattering data can be analyzed.

Recent Progress

We made several important discoveries outlined below. This work is still mostly unpublished.

1. **Electron-momentum dependence of electron-phonon coupling underling dramatic phonon renormalization in YNi_2B_2C**. Electron-phonon coupling, i.e., the scattering of lattice vibrations by electrons and vice versa, is ubiquitous in solids and can lead to emergent ground states such as superconductivity and charge-density wave order. A broad spectral phonon line shape is often interpreted as a marker of strong electron-phonon coupling associated with Fermi surface nesting, i.e., parallel sections of the Fermi surface connected by the phonon momentum. Alternatively broad phonons are known to arise from strong atomic lattice anharmonicity. We showed that strong phonon broadening can occur in the absence of both Fermi surface nesting and lattice anharmonicity, if electron-phonon coupling is strongly enhanced for specific values of electron-momentum, k. We used inelastic neutron scattering, soft x-ray angle-resolved photoemission spectroscopy measurements and DFT-based lattice dynamical and electronic band structure calculations to demonstrate this scenario in the highly anisotropic tetragonal electron-phonon superconductor YNi_2B_2C. This new scenario likely applies to a wide range of compounds.

2. **Effect of the electronic charge gap on LO bond-stretching phonons in undoped La2CuO4 calculated using LDA+U**. Typical DFT calculations wrongly predict undoped cuprates (known to be Mott insulators) to be metallic. They also predict Cu-O half- and full-breathing phonon energies that are significantly softer than observed, presumably because of weak on-site Coulomb repulsion on the Cu *3d* orbitals. We used DFT+U calculations with antiferromagnetic supercells of La_2CuO_4 to establish correlation between the on-site repulsion strength, tuned via adjusting the value of U, and phonon dispersions. We find that breathing and half-breathing phonons reach experimental values when U is tuned to obtain the correct optical gap and magnetic moments. We demonstrated that using distorted supercells within DFT+U is a

promising framework to model phonons in undoped cuprates and other perovskite oxides with complex, interrelated structural and electronic degrees of freedom [1]. These calculations have already played a key role in a different investigation led by J.M. Tranquada that focused on chiral phonons that may be responsible for the thermal Hall effect in the same compound [2].

3. **Spinons and damped phonons in spin-1/2 quantum-liquid Ba4Ir3O10 observed by Raman scattering**. In spin-1/2 Mott insulators, non-magnetic quantum liquid phases are often argued to arise when the system shows no magnetic ordering, but identifying positive signatures of these phases or related spinon quasiparticles can be elusive. We used Raman scattering to provide three signatures for spinons in a possible spin-orbit quantum liquid material $Ba_4Ir_3O_{10}$: (1) A broad hump, which we show can arise from Luttinger Liquid spinons in Raman with parallel photon polarizations normal to 1D chains; (2) Strong phonon damping from phonon-spin coupling via the spin-orbit interaction; and (3) the absence of (1) and (2) in the magnetically ordered phase that is produced when 2% of Ba is substituted by Sr ($(Ba_{0.98}Sr_{0.02})_4Ir_3O_{10}$). The phonon damping via itinerant spinons seen in this quantum-liquid insulator suggests a new mechanism for enhancing thermoelectricity in strongly correlated conductors, through a neutral quantum liquid that need not affect electronic transport [3].

4. **Disorder-induced flattening of phonon branches in the clathrate $Ba_8Ga_{16}Ge_{30}$.** In the search for high-performance thermoelectric materials, phonon-glass electron crystal (PGEC) materials such as clathrates have drawn attention due to having both glass-like low phonon thermal conductivity and crystal-like high electrical conductivity. $Ba_8Ga_{16}Ge_{30}$ (BGG) has a guest Ba atom trapped inside Ga/Ge cage structures is known for avoided crossings between acoustic phonons and the flat guest atom modes proposed to be the source of the low lattice thermal conductivity. Ga/Ge site disorder with Ga and Ge exchanging places in different unit cells has also been reported. We used TOF neutron scattering to measure the complete phonon spectrum in a large single crystal of BGG. Calculations assuming the structure where Ga/Ge atoms occupy their nominal sites, as well as a disordered configuration showed that the latter agrees much better with the data. (Fig. 1) Disorder strongly reduces phonon group velocities despite nearly identical masses of Ga and Ge, which accounts for exceptionally low thermal conductivity. Our work points at a new path towards optimizing thermoelectrics.

5. **Automating Analysis of Neutron Scattering Time-of-Flight Single Crystal Phonon Data.** We have been developing software called Phonon Explorer that implements a data mining workflow for large datasets of the neutron scattering function, $S(\mathbf{Q}, \omega)$, measured on time-of-flight neutron spectrometers. This systematic approach takes advantage of all useful data contained in the dataset. It includes finding Brillouin zones where specific phonons have the highest scattering intensity, background subtraction, combining statistics in multiple Brillouin zones, and separating closely spaced phonon peaks. Using the software reduces the time needed to determine phonon dispersions, linewidths, and eigenvectors by more than an order of magnitude. We recently published a paper describing the software as well as released a new version 1.1, with significant performance improvements and new functionality [4].

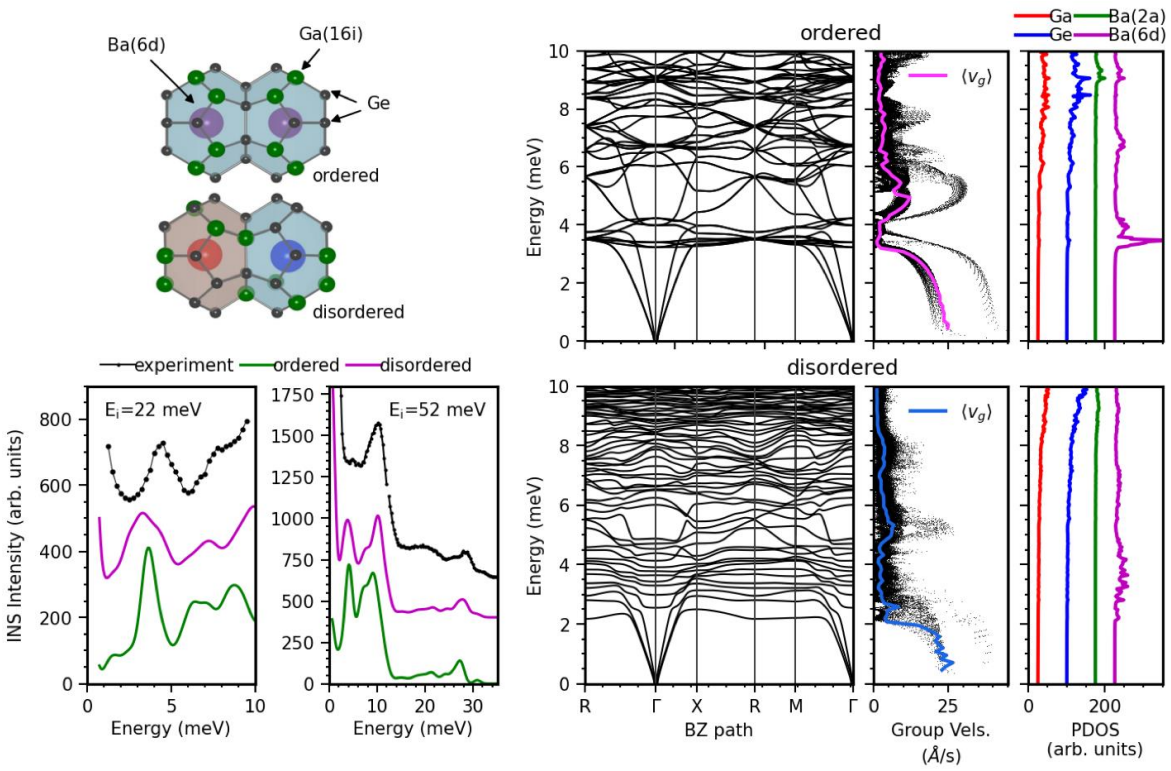

Fig. 1. Summary of the lattice dynamical phenomena in BGG. The top left panel shows part of the Ba rattler atom containing (Ga, Ge)24 cage portion of the 3d unitcells of (top) perfectly ordered and (bottom) disordered BGG. In the disordered phase, the Ge/Ga atom occupations are scrambled and the Ba sites are no longer equivalent. The bottom left panel shows the neutron-weighted densities of states (DoS) (inelastic neutron scattering intensities integrated over the 3<H<6, 3<K<7, 4.5<L<6.5 r.l.u. region of reciprocal space.) Black dotted lines are experimental data taken with incident energy Ei=52 meV (top) and Ei=22 meV (bottom). The green/pink lines are the same quantity calculated from DFT using the ordered/disordered unitcells. The disordered calculation and the experimental curves for Ei=22 meV are offset vertically by 250 counts to aid visibility. The experimental curve has an additional large (~250 counts) background that is not present in the calculations. For Ei=52 meV, the disordered and experimental curves are offset by 400 and 600 counts respectively. The top (ordered unitcell) and bottom (disordered unitcell) panels on the right show phonon dispersions (left column), phonon group velocities vk = |dω| (middle column), and atom projected densities of states, PDoS (right).

Future Plans

1. Interplay between phonon anomalies and polaron formation in perovskite oxides. Recently we performed inelastic neutron scattering measurements at the SNS and JPARC of optic phonons in several stripe-ordered nickelates, superconducting cuprates, and colossal magnetoresistance manganites. We plan to use the Phonon Explorer software to establish how phonon anomalies in these compounds correlate with features in published electrical conductivity and optical properties associated with polarons. DFT calculations will establish the degree to which DFT can be used to model phonons in materials with polaronic physics.

2. Atomistic mechanism underlying the effect of flash. Subjecting most materials to strong electric fields drastically changes their properties. In particular their electrical conductivity

increases dramatically, and they start glow due to intense luminescence, hence the name "flash". This fascinating phenomenon has been discovered recently and has an immense potential for applications, yet, its atomistic mechanism remains a mystery. There is a lot of circumstantial evidence that local structure is strongly modified and that phonons are intimately involved. We leverage our expertise in phonons and in neutron scattering to investigate the flash phenomenon in collaboration with the SNS, which invested significant funds into engineering and building the sample environment that allows passing large currents at high temperatures through single crystal samples. The first experiment on CORELLI was very successful and we hope to get beamtime for the followup measurement of phonons on ARCS. This will be followed by detailed data analysis with the purpose to discover of new physics of this phenomenon.

3. Upgrades of the Phonon Explorer software. We plan to incorporate instrument resolution functions into multizone fit. This will significantly improve fitting accuracy, especially extracting intrinsic phonon linewidths from the fits. We will also try to parallelize generation of slices, which will increase the speed of the program by an order of magnitude.

References

1. T. C. Sterling and D. Reznik, Phys. Rev. B **104**, 134311 (2021).
2. A. Sapkota, T. C. Sterling, P. M. Lozano, Yangmu Li, Huibo Cao, V. O. Garlea, D. Reznik, Qiang Li, I. A. Zaliznyak, G. D. Gu, and J. M. Tranquada, Phys. Rev. B **104**, 014304 (2021).
3. A. Sokolik, S. Hakani, S. Roy, N. Pellatz, H. Zhao, G. Cao, I. Kimchi, D. Reznik, arXiv:2110.15916 (2021), submitted to Phys. Rev. B Lett.
4. D. Reznik and I. Ahmadova, Quantum Beam Science **4**, 41 (2020).

Publications

1. **Spinons and damped phonons in spin-1/2 quantum-liquid Ba4Ir3O10 observed by Raman scattering,** A. Sokolik, S. Hakani, S. Roy, N. Pellatz, H. Zhao, G. Cao, I. Kimchi, D. Reznik, arXiv:2110.15916 (2021), submitted to Phys. Rev. B Lett.
2. **Effect of the electronic charge gap on LO bond-stretching phonons in undoped La_2CuO_4 calculated using LDA+U**, T. C. Sterling and D. Reznik, Phys. Rev. B **104**, 134311 (2021).
3. **Reinvestigation of crystal symmetry and fluctuations in La_2CuO_4**, A. Sapkota, T. C. Sterling, P. M. Lozano, Yangmu Li, Huibo Cao, V. O. Garlea, D. Reznik, Qiang Li, I. A. Zaliznyak, G. D. Gu, and J. M. Tranquada, Phys. Rev. B **104**, 014304 (2021).
4. **Lattice dynamics in the double-helix antiferromagnet FeP**, A.S. Sukhanov, S.E. Nikitin, M.S. Pavlovskii, T.C. Sterling, N.D. Andryushin, A.S. Cameron, Y.V. Tymoshenko, H.C. Walker, I.V. Morozov, I.O. Chernyavskii, S. Aswartham, D. Reznik, D.S. Inosov, Physical Review Research **2**, 043405 (2020).
5. **Automating Analysis of Neutron Scattering Time-of-Flight Single Crystal Phonon Data**, D. Reznik and I. Ahmadova, Quantum Beam Science **4**, 41 (2020).
6. **Quest for quantum states via field-altering technology**, G. Cao, H. Zhao, B. Hu, N. Pellatz, D. Reznik, P. Schlottmann, I. Kimchi, npj Quantum Materials **5**, 1 (2020).

7. **Giant electron-phonon coupling of the breathing plane oxygen phonons in the dynamic stripe phase of $La_{1.67}Sr_{0.33}NiO_4$,** A. M. Merritt, A. D. Christianson, A. Banerjee, G. D. Gu, A. S. Mishchenko, and, D. Reznik, Scientific Reports **10**, 11426 (2020).
8. **Phonon spectrum of underdoped $HgBa_2CuO_{4+\delta}$ investigated by neutron scattering**, I. Ahmadova, T.C. Sterling, A.C. Sokolik, D.L. Abernathy, M. Greven, D. Reznik, Phys. Rev. B **101**, 184508 (2020).
9. **Nematic correlation length in iron-based superconductors probed by inelastic x-ray scattering**, A. M. Merritt, F. Weber, J.-P. Castellan, Th. Wolf, D. Ishikawa, A. H. Said, A. Alatas, R. M. Fernandes, A. Q. R. Baron, and D. Reznik, Phys. Rev. Lett. **124**, 157001 (2020).

Structure-Property Relationships in Porous Electrodes for Electrochemical Energy Storage

Dr. Jeffrey J. Richards, Department of Chemical and Biological Engineering Northwestern University

Program Scope

Lithium-ion batteries are a mature electrochemical energy storage technology deployed at the TW scale today. This wide-scale adoption has only been made recently possible after 40 years of research and development.[1] In part, the slow pace of research and development and the reduction of system cost was a result of insufficient knowledge regarding the fundamental connection between the processing-performance relationships that persists today. In particular, the porous electrodes, a key component of rechargeable lithium-ion batteries[2], are highly non-equilibrium structures whose optimization was only realized after careful control of the formulation, coating, and post-processing steps.[3] The performance of a battery is therefore currently dependent on the details of the manufacturing process and not on a more fundamental appreciation of the material properties. Understanding the link between how porous electrodes are manufactured and the structure-function relationships that determine the microstructure is critical to accelerating the development of emergent battery technologies with higher rate cycling and capacity.

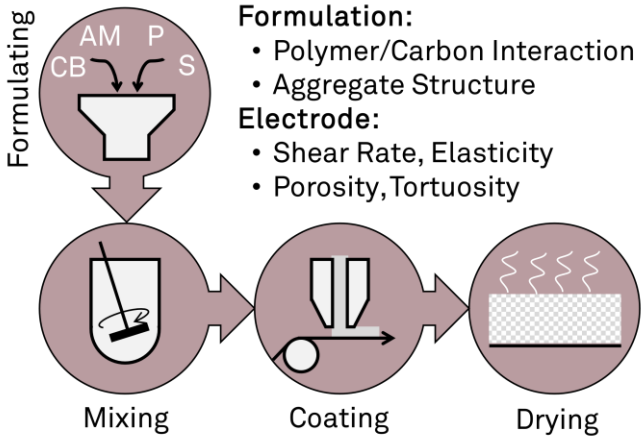

Figure 1: Manufacturing porous electrodes requires understanding the formulation and processing steps that determine the microstructure of porous electrodes. The electrode is a composite manufactured through the combination of carbon black (CB), active material (AM), and polymer binder (PB) dispersed in a solvent (S). These components are mixed and then coated into a thin-film electrode that is post-processed to yield a porous electrode.

Porous electrodes are manufactured by suspending a mixture of micron-sized electrochemically active material (AM), polymer binder (PB)[4–6], and carbon black (CB) [7,8] in a solvent (S) and depositing it onto a metallic current collector[9] as depicted in Figure 1. The complex processing conditions encountered during formulation crate many challenges for quantifying structure-property relationships. The overall goal of this project is to leverage advanced neutron scattering techniques to understand how formulation, coating, and electrochemical cycling influence the structure of porous electrodes and how that structure can be influenced by the processing conditions.

To gain this fundamental understanding, the focus of the research effort includes three objectives:

1. Quantifying polymer-particle interactions in flow using neutron scattering.
2. Processing-structure relationships in slurries using slot-die coating.
3. *In operando* studies of porous electrodes in relevant electrochemical contexts.

What will emerge from this proposal is a comprehensive microstructural picture of how porous electrodes gain and maintain their properties. On the way to this goal, this project will develop new

sample environments that will be available to the broader scientific community to examine technologies that go beyond batteries, such as fuel cells and coating formulations. Finally, this proposal will also serve to train the next generation of graduate student engineers in advanced neutron scattering methods.

Recent Progress: Our initial work has focused on Objective #1, understanding polymer-particle interactions in flow using neutron scattering. In preparation for these studies, we performed rheological and structural characterization on solutions containing poly(vinylidene fluoride) (PVDF) and carbon black (CB) in n-methyl pyrrolidine (NMP), typical of slurries used for cathodes.

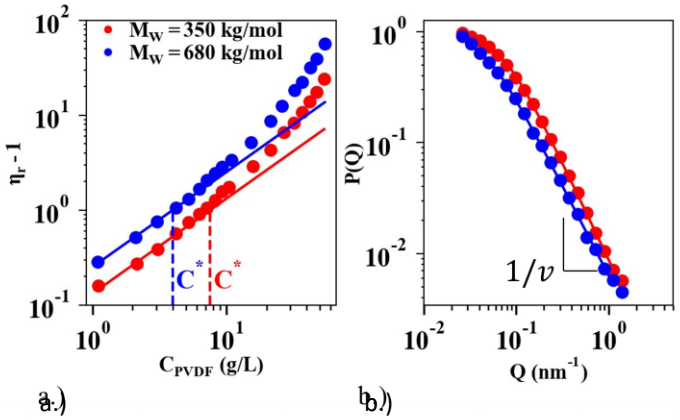

	M_W (kg/mol)	C^* (g/L)	R_v (nm)	R_G (nm)	v
A-741	350	7.6	19.4	20	0.57
A-761	680	4.0	30	30	0.63

Figure 2: Property summary of Arkema polymer conformation in NMP: a.) Reduced viscosity versus PVDF concentration. Overlaid on the curves are the linear predictions based on the Einstein equation and the experimentally determined values of C^* b.) Small angle scattering form factor, $P(Q)$, versus wavevector Q for two polymers. Fits to the polymer excluded volume model are overlaid on-top of the experimentally determined form factors. The power-law slope is indicated on the plots.

Initially, we examined the rheology of PVDF/NMP solutions for two commercial polymers (Arkema 741 (A-741) and 761 (A-761)). The results of these measurements are shown in Figure 2a. In the dilute limit, the reduced viscosity exhibits a linear scaling with C_{PVDF} (as shown by the solid lines). This linear scaling is preserved up to the overlap concentration, C^*, where the scaling becomes enhanced indicating a transition from the dilute to the semi-dilute regime. Our measurements show that C^* decreased with increasing polymer molecular weight (as indicated in the table in Figure 2). For a dilute polymer in a good solvent $\frac{1}{C^*} = [\eta_0] = \frac{10\pi}{3}\frac{N_A}{M_W}R_v^3$, where R_v is the viscometric radius of the polymer coil.[10] The numerical values of the intrinsic viscosities agree well with scaling predictions based on molecular weights measured using GPC the radius of gyration of the polymer, determined from fits to the measured polymer form factor shown in Figure 2b. The power-law index determined from these fits yields a confirmation consistent with swollen chains[11] and close quantitative agreement between the viscometric radius and the radius of gyration.

Our prior work has shown that suspensions of CB subjected to well-defined shear flow undergo structural break down with increasing shear intensity.[12–14] This break up can be described by a Mason number, a dimensionless balance of the shear forces acting to tear the agglomerates apart against the cohesive forces holding them together. The Mason number is given as $Mn = \frac{6\pi\phi^2\sigma(\dot{\gamma})}{\sigma_y}$ where $\sigma(\dot{\gamma})$ is the measured shear stress at a given shear rate $\dot{\gamma}$, σ_y is the yield stress, and

ϕ is the volume fraction of carbon black. While our prior work showed well-defined scaling behavior that depended on the solvent viscosity, suspensions consisting of mixtures of CB+P are expected to have an additional polymeric stress that has an unknown contribution to break down of carbon black agglomerates when suspended in polymer solutions.

To test this hypothesis, we seek to measure the shear-driven break up of carbon black agglomerates in suspensions of PVDF and NMP at relevant weight loadings for slurry coatings. In our preliminary work, we have measured the shear dependent steady state stress, $\sigma(\dot{\gamma})$, for a 3 wt% suspension of CB (Vulcan XC 72R) as a function of polymer concentration (0.0, 1.0, 2.0, and 3.0 wt%). We found that in general the shear stress depended on the polymer concentration at all shear rates. We fit our steady state flow curves to $\sigma(\dot{\gamma}) = \sigma_y(1 + (\tau\dot{\gamma})^{0.5}) + \eta_\infty\dot{\gamma}$, where σ_y is the yield stress, τ is a pseudo-plastic deformation timescale, and η_∞ is the infinite shear viscosity. We expect that $\eta_\infty = \eta_p + \eta_{CB}$, where the η_p should exhibit similar numerical values as those measured in Figure 2a. Figure 3 shows that this model describes the steady state stress well over the entire shear rate range for each sample.

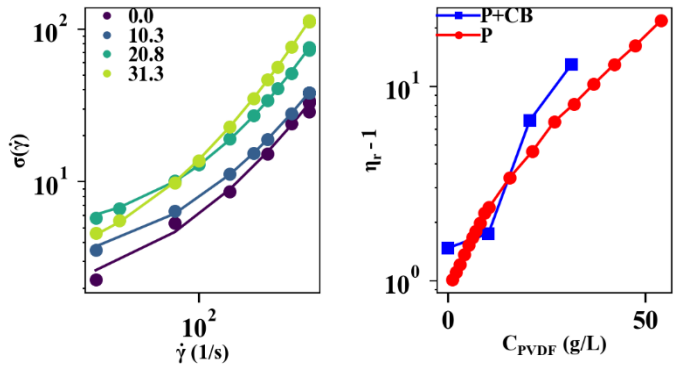

Figure 3: Nonlinear rheology of carbon black and polymer suspensions - four polymer concentrations (shown in g/L in the legend) at a fixed carbon content (3 wt%): a.) Structural contribution to the shear stress versus shear rate for 0.0, 1.0, 2.0, and 3.0 wt% samples. The solid lines are model fits, and b.) concentration dependent reduced viscosity and infinite shear viscosity for samples with (P+CB) and without carbon black (P).

In this representation, we observed a non-monotonic scaling of the σ_y and τ with polymer concentration, indicating that PVDF influences the structural trajectory of the carbon black agglomerates. Interestingly, this transition to non-monotonic scaling occurred at concentrations approximately equivalent to C^* for the A-741 polymer. This indicates that there may be important differences in the way that polymeric stress couples to the shear force in the dilute vs. semi-dilute regimes. We can further compare the infinite shear viscosity to measurements performed on A-841 and we see close agreement between η_∞ for CB +P and neat P solutions with CB+P sample showing a viscosity enhancement, likely due to the polymer-carbon interactions.

Future Plans

Over the next year, we will initiate work on Objective #2 with the acquisition of a slot-die coater to study the structural evolution of slurries. We have two pending beam-time proposals to study the structural evolution using ultra small angle neutron scattering (rheo-USANS) to study the breakup of carbon black agglomerates as a function of shear rate for these samples and to examine using small angle neutron scattering (SANS) the contrast dependent polymer form factor to quantify PVDF-CB interactions. These studies will be carried out at the Spallation Neutron Source (SNS) and the High-Flux Isotope Reactor (HFIR) at Oak Ridge National Laboratory. Finally, we

will initiate collaboration with Jeff Lopez at Northwestern in the Spring/Summer of 2022 to begin fabrication of electrochemical half cells capable of in situ electrochemical cycling (Objective 3).

References

(1) Whittingham, M. S.; Fanwood; N.J. Chalcogenide Battery. *Exxon Res. Eng. Co.* **1977**, 1–5.

(2) Armand, M. Issues and Challenges Facing Rechargeable Lithium Batteries. *Nature* **2001**, *414* (November), 359–367.

(3) Hawley, W. B.; Li, J. Electrode Manufacturing for Lithium-Ion Batteries—Analysis of Current and next Generation Processing. *J. Energy Storage* **2019**, *25* (June), 100862. https://doi.org/10.1016/j.est.2019.100862.

(4) Chou, S. L.; Pan, Y.; Wang, J. Z.; Liu, H. K.; Dou, S. X. Small Things Make a Big Difference: Binder Effects on the Performance of Li and Na Batteries. *Phys. Chem. Chem. Phys.* **2014**, *16* (38), 20347–20359. https://doi.org/10.1039/c4cp02475c.

(5) Bresser, D.; Buchholz, D.; Moretti, A.; Varzi, A.; Passerini, S. Alternative Binders for Sustainable Electrochemical Energy Storage-the Transition to Aqueous Electrode Processing and Bio-Derived Polymers. *Energy Environ. Sci.* **2018**, *11* (11), 3096–3127. https://doi.org/10.1039/c8ee00640g.

(6) Lestriez, B. Functions of Polymers in Composite Electrodes of Lithium Ion Batteries. *Comptes Rendus Chim.* **2010**, *13* (11), 1341–1350. https://doi.org/10.1016/j.crci.2010.01.018.

(7) Raccichini, R.; Varzi, A.; Passerini, S.; Scrosati, B. The Role of Graphene for Electrochemical Energy Storage. *Nat. Mater.* **2015**, *14* (3), 271–279. https://doi.org/10.1038/nmat4170.

(8) Spahr, M. E.; Goers, D.; Leone, A.; Stallone, S.; Grivei, E. Development of Carbon Conductive Additives for Advanced Lithium Ion Batteries. *J. Power Sources* **2011**, *196* (7), 3404–3413. https://doi.org/10.1016/j.jpowsour.2010.07.002.

(9) Myung, S. T.; Hitoshi, Y.; Sun, Y. K. Electrochemical Behavior and Passivation of Current Collectors in Lithium-Ion Batteries. *J. Mater. Chem.* **2011**, *21* (27), 9891–9911. https://doi.org/10.1039/c0jm04353b.

(10) Heo, Y.; Larson, R. G. The Scaling of Zero-Shear Viscosities of Semidilute Polymer Solutions with Concentration. *J. Rheol. (N. Y. N. Y).* **2005**, *49* (5), 1117–1128. https://doi.org/10.1122/1.1993595.

(11) Hore, M. J. A.; Hammouda, B.; Li, Y.; Cheng, H. Co-Nonsolvency of Poly(n - Isopropylacrylamide) in Deuterated Water/Ethanol Mixtures. **2013**.

(12) Hipp, J. B.; Richards, J. J.; Wagner, N. J. Direct Measurements of the Microstructural Origin of Shear-Thinning in Carbon Black Suspensions. *J. Rheol. (N. Y. N. Y).* **2021**, *Accepted*.

(13) Richards, J. J.; Hipp, J. B.; Riley, J. K.; Wagner, N. J.; Butler, P. D. Clustering and Percolation in Suspensions of Carbon Black. *Langmuir* **2017**, *33* (43), 12260–12266. https://doi.org/10.1021/acs.langmuir.7b02538.

(14) Hipp, J. B.; Richards, J. J.; Wagner, N. J. Shear-Induced Structure-Property Relationships of Carbon Black Suspensions Determined by Simultaneous Rheological and Structural Measurements. *J. Rheol. (N. Y. N. Y).* **2018**, *In prepara* (In preparation for submission).

Publications

N/A

Discovering Toroidal Materials with Spherical Neutron Polarimetry

Efrain E. Rodriguez
Dept. of Chemistry and Biochemistry, University of Maryland, College Park, MD 20742

Program Scope

Neutron scattering remains one of the most versatile and useful methods for probing the internal structure of condensed matter. Here, we use two aspects of the neutron's interaction with matter, its momentum and spin, to explore how symmetry is broken in ferroic materials and specifically ferrotoroidic materials. Briefly, a ferrotoroidic material is one in which toroidal moments order spontaneously at a given temperature and break both space inversion and time reversal symmetries simultaneously, making it a unique member of the ferroic classification table.[1,2] Currently, our project has two main components: 1) the exploration of toroidal materials with neutron scattering and 2) the development of spherical neutron polarimetry capabilities within North American sources. With respect to the first part of the project, we have furthered our understanding of how toroidal moments, which are much less understood than electric dipole and magnetic axial moments, can develop in magnetoelectric materials. We have explored transition metal phosphates and metal thiophosphates as the antiferromagnetic systems that can support such toroidal moments. With respect to the second part of our project, we have built an SNP apparatus that can be operated in a small angle configuration and have a design and components to extend it to wide angle operation.

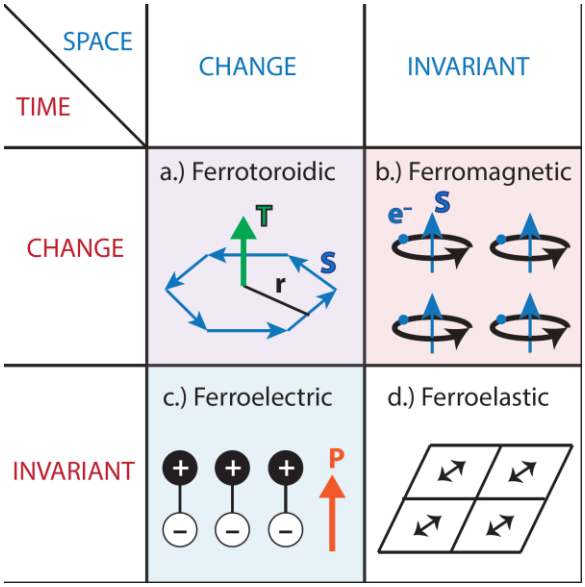

Figure 1. The four ferroics according to how they break space inversion or time reversal symmetries.

Recent Progress

Understanding the design of ferrotoroidics and magnetoelectrics: Since this funding period started in 2019, we have a better understanding of how materials can be designed to express ferrotoroidic behavior. The toroidal moment is a 'moment of a moment', and in our case it is specifically derived from a ring of spins centered on a transition metal such as iron, cobalt, and nickel [5]. These materials have implications for all materials where spontaneous breaking of symmetry can be harnessed for memory and sensing applications, as has been the case for ferromagnets, ferroelectrics, and ferroelastics. We conclude four major findings on the subject of ferrotoroidics.

i. Candidate materials for toroidal behavior should include complex oxoanions such as phosphates, germanates, and silicates that facilitate super-super exchange interactions between metal centers. It is not enough for M—O—M superexchange (where M = magnetic metal) to be present in a candidate material. Within a ferrotoroidic material, M—O—O—M interactions promote toroidal arrangement of spins where the O—O pathway is provided by the $(PO_4)^{3-}$, $(GeO_4)^{4-}$, or $(SiO_4)^{4-}$ anions.

ii. The location of the toroidal moments is exactly at the location of the symmetry operation $\bar{1}$'. In literature, the location of toroidal moments is ambiguous and much the confusion comes from a lack of consensus on where toroidal moments should be located in a crystal. My student Stephanie Gnewuch has advanced the crystallography of these materials, and we now hypothesize that these toroidal moments need to be located at the point where both time-reversal and space inversion symmetries simultaneously occur. This location also happens to be located at the center of rings that consist of M—$(PO_4)^{3-}$—M —$(PO_4)^{3-}$ in $LiFePO_4$ and $LiCoPO_4$. Hence, our hypothesis that these oxoanions are necessary in the composition is strengthened by our crystallographic arguments.

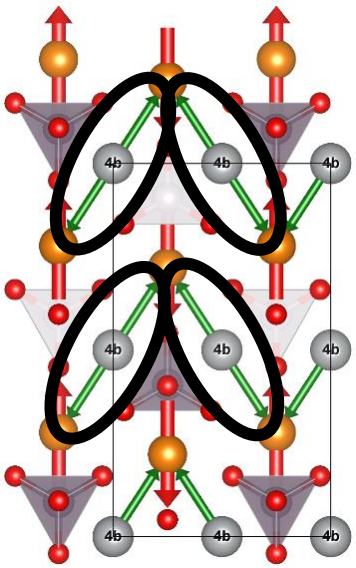

Figure 2. The location of the toroidal moments are centered in the 4b Wyckoff site for magnetic space group *Pnma*' in $LiCoPO_4$ and $LiFePO_4$. These toroidal moments are located at the center of rings that include super-superexchange interactions between the transition metal centers (in orange) that include the O—O edges of the phosphate $(PO_4)^{3-}$ groups (grey tetrahedra).

iii. We can increase the Néel temperature (T_N) in the olivine-type Li*M*PO_4 by de-intercalation of the lithium cation using a chemical oxidative technique. For the case of $LiFePO_4$, however, the magnetic space group switches to one that does not support ferrotoroidicity. We work around this challenge by making the solid solutions $LiFe_{1-x}Mn_xPO4$ and then de-lithiate these phases. This way, we arrive at a magnetic space group that supports ferrotoroidicity and raises the temperature from T_N = 47 K to 121 K, which makes potential investigation of these materials for applications more probable.

iv. SNP can be used to solve the domain population of a ferrotoroidic material. We have now successfully performed a CryoPAD experiment on a single crystal of $LiFePO_4$ under zero-field and field-cooled conditions. Under zero-field, we see equal domain population of the up and down toroidal state. Once we cool in a conjugate field of E x H (where E = electric field and H = magnetic field), we observer nearly 100 percent population of one domain over the other. This is easily demonstrated in the off-diagonal terms in the polarization matrix one measures during an SNP experiment. By reversing the field (e.g. -E x H), we can populate the other domain. We have now systematically demonstrated this in $LiFePO_4$ and hope the technique can be extended to other candidate ferrotoroidic materials.

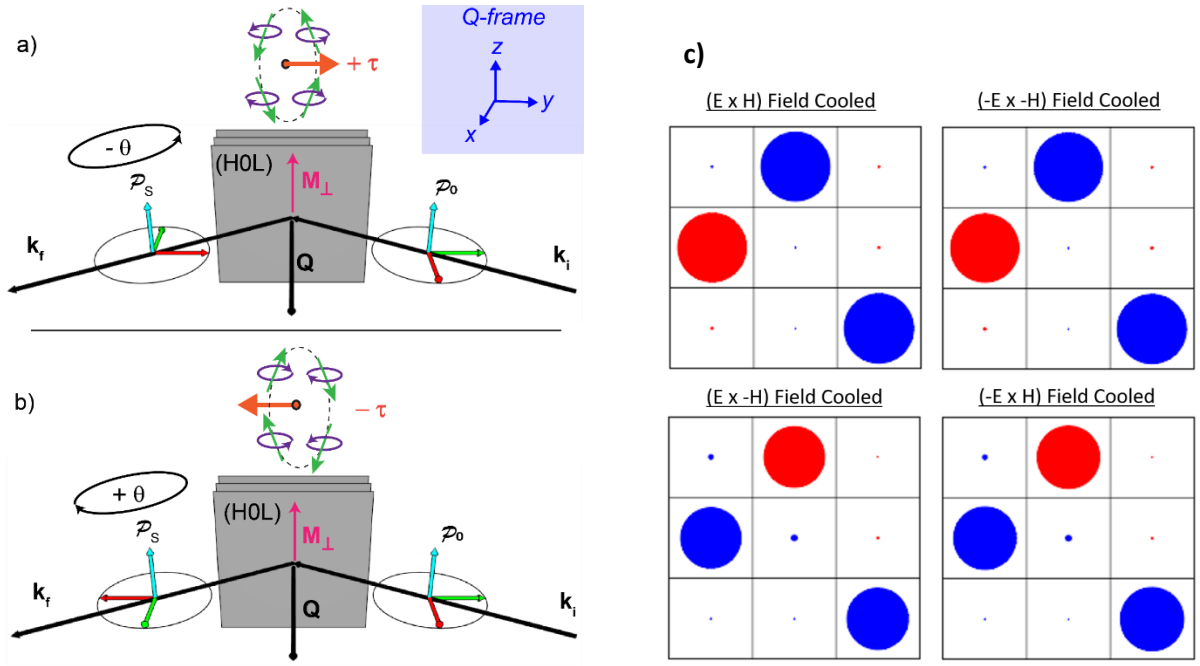

Figure 3. Rotation of the polarization $\mathcal{P}$ of the neutron beam after interacting with a $LiFePO_4$ single crystal that has been field cooled. In a) the toroidal moment τ is oriented in one direction after being cooled in either the (E x H) or (-E x -H) field, and the rotation angle -θ, is about the magnetic interaction vector M⊥. b) When the $LiFePO_4$ crystal is cooled under the opposite crossed field (E x -H) or (-E x H), then the polarization is about the +θ angle. c) The components of the 3x3 polarization matrix for the (101) Bragg reflection as shown by circles proportional to the percent polarized. One can see that it shows how the off-diagonal terms are filled in to represent a rotation about the z-axis. Red is negative, blue is positive.

Spherical neutron polarimetry: At the NIST Center for Neutron Scattering (NCNR), we worked with the polarization team (Wangchun Chen) to build a prototype whereby we tested the major components for an SNP experiment. Namely, we built electrically-controlled adiabatic rotation devices (ARD), before and after the sample space in order to prepare and analyze the beam's polarization in the *x*,*y*,*z*-directions. We then constructed a sample space consisting of a superconducting niobium shield connected to a cryogen-free closed cycle refrigerator (CCR). After building the software and hardware to interface with the PHADES instrument at NCNR, we were able to carry out enough measurements to calibrate the apparatus, which we called SANPA (Small Angle Neutron Polarimetry Apparatus).[3] Unfortunately, we hit a major roadblock in 2020, which was the pandemic and the exclusion of users from NCNR and other neutron facilities. Our current plan is to migrate our work to Oak Ridge National Laboratory to collaborate with the Neutron Sciences group to continue to develop neutron beam polarization techniques.

Future Plans

Inspired by our work on ferrotoroidic materials and a study that proposed $MnPS_3$ is a ferrotoroidic,[4] we are interested in pursuing such 2D materials that have a van der Waals (vdW)

gap, which allows us to manipulate them to study magnetism at the 2D limit. For the next phase of our neutron scattering work, we would like to continue our polarized neutron work but broaden our work and pivot from only ferroic materials and towards materials where the magnetism is confined to 2D-vdW materials. These 2D-vdW magnetic materials could play a crucial role in novel electronic materials since they can be isolated as monolayers.[5-7] We propose to elucidate the magnetic structures of new 2D-vDW magnetic materials with polarized neutron scattering. We are specifically interested in the transition metal thiophosphates and selenophosphates, which are 2D-vDW magnetic materials. These materials may express either long-range magnetic order or spin glassiness (i.e short-range order), and polarized neutrons will allow us to isolate the magnetic from the nuclear contribution and distinguish between multiple domains that can develop in these 2D-vDW materials. Furthermore, since these are vdW-materials, they exhibit extensive intercalation chemistry. Complex organic structures can be inserted to affect the magnetic, optoelectronic, and transport properties. Such hybrid organic-inorganic materials traditionally pose many challenges to unpolarized neutron diffraction, but with polarized neutron capabilities, we can solve their magnetic and nuclear structures.

As stated earlier, we are pivoting our polarized work away from NCNR to ORNL for the next couple of years. We have already sent several components of SANPA to the High Flux Isotope Reactor (HFIR) and hope to send the rest of it by the end of the year, so we can test it along with other apparatus at ORNL. We are currently purchasing a CCR that will be used to cool the superconducting Meissner shield for the wide-angle analogue to SANPA.

References

1) Spaldin, N.; Fiebig, M.; Mostovoy, M., "The toroidal moment in condensed-matter physics and its relation to the magnetoelectric effect" *Journal of Physics: Condensed Matter* **20,** 63 (2008).
2) Zimmermann, A. S.; Meier, D.; Fiebig, M., Ferroic nature of magnetic toroidal order. *Nature Communications* **5**, 4796 (2014). Gnewuch, S.; Rodriguez, E. E., "The fourth ferroic order: Current status on ferrotoroidic materials" *Journal of Solid State Chemistry* **271**, 175 (2019).
3) J. Tosado, W. C. Chen, S. Gnewuch, T. Hasaan, T. Dax, E. E. Rodriguez "Small-angle neutron polarimetry apparatus (SANPA): Development at the NIST Center for Neutron Research" *Review of Scientific Instruments* **90**, 063303 (2019).
4) Ressouche, E. *et al.* Magnetoelectric $MnPS_3$ as a candidate for ferrotoroidicity. *Physical Review B* **82**, 100408 (2010).
5) Susner, M. A.; Chyasnavichyus, M.; McGuire, M. A.; Ganesh, P.; Maksymovych, P. "Metal Thio- and Selenophosphates as Multifunctional van der Waals Layered Materials" *Advanced Materials* **29**, 1602852 (2017).
6) Gong, C.; Zhang, X. "Two-dimensional magnetic crystals and emergent heterostructure devices" *Science* **363**, 706 (2019).
7) Coak, M.J. et al. "Tuning dimensionality in van-der-Waals antiferromagnetic Mott insulators TMPS3" *Journal of Physics: Condensed Matter* **32**, 124003 (2020).

Publications

- S. Gnewuch and E. E. Rodriguez, "The fourth ferroic order: Current status on ferrotoroidic materials" *Journal of Solid State Chemistry* (2019) **271**, 175.
- J. Tosado, W. C. Chen, S. Gnewuch, T. Hasaan, T. Dax, E. E. Rodriguez "Small-angle neutron polarimetry apparatus (SANPA): Development at the NIST Center for Neutron Research", *Review of Scientific Instruments* (2019) **90**, 063303.
- S. Gnewuch and E. E. Rodriguez "Distinguishing the Intrinsic Antiferromagnetism in Polycrystalline $LiCoPO_4$ and $LiMnPO_4$ Olivines", *Inorganic Chemistry* (2020) **59**, 9, 5883-5895.
- T. Diethrich, P. Y. Zavalij, S. Gnewuch, and E. E. Rodriguez "Orbital Contribution to Paramagnetism and Noninnocent Thiophosphate Anions in Layered $Li_2MP_2S_6$ Where *M* = Fe and Co", *Inorganic Chemistry* (2021) **60**, 14, 10280–10290.
- H. Lane, E. E. Rodriguez, H. C. Walker, Ch. Niedermayer, U. Stuhr, R. I. Bewley, D. J. Voneshen, M. A. Green, J. A. Rodriguez-Rivera, P. Fouquet, S-W. Cheong, J. P. Attfield, R. A. Ewings, C. Stock, "Metastable antiphase boundary ordering in $CaFe_2O_4$", *Physical Review B*, (2021) **104**, 104404.

Non-Equilibrium Effects in Quantum Magnets

Kate A. Ross, Colorado State University

Program Scope

The project aims to achieve non-equilibrium conditions in solid state quantum magnets and measure the resulting properties via neutron scattering and ac susceptibility. I will report on the following areas: 1) Exploration of Kibble Zurek scaling effects in a transverse field Ising magnet using ac susceptibility, generated by quantum quenches (in this case, magnetic field ramps at low temperatures) performed at different quench rates spanning several orders of magnitude [1], 2) The study the spin-spin correlations after "quantum annealing" protocols vs. "thermal annealing" protocols in glassy Transverse Field Ising Model material using neutron scattering [2].

Recent Progress

Using AC susceptibility, we have investigated whether Kibble-Zurek (KZ) scaling is observable in the transverse-field Ising model material $CoNb_2O_6$ following magnetic field quenches [1]. As part of this work, we re-discovered and characterized (for the first time) a frozen state in this material that exists within its previously reported antiferromagnetically ordered phase at zero field. By varying the field quench rate and observing the initial ac susceptibility at zero field, we determined that Kibble-Zurek scaling is *not* observed. Namely, we do not observe strong evidence for a power-law scaling of initial ac susceptibility with quench rate. Instead, quenches into this phase result in a logarithmic scaling of the initial ac susceptibility. Our results are consistent with coarsening of domains over the timescale of the quench. Thus, we have not observed any form of Kibble-Zurek scaling in $CoNb_2O_6$, which itself is a somewhat surprising result; KZ scaling is expected to be ubiquitous for quenches across all second order transitions, including quantum, classical, and freezing transitions [3-6]. Our results imply that when coarsening happens on the timescale of the quenches, KZ scaling is possibly obscured.

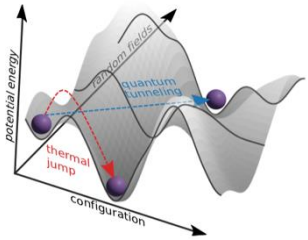

Figure 1: Cartoon of the effect of annealing protocols in $LiHo_xY_{1-x}F_4$. The transverse field induces quantum fluctuations, but also increases randomness.

We have also studied the effect of quantum annealing in the spin-spin correlations in the disordered Transverse Field Ising Model material, $LiHo_xY_{1-x}F_4$ (x=0.44) [2]. We used the CORELLI instrument to track the diffuse magnetic scattering this material for two annealing protocols; one which involves cooling in zero field (Thermal Annealing, TA), and the other involving cooling in a transverse field that induces quantum fluctuations (Quantum Annealing, QA). These two protocols in this material had been studied decades ago via ac

susceptibility, a study which provided the first evidence for a “quantum speedup” in this material [7]. In our neutron scattering experiment, at the shared end-point for both protocols, we observed very similar final spin-spin correlations, which produced of pinch-point scattering as expected based on critical scattering a phase boundary in the dipolar Ising ferromagnet model. However, comparing the time evolution at the end of the protocols, we find that the spin correlations evolve more significantly after TA, suggesting that QA produces a state closer to equilibrium. We also observe experimental evidence that the transverse field produces random fields, which had been previously predicted for this material and studied in other contexts. Thus, we argue that while the material does exhibit a “quantum speedup” under quantum annealing conditions, it is not a simple annealing problem; the energy landscape being optimized is changing as the optimization proceeds (see Figure 1).

Future Plans

We are now focusing on exploring non-equilibrium quantum dynamics via *inelastic* neutron scattering. In particular, we are interested in measuring non-equilibrium states via a departure from detailed balance. We will use a pulsed magnet setup on CNCS to try to measure higher effective temperatures in quantum magnets following a field quench, by comparing the inelastic signals at positive and negative energy-transfers. Once this principle is demonstrated, will then use this “effective thermometry” to investigate many-body localization (known as MBL [8]) by systematically introducing disorder into the materials of interest.

References

[1] C.L. Sarkis, S. Säubert, V. Williams, E.S. Choi, T.R. Reeder, H.S. Nair, K.A. Ross, "Low Temperature Domain Wall Freezing and Non-Equilibrium Dynamics in the Transverse-Field Ising Model Material CoNb2O6", Physical Review B. [Accepted Nov 2021].

[2] S. Säubert, C.L. Sarkis, F. Ye, G. Luke, K.A. Ross, "Microscopics of Quantum Annealing in the Disordered Dipolar Ising Ferromagnet LiHoxY1−xF4". arXiv:2105.03408v2 [cond-mat.str-el]

[3] W. H. Zurek, Cosmological experiments in superfluid helium?, Nature 317, 505 (1985)

[4] A. Chandran, A. Erez, S. S. Gubser, and S. L. Sondhi, Kibble- zurek problem: Universality and the scaling limit, Physical Re- view B 86, 064304 (2012).

[5] C.-W. Liu, A. Polkovnikov, A. W. Sandvik, and A. Young, Uni- versal dynamic scaling in three-dimensional ising spin glasses, Physical Review E 92, 022128 (2015).

[6] N. Xu, K.-H. Wu, S. J. Rubin, Y.-J. Kao, and A. W. Sandvik, Dynamic scaling in the two-dimensional ising spin glass with normal-distributed couplings, Physical Review E 96, 052102 (2017).

[7] J. Brooke, D. Bitko, T. Rosenbaum, and G. Aeppli, Quantum Annealing of a Disordered Magnet, Science 284, 779 (1999)

[8] A. C. Potter, R. Vasseur, and S. A. Parameswaran, Universal Properties of Many-Body Delocalization Transitions, Phys. Rev. X 5, 031033 (2015).

Publications

Colin L. Sarkis, "FRUSTRATION DRIVEN EMERGENT PHENOMENA IN QUANTUM AND CLASSICAL MAGNETS", Ph.D. Dissertation, Colorado State University, 04/01/2021.

C.L. Sarkis, S. Säubert, V. Williams, E.S. Choi, T.R. Reeder, H.S. Nair, K.A. Ross, "Low Temperature Domain Wall Freezing and Non-Equilibrium Dynamics in the Transverse-Field Ising Model Material CoNb2O6", Physical Review B. [Accepted Nov 2021].

S. Säubert, C.L. Sarkis, F. Ye, G. Luke, K.A. Ross, "Microscopics of Quantum Annealing in the Disordered Dipolar Ising Ferromagnet LiHoxY1−xF4". arXiv:2105.03408v2 [cond-mat.str-el]

Fundamental Understanding of Bottlebrush Polymers Based on Structure and Dynamics

Gerald J. Schneider, Department of Chemistry and Department of Physics & Astronomy, Louisiana State University, Baton Rouge, LA 70803

Program Scope

Our goal is a better fundamental understanding of bottlebrushes. Figure 1 illustrates the classification of graft polymers, from comb polymers to bottlebrushes, accomplished by increasing the number of side chains per backbone unit. The polymer reaches the bottlebrush regime once it can no longer form a random coil.[1] The high grafting density of side chains attached to a backbone leads to materials with ultralow viscosities, and hyperelasticity.[2]

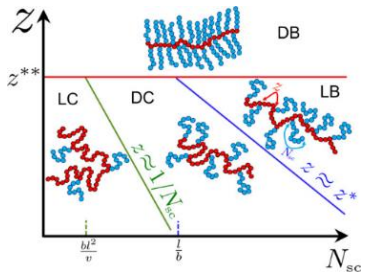

Figure 1. Classification of graft polymers by the grafting density, z, and degree of polymerization of side chains N_{sc}, distinguishing 4 regions, (1) loosely grafted comb-like, LC, (2) densely grafted comb, DC, (3) loosely grafted, LB, and (4) and densely grafted bottlebrush, DB.[3]

To understand systems with increasingly complex architectures, the project is divided into sub-tasks. (i) Identification of scaling relationships. (ii) Understanding of underlying molecular relaxation mechanisms. (iii) Correlation of results with viscoelastic data. Step (i) requires acquiring information on structure, and dynamics over a broad time and temperature-range. Step (ii) needs high-spatial resolution provided only by neutron spectroscopy and identification of local relaxations which requires isotopic sensitivity. Knowledge of scaling relationships and underlying relaxation mechanisms is highly transformative and can be utilized to further advance the understanding of viscoelastic data.

Recent Progress

This project combines information on structure and dynamics to advance fundamental understanding of bottlebrushes. Only neutron spectroscopy can provide simultaneous information on length- and timescale, e.g., central to distinguish two processes with the same relaxation time by the length-scale.

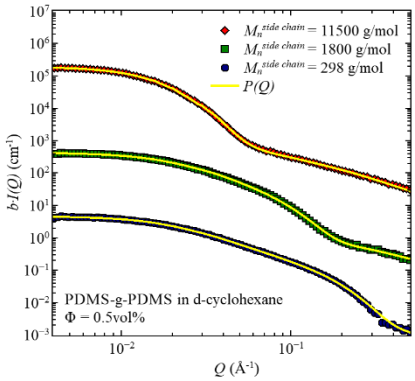

Figure 2. Small angle neutron scattering of PDMS-g-PDMS bottlebrush polymers with different side chain lengths.[4]

Our key results are: (1) We synthesized PDMS based bottlebrushes and verified stretching of the backbone by SANS experiments, which shows chain stretching occurs independently of side chain or backbone flexibility. (2) Via variation of the length of the side chains, we accomplished spherical and elongated shapes, as illustrated in Figure 2. Both shapes are of equal interest, e.g., as additives or standalone elastomers. (3) We showed that the shape of bottlebrushes is independent of the chemical environment and can be retained changing the host system from solvent to

polymer. (4) Bottlebrushes can be used as shell-only particles, with SANS being the unique tool to verify particle shape, size, and spatial distribution of shell-only particles in host matrices such as linear polymer melts. (5) Unlike any other system, the core of these shell-only particles has a negligible dimension, which facilitates a detailed investigation of the shell, compared to other systems like grafted nanoparticles, micelles, and star polymers. Additionally, it creates the opportunity to develop new light-weight materials by avoiding nanoparticles.

Figure 3 is a graphical illustration of the results obtained by SANS. It shows that the shell can swell in low molecular weight polymer melts. Shrinkage at higher molecular weight matrices is accompanied by agglomeration, at higher concentrations reflecting decreasing miscibility. (6) Knowledge of the ratio of side chain and host matrix molecular weights can be used to switch between colloidal and agglomerated systems.[5]

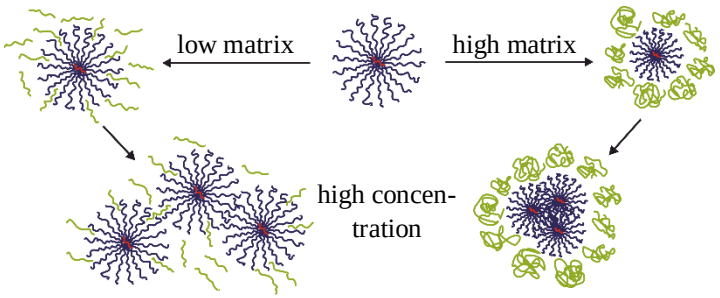

Figure 3. Pictorial illustration of the size changes and agglomeration behavior of bottlebrush polymers in linear host matrices.[5]

Dynamics largely determine the macroscopic material behavior. The recent progress concentrates on the fast relaxation at smaller length-scale. (7) Segmental relaxation of bottlebrushes strongly depends on the length of the side chain. In our project, the relaxation times of the segmental dynamics of bottlebrush polymers compared to their linear side chain changed by more than 2 orders of magnitude. A comparison with simulations on our samples reveals the surprising fact that this change can be turned to its opposite when going from stiff to flexible side chains. (8) Similar to linear polymers, the segmental dynamics of bottlebrushes changes over more than 10 orders of magnitude in time with temperature, obtained from complementary dielectric spectroscopy and fast field cycling relaxometry as seen in Figure 4. (9) Using the time scale of QENS in combination with the length scale resolution, reveals a length scale or Q dependent relaxation time, giving information whether the dynamics is homogenous or heterogenous. In case of our bottlebrush polymers, the segmental dynamics is heterogenous which is only visible due to the length scale resolution of QENS (Figure 5). Since dielectric spectroscopy would suggest homogenous dynamics due to a temperature independent shape of the segmental relaxation spectra, length scale information is an important part for understanding the dynamical processes.

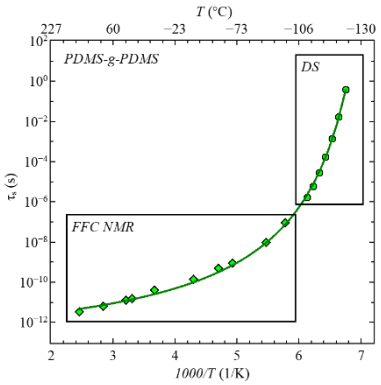

Figure 4. Segmental relaxation time as a function of inverse temperature.[6]

Experiments on materials, including but not limited to polymer melts, are often conducted at elevated temperatures to draw conclusions on the relaxation behavior at ambient temperature.

This assumption plays a crucial role in basic science in the construction of master plots from several measurements at various conditions. It is often the only way to predict the properties of a material over its lifecycle. However, the breakdown of the underlying time temperature superposition principle is known since a long time.[9] Understanding the reason for its breakdown has an enormous societal impact, and only neutron spectroscopy can give the answer, using a combination of experiments that covers a frequency/time range broad enough to create time temperature superposition together with the selection of the length-scale to separate processes.[9]

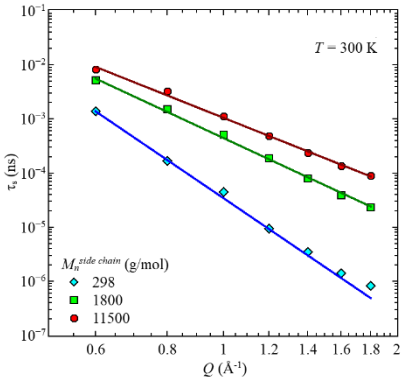

Figure 5. Segmental relaxation times as a function of momentum transfer.[7]

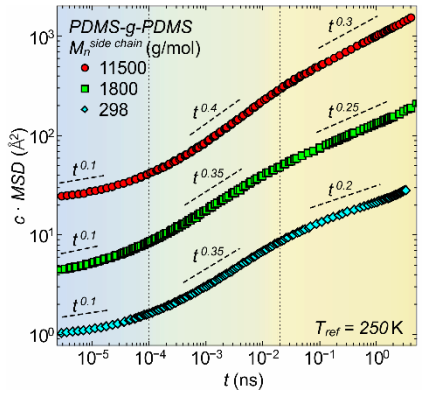

Figure 6. Mean square displacement as a function of time for the three different bottlebrush polymers.[9]

Here, we selected the small length-scale region less than the size of a polymer segment and concentrate on PDMS bottlebrushes and a broad time range to capture vibrations, methyl group rotation, and segmental relaxation. We demonstrate that the superposition of two or more processes is the main reason for the breakdown of the scaling at this small-length scale. However, we also demonstrate that the heterogeneity, very typical for the segmental relaxation, does not impact the time temperature scaling. The method we have developed is useful for the expert, but also designed for a beginner. It is highly transformative, e.g., shows why characterization tools like rheology and dielectric spectroscopy report a breakdown at vastly different temperature values. It is important, because it explains that a change of the MSD in the intermediate time range of Figure 6, is due to the superposition of the methyl group rotation and the segmental relaxation. The partial mean square displacement shows the independence of the methyl group rotation on temperature and molecular weight of the bottlebrush.

Future Plans

Up to now, our experiments concentrated on the fast relaxations, with a length-scale at the polymer segment scale or below. Our experiments identified the segmental relaxation as heterogeneous based on the Q dependence of the relaxation time.[7] The next step forward will capture the transition to the homogeneous region, and the homogeneous region itself. Estimates suggest a molecular weight dependent Q* between 0.1 to 0.6 Å^{-1} (Figure 7). At this value we expect a change of the power law. This beamtime is already granted at NIST, Gaithersburg.

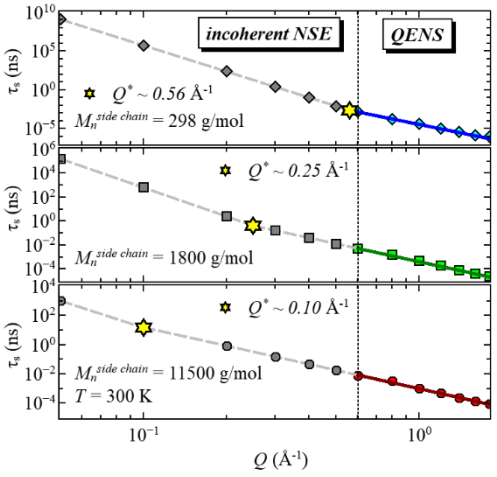

Figure 7. Estimated relaxation times and Q^*.

Inspired by the combined results of dielectric spectroscopy and QENS, which are in favor of a gradual relaxation behavior from the grafted to the free chain end, we are going one step further and conducting QENS experiments on specifically labeled bottlebrush polymers, highlighting two parts of the side chain to study the segmental dynamics as a function of the distance to the backbone, cf. Figure 8. Here we emphasize the important difference, because we use polypropyleneoxide, PPO, with the advantage that chain relaxation, or normal mode, is visible in dielectric spectroscopy.

By means of the planned QENS experiments (two out of three beamtime proposals are already scheduled, the third beamtime proposal is submitted) we can compare the confinement of the different blocks of the side chain with the fully protonated sample and unattached side chain using the time and length scale resolution of neutron spectroscopy.

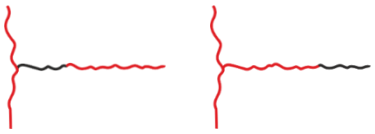

Figure 8. Specifically labeled bottlebrush polymers with inner part (left) and outer part (right) highlighted.

References

1. Polymeropoulos, G.; Zapsas, G.; Ntetsikas, K.; Bilalis, P.; Gnanou, Y.; Hadjichristidis, N., 50th Anniversary Perspective: Polymers with Complex Architectures. *Macromolecules* **2017,** *50* (4), 1253-1290.
2. Daniel, W. F.; Burdynska, J.; Vatankhah-Varnoosfaderani, M.; Matyjaszewski, K.; Paturej, J.; Rubinstein, M.; Dobrynin, A. V.; Sheiko, S. S., Solvent-Free, Supersoft and Superelastic Bottlebrush Melts and Networks. *Nat Mater* **2016,** *15* (2), 183-9.
3. Paturej, J.; Sheiko, S. S.; Panyukov, S.; Rubinstein, M., Molecular Structure of Bottlebrush Polymers in Melts. *Sci Adv* **2016,** *2* (11), e1601478.
4. Jakobi, B.; Bichler, K. J.; Sokolova, A.; Schneider, G. J., Dynamics of PDMS-g-PDMS Bottlebrush Polymers by Broadband Dielectric Spectroscopy. *Macromolecules* **2020,** *53* (19), 8450-8458.
5. Bichler, K. J.; Jakobi, B.; Huber, S. O.; Gilbert, E. P.; Schneider, G. J., Structural Analysis of Ultrasoft PDMS-g-PDMS Shell-Only Particles. *Macromolecules* **2020,** *53* (1), 78-89.
6. Bichler, K. J.; Jakobi, B.; Schneider, G. J., Dynamical Comparison of Different Polymer Architectures-Bottlebrush vs Linear Polymer. *Macromolecules* **2021,** *54* (4), 1829-1837.
7. Bichler, K. J.; Jakobi, B.; Sakai, V. G.; Klapproth, A.; Mole, R. A.; Schneider, G. J., Short-Time Dynamics of PDMS-g-PDMS Bottlebrush Polymer Melts Investigated by Quasi-Elastic Neutron Scattering. *Macromolecules* **2020,** *53* (21), 9553-9562.
8. Plazek, D. J.; Temperature Dependence of the Viscoelastic Behavior of Polystyrene. J. Phys. Chem. 1965, 69, 10, 3480–3487.
9. Bichler, K. J.; Jakobi, B.; Sakai, V. G.; Klapproth, A.; Mole, R. A.; Schneider, G. J., Universality of Time–Temperature Scaling Observed by Neutron Spectroscopy on Bottlebrush Polymers. *Nano Lett.* **2021,** *21* (10), 4494-4499.

Publications

- Bichler, K. J., *Morphology and Dynamics of Bottlebrush Polymers*. Springer Theses, Springer **2021**.
- Bichler, K. J.; Jakobi, B.; Sakai, V. G.; Klapproth, A.; Mole, R. A.; Schneider, G. J., Universality of Time–Temperature Scaling Observed by Neutron Spectroscopy on Bottlebrush Polymers. *Nano Lett.* **2021,** *21* (10), 4494-4499.
- Bichler, K. J.; Jakobi, B.; Schneider, G. J., Dynamical Comparison of Different Polymer Architectures-Bottlebrush vs Linear Polymer. *Macromolecules* **2021,** *54* (4), 1829-1837.
- Bichler, K. J.; Jakobi, B.; Sakai, V. G.; Klapproth, A.; Mole, R. A.; Schneider, G. J., Short-Time Dynamics of PDMS-g-PDMS Bottlebrush Polymer Melts Investigated by Quasi-Elastic Neutron Scattering. *Macromolecules* **2020,** *53* (21), 9553-9562.
- Jakobi, B.; Bichler, K. J.; Sokolova, A.; Schneider, G. J., Dynamics of PDMS-g-PDMS Bottlebrush Polymers by Broadband Dielectric Spectroscopy. *Macromolecules* **2020,** *53* (19), 8450-8458.
- Bichler, K. J.; Jakobi, B.; Huber, S. O.; Gilbert, E. P.; Schneider, G. J., Structural Analysis of Ultrasoft PDMS-g-PDMS Shell-Only Particles. *Macromolecules* **2020,** *53* (1), 78-89.

Neutron and X-Ray Studies of Spin and Change Manipulation in Magnetic Nanostructures

Sunil K Sinha, Dept. of Physics, University of California San Diego and Eric Fullerton, Center for Memory and Recording Research, University of California San Diego

Program Scope: Our program is focused on the study of competing, frustrated and disordered magnetic systems. In particular, we are interested in (i) the static and dynamic properties of chiral magnetic systems, (ii) spin fluctuations in jammed and frustrated magnetic systems, such as spin glasses, domain walls in antiferromagnets, and slow fluctuations in spin liquids and spin glasses, which can be probed with neutron spin echo techniques and XPCS and (iii) magnetic/superconducting heterostructures. We believe this research could lead us to new understandings of basic physics processes in magnetic and electronic systems using a combination of neutron and x-ray techniques.

Recent Progress:

(a) Magnetic Skyrmions: We have continued to use Fe/Gd multilayers as a model system to study chiral magnetic structures and we have probed them by SANS (see Fig. 1), resonant soft x-ray scattering, resonant soft x-ray imaging, XPCS, Lorentz TEM, ferromagnetic resonance, magneto-transport and modeling. In particular we demonstrated that the tunable magnetic properties of amorphous Fe/Gd mulitlayers enable the formation of well-ordered skyrmion lattices which are stable over a large temperature and magnetic field parameter space, including room temperature and zero magnetic field (see Fig. 1). We further used SANS to capture the skyrmion. Using perpendicular DC fields and in-plane RF fields, we explored the gyration modes of hybrid skyrmions away, below, at, and above resonance [Fig. 2(a-d)]. We find the dynamic modes of hybrid skyrmions contribute to the SANS signal in two ways: first, the scattered neutrons incur additional transverse momentum as a result of scattering from a moving

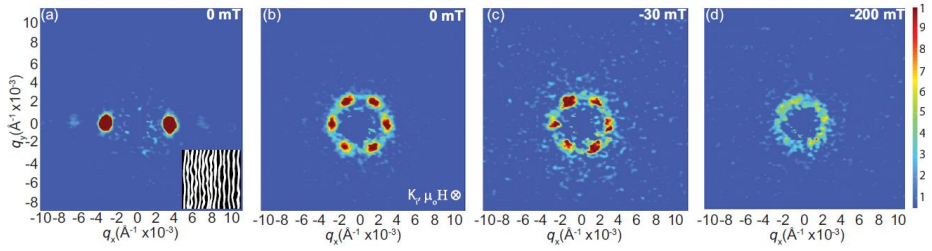

Figure 1: SANS pattern at sequential fields for Fe/Gd multilayer. (a) SANS pattern showing two peaks indicating a well-ordered stripe domain structure. The inset is an illustration of the artificially ordered stripe phase. The out-of-plane magnetic field was increased to μ_0H = 185 mT (not shown). SANS patterns were measured as the magnetic field was reduced towards negative saturation, with measurements shown at (b) μ_0H = 0 T (skyrmion phase), (c) μ_0H =−30 mT, (d) μ_0H =−200 mT.

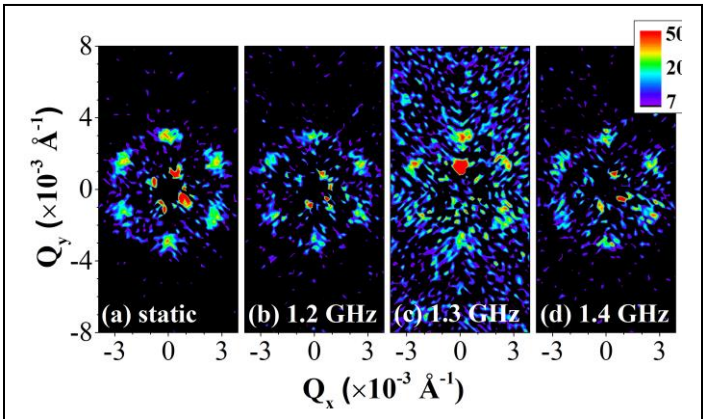

Figure 2: 2D SANS pattern of magnetic skyrmions under different magnetic fields and excitation frequencies: (a) Static state (H=0, RF=0), (b) below-resonance state (H=150 mT, RF=1.2 GHz), (c) at-resonance state (H=150 mT, RF=1.3 GHz) and (d) above-resonance state (H=150 mT, RF=1.4 GHz). All 2D images are plotted with the same intensity scale.

source, and second, the gyration skyrmions disrupt ordering of the lattice giving rise to enhancement form-factor scattering.

By using coherent resonant x-ray magnetic scattering, we studied spontaneous fluctuations on nanosecond time scales in thin films of multilayered Fe/Gd that exhibit ordered stripe and skyrmion lattice phases. We first measure spontaneous fluctuations of the skyrmion lattice phase and find an inherent, collective mode showing an underdamped oscillation with a relaxation of a couple of nanoseconds. Further observations track the response towards the continuous phase transition and a "critical-like" slowing down of fluctuations is observed well before the critical point. These results suggest that the skyrmion lattice phase never fully freezes into a static crystal. This constant state of fluctuation indicates that the physics of topological magnetic phases may have more in common with high-temperature superconductors with disorder.

(b) Study of the Griffiths Phase and high-field magnetic phase transitions in disordered binary rare earth compounds: The binary rare-earth dialuminides reveal interesting physics, such as strong crystal field (CF) effects due to anisotropic *4f* charge density as well as the competition between different magnetic and crystal structures. $PrAl_2$ and $ErAl_2$ exhibit ferromagnetic to paramagnetic transitions at 32.5 K and 14 K, respectively. On the other hand, $(Pr,Er)Al_2$ undergoes a paramagnetic to ferrimagnetic (FIM) transition at T_C = 24 K. In the FIM phase, the Pr and Er moments are aligned antiparallel, and this material shows several further magnetic transitions at high applied magnetic fields. In particular, at low fields and below a temperature of 26 K, it shows what is believed to be a Griffiths phase [1]. We have used a combination of SANS and XMCD to understand several of the novel magnetic phases observed in $(Pr_{0.6}Er_{0.4})Al_2$, including the detailed nature of the ferrimagnetic phase. For reasons of space we will not include the XMCD results in this report. We have used SANS at the NIST NCNR facility to study the Griffiths phase in a single crystal of $(Pr_{0.6}Er_{0.4})Al_2$ in the temperature region just above Tc. The Griffiths phase [1] in a system with quenched-in disorder, is a phase which exists at temperatures above the true long-range ordering temperature where quantities such as the magnetization, free energy, etc. are non-analytic functions of magnetic field and temperature. It is characterized by local clusters of ordered spins, presumably ferrimagnetic clusters in this case. Using polarized SANS we have confirmed the existence of these clusters, demonstrated that they are anisotropic and measured their temperature dependence. Unfortunately, we were unable to get a complete set of data, as the detector on the spectrometer had to be replaced and then the NIST reactor shut down. We were able to get beam time at the SANS instrument at the ANSTO neutron facility in Australia (which have to be run remotely as we are barred from access due to COVID restrictions) which is now scheduled for January. We then hope to measure down to Q values of ~ 10 ^-4 $Å^{-1}$ and get a complete set of temperature data, which will enable us to publish these results.

(c) Interfacial Spin Structure, Spin-Triplet Superconductivity, and Long-Range Proximity Effects in Magnetic-Superconducting Heterostructures: Combining superconductivity with spintronics can lead to different superconducting states which can be useful for spin transport applications. For superconducting/ferromagnetic (S/F) composites, the penetration of the spin-singlet Cooper pairs into a ferromagnet typically decays quickly over the order one or two nanometers. However, if the magnetization vectors at the S/F interface are non-collinear with respect to the magnetization vector in the ferromagnet, one can obtain spin-triplets, which persist over long distances giving rise to a long-range proximity effect. We have used polarized neutron reflectivity combined with transport measurements to probe the interface spin structure of this heterostructure consisting of a fixed hard magnetic layer (F), a free magnetic layer (F') and superconducting layer (S).

The samples studied are MgO(110)/Cr/Co/Au/NiFe/Au/Nb/Au with different thicknesses of a free magnetic (NiFe) layer (F').. Figure 3(a) shows the resistivity measurement in magnetic field along MgO[100] direction (black curves), and MgO[011] direction (red curves) for multilayer sample MgO(110)/Cr(6nm)/Co(2.5nm) /Au(4nm)/NiFe(0.6nm) /Nb(21nm) /Au(4nm). The GMR effect (Fig 3(a)) is directly related to the angle between the magnetic orientations of two magnetic layers. It shows that the maximum resistance state shows up at antiparallel magnetic orientations and switch to the minimum resistance state when magnetic orientations are in parallel.

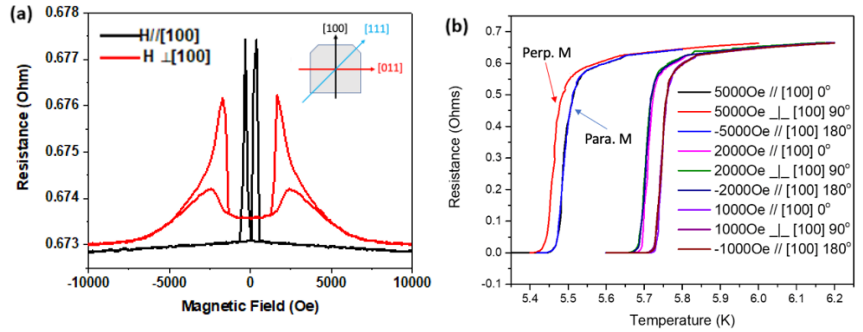

Figure 3: (a) GMR curves measured at 10 K with the field parallel and perpendicular to MgO[100], and (b) T_C at a different angle and field strength for multilayer sample with d(NiFe) = 0.6 nm.

The indirect manifestation of spin-triplet tunneling is a relative shift of T_C when spins in F and F' are canted relative to each other. For our multilayer sample with NiFe = 0.6 nm shows lower critical temperature (*Tc*) at non-linear configuration (when applying magnetic field 90 degree to the easy axis of Co layer below the saturation field and above the NiFe switching field) (see Fig. 3(b)). However, a multilayer with NiFe=3 nm (not shown here) shows the opposite trend, where non-linear configuration shows higher T_c. The transport measurements were done off-line, but in principle could be done simultaneously with the neutron measurements. A device with no F' layer with a Nb film showed an overall downward shift of Tc with increasing field (presumably due to the field penetration into the Nb film) but no relative shift of Tc dependent on the direction of applied field.

We performed our preliminary studied of polarized neutron reflectometry (PNR) measurements at temperature 4 K at NIST. We measured at three different conditions to achieve three different magnetic orientation configuration: a) H = 5000 Oe and field applied along with MgO[100] direction: parallel orientation; b) H = -200 Oe and field applied along minus MgO[100] direction: antiparallel orientation; c) H = 3000 Oe and field applied along with MgO[011] direction: perpendicular orientation. We observed that the relative angle between the two layers is consistent with the value we get from VSM and GMR measurements. We observed that the behavior of the spin valve is highly sensitive to the thickness (*d*) of F', F and S. We have a proposal in to pursue more exhaustive measurements at the SNS.

(d) Development of theory for phase retrieval imaging in GISAXS mode using the Distorted Wave Born Approximation.

"Diffraction Imaging" has attracted much attention over the last few years. The method uses oversampling methods and iterative schemes to retrieve the phase of the speckle pattern produced by the scattering of a coherent X-ray beam to reconstruct the image of samples at nanometer length scales. Most of such measurements have been made in transmission geometry set of samples that show spin triplet behavior with different signs of critical temperature when the magnetic configuration of two layers is perpendicular to each other. We have a proposal in to

pursue more exhaustive measurements at the SNS.and have assumed that the speckle pattern is the Fourier Transform (FT) of the object, as in the Born Approximation.

However, for many experiments it may be desirable for many reasons to mount the samples on a surface or interface, so that GISAXS would be the technique of choice. In this case the existence of a reflected beam from the substrate causes the speckle pattern to deviate significantly from the simple FT of the object. We have extended the phase retrieval method to use the full DWBA expression for the speckle pattern which takes the specularly reflected beam into account. The results obtained from detailed computer simulations of the scattering and reconstruction are very encouraging in showing that the method works. (see Fig. 4) Verification with real experiments is planned.

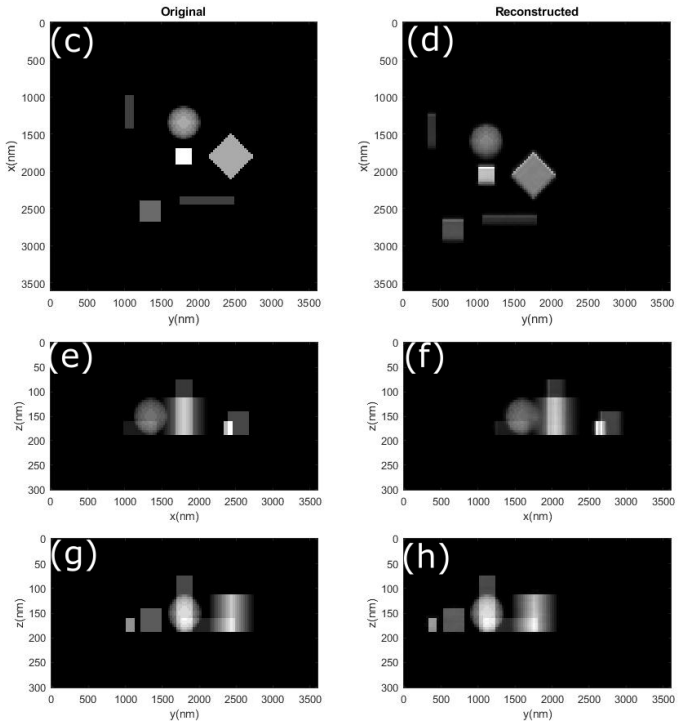

Figure 4: (c), (e) and (g) show the 3 projections of the model objects (assumed to be gold, sitting on a smooth Si surface – not shown) in the x-y, x-z and y-z planes, respectively. The GISAXS scattering from these objects was simulated using the DWBA and reconstructed using the DWBA-extended phase reconstruction methods. (d),(f) and (h) on the right show the reconstructed images and corresponding projections.

(e) XPCS and X-ray microscopy studies of ion transport in polymer electrolytes

Quantitative understanding of ion and mass transport in liquid and polymeric electrolytes is at the heart of electrochemistry and many other energy related fields. Here, the goal is to accurately predict the concentration-dependent transport properties of the electrolyte and the resulting performance of an electrochemical device. In this context, one challenge is to unravel the transport phenomena occurring in concentrated solutions and determine the corresponding transport coefficients, as these are foundational to the performance of electrolytes in ion batteries. In this study, we employed a novel approach to understand the ion transport mechanism and evaluate transport coefficients, including transference numbers, in a baseline polymeric electrolyte. Specifically, we utilized in-situ synchrotron XPCS and X-ray microscopy to directly measure the electrolyte velocity and ion concentration profiles in a Li–polymer electrolyte cell. These were directly compared to calculations based on macroscopic concentrated solution theory, which contain the transference numbers as an input. Our results provide length- and time-scale bridging understanding of ion transport. The results have been published in *Energy and Environmental Science*.

PUBLICATIONS

(1) A. Singh, J. C. T Lee, K. E. Avila, Y. Chen, S. Montoya, E. E. Fullerton, P. Fischer, K. A. Dahmen, S. D. Kevan, M. K. Sanyal, S. Roy, "Scaling of domain cascades in stripe and skyrmion phases", *Nature Communications*, Vol. 10, No. 01, (Apr. 2019) pp 1988/1-9.

(2) T.O.Farmer, E.-J. Guo, R.D. Desautels, L. DeBeer-Schmitt, A.Chen, Z.C.Wang, Q. Jia, J.A.Borchers, D.A. GilberT, B. Holladay, S.K.Sinha, M.R. Fitzsimmons, "Nanoscale magnetization inhomogeneity within single phase nanopillars", *Phys. Rev. Materials*, **3**, No.8 (Aug, 2019) 081401

(3) L. M. DeBeer-Schmitt, R. D. Desautels, S. Montoya, J. A. Borchers, S.-G. Je, M.-Y. Im, M. R. Fitzsimmons, E. E. Fullerton, Dustin A. Gilbert, "Realization of magnetic skyrmions in thin films at ambient conditions", *Physical Review Materials,* Vol. 3, No. 10 (Oct. 2019) pp 104406/1-9.

(4) V. Esposito, X. Y. Zheng, M. H. Seaberg, S. A. Montoya, B. Holladay, A. H. Reid, R. Streubel, J. C. T. Lee, L. Shen, J. D. Koralek, G. Coslovich, P. Walter, S. Zohar, V. Thampy, M. F. Lin, P. Hart, K. Nakahara, P. Fischer, W. Colocho, A. Lutman, F.-J. Decker, S. K. Sinha, E. E. Fullerton, S. D. Kevan, S. Roy, M. Dunne, and J. J. Turner. "Skyrmion fluctuations at a first-order phase transition boundary", *Applied Physics Letters*, Vol. 116, No. 18 (May 2020) pp 181901/1-4.

(5) J. Wingert, A. Singer, S. K. K. Patel, R. Kukreja, M. Verstraete, A. Romero, V. Uhl´ıˇr, S. Festersen, D. Zhu, J. M. Glownia, H. T. Lemke, S. Nelson, M. Kozina, K. Rossnagel, M. Bauer, B. M. Murphy, O. M. Magnussen, E. E. Fullerton, and O. G. Shpyrko, "Direct time-domain determination of electron-phonon coupling strengths in chromium" *Physical Review B,* Vol. 102, No. 04 (July 2020) pp 041101(R)/1-6.

(6) M. S. El Hadri, V. Polewczyk. Y. Xiao, S. Mangin and E. E. Fullerton, "Large anisotropic magnetocaloric effect in all-sputtered epitaxial terbium thin films" *Physical Review Materials,* Vol. 4, No. 12 (Dec. 2020) pp 124404/1-7.

(7) H.-G. Steinruck, C.J.Takacs, H.-K. Kim, D.G. Mackanic, B.Holladay, C.T.Cao, S.Narayanan, E.M.Dufresne, Y.Chushkin, B.Ruta, F.Zontone, J.Will, O.Borodin, S.K.Sinha, V.Srinivasan and M.F.Toney, "Concentration and velocity profiles in a polymeric lithium-ion battery electrolyte" *Energy and Environmental Science*, Vol. 13, Issue 11 (2020) pp. 4312-4321

(8) L. Fallarino, B. J. Kirby, and E. E. Fullerton, "Graded magnetic materials", *Journal of Physics D: Applied Physics,* Vol. 54, No. 30, (May 2021), pp. 303002/1-15.

(9) M. H. Seaberg, B. Holladay, S. A. Montoya, X. Y. Zheng, J. C. T. Lee, A. H. Reid, J. D. Koralek, L. Shen, V. Esposito, G. Coslovich, P. Walter, S. Zohar, V. Thampy, M. F. Lin, P. Hart, K. Nakahara, R. Streubel, S. D. Kevan, P. Fischer, W. Colocho, A. Lutman,

F.-J. Decker, E. E. Fullerton, M. Dunne, S. Roy, S. K. Sinha, and J. J. Turner, "Spontaneous fluctuations in a magnetic Fe/Gd skyrmion lattice", *Physical Review Research,* Vol. 3, No. 3, (Sept. 2021), pp. 033249-1-8.

(10) T. D. Frazer, Y. Zhu, Z. Cai, D. A. Walko, C. Adamo, D. G. Schlom, E. E. Fullerton, S. O. Hruszkewycz, Y. Cao, H. Wen, "Optical-transient-grating-pumped x-ray diffraction microscopy for studying mesoscale structural dynamics", *Scientific Reports* Vol. 11, No. 1, (Sept. 2021), pp. 19322-1-8.

Revealing the molecular origin of interactions between nanocrystals

James Swan, MIT (PI)

William Tisdale, MIT (co-PI)

Program Scope

The goal of this research program is to identify and quantify the role of surface-bound molecular ligand layers in directing the self-assembly of colloidal nanocrystals into ordered superlattices. Apart from shape-driven excluded volume interactions or ligand-driven enthalpic interactions, we hypothesize that molecular organization on and around nanocrystal surfaces sensitively biases the self-assembly of particular nanocrystal superlattice morphologies. To test this hypothesis, we are using small angle scattering (**Fig. 1**) and molecular simulation to investigate how interactions among surface-bound ligands, solvent, and free ligands in solution control the formation of nanocrystal superlattices.

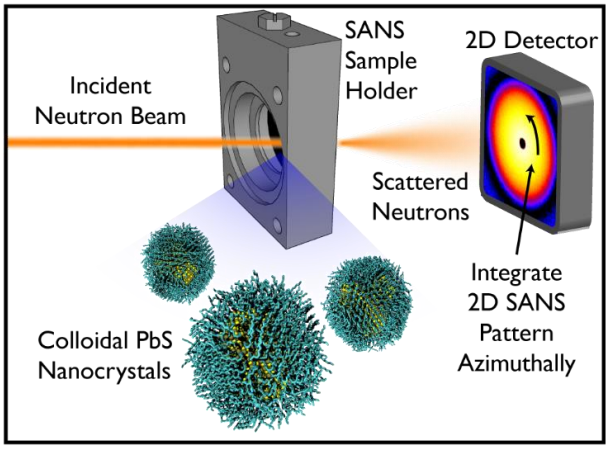

Figure 1. Schematic illustration of small-angle neutron scattering (SANS) of oleate-capped PbS nanocrystals in solution.

The specific aims of this program are 1) to quantify molecular structure on isolated nanocrystal surfaces using small-angle neutron scattering (SANS), 2) to understand how free and bound ligands mediate nanocrystal interactions in concentrated solutions, and 3) to determine the structural organization of molecular ligands in self-assembled nanocrystal superlattices.

Recent Progress

1) Quantifying interaction potentials between nanocrystals in dense solutions

In Year 1 of the program, we used small-angle neutron scattering (SANS) to measure the solution structure factor in dispersions of fully passivated, oleate-capped PbS NCs up to concentrations of 16 v/v%. Fitting the data by assuming an attractive square well interaction potential between NCs yielded a repulsive core diameter larger than the physical NC core diameter. This repulsive core stems from a densely packed region of the ligand-shell near the NC surface. The spatial extent of the repulsive core increases with temperature as ligand motion increases, becoming repulsive

farther out in the ligand-shell, while the portion of ligand-shell outside of the repulsive region remains attractive with a strength ~1 k_BT (**Fig. 2**). SANS provides a molecular interpretation of the fundamental inter-particle interactions in colloidal nanocrystal suspensions, ultimately relevant to understanding the self-organization of nanoscale materials. This work is summarized in Publication #1.

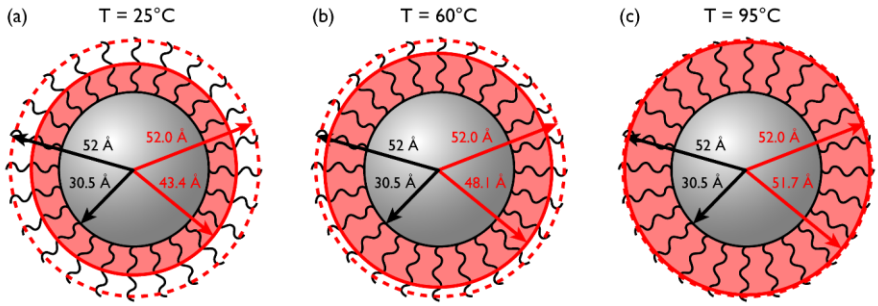

Figure 2. Schematic comparison across temperature. (a-c) Comparison of the square well fit dimension parameters (red) to the physical dimensions of the NC (black) for the high ligand coverage batch of PbS NCs ($D = 6.1\ nm$, $\sigma_D \leq 3.4\%$, $\gamma = 5.8\ ligands/nm^2$, $\phi_f = 0.12$). The repulsive core diameter σ is larger than the NC core diameter and increases with temperature as ligand bulk material density decreases.

2) **Prediction of superlattice structure with large-scale patchy particle simulations**

Predictive control over the assembly of PbS nanocrystals (NCs) into ordered, oriented superlattices (SLs) and a comprehensive theoretical framework consistent with experimental observations has remained elusive. PbS NC SLs can adopt any number of configurations along the Bain path from body-centered cubic (BCC) to face-centered cubic (FCC) pathway through body-centered tetragonal (BCT) intermediates. In early work from this program, we showed that NC interactions are well-characterized by an isotropic, repulsive, densely packed ligand-shell larger than the NC core with weak attractions also present (Publication #1). Recently, we have extended that molecular understanding to parameterize a patchy particle representation of PbS NCs for large-scale Brownian dynamics (BD) simulations (**Fig. 3**).

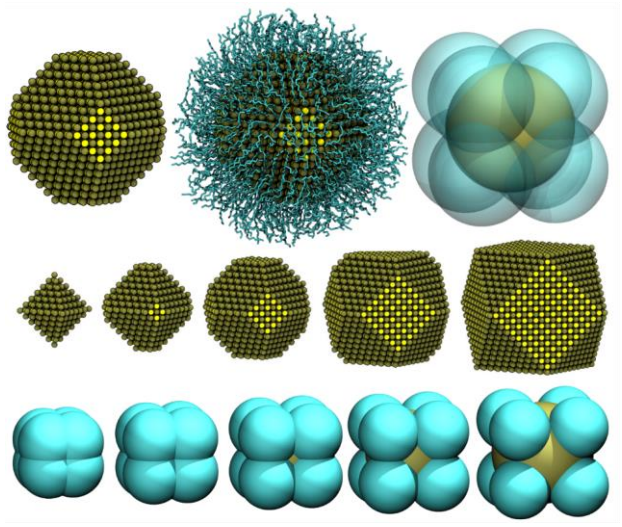

Figure 3. Comparison of atomistic and patchy particle NC representations. (top row) Bare NC core, NC with ligands, and patchy particle with ligand patches on the 8 $(111)_{NC}$ facets. (bottom row) Equivalent patchy particle representations with ligand patches matching length of oleate capping ligands ($L = 2.19$ nm).

The ligand patch attractive strength is determined by comparison of the solution structure to that measured by small-angle neutron scattering (SANS) for oleate-capped PbS NCs (**Fig. 4**). The patchy particle self-assembly behavior is probed using a sedimentation equilibrium methodology which returns a complete equation of state with a single simulation and allows extraction of the SL parameters and NC orientations. As the size of the repulsive ligand core increases, the lattice transitions predictably along the pathway BCC → BCT → FCC with unit cell axes lengths that perfectly match experimentally realized PbS NC SLs characterized by grazing-incidence small-angle X-ray scattering (GISAXS). Weak attractions between ligand patches, consistent with anisotropic ligand coverage on lead chalcogenide NCs, stabilize NC orientations in the SL. The nearest-neighbor spacing corresponds well with the repulsive core size. We have mapped the phase diagram across typical NC core diameters and ligand lengths and present a predictive framework that agrees with the observed SLs. A manuscript detailing these advances is in preparation.

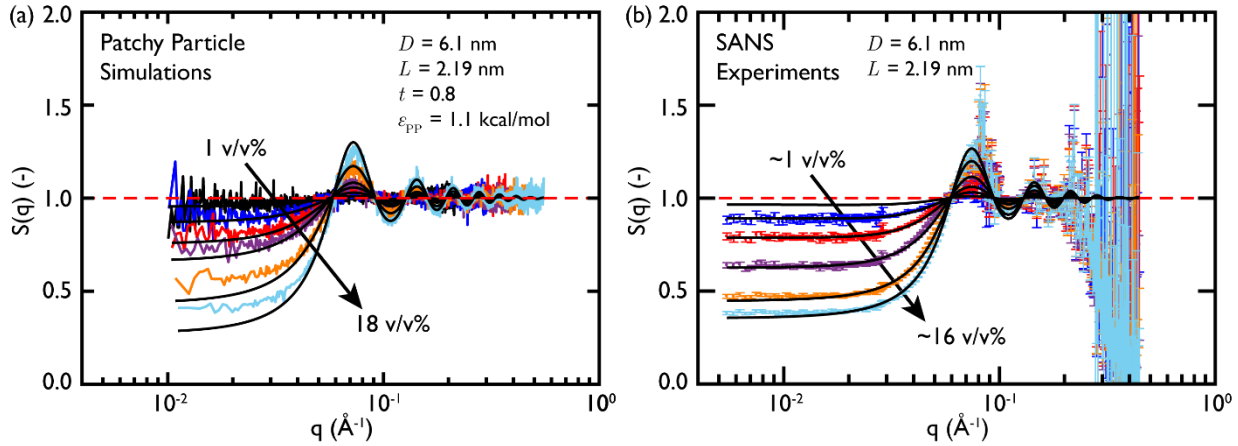

Figure 4. Comparing simulation and experimental structure factors. (a) Solution structure factor from patchy particle simulations (colored) and fits to the square-well model (black, dashed) for semi-dilute solutions (ϕ = 1, 3, 5, 9, 14, and 18 v/v%) of patchy particles with comparable dimensions to those measured using SANS at an interaction strength of 1.1 kcal/mol. (b) Experimental structure factor from SANS experiments for 6.1 nm diameter oleate-capped PbS NCs. Volume fractions (ϕ = 1.0, 3.2, 5.6, 9.4, 14.2, and 16.5 v/v%) are different from panel (a).

Future Plans

Work under this program so far has focused exclusively on understanding interactions between NC ligand layers in solution. Moving forward, the focus will shift toward understanding molecular organization in self-assembled NC superlattices. A key goal for the coming program year is acquisition of high-quality SANS data on NC superlattices. This is a challenging undertaking, as this will require an unusually large quantity of NC material.

Publications (2021)

1. "Repulsive, Densely Packed Ligand-Shells Mediate Interactions between PbS Nanocrystals in Solution"
   S.W. Winslow, Y. Liu, J.W. Swan,* W.A. Tisdale;*
   J. Phys. Chem. C. 125, 8014-8020 (2021).

Orbitally-Active AMX_2 as a Platform for Novel Magnetism and Entangled Electronic States

Stephen D. Wilson

Materials Department, University of California, Santa Barbara

Program Scope

This program supports the synthesis and study of orbitally-active AMX_2 (A=alkali metal, *M*=transition metal or rare earth ion, *X*=chalcogen ion) compounds. These compounds typically form into delafossite-like structures comprised of triangular lattice, edge-sharing networks of MX_6 octahedra separated by layers of *A*-site ions (though other interesting structures occasionally also form). The goal is to understand whether members of this family of materials that host magnetic ions with intertwined orbital and spin degrees of freedom can stabilize new magnetic states and quasiparticles. For instance, novel Higgs-like amplitude modes, quantum spin liquid states, and emergent Majorana quasiparticle excitations are predicted to emerge in certain scenarios.

The specific structural motifs of AMX_2 systems targeted in this program form highly frustrated networks of *M*-site spins either in a layered triangular lattice structure or within a stretched, diamond-like lattice. By tuning the interaction energies, single-ion anisotropies, and exchange anisotropies, a rich frontier of emergent electronic phase behavior is predicted to be accessible. Furthermore, in layered triangular lattice variants, the large ionic mobility of the *A*-site cations provides a materials-based tuning parameter for controlling doping and vacancy- coupled electronic order. Key variants under exploration are the $NaMO_2$ compounds with *M*=Mn, Ru transition metal cations and ARX_2 compounds with *A*=Li, Na, K, Rb and *R*=Yb, Ce and *X*=O, S, Se, Te. This program endeavors to synthesize both powders and single crystals of these compounds and to explore their electronic ground states via an array of neutron scattering techniques.

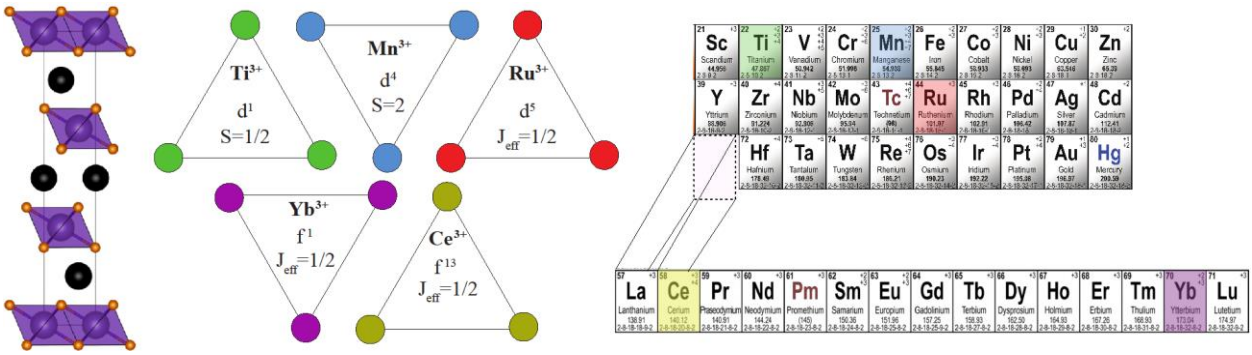

Fig. 1: Side view of the AMX_2 delafossite-like structure comprised of layers of edge-sharing MX_6 octahedra (purple spheres coordinated by orange spheres) separated by *A*-site ions (black spheres). Triangles show targeted *M*-site ions, their electronic configurations and resulting angular momenta. Periodic table illustrates the relative positions of targeted *M*-site cations.

Recent Progress

Our recent work has focused on the study of AMX_2 variants with M=Mn, Yb, and Ce. This involved the synthesis of powders and single crystals of select variants as well as neutron scattering-led studies of their spin/lattice structures and spin dynamics. Brief highlights of progress realized in select materials are provided below.

$NaMnO_2$: Building from our previous discovery of a longitudinally polarized, highly coherent two-magnon bound state in this $NaMnO_2$, we continued our study in search of higher-order bound states. In particular, due to the relatively strong binding energy and anomalously long lifetime of the two-magnon bound state, $NaMnO_2$ presents a unique platform for attempting to realize a native three-magnon bound state in an antiferromagnet for the first time. Our measurements indeed provided the first observation of a three-magnon bound state quasiparticle predicted to form from DMRG calculations [2]. This demonstrated that remarkable "few-body" states with relevance to droplet models pursued in the cold-atom community can form in quasi-1D "classical" S=1 chains with uniaxial anisotropy.

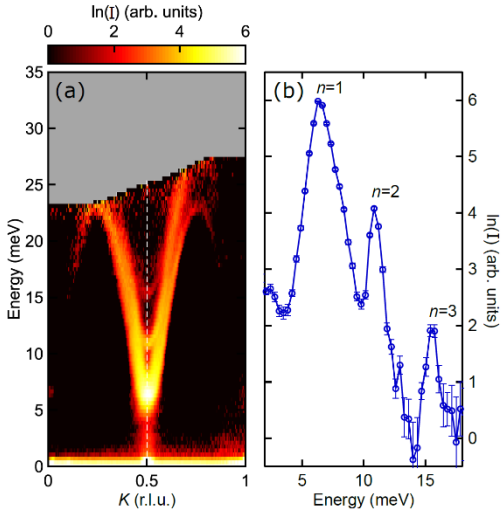

Fig. 2: (a) Inelastic neutron scattering showing the dispersion of single, two-, and three-magnon bound states. (b) A cut through the K=0.5 zone center showing peaks at n=1, 2, and 3 magnon states. From Ref. [2]

$NaYbO_2$: In exploring the delafossite rare-earth oxide with Yb^{3+} M-site ions, we sought to understand how a frustrated lattice of J_{eff}=1/2 Yb ions would order and how the spin-orbit intertwined f-electron orbitals (and their associated anisotropies) would affect the predicted patterns of order on the triangular lattice. By studying this system, we discovered that the Yb moments form a chemically clean lattice and an intrinsically quantum disordered ground state [1]. What makes this quantum disordered state unique is its clean evolution into an ordered "up-up-down" collinear ordered state under the application of a magnetic field. The presence of this sharp phase boundary and the stability of the up-up-down state relative to the predicted zero-field ordered states on a triangular lattice preclude extrinsic chemical disorder as the origin of the zero-field quantum disorder and establish $NaYbO_2$ as an ideal platform for understanding the formation of quantum spin liquid states.

We further explored the phase boundary in $NaYbO_2$ between quantum disorder and field-driven (fluctuation-stabilized) order. A first-order phase boundary was observed at the high-field phase boundary of the ordered state [3], consistent with numerical models of classical spins on the triangular lattice. The crystal electric field split excitation scheme of the Yb^{3+} was also modeled and the evolution of the low energy spin dynamics studied as an H-field drove $NaYbO_2$ from its native spin liquid state into the ordered phase and then into the quantum paramagnetic regime.

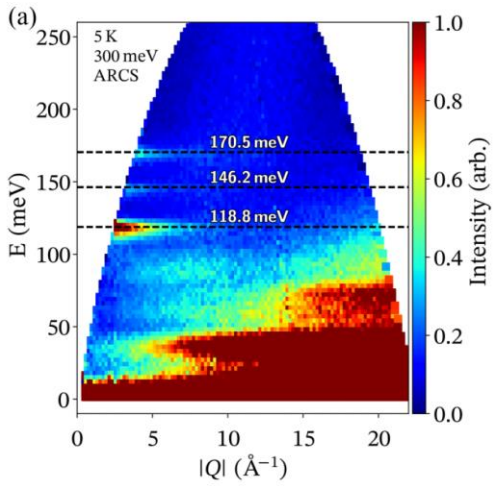

Fig. 3: Inelastic neutron scattering data collected on ARCS showing the CEF level scheme of $KCeO_2$ as well as an additional, extra mode present at 170 meV. Fig. from Ref. [10]

$KCeO_2$: Furthering our studies of $NaYbO_2$, we explored the impact of using a single electron *M*-site ion Ce^{3+}. This material forms the same triangular lattice network of J_{eff}=1/2 ions; however the introduction of the Ce^{3+} spin-orbit entangled wavefunction in place of Yb^{3+} causes the system to order. We established signatures of the formation of long-range order below 300 mK in this material [10] and also verified predictions of an anomalously large crystal electric field (CEF) splitting of the Ce^{3+} J=5/2 states. By solving the CEF Hamiltonian, we established that this system is far from predictions of a dipole-octopole doublet and instead has conventional dipole-dipole character; however we also discovered an anomalous excitation in the CEF spectrum. This additional mode is a subject of continued study, and likely originates from a dynamic Jahn-Teller-like mode in this and related materials.

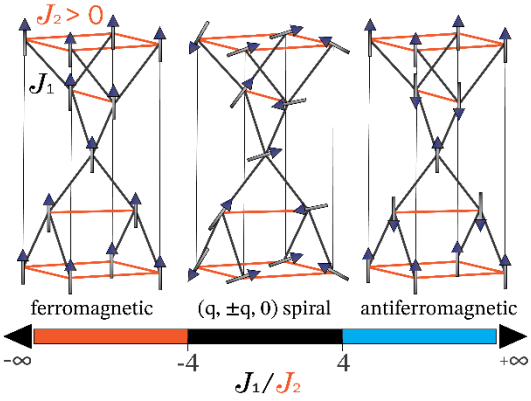

Fig. 4: The diamond-like lattice of moments in the $I4_1/amd$ structure of AMO_2. The J1-J2 phase diagram for Heisenberg spins on this lattice is illustrated below.

$LiYbO_2$/$NaCeO_2$: AMO_2 compounds with a rare-earth *M*-site can also form an unusual, distorted diamond-like lattice if the ratio of the *A*-site and the *M*-site sizes exceeds a certain threshold. The rare earth ions form a frustrated, diamond-like network that is predicted to harbor spiral spin liquid and other unusual magnetic states. We explored two such variants: $LiYbO_2$ with single-hole Yb^{3+} J_{eff}=1/2 moments [7] and $NaCeO_2$ with single-electron Ce^{3+} J_{eff}=1/2 moments [5]. While $NaCeO_2$ orders into a conventional Neel state, $LiYbO_2$ forms a highly unusual spiral magnetic state that hosts an intermediate partially disordered phase. Fluctuations in this partially disordered state drive a rich magnetic phase diagram that we mapped out via neutron scattering measurements. The resulting phase diagram and ground states can be well fit with a J_1-J_2 Heisenberg model on a stretched diamond lattice.

Future Plans

The program is focusing on the study of single crystal specimens of rare-earth based delafossites that realize quantum disordered ground states. This allows us to establish the precise details of their magnetic phase diagrams in order to inform more precise computational models of their underlying Hamiltonians. The goal is to provide deeper insights into the mechanism that stabilizes quantum spin liquid states in these triangular lattice systems.

We are also working on exploring the magnetic ground states of *M*-site ions that realize a $J_{eff}=1/2$ ground state wavefunction built from *d*-electron t_{2g} orbitals rather than *f*-electron orbitals. We are completing a series of initial studies of materials like $NaRuO_2$ in this space, and it is an exciting new direction where strong anisotropic exchange (e.g. Kitaev-like interactions) can provide an alternative pathway to realizing quantum disordered ground states. New materials synthesis, new crystal growth, and neutron scattering-based characterization are ongoing activities that will develop further in the coming year.

Publications in the past two-years:

[1] Mitchell M. Bordelon et al., Field-tunable quantum disordered ground state in the triangular lattice antiferromagnet $NaYbO_2$. Nature Physics 15, 1058 (2019).

[2] R. L. Dally et al. Three-Magnon Bound State in the Quasi-One-Dimensional Antiferromagnet a-$NaMnO_2$. Phys. Rev. Lett. 124, 197203 (2020).

[3] M. M. Bordelon et al. Spin excitations in the frustrated triangular lattice antiferromagnet $NaYbO_2$. Phys. Rev. B 101, 224427 (2020).

[4] P. M. Sarte, et al. Magnetic fluctuations and the spin–orbit interaction in Mott insulating CoO. Journal of Physics: Condensed Matter 32, 374011 (2020).

[5] M. M. Bordelon, et al. Antiferromagnetism and crystalline electric field excitations in tetragonal $NaCeO_2$. Phys. Rev. B 103, 024430 (2021).

[6] P. M. Sarte et al. Dynamical ground state in the XY pyrochlore Yb_2GaSbO_7. npj Quantum Materials 6, 42 (2021).

[7] M. M. Bordelon, et al. Frustrated Heisenberg J1-J2 model within the stretched diamond lattice of $LiYbO_2$. Phys. Rev. B 103, 014420 (2021). [Editors suggestion]

[8] S. J. Gomez, et al., "Absence of moment fragmentation in the mixed B-site pyrochlore Nd_2GaSbO_7", Phys. Rev. B 103, 214419 (2021). [Editors suggestion]

[9] S. Wilson, and M. M. Bordelon, Quantum disorder and unconventional magnetism in $ALnX_2$ (A = alkali; Ln = lanthanide; X = chalcogen) materials. Neutron News 32, 19-21 (2021).

[10] M. M. Bordelon et al. Magnetic properties and signatures of moment ordering in the triangular lattice antiferromagnet $KCeO_2$. Phys. Rev. B 104, 094421 (2021).

Bound Layer Exchange in Polymer Nanocomposite Melts

Karen I. Winey, Materials Science and Engineering, University of Pennsylvania
Robert A. Riggleman, Chemical and Biomolecular Engineering, University of Pennsylvania

Program Scope

Polymer nanocomposites (PNCs) are an important class of materials in a variety of applications ranging from structural materials to membranes for separations or to membranes in battery applications. Preventing aggregation of nanoparticles (NPs) in PNCs frequently requires systems with strong attractions between the polymer and the particles, leading to polymer adsorption on the particle surfaces. This bound layer of polymers exhibits conformations and dynamics distinct from bulk polymers and are critical to the properties and performance of polymer nanocomposites. In fact, bound polymer layers can prevent NPs aggregation and promote dispersion and are responsible for the superior mechanical and transport properties of PNCs. The goal of our collaborative proposed work is to develop and demonstrate a small-angle neutron scattering (SANS) technique to probe chain-scale exchange of bound polymers in bulk PNCs and polymer-nanoparticle suspensions. We will combine this technique with course-grained molecular dynamics (MD) simulations to study the effect of annealing temperature and time on bound layer exchange dynamics and demonstrate control of exchange dynamics by altering the NP-polymer and NP-polymer-solvent interactions. Achieving these goals will broadly impact the fabrication and use of polymer nanocomposites. When polymer nanocomposites are fabricated from polymer-nanoparticle suspension, the characteristics of the bound polymer in solution controls the nature of the bound layer and subsequently the exchange dynamics in the polymer nanocomposites.

Recent progress: Simulations of Nanoparticles and Polymers in Solutions

Details of MD Simulation: To model the bound layer formation process in polymer-nanoparticle suspensions, we constructed a series of systems that has one amorphous nanoparticle (or flat surface) fixed in the center of the simulation box. We then fill the simulation box with polymer chains and solvent, where polymer density is 0.1 and solvent density is 0.6. The polymer chains are modeled using a canonical bead-spring coarse grain model [1]. Each polymer chain consists of N LJ interaction sites connected fully flexible harmonic bonds. We employed the same interaction parameter setting presented in our group's recent work [2], and the nanoparticle-polymer interaction, ε_{wp}, is varied. We define $\Delta\varepsilon_{wf} = \varepsilon_{wp} - \varepsilon_{ws}$ to measure the relative affinity of the polymer and solvent with the nanoparticles, and for $\Delta\varepsilon_{wf} > 0$, polymers preferentially wet the nanoparticle surface. The primary aim of this work is to study the effect of nanoparticle curvature, polymer chain length, and polymer-nanoparticle interactions on the bound layer formation process. Thus, we employed three different curvatures ($r_{NP} = 6\,\sigma, 10\,\sigma$, and flat surface) and three different chain lengths ($N = 10, 40$, and 100). For each chain length, we have four different polymer-

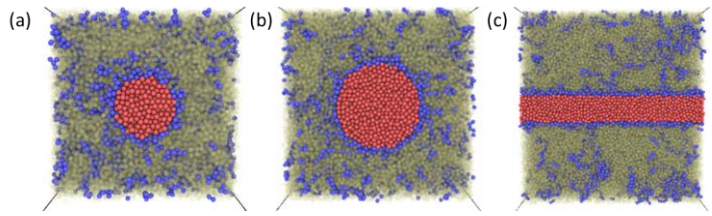

Figure 1. Visualizations of our MD simulation systems with (a) nanoparticle $r_{NP} = 6\,\sigma$, (b) nanoparticle $r_{NP} = 10\,\sigma$, and (c) flat surface in a polymer solution. Nanoparticle (red), polymer chains (blue), and solvent (yellow) are all modeled as LJ interaction sites. The visualizations presented are a cut through the center of the simulation box for clarity.

nanoparticle interaction strengths, which is controlled through $\Delta\varepsilon_{wf}$ ($\Delta\varepsilon_{wf} = 0.1, 0.3, 0.5$, and 0.7). Typical snapshots of our systems are shown in **Figure 1**.

Bound polymer density: After equilibrating our systems at constant density where both the polymer and the solvent do not wet the particle surface, we then turn on the particle/solvent and particle/polymer interactions to induce adsorption. We begin our analysis by measuring the polymer density in the bound layer. Representative results are presented in **Figure 2**. In **Figure 2a**, we plot the polymer density as a function of distance to nanoparticle center for systems with $N = 40$ at four different $\Delta\varepsilon_{wf}$. As expected, a more favorable polymer-nanoparticle interaction can increase the polymer density in the bound layer. We then plot the peak height of the density profile as a function of time in Fig. 2b and find that $\Delta\varepsilon_{wf}$ has little effect on the bound layer formation time. If we compare the formation process of different chain lengths, we can find that for a given interaction strength, it takes longer for long polymer chains to form the bound layer, though the final polymer densities are quite similar (Fig. 2c). We also measured the total number of adsorbed polymer monomers, which is defined as monomers within 2.5 σ to the nanoparticle surface, observing qualitatively similar results as the density peak height shown in **Figure 2**.

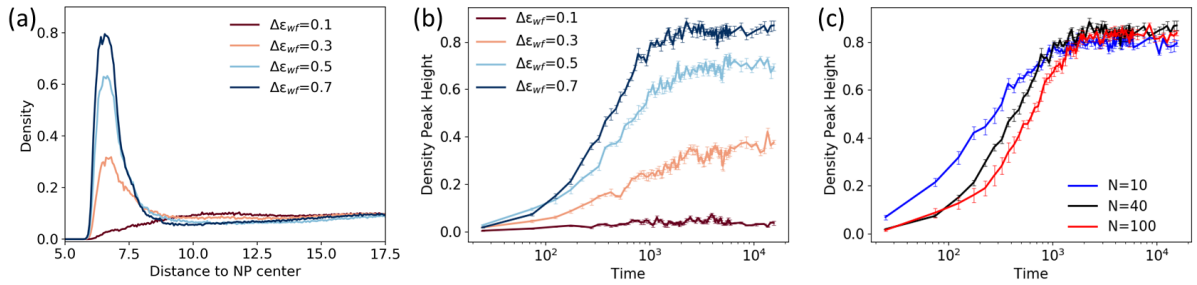

Figure 2. Representative results of bound polymer density (using systems with $r_{NP} = 6\,\sigma$): (a) polymer density as a function of distance to nanoparticle center for chain length $N = 40$; (b) density peak height of different polymer-nanoparticle interactions for chain length $N = 40$; (c) density peak height of different polymer chains lengths for $\Delta\varepsilon_{wf} = 0.7$.

Average coordination number: We also studied the chain scale dynamics of bound layer formation, by measuring the average coordination number of bound polymer chains. Here, we define the coordination number as the number of monomers in contact with the nanoparticle (within 2.5 σ to the nanoparticle surface). Interestingly, we observe a non-monotonic trend in the average coordination number when the interaction is large enough ($\Delta\varepsilon_{wf} \geq 0.5$), and the effect is more pronounced for short polymer chains. These results indicate that there are two stages during the bound layer formation. Initially, a large portion of bound polymer chains adsorb to the nanoparticle since there is enough available space on the nanoparticle surface. Later when more polymers get adsorbed and cover the nanoparticle surface, new adsorbed chains with only a few monomers adsorb, and the chains that initially had a large fraction of their monomers adsorbed become less tightly bound by desorbing some of their monomers.

Implicit solvent simulation: Our simulations become much more expensive when chain length exceeds $N = 100$. Therefore, we employed systematic coarse-graining methods to model systems with an implicit solvent by varying the effective polymer-polymer and polymer-nanoparticle interactions (ε_{pn}). Like the explicit solvent systems, we also vary ε_{pn} to study the effect of polymer-nanoparticle interactions. Implicit

solvent enables us to simulate much longer chains with a reasonable computational cost and we can reproduce the analyses from the explicit solvent simulation.

Longer chains enable us to study the development of entanglements during the bound layer formation. To do this analysis, we define bound layer as regions within 2.5 σ to the nanoparticle surface, and a polymer chain is defined as a bound polymer if at least one of its monomers is in the bound layer. A typical snapshot of the bound polymer chains can be found in **Figure 3a**. We then calculate the entanglements between these bound polymer chains using the Z1 algorithm [4]. In **Figure 3b**, we plot the average entanglements per bound polymer chain as a function of time for three different ε_{pn}. We observed a significant increase of average number entanglements for all three interactions, suggesting that chains unentangled with each other are more likely to be adsorbed by the nanoparticle first during the bound layer formation. This result is important for experimental systems where polymers are commonly adsorbed to the nanoparticles in solution prior to drying, and it shows that even within the bound polymer layer, the bulk entanglement density is reached when the interactions are sufficiently strong.

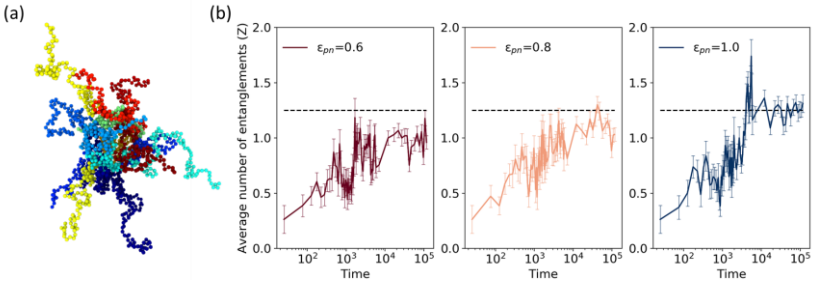

Figure 3. (a) Bound polymers (N=400) used to calculate the entanglements. Different colors represent different polymer chains, and the nanoparticle is removed for better visualization. (b) Average entanglements per bound polymer chain during the bound layer formation. The black dash line represents the average entanglements in the bulk region. Results are averaged over five configurations.

Recent progress: Small Angle Neutron Scattering of Nanoparticles in Polymer Melts

We have devised a method by which nanoparticles are preferentially coated with non-deuterated polymers within a matrix of mixed deuterated and non-deuterated polymer. Ex situ small angle neutron scattering can be used to detect the extent of exchange between the bound polymer at the NP surface and the free polymer in the matrix as a function of annealing time. Limited and unpredictable access to neutron sources since March 2020 has significantly hampered the progress of these experiments. For example, contrast matching experiments are necessary for selecting the ratio of deuterate to non-deuterated polymer in the matrix to maximize the contrast between the initial state and the fully exchanged state. After our beam time at NIST was canceled, we secure time at the Quokka Beamline in Australia to perform these experiments in early August 2021. Closures at that facility due to the pandemic postpone our (remote) beamtime until November/December 2021 (tentatively). Thus, we were forced to estimate the contrast matching conditions for the nanocomposites measured at ORNL in October 2021. Initial analysis of those data is intriguing in that the polymer exchange is faster than expected, but the nanoparticle SLD is necessary to quantify the rate of polymer exchange. Moreover, in person SANS experiments are necessary to track the polymer exchange in solutions.

Future work

For our future work, we plan to extend our simulation to systems with implicit solvent and block copolymers consisting of two different types of monomers, A and B. We use the same system setting as discussed above,

except we fix the interaction between the nanoparticle and monomer A (ε_{nA}) and monomer B (ε_{nB}) to be 1.0 and 0.6, respectively. Both the ratio of monomer A, f_A, and monomer sequence are varied to study their effects on the bound layer formation. We have used diblock copolymers with 5 different f_A $(0.1\sim0.5)$ and five different monomer sequences with a fixed $f_A = 0.2$. Preliminary results suggest that a higher f_A leads to a higher polymer density in the bound layer, and polymer sequence can affect both the adsorption rate and polymer density in the final bound layer.

Reference

[1] K. Kremer and G. S. Grest, *Dynamics of Entangled Linear Polymer Melts: A Molecular-Dynamics Simulation*, J. Chem. Phys. **92**, 5057 (1990).

[2] E. Y. Lin, A. L. Frischknecht, K. I. Winey, and R. A. Riggleman, *Effect of Surface Properties and Polymer Chain Length on Polymer Adsorption in Solution*, J. Chem. Phys. **155**, (2021).

[3] S. Plimpton, *Fast Parallel Algorithms for Short-Range Molecular Dynamics*, J. Comput. Phys. **117**, 1 (1995).

[4] N. C. Karayiannis and M. Kröger, *Combined Molecular Algorithms for the Generation, Equilibration and Topological Analysis of Entangled Polymers: Methodology and Performance*, Int. J. Mol. Sci. **10**, 5054 (2009).

Publications (November 2019 – present)

1. E. J. Bailey*, K. I. Winey*, *Progress in Polymer Science*, **105**, 101242, **2020**. "Dynamics of polymer segments, polymer chains, and nanoparticles in polymer nanocomposite melts: A review."
2. E. J. Bailey, M. Tyagi, K. I. Winey*, *Journal of Polymer Science*, 1-8, **2020**. "Correlation between backbone and pyridine dynamics in poly(2-vinyl pyridine)/silica polymer nanocomposites."
3. E. J. Bailey, R. A. Riggleman, K. I. Winey*, *Macromolecules*, **53**, 8171-8180, **2020**. "Polymer conformations and diffusion through a monolayer of confining nanoparticles."
4. Tianren Zhang, K. I. Winey*, R. A. Riggleman*, *Journal of Chemical Physics*, **153**, 184095, **2020**. "Conformation and dynamics of ring polymers under symmetric thin film confinement."
5. Emily Y. Lin, A. L. Frischknecht, K. I. Winey, R. A. Riggleman, *Journal of Chemical Physics* **155** 034701, **2021**. "Effect of surface properties and polymer chain length on polymer adsorption in solution",
6. Entao Yang, J. Pressly, B. Natarajan, K. I. Winey, R. A. Riggleman, submitted. "Dynamical decomposition of creep in model polymer nanocomposites."

Unraveling Emergent Quantum States in Magnetic Topological Insulators using High Pressure Neutron Scattering

Weiwei Xie, Chemistry and Chemical Biology, Rutgers University – New Brunswick

Program Scope

This program supports a combined neutron scattering and materials discovery of novel magnetic materials that display the coexistence of magnetism plus other physical phenomena such as a non-trivial electronic band topology under high pressure. The goal of this project is to close a long-standing knowledge gap in quantum materials research by developing a high-pressure neutron scattering (HP-NS) toolbox to systematically determine the magnetic structures and electronic interactions present at high pressure. To attain this goal, we have designed and tested multiple high-pressure experimental approaches through the study of trigonal 122-type AMn_2M_2 (alkaline earth manganese pnictide) and 112-type phases using neutron scattering with a focus on: 1) quantifying the effect of pressure on magnetism and crystal structure; 2) validating the role of magnetism in stabilizing its coexistence with topological electronic states; 3) modeling magnetic interactions and spin dynamics by computational theory. and 4) centrally, using high pressure to manipulate the interplay of multiple quantum phenomena both experimentally and theoretically. Moreover, stabilizing these metastable phases detected under high pressure is another goal of proposed research. The proposed high-pressure neutron scattering studies will open new avenues for unraveling the effects of pressure on the interacting electrons that dominate the magnetic properties in various quantum materials. The establishment of structure-magnetism-electronic property relationships in forefront quantum materials is critical for understanding and predicting the properties of matter and energy at the atomic and molecular level, thus inspiring new strategies for materials discovery and characterization, and, over the long term, benefits the development of future energy technologies.

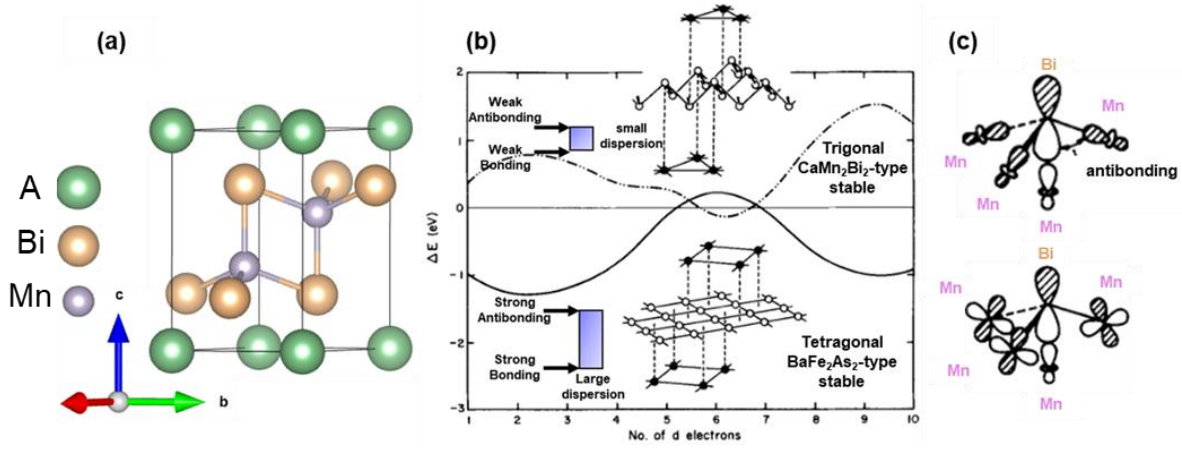

Recent Progress

1. Incommensurate Magnetic Ordering in 122-phases: To obtain the accurate magnetic structure and understand how magnetism behaves under high-pressure, high-pressure neutron scattering measurements were conducted on 122-phases. Single crystal $CaMn_2Bi_2$ was crushed into a powder and measured using a Paris-Edinburgh cell up to 7 GPa and down to 100 K at the Spallation Neutron and Pressure Diffractometer (SNAP) at Oak Ridge National Laboratory (ORNL). The two magnetic structures refined based on the high-pressure neutron diffraction data show antiferromagnetic ordering dominating in $CaMn_2Bi_2$ at ambient and high pressures. Moreover, incommensurate magnetic ordering was observed, which is consistent with what we observed in the high-pressure electric resistivity measurements.

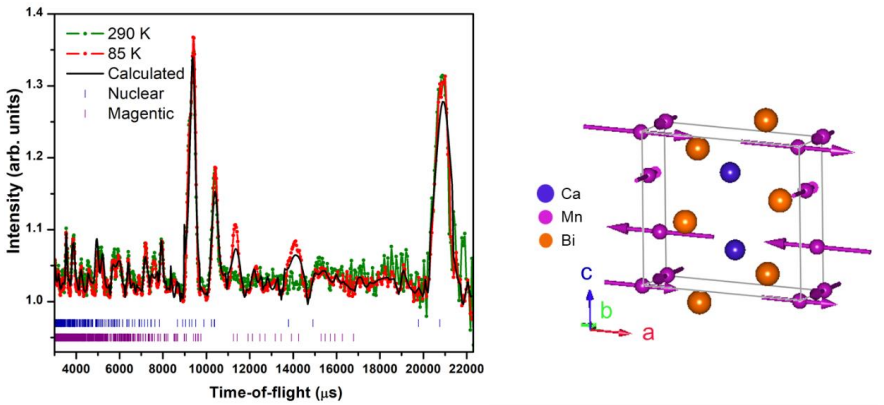

Fig. 1 (Left) Neutron powder scattering on $CaMn_2Bi_2$ at 5 GPa at both low (85 K) and high (290 K) temperatures. (Right) Refined magnetic structure of $CaMn_2Bi_2$.

2. Structural Phase Transition Observed in other 122-type Compounds: To experimentally explore structural transitions in other 122-type compounds, we studied the materials using high pressure X-ray diffraction. High-pressure X-ray diffraction can provide information about crystal orientation and geometrical relationships in addition to the *d*-spacing commonly obtained by powder X-ray diffraction. According to the high-pressure PXRD results, we successfully obtained the structural information and critical pressures for structural transitions. For example, $CaMn_2Sb_2$ transforms into monoclinic structure at around 5.0 GPa shown in Fig. 2; the structural transition occurs around 2.1 GPa in $EuMg_2Bi_2$. However, no structural transition was detected in $EuSn_2P_2$ and $EuSn_2As_2$ up to 25 GPa.

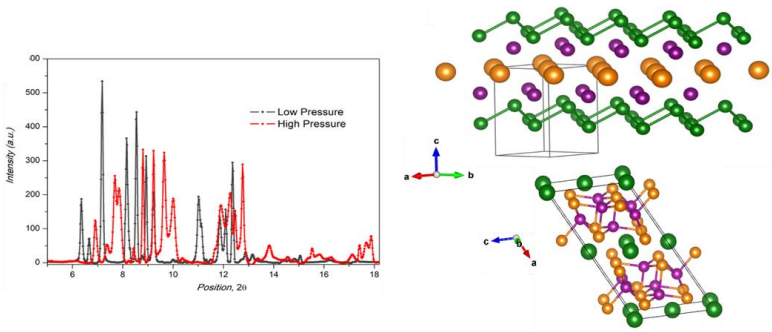

Fig. 2 (Left) X-ray powder scattering on $CaMn_2Sb_2$ at 0.2 and 7.3 GPa. (Right) Refined crystal structures of $CaMn_2Sb_2$ at 0.2 and 7.3 GPa.

3. $Eu_2Mg_3Bi_4$ in Buckled Honeycomb Structure obtained under High Pressure: Honeycomb lattice and its derived variants are paramount in modelling and designing quantum magnets. A novel magnetic material, $Eu_2Mg_3Bi_4$, which stabilizes in a previously unknown buckled honeycomb lattice, was discovered by high-pressure and high-temperature methods. On the synthesis exploration of pure single crystals, structural determination of buckled honeycomb lattice of Europium moments, and experimental observation of competing magnetic phases in metallic $Eu_2Mg_3Bi_4$. The crystal structure of $Eu_2Mg_3Bi_4$ is orthorhombically centrosymmetric with the space group *Cmca*. Eu atoms form an Eu buckled honeycomb lattice in perfect layers. The dominate antiferromagnetic interaction associated with magnetic coupling within the buckled honeycomb layers is confirmed based on the high Curie-Weiss fitting with T_{CW} ~ -24 K. However, the long-range magnetism orders in the temperature range far below T_{CW}. Two transitions observed at T_{N1} = 4.0 K and T_{N2} = 6.0 K originate from the competing magnetic interactions in $Eu_2Mg_3Bi_4$. Two sharp anomalies occur in the magnetic susceptibility, zero-field resistivity, as well as heat capacity all suggest successive evolution of magnetic order parameters, which is frequently observed in magnets with competing interactions. This magnetism and structure entanglement provides an ideal platform to study the interplay between honeycomb lattice rare-earths and quantum magnets, thus realizing the design and control of magnetism from the structural aspects.

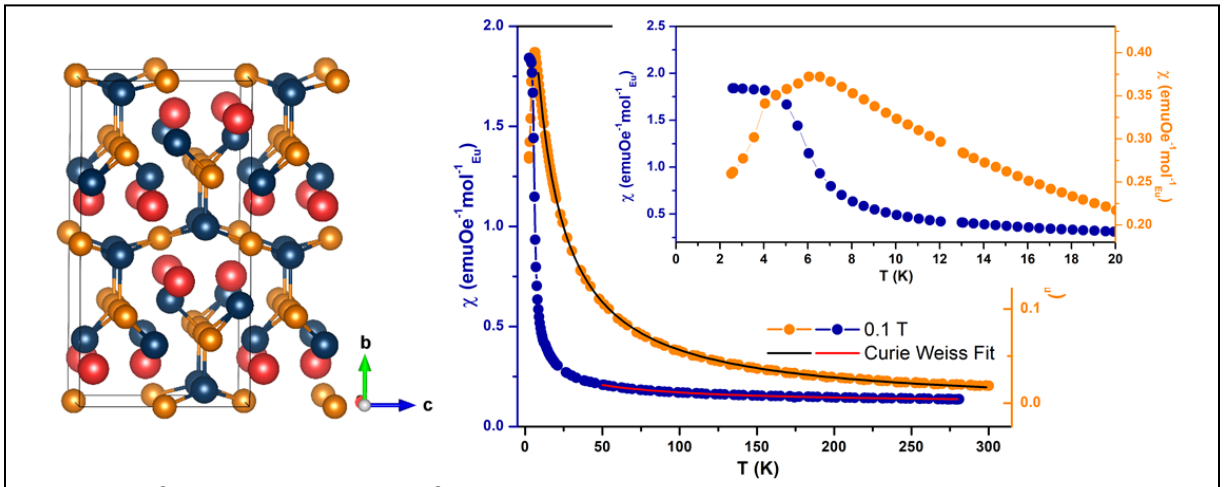

Fig. 3 (Left) Crystal structure of $Eu_2Mg_3Bi_4$ synthesized at 6GPa, 800 ºC. (Right) Magnetic properties of $Eu_2Mg_3Bi_4$ with competing magnetic orders in buckled honeycomb lattice.

4. Tuning Chemical Pressure to Discover a New Type Pyrochlore Lattice: The single crystal of $LiYbSe_2$ was grown from LiCl flux. Distinct from the quantum spin-liquid candidate $NaYbSe_2$ hosting a perfect triangular lattice of Yb^{3+}, $LiYbSe_2$ crystallizes in the cubic pyrochlore structure with space group F*d*-3*m* (No. 227). The Yb^{3+} ions in $LiYbSe_2$ are arranged on a network of corner-sharing tetrahedral, which is particularly susceptible to geometrical frustration. According to our temperature-dependent magnetic susceptibility measurements, the dominant antiferromagnetic interaction in $LiYbSe_2$ is θ_{CW} ~ -1.5 K and no long-range magnetic order is observed in thermomagnetic measurements above 70 mK, likely due to geometrical frustration. Specific heat measurements also show magnetic correlations shifting with applied magnetic field with a degree

of missing entropy that may be related to the slight mixture of Yb^{3+} on the Li site. $LiYbSe_2$ is an important material to understand exotic magnetic effects with anisotropic Yb^{3+} moments on the pyrochlore lattice.

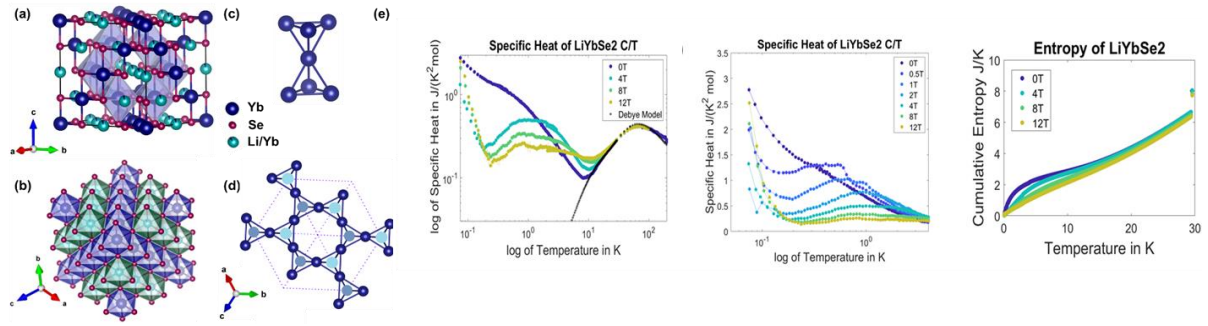

Fig. 4 (Left) Crystal structure of $LiYbSe_2$. (Right) Heat Capacity measurements on $LiYbSe_2$ with down to 70mK without observing any long-range or short-range magnetic interactions.

5. Non-centrosymmetric Sr2IrO4 obtained under High Pressure: Sr_2IrO_4 with strong spin-orbit coupling (SOC) and Hubbard repulsion (U) hosts Mott insulating states. The similar crystal structure, magnetic and electronic properties, particularly the *d*-wave gap observed in Sr_2IrO_4 enhanced the analogies to cuprate high-T_c superconductor, La_2CuO_4. The incomplete analogy was due to the lacking in broken inversion symmetry in Sr_2IrO_4. Here, we describe the synthesis of non-centrosymmetric Sr_2IrO_4 under high pressure and high temperature. The crystal structure and non-centro-symmetry were determined by both single crystal X-ray diffraction and high-resolution transmission electron microscopy (HR-TEM). The magnetic characterization confirms the Ir^{4+} with S = ½ at low temperatures in Sr_2IrO_4 with magnetic ordering temperature around 80(2) K, which is much larger than the moment observed in ambient pressure Sr_2IrO_4. Moreover, the resistivity measurement shows the non-centrosymmetric high pressure Sr_2IrO_4 phase exists a bandgap around 68(1) meV without an applied magnetic field and keeps decreasing as increasing the magnetic fields. Non-centrosymmetric Sr_2IrO_4 appears to be a unique material to understand high-T_c superconductivity.

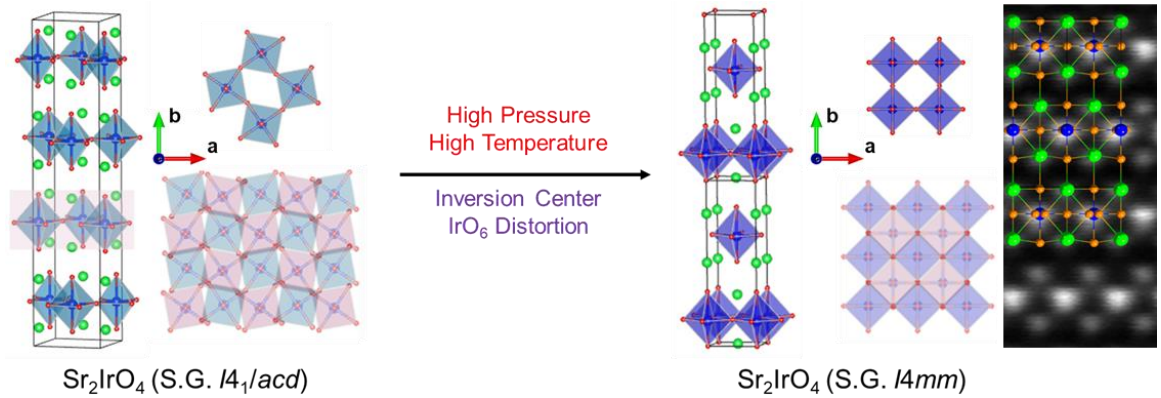

Fig. 5 Crystal structure changes of Sr_2IrO_4 under high pressure.

Future Plans

We will experimentally study how pressure impacts structural stability and structural preference. We will perform chemical bonding analysis and theoretical assessment of the new phases obtained under high pressure and compare the results to the phase obtained at ambient pressure to investigate how the chemical bonding dominates structural stability. We will study the comparison between chemical pressure and physical pressure in other 122-type and 112-type phases. Sr and Bi are larger than Ca and Sb, which indicates that solid solutions will have different degrees of chemical pressure present. We will investigate structural stabilities of these materials at various chemical and physical pressures and map the tuning parameters between chemical and physical pressures to obtain targeted phases. Moreover, we will perform high pressure neutron scattering at the ORNL high pressure neutron scattering facility to gain knowledge of the atomic interactions and spin dynamics emerging in these materials at various temperatures and pressures. We will focus on the construction of magnetic and potential superconducting domes and possible non-Fermi liquid behavior. We will study the surface band structures of high-pressure phases both experimentally and theoretically with a focus on the search for emerging interacting magnetic and topological surface states in new high-pressure phases. To understand the interplay of band topology and magnetism deeply in the metastable phases synthesized by high pressure high temperature methods. Finally, to understand the atomic and electronic interactions deeply, theoretical calculations using WIEN2k DFT-calculations will be performed. Moreover, the electron-electron coupling strength will be calculated and compared to illustrate the effect of pressure on the magnetic interactions. We will perform theoretical calculations, especially band structure and Fermi surface calculations, to study how the electrons in 3*d* orbitals interact with electrons in 4*f* orbitals under high pressure.

References

1. Hirschberger, M.; Nakajima, T.; Gao, S.; Peng, L.; Kikkawa, A.; Kurumaji, T.; Kriener, M.; Yamasaki, Y.; Sagayama, H.; Nakao, H.; Ohishi, K.; Kakurai, K.; Taguchi, Y.; Yu, X.; Arima, T.; Tokura, Y. Skyrmion Phase and Competing Magnetic Orders on a Breathing Kagomé Lattice. *Nat Commun* **2019**, *10* (1), 5831. https://doi.org/10.1038/s41467-019-13675-4.

2. Bramwell, S. T.; Gingras, M. J. Spin Ice State in Frustrated Magnetic Pyrochlore Materials. *Science* **2001**, *294* (5546), 1495–1501. https://doi.org/10.1126/science.1064761.

3. Castelnovo, C.; Moessner, R.; Sondhi, S. L. Magnetic Monopoles in Spin Ice. *Nature* **2008**, *451* (7174), 42–45. https://doi.org/10.1038/nature06433.

4. Zhou, Y.; Kanoda, K.; Ng, T.-K. Quantum Spin Liquid States. *Rev. Mod. Phys.* **2017**, *89* (2), 025003. https://doi.org/10.1103/RevModPhys.89.025003.

5. G. Cao; J. Bolivar; S. McCall; J. E. Crow; R. P. Guertin. Weak Ferromagnetism, Metal-to-Nonmetal Transition, and Negative Differential Resistivity in Single-Crystal Sr_2IrO_4, *Phys. Rev. B* **1998**, *57*, R11039. https://doi.org/10.1103/PhysRevB.57.R11039.

Publications (since Sept. 2021)

1. M. Marshall; W. Xie. Crystal Defect Doping on Antiferromagnetic Topological Insulator Candidate $EuMg_2Bi_2$ *J. Phys. Chem. C*, under review.

2. R. S. Dissanayaka Mudiyanselage; O.Vilella; M. Mourigal, G. Kotliar; W. Xie. $LiYbSe_2$: Magnetism in a New Type Pyrochlore Lattice *Phys. Rev. X*, under review.

3. M. Marshall; W. Xie. Comprehensive Inorganic Chemistry III, Chapter 76: 00320. Topological and quantum materials, *accepted*.

4. M. Marshall; Z. Wang; R. S. Dissanayaka Mudiyanselage; M. Greenblatt; Y. Zhu; D. Walker; W. Xie. Non-centrosymmetric Sr_2IrO_4 obtained under High Pressure *Phys. Rev. Lett.* under review.

5. M. Marshall1; F. Wang; T. Klimczuk; M. Greenblatt; G. Kotliar, D. Walker; W. Xie. $Eu_2Mg_3Bi_4$: Competing Magnetic Orders on a Buckled Honeycomb Lattice *Chem. Mater.* under review.

Project title: Exotic Magnetic Orders and Dynamics in Chiral Magnets

PI: Junjie Yang, Department of Physics, New Jersey Institute of Technology, NJ 07102

Program Scope

Since broken symmetry often accompany new physics, new physical phenomena are bound to happen in chiral magnets where all of space inversion, mirror, and timer reversal symmetries are broken.[1-7] For instance, chiral magnets exhibit various exotic magnetic structures including the chiral soliton lattice and Skyrmions which originate from the interplay between the asymmetric Dzyaloshinskii Moriya (*DM*) interactions, the symmetric exchange interactions, and the magnetic anisotropy.[1-9] Moreover, when chemical substitution is introduced in chiral magnets, the magnetic interactions and anisotropy could be significantly changed, and their complicated correlations with the modified structural features may result in exotic magnetic orders and dynamics. The chemical substitution effect in chiral magnets has been little studied. It is quite essential to make clear the role of the chemical substitution in chiral magnets, as chemical substitution provides an effective way to tune the physical properties for desired material functions. We choose 2 chiral material systems to study the effect of chemical substitution: $Ni_{3-x}M_xTeO_6$ (M = Mn, Co) with $0 \leq x \leq 3$ and the $Cr_{1/3-x}M_xTaS_2$ (M = Fe, Co and Ni) with $0 \leq x \leq 1/3$. In the chiral lattice environment of the parent compounds, the chemical substitutions could modify the chiral lattice structure, adopt various magnetic anisotropies and tune the competing magnetic interactions, giving rise to novel physics in chemical-substituted chiral magnets. The ultimate goal of this project is to reveal the complex correlations between chemical substitution, chiral crystal structure, magnetic interactions and exotic magnetic orders in chemical-substituted chiral magnets, through a series of neutron diffraction and inelastic neutron scattering experiments.

Recent Progress

We progressed in the several directions. First, we confirmed that the Mn substitution in $Ni_{3-x}M_xTeO_6$ can induce chiral helical magnetic structures. The parent compound Ni_3TeO_6 has a chiral and polar crystal structure which can be described by the $R3$ space group.[10,11] Ni_3TeO_6 has been found to exhibit a collinear antiferromagnetic order with spins aligned along the c axis below 50 K.[10,11] In pure Ni_3TeO_6, the magnetic Ni^{2+} ions occupy 3 distinct sites denoted as TM^I, TM^{II} and

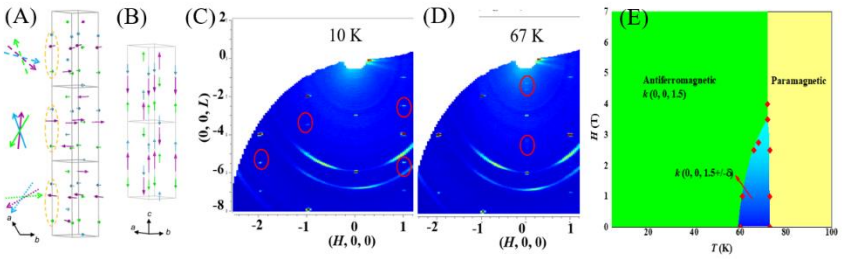

Figure 1. (A) The helical magnetic structure of NMTO at 68 K. (B) The collinear magnetic structure of NMOT at 4 K. Neutron single crystal diffraction patterns for NMTO at 10 K (C) and 67 K (D), red circles mark the magnetic peaks. (E) *H-T* phase diagram of NMTO.

TM^{III}, respectively. Our neutron powder diffraction results (obtained at BT1 at NCNR) suggest that Mn doped $Ni_{3-x}Mn_xTeO_6$ (NMTO) is isostructural to Ni_3TeO_6. Mn^{2+} ions substitute Ni^{2+} ions and mainly occupy the TM^{II} site.[12] The ground state of NMTO (x = 0.9) maintains the commensurate collinear (CC) antiferromagnetic order (T < 63 K) as depicted in Fig. 1(B) and (C), but a new phase with XY-type magnetic anisotropy is discovered at an intermediate temperature range (63 K < T < 75 K). Our neutron single crystal diffraction experiments (performed at WAND^2 at HFIR) reveal that the intermediate phase is an incommensurate (IC) helical magnetic state propagating along the c axis with a vector k = (0, 0, 1.5 ± δ) with δ = 0.146, as shown in Fig. 1(D). Moreover, the temperature and magnetic field dependence of neutron diffraction experiments (performed at BT1 at NCNR and $WAND_2$ at HFIR) indicates that the balance between these two magnetic states can be readily manipulated with magnetic fields. Our neutron diffraction results are summarized in the H-T phase diagram in Fig. 1(E) which is consistent with the phase diagram obtained from magnetic susceptibility and dielectric constant.[12]

We also obtained high-quality single crystals of $NiCo_2TeO_6$ (NCTO). Neutron powder diffraction results (obtained at BT1 at NCNR) confirm that the space group of NCTO is chiral and polar $R3$. However, different from the two magnetic transitions in NMTO, neutron diffraction experiments on NCTO indicate that the spins order into an IC helical magnetic ground state below T_N ~ 54 K, as shown Fig. 2(C). The helical magnetic structure consists of spins aligned in the ab-plane which stack helically along the c-axis with an incommensurate propagation vector k ~ (0, 0, 1.5 ± δ) with δ = 0.255. Figure 2(A) exhibits the temperature dependence of the two IC magnetic peaks at (0, 0, 1.5 ± δ) (data obtained at HB-1A at HFIR). Furthermore, as shown in Fig. 2(B), the magnetic field dependence of the two IC peaks reveals that the IC helical magnetic structure can be readily switched to commensurate structure with a vector k ~ (0, 0, 1.5) by external magnetic fields.

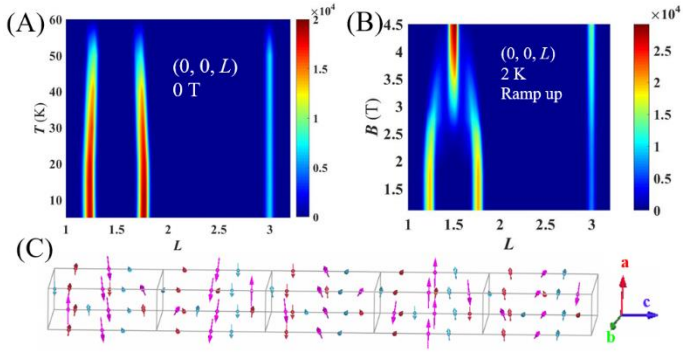

Figure 2. (A) Neutron single crystal diffraction intensities near (0, 0, 1.5) vs temperature for NCTO. (B) Neutron diffraction intensities near (0, 0, 1.5) vs magnetic field at 2 K. (C) Helical magnetic structure of NCTO.

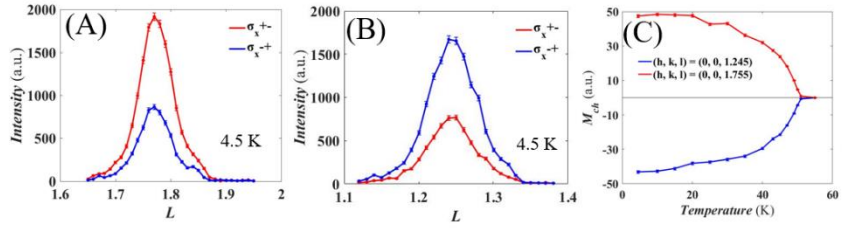

Figure 3. (A) and (B) Polarized neutron single crystal diffraction intensities near (0, 0, 1.5) for NCTO at 4.5 K. (C) Estimated magnetic chirality vs temperature.

We also obtained NCTO single crystals with mono-chiral domain and performed polarized neutron diffraction experiments on the single crystals at HB-1 at HFIR. Using polarized neutron diffraction method and longitudinal polarization

analysis, we clearly clarified the magnetic chirality of the helical magnetic structure of NCTO. As shown in Fig. 3(A), at 4.5 K, the intensity of the σ_{x+-} channel is much higher than that of the σ_{x-+} channel near the IC peak of (0, 0, 1.755), whereas near the IC peak of (0, 0, 1.245) the intensity of the σ_{x+-} channel is much lower than that of the σ_{x-+} channel. The magnetic chirality is estimated by $(\sigma_{x+-} - \sigma_{x-+})/2P_i$ where P_i is the polarization of the incident neutron beam. The temperature dependence of magnetic chirality is shown in Fig. 3(C).

For the metallic $Cr_{1/3-x}M_xTaS_2$, we confirmed the chiral helimagnetic transition in the pure $Cr_{1/3}TaS_2$ and observed nontrivial magneto-transport properties associated with the topological chiral magnetic solitons.[13] The propagation vector of the helical magnetic structure in $Cr_{1/3}TaS_2$ is (0, 0, 0.042). Our neutron diffraction experiments on the Co and Ni doped $Cr_{1/3}TaS_2$ single crystals suggest that the Co and Ni substitutions can significantly tune the chiral helimagnetic structure. As shown in Fig. 4(A), the Co doped $Cr_{1/3}TaS_2$ exhibits a pair of IC peaks which can be indexed by a *k* vector of (0, 0, 0.038). The Ni doped $Cr_{1/3}TaS_2$ also exhibits a pair of IC peaks and the peaks can be indexed with a *k* vector of (0, 0, 0.09). The Co and Ni ions are expected to modify the microscopic magnetic interactions in $Cr_{1/3}TaS_2$ and induce the significant change in the *k* vector.

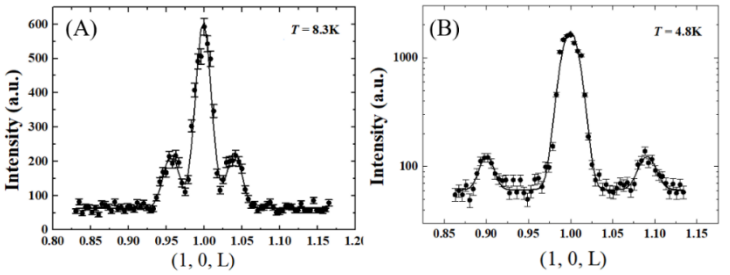

Figure 4. (A) Neutron single crystal diffraction intensities near (1, 0, 1) for Co doped $Cr_{1/3}TaS_2$. (B) Neutron single crystal diffraction intensities near (1, 0, 1) for Ni doped $Cr_{1/3}TaS_2$.

Future Plans

We will continue our efforts to understand the complex correlations between chemical substitution, chiral crystal structure, structural disorders, magnetic interactions and exotic magnetic orders in chemical-substituted chiral magnets.

The magnetic chirality of the IC helical phase in NMTO has not been clarified. We will perform polarized neutron diffraction on NMTO single crystal to reveal the magnetic chirality for the intermediate IC helical phase. It is not clear why the NMTO exhibits two magnetic transitions whereas the NCTO only shows one IC helical magnetic transition. We have obtained high-quality inelastic neutron scattering data on NCTO and we will perform inelastic neutron scattering experiments on NMTO. We will compare the data, analyze the magnetic interactions in these two samples, and figure out the microscopic reasons for the exotic magnetic transitions. Furthermore, the chiral helical magnetic phases of these doped chiral magnets are also expected to show novel non-reciprocal spin wave features.[1-7] We will perform polarized inelastic neuron scattering experiments on NMTO and NCTO single crystals to verify the possible non-reciprocal spin wave features. The magnetic field dependence of the magnetic structures of NMTO and NCTO also indicate that the topological chiral magnetic solitons could exist in these insulating oxides. To search for the possible topological chiral soliton state in NMTO and NCTO, we will perform small

angle neutron diffraction experiments on these single crystals. The Co and Ni substitutions can significantly tune the chiral helical magnetic structure of the pure $Cr_{1/3}TaS_2$ single crystals. However, the underneath reasons are still not clear. To reveal the microscopic reasons, we will also perform inelastic neutron scattering experiments on the doped $Cr_{1/3}TaS_2$ single crystals.

References

[1]. Cheong, S. W., SOS: symmetry-operational similarity. npj Quantum Mater. 2019, 4 (1).

[4]. Cheong, S. W.; Talbayev, D.; Kiryukhin, V.; Saxena, A., Broken symmetries, non-reciprocity, and multiferroicity. npj Quantum Mater. 2018, 3 (1).

[5]. Togawa, Y.; Koyama, T.; Takayanagi, K.; Mori, S.; Kousaka, Y.; Akimitsu, J.; Nishihara, S.; Inoue, K.; Ovchinnikov, A. S.; Kishine, J., Chiral magnetic soliton lattice on a chiral helimagnet. Phys. Rev. Lett. 2012, 108 (10).

[6]. Mühlbauer, S.; Binz, B.; Jonietz, F.; Pfleiderer, C.; Rosch, A.; Neubauer, A.; Georgii, R.; Böni, P., Skyrmion lattice in a chiral magnet. Science 2009, 323 (5916), 915-919.

[7]. Yu, X. Z.; Onose, Y.; Kanazawa, N.; Park, J. H.; Han, J. H.; Matsui, Y.; Nagaosa, N.; Tokura, Y., Real-space observation of a two-dimensional skyrmion crystal. Nature 2010, 465 (7300), 901-904.

[8]. Dzyaloshinsky, I., A thermodynamic theory of "weak" ferromagnetism of antiferromagnetics. Journal of Physics and Chemistry of Solids 1958, 4 (4), 241-255.

[9]. Moriya, T., Anisotropic superexchange interaction and weak ferromagnetism. Physical Review 1960, 120 (1), 91-98.

[10]. Kim, J. W.; Artyukhin, S.; Mun, E. D.; Jaime, M.; Harrison, N.; Hansen, A.; Yang, J. J.; Oh, Y. S.; Vanderbilt, D.; Zapf, V. S.; Cheong, S. W., Successive magnetic-field-induced transitions and colossal magnetoelectric effect in Ni3TeO6. Phys. Rev. Lett. 2015, 115 (13).

[11]. Oh, Y. S.; Artyukhin, S.; Yang, J. J.; Zapf, V.; Kim, J. W.; Vanderbilt, D.; Cheong, S. W., Non-hysteretic colossal magnetoelectricity in a collinear antiferromagnet. Nat. Commun. 2014, 5.

[12] Kim, J.W.; Yang, J.J.; Won, C.J.; Kim, K; Kim, B; Obeysekera, D; Lee, D.W.; Cheong, S.-W*, "Helical versus collinear antiferromagnetic order tuned by magnetic anisotropy in polar and chiral $(Ni,Mn)_3TeO_6$", Phys. Rev. Materials. 2021, 5, 094405.

[13]. Obeysekera, D; Gamage, K; Gao, Y. P.; Cheong, S.-W; Yang, J. J.*, "The Magneto-Transport Properties of $Cr_{1/3}TaS_2$ with Chiral Magnetic Solitons", Adv. Electron. Mater. 2021, 7, 2100424.

Publications

[1]. Obeysekera, D; Gamage, K; Gao, Y. P.; Cheong, S.-W; Yang, J. J.*, "The Magneto-Transport Properties of $Cr_{1/3}TaS_2$ with Chiral Magnetic Solitons", Adv. Electron. Mater. 2021, 7, 2100424.

[2] Kim, J.W.; Yang, J.J.; Won, C.J.; Kim, K; Kim, B; Obeysekera, D; Lee, D.W.; Cheong, S.-W*, "Helical versus collinear antiferromagnetic order tuned by magnetic anisotropy in polar and chiral $(Ni,Mn)_3TeO_6$", Phys. Rev. Materials. 2021, 5, 094405.

Universality of Collective Dynamics in Liquids at and away from Equilibrium

Professor Yang Zhang (YZ), Department of Nuclear, Plasma, and Radiological Engineering, Department of Electrical and Computer Engineering, Program of Computational Science and Engineering, Center for Biophysics and Quantitative Biology, Beckman Institute for Advanced Science and Technology, University of Illinois at Urbana-Champaign

Program Scope

Liquids, including complex fluids, as one of the three phases of matter, are ubiquitous on earth and are prototypical disordered condensed matter. However, the physics of liquids is far from being completely understood and therefore excluded by Landau and Lifshitz from their *Course of Theoretical Physics*. As the mediate phase between non-structured gases and ordered solids, liquids possess intriguing complexities that are absent on either extreme counter phase, especially when they are driven away from equilibrium. Despite decades of studies, the physics of liquids still keeps surprising us and challenges our understanding of condensed matter, emergent phenomena, and complex systems. Furthermore, numerous soft and biological materials of amazing far-from-equilibrium complexity seem to share many intriguing features of liquids. Therefore, quantitative descriptions of the structure and dynamics of liquids and liquid-like matter will likely impact a wide range of disciplines.

Among the many interesting properties of liquids, the nature of *collective dynamics* in liquids remains elusive because of both the presence of strong interactions and the absence of translational invariance. Our research activities center around the understanding of *collective density fluctuations (*or *collective modes)*, which include both phonon-like excitations and collective relaxations, in the Q-dependent generalized hydrodynamic regime in liquids and liquid-like matter both at and away from equilibrium. We perform systematic studies of the fast collective dynamics of a variety of liquids characterized by different fragilities and interactions (ionic, metallic, hydrogen-bonded, van der Waals) using synergistically integrated coherent neutron scattering experiments, a ViscoElastic Hydrodynamics theory we have been developing, and Molecular Dynamics (MD) simulations and our analysis package LiquidLib. The transformative knowledge of the collective dynamics in liquids is important to understand and ultimately control the transport of mass, energy, and charge in liquids, both at and away from thermal equilibrium, which may will likely impact a wide range of disciplines.

Recent Progress

1. Using a combination of the new wide-angle neutron spin-echo **(WASP)** at ILL and the time-of-flight direct geometry chopper spectrometer AMATERAS at J-PARC, we measured the collective relaxation dynamics of a **model fragile glass-forming liquid CKN** covering a wide Q range and time range. The results show, for the first time experimentally, temperature

independent dynamic heterogeneity with more Arrhenius-like behavior at the local length scales. (*Nature Communications*, in revision) [1]

It has been known that the relaxation of glass formers is spatially heterogeneous, however, the dynamics at different microscopic length scales are not fully explored. Employing wide-angle neutron spin-echo spectroscopy, we measured the Q-dependent coherent intermediate scattering function of a prototypical ionic glass former Ca0.4K0.6(NO3)1.4, in the equilibrium and supercooled liquid states beyond the hydrodynamic regime. de Gennes narrowing is observed in all characteristic variables of the slow α-relaxation: the relaxation time, amplitude, and stretching exponent. In contrast to that around the structure factor peak, the stretching exponent exhibits no temperature dependence and concomitantly the relaxation time shows smaller deviations from Arrhenius temperature dependence at the structure factor valley, indicating temperature independent dynamic heterogeneity with more Arrhenius-like behavior at the local length scales. These observations reveal the length scale dependent relaxation dynamics and shed new light to the microscopic relaxation mechanism of supercooled liquids.

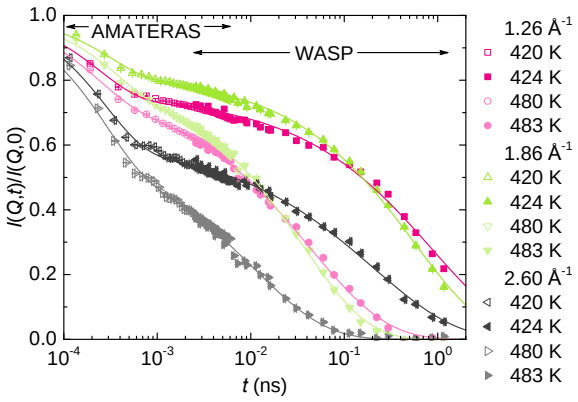

Figure 1. ISF of CKN covering a broad time window at three representative *Q*'s: (1.26, 1.86 and 2.60) Å^{-1}. The data presented by open symbols from 0.1 ps to 6 ps are Fourier deconvoluted time-of-flight spectra measured on AMATERAS, those presented by solid symbols from 2.6 ps to 1.2 ns are the WASP data. The AMATERAS data are measured at T = 420 K and 480 K, and the WASP data are at T = 424 K and 483 K. These two sets of data match in the overlapping time range without any artificial adjustment.

2. Using neutron spin-echo (NSE), we measured the microscopic structural relaxation of a **prototypical network ionic liquid (also molten salt) $ZnCl_2$** at two characteristic length scales associated to the nearest-neighboring ionic correlation and the ordering of the tetrahedral motifs. We discovered an unusual increase of the stretching exponent upon cooling, which is rationalized by the formation of network structure on cooling from simulations. (*JPCL*) [8]

$ZnCl_2$ constitutes a rare prototype of ionic network glass former and has received recent technological interests because of its relevance in applications as heat transfer fluid for molten salt reactors and concentrated solar power plants, and in applications of molten salt synthesis of electrodes and luminescent materials. Liquid $ZnCl_2$ has been found to exhibit unique properties in contrast to other molten salts, for example, it melts at a fairly low temperature and has nearly 3 orders of magnitude larger viscosity than other salts, together with low ionic mobility and

conductivity at the melting point. These striking properties imply distinct dynamical behaviors of liquid $ZnCl_2$. Our results show that the relaxation at the primary peak is faster than the pre-peak and the activation energy is ≈33% higher. Stretched exponential relaxation is observed even at temperatures well above the melting point T_m. Surprisingly, the stretching exponent shows a rapid increase upon cooling, especially at the primary peak, where it changes from stretched exponential to simple exponential on approaching T_m. These results suggest that the appearance of heterogeneous glassy dynamics typical of the supercooled state even in the equilibrium liquid state of $ZnCl_2$ as well as the different temperature dependence of the relaxation time at the two investigated lengthscales, suggesting that the formation of network structure on cooling induces qualitative modifications of the microscopic dynamics.

3. Using QENS, we revealed the distinctively different collective dynamics behavior in the **kosmotrope** as opposed to the **chaotrope aqueous solutions of salts**, increasing with the salt concentration in the former and decreasing in the latter. (*JPCL*) [10]

Aqueous solutions of salts are the focus of ever-present scientific interest because of their relevance in chemistry, biology, and physics. In fact, the presence of ions plays a critical role in many processes, for example in biology, in the selectivity of ion channels; highly concentrated aqueous salt solutions are also the object of increasing interest in the search of novel electrolytes for better performing batteries. Despite the intense scrutiny, one of the most intriguing phenomena, the reduction of the viscosity observed for aqueous solutions of certain salts, is still not fully understood. In fact, no significant difference has been observed in the way the molecular structure of water is affected by the presence of kosmotrope (which increase the viscosity) or chaotrope (which decrease the viscosity) salts in solution. Spectroscopic and computer simulations studies suggest that the effect of salts on the H-bond lifetime is mostly limited to the first solvation shell. Using QENS, we studied the structural relaxation in heavy water solutions of kosmotrope (structure maker) and chaotrope (structure breaker) salts, namely sodium chloride, potassium chloride, and cesium chloride. Our data indicate that kosmotrope salts dynamically stabilize (increase the lifetime of) the hydrogen bond network, whereas chaotrope salts have the opposite effect. In both cases the trends are proportional to the concentration dependence of the relative viscosity of the solutions. These results indicate that kosmotropes and chaotropes influence the solution's viscosity by impacting in opposite ways the hydrogen bond network of water, strengthening it in one case and softening it in the other, and thus provide a new perspective to the understanding of the effect of salts on water, underlying the relevance of the hydrogen bond network dynamics beyond a physical picture, strictly structural, and the insight from spectroscopic studies of the H-bond lifetime.

4. Using neutron vibrational spectroscopy, QENS, and MD simulation, we continue studying the unique molecular dynamics of **ionic liquids**. [2, 11, 14]

The competition between Coulomb and van der Waals interactions brings forth unique dynamic features and broad applications to ionic liquids. We use neutron vibrational spectroscopy, QENS,

Raman, far-infrared, calorimetric, X-ray diffraction, and MD simulation to study the relaxational dynamics of the liquid, supercooled liquid, crystalline, glassy, and glacial states of two model ionic liquids: tributylmethylammonium (a good glass-former) and butyltrimethylammonium (a good crystal-former) cations and the bis(trifluoromethanesulfonyl)imide anion, over a wide temperature range.

5. Using QENS and MD simulation, we continue to measure the atomic dynamics of **metallic glass melts and surfaces** and elucidate the role of phonon softening induced by anisotropic fluctuations in the enhanced surface mobility. We also used low-energy ion irradiation and created highly coherent atomic-scale ripple patterns on bulk metallic glass surfaces, which is attributed to the enhanced surface mobility of glasses. [3, 7, 9]

6. Using neutron PDF, QENS, neutron vibrational spectroscopy, and MD simulations, we continue to study the structure and dynamics of **concentrated electrolyte solutions** used in flow batteries. [12, 13]

7. We continue to develop and maintain ***LiquidLib*®** for computing various weighted statistical quantities of liquids and liquid-like systems from classical and *ab initio* molecular dynamics trajectories, which can be directly compared with both elastic and inelastic neutron scattering experiments. Up to date, *LiquidLib*® has >250 users worldwide. [http://z-laboratory.github.io/LiquidLib/]

Future Plans

We will perform systematic studies of the *collective dynamics (including both phonon-like excitations and collective relaxations)* of four classes of liquids characterized by different fragilities (fragile vs. strong) and interactions (ionic, metallic, hydrogen-bonded, van der Waals) using synergistically integrated coherent neutron scattering experiments (Inelastic Neutron Scattering (INS), Quasi-Elastic Neutron Scattering (QENS), and Neutron Spin Echo (NSE)), a ViscoElastic Hydrodynamics theory we have been developing, and Molecular Dynamics (MD) simulations and our analysis package *LiquidLib*®. We will use a combination of several INS/QENS/NSE spectrometers to cover a wide dynamic/time range and wave vector transfer range. We will measure the "dispersion relation" (Q dependence) of the representative model liquid systems over a wide temperature range. All the systems are picked to minimize incoherent scattering by choosing elements with small incoherent cross sections or with isotope substitution. Furthermore, we will use polarization analysis to further suppress the incoherent scattering when available. We will use MD simulations to achieve robust interpretations of the experimental results and gain deeper insights from computed physical quantities otherwise inaccessible by experiments. Inspired by the experimental data and simulations, we will develop a ViscoElastic Hydrodynamic (VEH) theory by generalizing the classical hydrodynamic theory to provide a unified framework to analyze the inelastic scattering data and understand the collective dynamics in liquids. We will maintain and further develop the functions and usability of *LiquidLib*.

Publications (2019.01 – 2021.11)

[1] P. Luo, Y. Zhai, P. Falus, V. Garcia-Sakai, M. Hartl, M. Kofu, K. Nakajima, A. Faraone, **Y Z*,** "Q-dependent collective relaxation dynamics of glass-forming liquid $Ca_{0.4}K_{0.6}(NO_3)_{1.4}$ investigated by wide-angle neutron spin-echo", *Nature Commun.* (in revision)

[2] I. F. T. de Souza, V. H. Paschoal, K. Bernardino, T. A. Lima, L. L. Daemen, **Y Z,** M. C. C. Ribeiro, "Vibrational spectroscopy and molecular dynamics simulation of choline oxyanions salts", *J. Mol. Liq.* 340(15), 117100 (2021)

[3] P. Luo, A. Jaiswal, Y. Zhai, Z. Cai, N. P. Walter, L. Zhou, M. Liu, R. Mills, A. Podlesynak, G. Ehlers, A. Faraone, H. Bai, W. Wang, **Y Z*,** "Atomic dynamics of metallic glass melts $La_{50}Ni_{15}Al_{35}$ and $Ce_{69}Cu_{20}Al_{10}Nb_1$ studied by quasi-elastic neutron scattering", *Phys. Rev. B* 103, 224104 (2021)

[4] R. Nome, Pilar Cossio, **Y Z,** "Editorial: Integrating Timescales from Molecules Up", *Front. Chem.* 9, 680533 (2021)

[5] Y. Zhai, N. S. Martys, W. L. George, J. Nayem, **Y Z,** Y. Liu, "Intermediate scattering functions of a rigid body monoclonal antibody protein in solution studied by dissipative particle dynamic simulations", *Struc. Dyn.* 8, 024102 (2021)

[6] Y. Zhai, P. Luo, M. Nagao, K. Nakajima, T. Kukuchi, Y. Kawakita, P. Kienzle, **Y Z*,** A. Faraone, "Relevance of hydrogen bonded associates to the transport properties and nanoscale dynamics of liquid and supercooled 2-propanol", *Phys. Chem. Chem. Phys.* 23, 7220 (2021)

[7] Y. Zhai, P. Luo, **Y Z*,** "Role of phonon softening induced by anisotropic fluctuations in the enhanced mobility at free glassy surfaces", *Phys. Rev. B* 103, 085424 (2021)

[8] P. Luo, Y. Zhai, J. Leao, M. Kofu, K. Nakajima, A. Faraone, **Y Z*,** "Neutron spin echo studies of the structural relaxation of liquid $ZnCl_2$ at the structure factor primary peak and pre-peak", *J. Phys. Chem. Lett.* 12(1), 392 (2021)

[9] P. Luo, C. Jaramillo, A. M. Wallum, Z. Liu, R. Zhao, L. Shen, Y. Zhai, J. C. Spear, D. Curreli, J. W. Lyding, M. Gruebele, W. Wang, J. P. Allain, **Y Z*,** "Coherent atomic-scale ripples on metallic glasses patterned by low-energy ion irradiation for large-area surface structuring", *ACS Appl. Nano Mater.* 3(12), 12025 (2020)

[10] P. Luo, Y. Zhai, E. Senses, E. Mamontov, G. Xu, **Y Z*,** A. Faraone, "Influence of kosmotrope and chaotrope salts on water structural relaxation", *J. Phys. Chem. Lett.* 11(21), 8970 (2020)

[11] T. A. Lima, V. H. Paschoal, R. S. Freitas, L. F. O. Faria, Z. Li, M. Tyagi, **Y Z,** M. C. C. Ribeiro, "An inelastic neutron scattering, Raman, far-infrared, and molecular dynamics study of the intermolecular dynamics of two ionic liquids", *Phys. Chem. Chem. Phys.* 22, 9074 (2020)

[12] Z. Li, L. A. Robertson, I. A. Shkrob, K. C. Smith, L. Cheng, L. Zhang, J. S. Moore, and **Y Z***, "Realistic ion dynamics through charge renormalization in nonaqueous electrolytes", *J. Phys. Chem. B* 124(15), 3214 (2020)

[13] L. A. Robertson, Z. Li, Y. Cao, I. A. Shkrob, M. Tyagi, K. C. Smith, L. Zhang, J. S. Moore, and **Y Z***, "Observation of microheterogeneity in highly concentrated nonaqueous electrolyte solutions", *J. Am. Chem. Soc.* 141(20), 8041 (2019)

- ***"Stability and microheterogeneity in concentrated nonaqueous electrolyte solutions", 2020 Accomplishments and Opportunities, NIST Center for Neutron Research (2020)***

[14] T. A. Lima, Z. Li, M. Tyagi, M. C.C. Ribeiro**, Y Z***, "Spatial and thermal signatures of α and β relaxations in glassy and glacial aliphatic ionic liquids", *J. Chem. Phys.* 150, 144506 (2019)

Laboratory Abstracts

Local Site Magnetic Susceptibility for Quantum Materials

Huibo Cao

Neutron Scattering Division, Oak Ridge National Laboratory

Program Scope

Understanding the interactions leading to magnetic quantum phenomena in a wide range of quantum materials is extremely important for development of new quantum materials and future technologies. Quantifying these interactions in materials is currently being limited by a range of challenges including the lack of sizable high-quality crystals, limited high pressure capabilities, and the ability to disentangle the intrinsic quantum phenomena versus effects from the material's defects and site-disorder. This project is to develop Local Site Magnetic Susceptibility methods based on polarized neutron diffraction (PND) to understand the balance of subtle magnetic interactions in quantum materials that lead to the key quantum states.

Recent Progress

In the past two years since the instrument HB-3A was upgraded to DEMAND from the traditional Four-Circle Diffractometer, we have achieved polarized thermal neutrons with an in-situ-pumped ^{3}He polarizer at the polarization rate of 90%, all developed in-house. We studied several frustrated magnets with PND techniques. Both single crystal and powder samples were selected for commissioning experiments. With an optimized permanent magnet set, both powder (sample volume is limited) and single crystal samples can be studied. We are installing an automatic polarizer changing system to make this capability more convenient to general users. It will be available for commissioning in the January HFIR fuel cycle in 2022. An asymmetric cryomagnet has been commissioned with the ^{3}He polarizer, however the stray field and the sample environment background need to be further reduced for high-quality data. The small vertical opening of the current cryomagnet also limits the application of PND. We are working on a long-term instrument optimization package, which will overcome these issues. We are now focusing our ECA team's efforts on the theoretical modeling to extract exchange interactions from the PND data measured at low temperature, where the local magnetic susceptibility tensor is not symmetric anymore, i.e., beyond the application range of the current local magnetic susceptibility analysis software. We have defined the boundary of the current local magnetic susceptibility method and are working on the Hamiltonian optimization to fit the magnetization data measured by PND. The following lists the detailed scientific progress of the projects in the past two years.

Magnetization density map on a magnetic topological insulator $MnBi_4Te_7$. Inserting magnetic layer MnTe into topological insulator Bi_2Te_3 is one of chemical routes to design magnetic topological insulators. Structural defects occurring in these hybrid compounds seem to control the

magnetic and topological properties. We used neutrons to characterize such magnetic and structural defects. This was the first publication on the magnetization density map reconstructed from the DEMAND data. The map indicates the density of magnetic impurity is low in $MnBi_4Te$. It helps to understand the origin of ferromagnetism in the Mn-Bi-Te family and guide the design

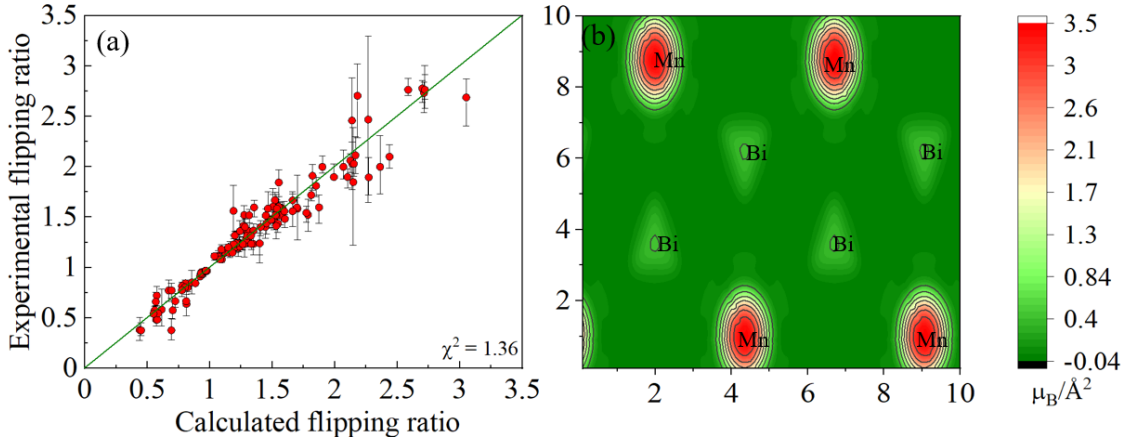

Figure 1 (a) The observed and calculated flipping ratios of 136 reflections. (b) Projection of the magnetization density within the unit cell on the ***ab***-plane for $MnBi_4Te_7$ under the magnetic field of 0.83 T.
L. Ding et al., *Journal of Physics D: Applied* **54** 174003 (2021)

of magnetic topological insulators (L. Ding et al., *Journal of Physics D: Applied Physics* **54** 174003 (2021)).

Field-tunable toroidal moment in a chiral-lattice magnet. Being one of few macroscopic manifestations of quantum coherence, magnetic order is at the crux of condensed matter physics. For millennia, only ferro(antiferro-,ferri-)magnetism had been known to humankind. Only in the last decades has it been realized that magnetism may extend to topologically nontrivial orders and in several ways on the next level compared to the ferromagnetic (dipolar) order. The notion of a toroidal order, which corresponds to a toroidal solenoid, was proposed around 1980, as an abstract theoretical concept, but came into the limelight lately after being found, or at least suggested in some real materials. Experimental studies of complex magnetic textures (such as skyrmions) and deep theoretical interest in topological orders led to recognition of several other unconventional magnetic orders, such as vector and scalar chiralities. All these orders break various combinations of global symmetries, such as time or space inversion. A toroidal order, a pseudovector in response to both spatial and temporal inversion, cannot be manipulated with either magnetic or electric field separately (without coupling to additional ferroic order), but only with a combination of both. This is rather impractical, and, besides, coupling of the toroidal moment with the electric field is extremely weak. This work presents the field-switching multi-stair toroidal transitions manifested by switching the arrangement of magnetic vortices and their chirality, which is unique and has not been observed before. Direct coupling to the magnetism (multi-stair magnetization) makes the chiral magnet $BaCoSiO_4$ an unusual multiferroic and serves as the driving force for the magnetic-

field switchable toroidal orders. The work was published in *Nature Communications* (L. Ding et al., *Nature Communications*, **12** 5339, 2021). The published work was selected as a highlight to DOE.

Realizing magnetic vortex liquid state in a rare-earth bilayer square lattice. By introducing Ising

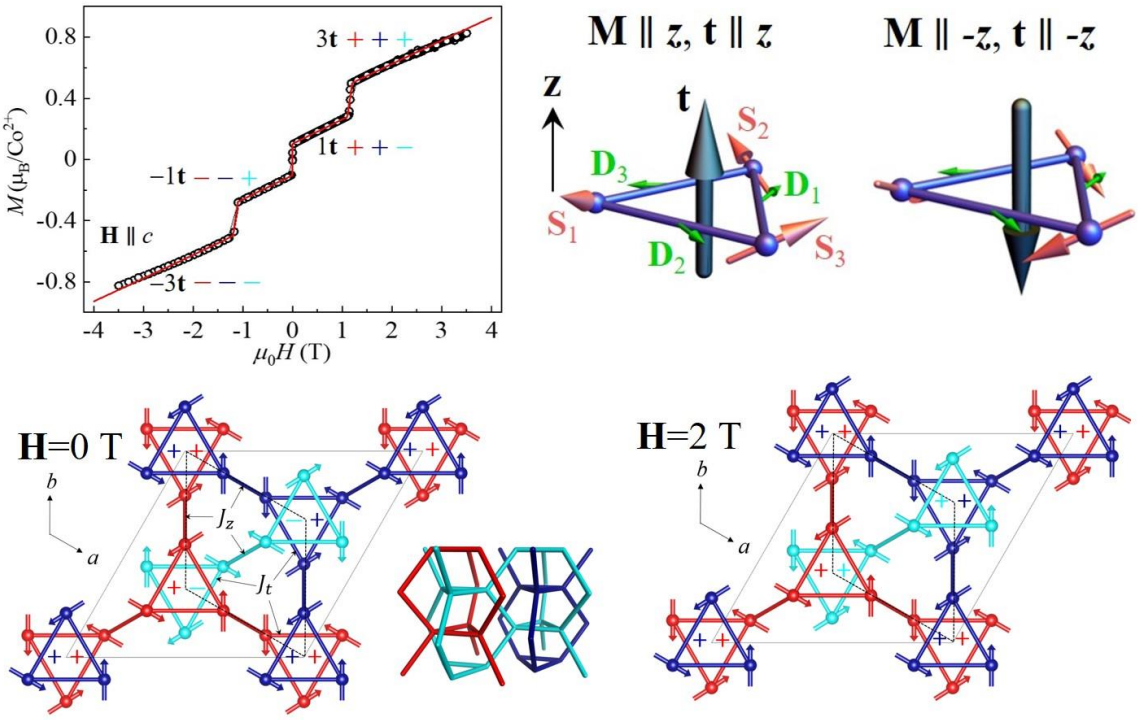

Figure 2 Field-induced ferri- to ferrotoroidal transition in $BaCoSiO_4$. Top-left: Magnetization data (circles) with the field H//c and the theoretical calculations (line) from the full spin Hamiltonian. Top-right: Minimal energy configurations for three spins S_i (i = 1,2,3) on a triangle with an antiferromagnetic Heisenberg interaction and an in-plane DM interaction D_i (i = 1, 2, 3). It illustrates how a field can switch a toroidal moment t. Bottom two plots show the magnetic structures at zero field and H = 2 T and corresponding toroidal moment t (+, - represent the toroidal moment up and down). L. Ding et al., *Nature Communications*, **12** 5339 (2021).

spins on a 2-dimensional bi-layer square lattice $Tb_2SrAl_2O_7$, we realized a frustrated magnet where no long-range magnetic order was found upon cooling to 100 mK. Using the local magnetic susceptibility method through PND, we revealed spins' Ising anisotropy and determined the tilt angle of Ising direction. With this information, we were able to simulate the neutron diffuse scattering patterns observed at 100 mK under selected magnetic fields through machine learning assisted spin Hamiltonian optimization. Our studies revealed a short-range ordered stripe magnetic phase wrapped by domain-wall phases. By applying magnetic field perpendicular to the square-lattice plane, the stripe magnetic phase melts and the condensed domain wall phases form a short-range ordered vortex lattice, so-called magnetic vortex liquid state, at a critical field of 2 T (see Fig. 3). Further application of the magnetic field to 4 T, makes all of the spins aligned nearly along the field direction, i.e., a polarized paramagnetic phase. Here the evolution of stripe phase and domain wall phase can be precisely controlled by a magnetic field and tracked by neutron

scattering. A Z4 vortex was found to be originated from two crossed domain walls. While the density of the domain wall and vortices increase with the field and reach their maximum before entering the fully polarized paramagnetic phase. The discovery highlights the role of local magnetic susceptibility method based on PND. The work is draft form and will be submitted this year.

Besides the studies on single crystal samples, we also explored the 2D polarized neutron diffraction on powder sample, which will help to understand local magnetic anisotropy of a frustrated magnet when single crystals are not available.

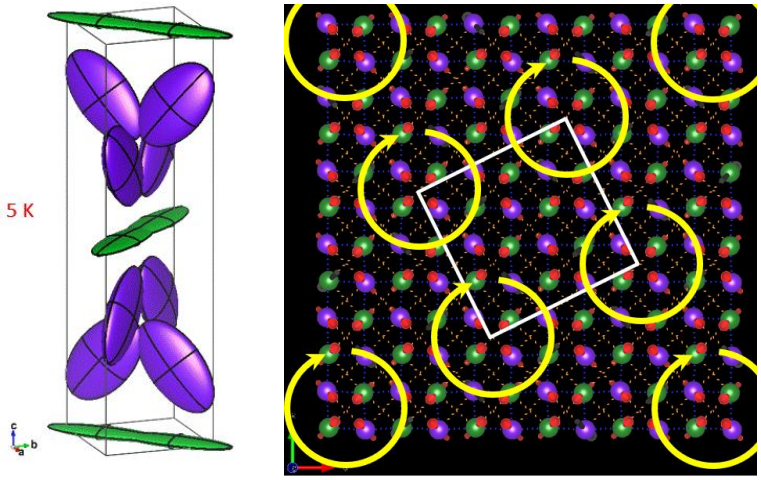

Figure 3 (left) Local site magnetic susceptibility tensors versus temperature (animated image). The purple ellipsoids indicate the susceptibility tensors on the major Tb-sites, and the green ones represent the Tb impurity on the Sr-sites. The tensors can help to identify the roles of Tb-spins on the major and impurity sites for forming the magnetic vortices shown on the right.

Future Plans

We have achieved the capability of studying the rare-earth magnets and the 3d-transition metal topological 2D magnets by the local magnetic susceptibility method through PND. The plan in the following years includes two directions.

1) By optimizing and stabilizing the performance of the neutron polarizer and the transportation of polarized neutrons, we will start to study 4*d* and 5*d* transition metal systems and other weak magnetic systems in the last two years of the ECA project. In this year, we are going to install the automated lifting device to conveniently switch between PND and unpolarized neutron diffraction, which can stabilize the performance of the ^{3}He polarizer and make PND available to all users.
2) Extracting magnetic interaction parameters from low temperature magnetization density measurement through PND. The current local magnetic susceptibility method assumes that the magnetic susceptibility tensor is symmetric, which is not true at low temperature. We reached the point where we need new methodology and new codes to model the PND data at low temperature to determine magnetic interaction beyond measuring single ion magnetic anisotropy. By achieving this, the local magnetic susceptibility method can become one of the important ways to understand spin Hamiltonians and magnetic ground state of a quantum material.

Publications

FY 2020-2021 Journal Publications:

- **Lei Ding**, Xianghan Xu, Harald O Jeschke, **Xiaojian Bai**, **Erxi Feng**, Admasu Solomon Alemayehu, Jaewook Kim, Feiting Huang, Qiang Zhang, Xiaxin Ding, Neil Harrison, Vivien Zapf, Daniel Khomskii, Igor I Mazin, Sang-Wook Cheong, **Huibo Cao**, "Field-tunable toroidal moment in a chiral-lattice magnet*", Nature Communications* **12**, 5339 (2021) https://doi.org/10.1038/s41467-021-25657-6

- **Lei Ding**, Chaowei Hu, **Erxi Feng**, Chenyang Jiang, Iurii A. Kibalin, Arsen Gukasov, MiaoFang Chi, Ni Ni, and **Huibo Cao**, "Neutron diffraction study of magnetism in van der Waals layered $MnBi_{2n}Te_{3n+1}$*", Journal of Physics D: Applied Physics* **54** 174003 (2021) **invited** https://www.doi.org/10.1088/1361-6463/abe0dd

- **Lei Ding**, Chaowei Hu, Feng Ye, **Erxi Feng**, Ni Ni, **Huibo Cao**, Crystal and magnetic structures of magnetic topological insulators $MnBi_{2n}Te_{3n+1}$. *Physical Review B* **101,** 020412(R) (2020). https://journals.aps.org/prb/abstract/10.1103/PhysRevB.101.020412

- **Lei Ding**, M. Lee, T. Hong, Z. L. Dun, R. Sinclair, S. X. Chi, H. K. Agrawal, E. S. Choi, B. C. Chakoumakos, H. D. Zhou, **Huibo Cao**, "Noncollinear magnetic structure and magnetoelectric coupling in buckled honeycomb $Co_4Nb_2O_9$: A single-crystal neutron diffraction study", *Physical Review B* **102,** 174443 (2020).

  http://doi.org/10.1103/PhysRevB.102.174443

- **Lei Ding**, Minseong Lee, Eun Sang Choi, Jing Zhang, Yan Wu, Ryan Sinclair, Bryan C. Chakoumakos, Yisheng Chai, Haidong Zhou, and **Huibo Cao**, "Large spin-driven dielectric response and magnetoelectric coupling in the buckled honeycomb $Fe_4Nb_2O_9$" *Physical Review Materials* **4**, 084403 (2020)

  https://doi.org/10.1103/PhysRevMaterials.4.084403

- **Xiaojian Bai**, Randy S Fishman, Gabriele Sala, Daniel M Pajerowski, V Ovidiu Garlea, Tao Hong, Minseong Lee, Jaime A Fernandez-Baca, **Huibo Cao**, Wei Tian, "Magnetic excitations of the hybrid multiferroic$(ND_4)_2FeCl_5 \cdot D_2O$", *Physical Review B* **103,** 224411 (2021). https://doi.org/10.1103/PhysRevB.103.224411

- Chaowei Hu, **Lei Ding**, Kyle N. Gordon, Barun Ghosh, Haoxiang Li, Shang-Wei Lian, A. Garrison Linn, Hung-Ju Tien, Cheng-Yi Huang, P. V. Sreenivasa Reddy, Bahadur Singh, Amit Agarwal, Arun Bansil, Su-Yang Xu, Hsin Lin, **Huibo Cao**, Tay-Rong Chang, Dan Dessau, Ni Ni, "Realization of an intrinsic ferromagnetic topological state in $MnBi_8Te_{13}$", *Science Advances*, **6,** eaba4275 (2020). **Lei Ding** is **the co-first author**.

  https://doi.org/10.1126/sciadv.aba4275

- J. Xing, **Erxi Feng**, Y. Liu, E. Emmanouilidou, C. Hu, J. Liu, D. Graf, A.P. Ramirez, G. Chen, **Huibo Cao**, N. Ni, "Néel-type antiferromagnetic order and magnetic field–temperature phase diagram in the spin- 1/2 rare-earth honeycomb compound $YbCl_3$", *Physical Review B,* **102,** 014427 (2020). Erxi Feng is the co-first author and Huibo Cao is the co-corresponding author. https://doi.org/10.1103/PhysRevB.102.014427
- Xin Gui, **Erxi Feng**, **Huibo Cao**, Robert J Cava, "Ferromagnetic Cr_4PtGa_{17}: A Half-Heusler-Type Compound with a Breathing Pyrochlore Lattice", *Journal of the American Chemical Society* **143,** 14342 (2021). https://doi.org/10.1021/jacs.1c06667
- Madalynn Marshall, Ivo Pletikosić, Mohammad Yahyavi, Hung-Ju Tien, Tay-Rong Chang, **Huibo Cao**, Weiwei Xie, **"**Magnetic and electronic structures of antiferromagnetic topological material candidate $EuMg_2Bi_2$**"**. *Journal of Applied Physics* **129** 035106 (2021) **invited.**
- P.-L. Dai, Gaoning Zhang, Yaofeng Xie, Chunruo Duan, Yonghao Gao, Zihao Zhu, **Erxi Feng**, Chien-Lung Huang, **Huibo Cao**, Andrey Podlesnyak, Garrett E. Granroth, David Voneshen, Shun Wang, Guotai Tan, Emilia Morosan, Xia Wang, Lei Shu, Gang Chen, Yanfeng Guo, Xingye Lu, Pengcheng Dai, "Spinon Fermi surface spin liquid in a triangular lattice antiferromagnet $NaYbSe_2$", *Physical Review X*, **11**, 021044 (2021).

  https://doi.org/10.1103/PhysRevX.11.021044
- Chaowei Hu, Xiaoqing Zhou, Pengfei Liu, Jinyu Liu, Peipei Hao, Eve Emmanouilidou, Hongyi Sun, Yuntian Liu, Harlan Brawer, Arthur P. Ramirez, **Huibo Cao**, Qihang Liu, Dan Dessau, Ni Ni, "A van der Waals antiferromagnetic topological insulator with weak interlayer magnetic coupling", *Nature Communications* **11**, 97 (2020) https://www.nature.com/articles/s41467-019-13814-x

Understanding Quantum Matter Beyond the Unit Cell

Andrew Christianson[1], Joseph Paddison[1], Andrew May[1], Gábor Halász[1], David Mandrus[1,2,3]

[1]Materials Science & Technology Division, Oak Ridge National Laboratory, Oak Ridge, TN
[2]Department of Physics & Astronomy, University of Tennessee, Knoxville, TN
[3]Department of Material Science & Engineering, University of Tennessee, Knoxville, TN

Program Scope

Our knowledge of how topological invariants influence a material's physical properties continues to evolve and is driving a "topological revolution" in condensed matter physics. Despite significant progress, understanding how topology impacts all the static and dynamic properties of quantum materials is a grand challenge of modern condensed matter physics. The Overarching Goal of this project is to achieve a fundamental understanding of how anisotropy, frustration, and topology acting in concert produce collective quantum phenomena. To achieve this goal, the Specific Aims of the project are: (1) Reveal the quantum mechanical origins of magnetic continua and how multi-magnon interactions both impact and reveal the nature of quantum magnetism; (2) Understand and tune topologically nontrivial character reflected in the excited states of quantum magnets; (3) Unravel the formation and properties of multi-$\boldsymbol{Q}$ magnetism with an emphasis on novel spin textures. These topics are pursued by employing sophisticated theoretical modeling and simulation to exploit the multi-faceted information available from various neutron scattering techniques. The principal outcomes will be the construction of physical models that describe how quantum magnetism and topology together influence macroscopic properties and guidelines for identifying and manipulating systems to produce specific, quantum phenomena.

Recent Progress

I. Breathing pyrochlore magnetism: A breathing pyrochlore lattice consists of a static array of alternating small and large corner-shared tetrahedra. Breathing pyrochlore materials provide an interesting lattice geometry to probe for novel behavior, ranging from frustrated magnetism to the possibility of Weyl magnons. We have studied several examples of breathing pyrochlore lattice materials, including $LiGaCr_4S_8$ and $CuInCr_4S_8$ that are ordered variants of the well-known ACr_4S_8 spinel structure.

To understand the nature of the spin-spin interactions in the Cr-based breathing pyrochlore materials, we studied the magnetic diffuse scattering and magnetic excitations in $LiGaCr_4S_8$, and these investigations have led to several interesting discoveries[1]. Through field theoretic simulations, we extracted the interaction parameters to reveal that further neighbor interactions, at least up to third nearest neighbors, play a key role in the magnetic properties. We additionally determined that the magnetic behavior was controlled by interacting ferromagnetic clusters (effectively) decorating an FCC lattice. Under these circumstances, conventional magnetic order is avoided due to frustrated interactions between clusters. The picture of interacting clusters is

likely to be important for many different breathing pyrochlore materials. Another important aspect of this work is that the methodology developed by the project demonstrates that diffuse scattering from powders can be extremely valuable for rapidly screening quantum materials, particularly when used in conjunction with more conventional techniques.

We have also studied $CuInCr_4S_8$ to examine a long range ordered example of a breathing pyrochlore lattice material [2]. Using inelastic neutron scattering, we showed that the spin excitations in the ordered phase are hierarchical and can be approximated at low energies by an effective model of correlated tetrahedra. At higher energies, intra-tetrahedron excitations and strong magnon-phonon couplings are observed, which suggests the possible role of the lattice degree of freedom in stabilizing the spin tetrahedra. The effective cluster model demonstrated can be generalized to understand spin dynamics in different breathing-type lattice compounds.

II. Quantum magnetism on the honeycomb lattice: Our work on the honeycomb lattice material $YbCl_3$ has resulted in the first observation of a Van Hove singularity in the continuum scattering of a quantum magnet [3]. The honeycomb lattice is a fascinating structural motif for the generation of collective quantum behavior. For instance, magnetic frustration on the honeycomb lattice can arise from geometric frustration in isotropic systems with further neighbor interactions or from exchange frustration through competing anisotropic interactions. When the spin interactions are strongly anisotropic, as is the case for the Kitaev materials, the result is strongly frustrated interactions and, hence, the honeycomb lattice is one of the primary contenders to host quantum spin liquids. In the opposite limit of isotropic spin interactions, frustrated quantum magnetism can arise through the competition of nearest neighbor and next nearest neighbor interactions. Complementary to these research directions, our work on $YbCl_3$ [3] was the first to carefully characterize such a system in the limit of the nearest neighbor honeycomb lattice Heisenberg model. This model, like many important models of quantum magnetism, is elegantly simple – only nearest neighbor Heisenberg interactions are considered, there is no frustration, and the ground state at T=0 is the antiferromagnetic Néel state. In such a simple case, quantum effects can be the subject of rigorous investigation.

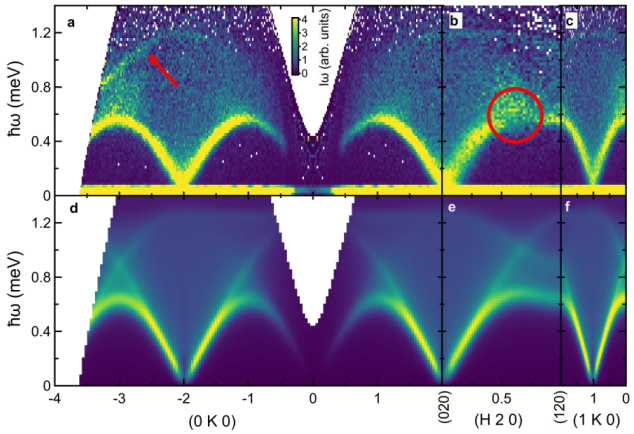

Figure 1: Inelastic neutron scattering data for $YbCl_3$ measured at T=0.24 K ((a)-(c)) and linear spin-wave calculations, including both transverse and longitudinal channels ((d)-(f)). Above the spin-wave mode, the response has a pronounced continuum component which contains a clearly observable sharp feature, a Van Hove singularity (red arrow), close to its upper edge [3]. The anomalous spectral distribution near the K-point is indicated by the red circle.

Our initial investigations of the basic physical properties showed that $YbCl_3$ could be viewed as an effective spin-1/2 quantum magnet [4]. We then synthesized large single crystals so that the collective properties could be examined though inelastic neutron scattering studies. These studies [3] revealed a rich excitation spectrum. In addition to conventional spin waves, the spectrum exhibits an unusually sharp feature within a broad continuum (Fig. 1). The spectrum is explained by a linear spin wave theory (LSWT) that includes both transverse and longitudinal channels of the neutron response. In particular, the broad continuum corresponds to a two-magnon contribution from the longitudinal channel, while the sharp feature within this continuum is identified as a Van Hove singularity in the joint density of states. The experimental demonstration of a sharp Van Hove singularity in a two-magnon continuum is important as a confirmation of broadly held expectations that such features should be present in the continua of quantum magnets. Also, analogous features in two-spinon continua could potentially be used to distinguish quantum spin liquids from classically disordered systems.

III. Understanding magnon decay and spectral renormalization in a S=1 quantum magnet: An ongoing challenge in the study of quantum materials is to incorporate quantum effects that are not captured by the simplest semiclassical approaches. This is particularly important for quantum magnets where one of the strongest signatures of quantum behavior is spontaneous quasiparticle decay. This many body process has been found to be accompanied by a significant renormalization (~40 %) of the overall spectrum [5,6] in triangular lattice materials. This spectral renormalization has an important implication, namely that the renormalized single-magnon dispersion provides a stringent test for theories that attempt to reproduce measurable effects of magnon decay. In other words, approaches which do not fully incorporate these many-body effects will not yield correct values of the interaction parameters extracted from fits of inelastic neutron scattering data. Our work clearly demonstrates these effects and also provides a new approach to understand them.

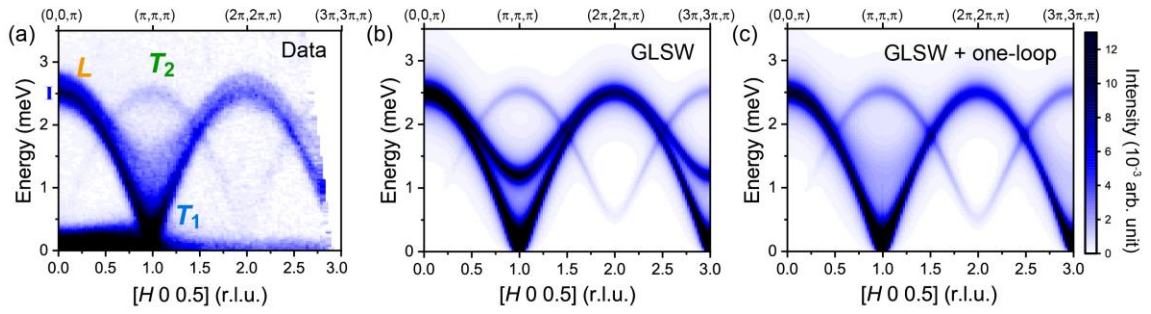

Figure 2: (a) Contour map of the inelastic neutron scattering data from $Ba_2FeSi_2O_7$ as a function of energy and momentum transfer along the [H,0,0.5] direction measured at T=1.6 K (< T_N). The two transverse modes and the longitudinal mode are labeled with T_1, T_2, and L, respectively. (b),(c), INS intensities calculated by the generalized linear spin wave theory (GLSWT) and GLSWT plus one-loop corrections (GLSWT+one-loop). [7]

Our combined neutron scattering and theory study [7] shows that $Ba_2FeSi_2O_7$ is a realization of a quasi-2D easy-plane antiferromagnet in the proximity of the quantum critical point (QCP) that signals the transition into a quantum paramagnetic phase. Previous examples of low-dimensional

easy-plane quantum magnets in the proximity of this QCP were typically on the quantum paramagnetic side of the quantum phase transition. $Ba_2FeSi_2O_7$ thus provides a unique platform to study the strong decay and renormalization effects of the transverse and longitudinal modes of the AFM state. In particular, we have measured the magnon spectrum over an entire Brillouin zone with inelastic neutron scattering measurements and used the data as means to test a loop expansion approach based on an SU(3) spin wave theory (Fig. 2). This loop expansion, which generalizes the well-known 1/*S* expansion of the SU(2) spin wave theory, allows us to reproduce the measured width and renormalization of the longitudinal and transverse modes near the zone center by just including a one-loop correction. This confirms that $Ba_2FeSi_2O_7$ is an ideal model system for studying many-body effects in the proximity of an O(2) QCP in D=3+1 dimensions. More generally, our work demonstrates a general scheme for treating quantum magnets with more than one type of low-energy mode.

Future Plans

- Investigate the fundamental aspects of quantum magnetism on the honeycomb lattice (such as magnon decay and continuum scattering) using sophisticated models to enable a deeper understanding of collective quantum phenomena.
- Understand mode interactions and resulting decays of various types in quantum magnets, with an emphasis on tuning magnon decay with applied field in square lattice materials.
- Study and manipulate topological magnons and the novel ground states they emerge from in honeycomb lattice, kagome lattice, and Shastry-Sutherland lattice geometries via diffuse and inelastic neutron scattering.
- Understand how novel spin textures are generated though geometric frustration and competing interactions. For example, we will use diffuse and inelastic neutron scattering to determine under what circumstances a spin texture can emerge from a spiral spin liquid.
- Understand the interplay of spin textures and chemical disorder. Knowledge of chemical disorder will be coupled with our neutron diffraction studies of the magnetic spin configuration to understand mechanisms for spin texture formation.
- We will develop techniques to rapidly screen new candidate quantum materials using diffuse neutron scattering and inelastic neutron scattering on polycrystalline materials.

References

[1] G. Pokharel, *et al*., *Phys. Rev. Lett*. **125**, 167201 (2020).
[2] S. Gao, *et al*., Phys. Rev. B **103**, 214418 (2021).
[3] G. Sala, *et al*., *Nat. Commun*. **12**, 171 (2021).
[4] G. Sala, *et al*., *Phys. Rev. B* **100**, 180406(R) (2019).
[5] A. L. Chernyshev and M. E. Zhitomirsky, *Phys. Rev. B* **79**,144416 (2009).
[6] W. Zheng, *et al*., *Phys. Rev. Lett*. **96**, 057201 (2006).
[7] S.-H. Do, *et al*., *Nat. Commun.* **12**, 5331 (2021).

Publications

1. G. Sala, M. B. Stone, B. K. Rai, A. F. May, D. S. Parker, G. B. Halász, Y. Q. Cheng, G. Ehlers, V. O. Garlea, Q. Zhang, M. D. Lumsden, and A. D. Christianson, Crystal field splitting, local anisotropy, and low energy excitations in the quantum magnet $YbCl_3$, *Phys. Rev. B* **100**, 180406(R) (2019).

2. W. R. Meier, J. Yan, M. A. McGuire, X. Wang, A. D. Christianson, and B. C. Sales, Reorientation of antiferromagnetism in cobalt doped FeSn, *Phys. Rev. B* **100**, 184421 (2019).

3. B. C. Sales, J. Yan, W. R. Meier, A. D. Christianson, S. Okamoto, and M. A. McGuire, Quasi 2-D magnetism in the Kagome layer compound FeSn, *Phys. Rev. Mater.* **3**, 114203 (2019).

4. L. Poudel, J. M. Lawrence, L. S. Wu, G. Ehlers, Y. Qiu, A. F. May, F. Ronning, M. D. Lumsden, D. Mandrus, and A. D. Christianson, Multicomponent fluctuation spectrum at the quantum critical point in $CeCu_{6-x}Ag_x$, *npj Quantum Mater*. **4**, 52 (2019).

5. J. Xing, L. D. Sanjeewa, J. Kim, W. R. Meier, A. F. May, Q. Zheng, R. Custelceean, G. R. Stewart, and A. S. Sefat, Synthesis, magnetization, and heat capacity of triangular lattice materials $NaErSe_2$ and $KErSe_2$, *Phys. Rev. Mater***. 3**, 114413 (2019).

6. B. K. Rai, A. D. Christianson, G. Sala, M. B. Stone, Y. Liu, and A. F. May, Magnetism of Nd_2O_3 single crystals near the Néel temperature, *Phys. Rev. B* **102**, 054434 (2020).

7. N. Sirica, P. Vilmercati, F. Bondino, I. Pis, S. Nappini, S.-K. Mo, A. V. Fedorov, P. K. Das, I. Vobornik, J. Fujii, L. Li, D. Sapkota, D. S. Parker, D. G. Mandrus, and N. Mannella, The nature of ferromagnetism in the chiral helimagnet $Cr_{1/3}NbS_2$, *Commun. Physics* **3**, 1 (2020).

8. E. M. Clements, R. Das, G. Pokharel, M. H. Phan, A. D. Christianson, D. Mandrus, J. C. Prestigiacomo, M. S. Osofsky, and H. Srikanth, Robust cycloid crossover driven by anisotropy in the skyrmion host GaV_4S_8, *Phys. Rev. B* **101**, 094425 (2020).

9. J. G. Vale, S. Calder, N. A. Bogdanov, C. Donnerer, M. Moretti Sala, N. R. Davies, D. Mandrus, J. van den Brink, A. D. Christianson, and D. F. McMorrow, Spin and orbital excitations through the metal-to-insulator transition in $Cd_2Os_2O_7$ probed with high-resolution resonant inelastic x-ray scattering, *Phys. Rev. B* **101**, 014441 (2020).

10. S.-S. Zhang, H. Ishizuka, H. Zhang, G. B. Halász, and C. D. Batista, Real-space Berry curvature of itinerant electron systems with spin-orbit interaction, *Phys. Rev. B* **101**, 024420 (2020).

11. H. K. Yoshida, S. E. Dissanayake, A. D. Christianson, C. de la Cruz, Y. -Q. Cheng, S. Okamoto, K. Yamaura, M. Isobe, and M. Matsuda, Static and dynamic spin properties in a quantum triangular lattice antiferromagnet Ag_2CoO_2, *Phys. Rev. B* **102**, 024445 (2020).

12. Y. Ishii, Jie Chen, H. K. Yoshida, M. Odaa, A. D. Christianson, and K. Yamaura, High-pressure synthesis, crystal structure, and magnetic properties of the Shastry-Sutherland-lattice oxides $BaLn_2ZnO_5$ (Ln = Pr, Sm, Eu), *J. Solid State Chem*. **289**, 121489 (2020).

13. Z. Dun, X. Bai, J. A. M. Paddison, E. Hollingworth, N. P. Butch, C. D. Cruz, M. B. Stone, T. Hong, F. Demmel, M Mourigal, and H. Zhou, Quantum versus classical spin fragmentation in dipolar Kagome ice $Ho_3Mg_2Sb_3O_{14}$, *Phys. Rev. X* **10**, 031069 (2020).

14. S. Gao, L.-F. Lin, A. F. May, B. K. Rai, Q. Zhang, E. Dagotto, A. D. Christianson, and M. B. Stone, Weakly coupled alternating S=1/2 chains in the distorted honeycomb lattice compound $Na_2Cu_2TeO_6$, *Phys. Rev. B* **102**, 220402(R) (2020).

15. G. Pokharel, H. S. Arachchige, T. J. Williams, A. F. May, R. S. Fishman, G. Sala, S. Calder, G. Ehlers, D. S. Parker, T. Hong, A. Wildes, D. Mandrus, J. A. M. Paddison, and A. D. Christianson, Cluster frustration in the breathing pyrochlore magnet $LiGaCr_4S_8$, *Phys. Rev. Lett.* **125**, 167201 (2020). Editors' Suggestion.

16. N. Mohanta, A. D. Christianson, S. Okamoto, and E. Dagotto, Signatures of a liquid-crystal transition in spin-wave excitations of skyrmions, *Commun. Physics* **3**, 229 (2020).

17. A. D. Christianson, V. R. Fanelli, L. Lindsay, S. Mu, M. C. Rahn, D. G. Mazzone, A. H. Said, F. Ronning, E. D. Bauer, and J. M. Lawrence, Phonons, Q-dependent Kondo spin fluctuations, and 4f phonon resonance in $YbAl_3$, *Phys. Rev. B* **102**, 205135 (2020).

18. J. A. M. Paddison, Scattering signatures of bond-dependent magnetic interactions, *Phys. Rev. Lett*. **125**, 247202 (2020).

19. X. Bai, S.-S. Zhang, Z. Dun, H. Zhang, Q. Huang, H. Zhou, M. B. Stone, A. I. Kolesnikov, F. Ye, C. D. Batista and M. Mourigal, Hybridized quadrupolar excitations in the spin-anisotropic frustrated magnet FeI_2. *Nat. Phys.* **17**, 467 (2021).

20. M. J. Coak, D. M. Jarvis, H. Hamidov, A. R. Wildes, J. A. M. Paddison, C. Liu, C. R. S. Haines, N. T. Dang, S. E. Kichanov, B. N. Savenko, S. Lee, M. Kratochvílová, S. Klotz, T. C. Hansen, D. P. Kozlenko. J.-G. Park, and S. S. Saxena, Emergent magnetic phases in pressure-tuned van der Waals antiferromagnet $FePS_3$, *Phys. Rev. X* **11**, 011024 (2021).

21. L.-F. Lin, N. Kaushal, C. Şen, A. D. Christianson, A. Moreo, and E. Dagotto, Oxygen magnetic polarization, nodes in spin density, and zigzag spin order in oxides, *Phys. Rev. B* **103**, 184414 (2021).

22. W. R. Meier, B. C. Chakoumakos, S. Okamoto, M. A. McGuire, R. P. Hermann, G. D. Samolyuk, S. Gao, Q. Zhang, M. B. Stone, A. D. Christianson, and B. C. Sales, A catastrophic charge density wave in $BaFe_2Al_9$, *Chem. Mater.* **33**, 2855 (2021).

23. B. C. Sales, W. R. Meier, A. F. May, J. Xing, J.-Q. Yan, S. Gao, Y. H. Liu, M. B. Stone, A. D. Christianson, Q. Zhang, and M. A. McGuire, Tuning the flat bands of the kagome metal CoSn with Fe, In, or Ni doping, *Phys. Rev. Mater*. **5**, 044202 (2021).

24. B. K. Rai, G. Pokharel, H. Suriya Arachchige, S.-H. Do, Q. Zhang, M. Matsuda, M. Frontzek, V. O. Garlea, A. D. Christianson, and A. F. May, Complex magnetic phases in polar tetragonal intermetallic $NdCoGe_3$, *Phys. Rev. B* **103**, 014426 (2021).

25. G. Sala, M. B. Stone, B. K. Rai, A. F. May, P. Laurell, V. O. Garlea, N. P. Butch, M. D. Lumsden, G. Ehlers, G. Pokharel, A. Podlesnyak, D. Mandrus, D. S. Parker, S. Okamoto, G. B. Halász, and A. D. Christianson, Van Hove singularity in the magnon spectrum of the antiferromagnetic quantum honeycomb lattice, *Nat. Commun.* **12**, 171 (2021).

26. Y. Ishii, G. Sala, M. B. Stone, V. O. Garlea, S. Calder, Jie Chen, H. K. Yoshida, S. Fukuoka, J. Yan, C. dela Cruz, M.-H. Du, D. S. Parker, H. Zhang, C. D. Batista, K. Yamaura, and A. D. Christianson, Magnetic properties of the Shastry-Sutherland lattice material $BaNd_2ZnO_5$, *Phys. Rev. Mater.* **5**, 064418 (2021).

27. S. Gao, A. F. May, M.-H. Du, J. A. M. Paddison, H. Suriya Arachchige, G. Pokharel, C. dela Cruz, Q. Zhang, G. Ehlers, D. S. Parker, D. G. Mandrus, M. B. Stone, and A. D. Christianson, Hierarchical excitations from correlated spin tetrahedra on the breathing pyrochlore lattice, *Phys. Rev. B* **103**, 214418 (2021).

28. S.-H. Do, H. Zhang, T. J. Williams, T. Hong, V. Ovidiu Garlea, T.-H., Jang, S.-W. Cheong, J.-H. Park, C. D. Batista, and A. D. Christianson, Decay and renormalization of a longitudinal mode in a quasi-two-dimensional antiferromagnet, *Nat. Commun*. **12**, 5331 (2021).

29. S. Gao, V. Kocsis, M. Soda, F. Ye, Y. Liu, A. F. May, Y. Taguchi, Y. Tokura, T.-h. Arima, W. Schweika, A. D. Christianson, M. B. Stone, Suppressed incommensurate order in the Swedenborgite $Ca_{0.5}Y_{0.5}BaCo_4O_7$, *Phys. Rev. B* **104**, L140408 (2021).

Neutron Studies of Hybrid Excitations

R. P. Hermann, M. E. Manley, R. S. Fishman
Materials Science & Technology Division, Oak Ridge National Laboratory, Oak Ridge, TN

Program Scope

This project studies how hybridized atomic vibrations control energy transport and functionalities in energy materials. First, we aim to understand how non-linearities modify lattice energy propagation. To this effect, we have focused on lattice dynamics in hybrid photovoltaic perovskites where the interplay of charge and lattice is crucial for energy conversion and we have focused on understanding the limits of thermal transport through the phonon, diffuson, and phason channels. Second, we aim to understand how to control spin directions and transport through the spin channel. Here, we have focused on how spin disorder affects magnon dispersions and on the spin structure and dynamics in MnTe. Our third aim is to understand how lattice topology and quantum fluctuations impact thermal transport and phase stability in the quantum regime. We have focused on identifying the microscopic origin of glass-like thermal transport in the $BaTiS_3$ hexagonal perovskites and on how structural chirality impacts dynamical structure factors and phonon polarization in TeO_2. Our work also includes methods and procedure, e.g., for absorption correction, enhanced resolution, and high-pressure. Investigating the microscopic energy transport mechanisms by inelastic neutron scattering contributes to fill the knowledge gaps in the interrelation of functionality and lattice dynamics in systems hosting hybrid excitations.

Recent Progress

Giant isotopic shift keeps charge carriers hot in photovoltaic perovskite. Neutron scattering from photovoltaic methylammonium lead iodide (*MA*PbI_3), (*MA*= H_3CNH_3), reveals a giant effect of isotopic substitution on phonons due to coupling with molecule dynamics that results in increased thermal resistivity and hot-carrier cooling times [1]. Harnessing charge carriers before they lose energy to heat could dramatically increases the solar-cell conversion efficiency. A big challenge is finding absorber materials from which charge carriers can be extracted before they have time to cool. Halide perovskites show a unique slow cooling of charge carriers owing to a "phonon bottleneck" that jams cooling [2]. Our neutron scattering study of phonons and molecular modes in protonated and deuterated *MA*PbI_3 reveals a coupling of phonons to molecular modes (Fig. 1) that leads to a giant effect: Heat transport is reduced by half and the charge-carrier cooling time doubles with deuteration – highlighting a route for enhancing hot-carrier solar cell efficiency.

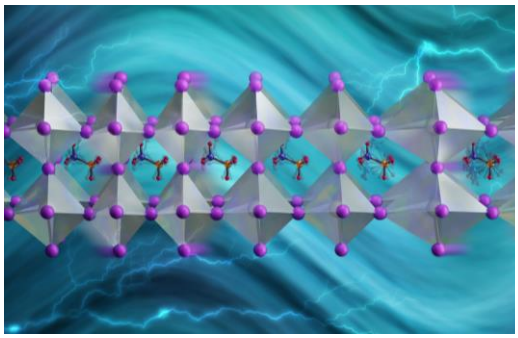

Fig. 1. The methylammonium libration mode slows down when the mass of hydrogen is doubled by deuteration. This slow down, in turn, dramatically slows down part of the longitudinal acoustic phonon branch. Image credit: Jill Hemman/ORNL, U.S. Dept. of Energy.

Diffuson thermal transport. We have explored the boundaries of thermal conductivity in systems poised at two extremes: crystalline $Yb_{14}MnSb_{11}$, which has traits of an amorphous thermal conductor [3], and amorphous silicon, with the traits of a crystal-like thermal conductor [4]. These studies provide new insights into the thermal conductivity mechanisms near or at the amorphous limit and ultimately can inform the future design of materials with tailored thermal transport. $Yb_{14}MnSb_{11}$ is a thermoelectric material with an extremely large unit-cell [5], with 312 phonon modes, all located below 25 meV. The proximity of these modes suggests the importance of diffuson channel transport i.e., the hopping of vibrational energy between neighboring phonon modes made possible by their quasi-degeneracy, for which a framework was recently developed [6]. Our work explains the low, almost constant thermal transport above 295 K, which does not exhibit the traditional $1/T$ Umklapp-scattering behavior. Using inelastic neutron scattering and calculations we have shown that this behavior corresponds to diffuson-, rather than phonon-channel-, dominated thermal transport at high temperature.

Spin structure and dynamics in MnTe and disorder materials. MnTe is an antiferromagnetic semiconductor with the NiAs-structure and has a Néel temperature of 307 K [7]. In earlier work, we linked the strong increase in thermopower at the Néel temperature to the robust long-lived paramagnons [8]. Besides yielding paramagnon lifetimes, our recent measurements on 0.3%-5% Li:MnTe suggest that, when doped with Li, MnTe exhibits a new magnetic structure with axial instead of the in-plane spins seen in pure MnTe. As little as 0.3%-Li doping is sufficient to tune the magnetic anisotropy [9]. Modelling also suggests that injecting small amounts of charge carriers reorients the spins and that Fermi-level-tuning of the magnetic anisotropy could functionalize this material as a spin-valve. We have also characterized and modelled spin disorder in entropy stabilized (Mg,Co,Ni,Zn,Cu)O. Inelastic neutron scattering and muon spin resonance showed the quasi-continuous nature of the ordering transition and the persistence of magnetic fluctuations at low temperatures[10]. Modelling the excitation spectrum reveals a coherent and incoherent component at low and high energies, respectively, and a spin-wave gap proportional to the average moment size per lattice site [11].

Atomic tunneling explains glass-like heat transport in simple crystal. Neutron measurements of a double-well local structure and associated two-level excitation, see Fig. 2, reveal that atomic tunneling is the source of an ultralow glass-like thermal conductivity in $BaTiS_3$ [12]. These were the first observations of translational atomic tunneling other than hydrogen using neutrons in a crystal. Such two-level systems are known in glasses, but this is first time where tunneling has sufficiently high frequency to disrupt thermal transport over a large temperature range in a crystal. This mechanism suggests an alternative route to controlling thermal transport in functional materials.

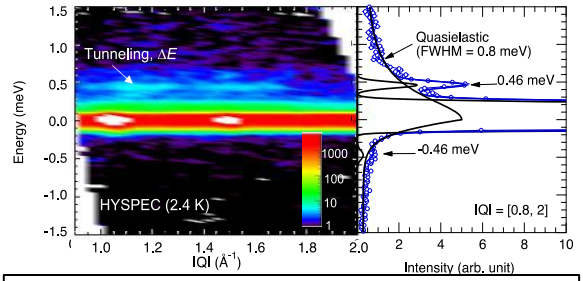

Fig. 2. High-energy-resolution inelastic neutron scattering of $BaTiS_3$ powder at 2.4 K at HYSPEC, SNS. A localized excitation is observed at 0.46 meV. Right: momentum-integrated spectra.

Dynamical structure factors in chiral materials. Structural chirality directly imposes non-trivial topology on electronic and phononic bands [13]. More simply, when the structural number *Z* of formula units per *primitive* unit-cell is larger than 1, *i.e.*, in non-symmorphic systems, crossing points and additional symmetries are expected in the phonon bands. We have analyzed in detail the phonon dispersions and polarizations, see Fig. 3, in chiral paratelluride, α-TeO_2. A novel kind of quantum number emerges from the chirality which yields conservation laws for phonon-phonon scattering terms and determines the dynamical structure factors [14]. In particular, phonons measured in a purely longitudinal geometry exhibit alternatingly all group velocities allowed by the three polarizations. These findings have implications for future thermal conductor and insulator design.

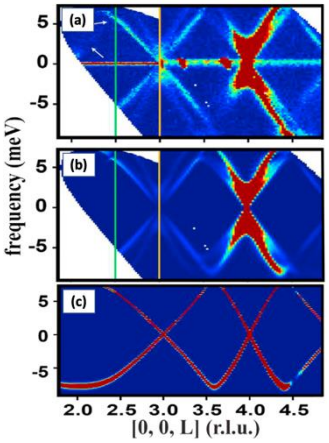

Fig. 3 $S(Q,E)$ in α-TeO_2. (a) HYSPEC, SNS; (b) DFT with matched resolution; (c) DFT without convolution.

Intrinsic absorption correction for time-of-flight instruments. As part of efforts to understand electron-phonon coupling and anharmonicity in simple systems, we have investigated iridium, one of the least studied elements, in part due to its large neutron-absorption cross-section [15]. To address the critical absorption, we have developed a method based on the principle of detailed balance which provides intrinsic absorption correction procedure [16]. This enabled a quantitative study of the density of phonon states and lattice thermodynamics in iridium as a function of temperature. Interestingly, the phonon anharmonicity determined by the van Hove singularity energy shift with temperature is substantially larger than calculated [16].

Future Plans

Lead-free hybrid perovskite photovoltaics. Whereas *MA*PbI_3 hybrid perovskite photovoltaics have spearheaded a revolution in photovoltaics research, lead-free alternatives are desirable. Our work on deuterated *MA*PbI_3 suggests the working hypothesis that tuning the moment of inertia of the organic (*A*-site) cation could extend the hot-carrier lifetime. We will use this idea to investigate the lattice dynamics in lead-free materials, based on the SnI_3 and Sb_2I_9 units, by means of vibrational neutron spectroscopy, using the SNS VISION spectrometer, which we will complement with nuclear resonant scattering to obtain Sn and Sb element-specific vibrational modes, and optical transient absorption work by collaborators. These investigations will benefit from and inform modelling efforts for the vibrational modes, which are challenging for these hybrid materials because they require dispersion corrections for van der Waals type interactions.

Clarifying the role of vibrational entropy in charge density wave (CDW) transitions. We have recently observed a catastrophic CDW that develops around 100 ± 20 K, that shatters the crystals, in the intermetallic compound $BaFe_2Al_9$.[17] $BaFe_2Al_9$ is a hexagonal, aluminum rich compound dominated by a 3D Al network, which is a rare example of a 3D intermetallic compound with CDW order. Intriguingly iron-57 Mossbauer spectroscopy indicates two discrete iron sites in the CDW phase, which contrasts with the incommensurate density wave. The driving mechanism of

the CDW transition is also still elusive. To understand the origin of the CDW, we will analyze inelastic neutron scattering data of $BaFe_2Al_9$ and $BaCo_2Al_9$, which does not exhibit this CDW, and determine the relative contribution of vibrational and electronic entropy to the phase transition.

Quantifying the impact of supersonic phasons on thermal transport in incommensurate crystals. Fast propagating acoustic-like waves in the phase of incommensurate structures, called phasons, have long been implicated to enhance thermal conductivity. Although faster than phonon (sound) group velocities have been observed in phason dispersion measurements [18], the linewidths, from which phason mean free paths can be determined, have never been resolved. Mean free paths and group velocities are both needed to evaluate the thermal conductivity. We will quantify the role that phasons play in piezoelectric fresnoite using high-resolution inelastic neutron scattering of the phason and phonon line shapes and temperature-dependent thermal conductivity measurements.

Beyond incoherent tunneling states in $BaTiS_3$. Tunneling phenomena are a hallmark manifestation of quantum mechanical that reveals the possibility of an object residing in a superposed state. Neutron scattering has played a critical role in identifying tunneling behavior, mostly in hydrogen-based materials. Tunneling of heavier atoms is, however, much more elusive – mostly because of the small energy scale and the destruction of tunneling states by thermal energy. Going beyond our first observation of Ti tunneling in $BaTiS_3$ [12] we will better characterize the tunneling peaks, their intrinsic linewidth, their thermal population, and their interaction with the phonon bath. Furthermore, we plan to probe and model possible correlations between Ti that would go beyond a simple double-well behavior, and provide the form factor of the tunneling state, and temperature dependence of the tunneling energy due to thermal expansion.

References

[1] M. Manley *et al.*, *Sci. Adv.* **6**, eaaz1842 (2020).
[2] Y. Yang *et al.*, *Nat. Photonics* **10**, 53 (2016).
[3] R. Hanus *et al.*, *Mat. Today Phys.* **18**, 100344 (2021).
[4] J. Moon *et al.*, *Phys. Rev. Mater.* **3**, 065601 (2019).
[5] S. Brown *et al.*, *Chem. Mater.* **18**, 1873 (2006).
[6] M. Simoncelli *et al.*, *Nat. Phys.* **15**, 809 (2019).
[7] J. Wasscher and C. Haas, *Phys. Lett.* **8**, 302 (1964).
[8] Y. Zheng *et al.*, *Sci. Adv.* **5**, eaat9461 (2019).
[9] D. Moseley *et al.*, Giant Doping Response of Magnetic Anisotropy in MnTe, subm. (2021).
[10] B. Frandsen *et al.*, *Phys. Rev. Mater.* **4**, 074405 (2020).
[11] T. Berlijn *et al.*, *Phys. Rev. Res.* **3**, 033273 (2021).
[12] B. Sun *et al.*, *Nat. Commun.* **11**, 6039 (2020).
[13] G. Chang *et al.*, *Nat. Mater.* **17**, 978 (2018).
[14] R. Juneja *et al.*, *Mat. Today Phys.* **21**, 100548 (2021).
[15] M. Kresch, *Ph.D. Thesis, California Institute of Technology* (2009).
[16] D. Moseley *et al.*, *Phys. Rev. Mater.* **4**, 113608 (2020).
[17] W. Meier *et al.*, *Chem. Mater.* **33**, 2855 (2021).
[18] M. Manley *et al.*, *Nature Commun.* **9**, 1823 (2018).

Publications

1. L. Lindsay, A. Katre, A. Cepellotti, and N. Mingo, Perspective on ab initio phonon thermal transport, *J. Appl. Phys.* **126**, 050902 (2019).
2. I. Sergueev, K. Glazyrin, M. G. Herrmann, P. Alexeev, H.-C. Wille, O. Leupold, A. F. May, T. Pandey, L. R. Lindsay, Friese K. and R. P. Hermann, High-pressure nuclear inelastic scattering with backscattering monochromatization, *J. Synch. Rad.* **26**, 1592 (2019).
3. Y. Zheng, T. Lu, Md M. H. Polash, M. Rasoulianboroujeni, N. Liu, M. E. Manley, Y. Deng, P. J. Sun, X. L. Chen, R. P. Hermann, D. Vashaee, J. P. Heremans, and H. Zhao, Paramagnon drag in high thermoelectric figure of merit Li-doped MnTe, *Sci. Adv.* **5**, eaat9461 (2019).
4. M. E. Manley, K. Hong, P. Yin, S. Chi, Y. Cai, C. Hua, L. L. Daemen, R. P. Hermann, H. Wang, A. F. May, M. Asta, and M. Ahmadi, Giant isotope effect on phonon dispersion and thermal conductivity in methylammonium lead iodide, *Sci. Adv.* **6**, eaaz1842 (2020).
5. Y. Sharma, R. Agarwal, C. Liam, Q. Zheng, A. Ievlev, R. P. Hermann, V. R. Cooper, Santosh Kc., I. N. Ivanov, R. S. Katiyar, S. V. Kalinin, H. N. Lee, S. Hong, and T. Z. Ward, Self-Assembled Room Temperature Multiferroic BiFeO3-LiFe5O8 Nanocomposites, *Adv. Funct. Mater.* **30**, 1906849 (2020).
6. M. G. Herrmann, R. P. Stoffel, I. Sergueev, H.-C. Wille, O. Leupold, M. Ait Haddouch, G. Sala, D. L. Abernathy, J. Voigt, R. P. Hermann, R. Dronskowski and K. Friese, Lattice dynamics of Sb2Se3 from inelastic neutron and X-ray scattering, *Phys. Stat. Solidi B* **257**, 2000063 (2020).
7. B. A. Frandsen, K. A. Petersen, N. A. Ducharme, A. G. Shaw, E. J. Gibson, B. Winn, J. Yan, J. Zhang, M. E. Manley, and R. P. Hermann, Spin dynamics and a nearly continuous magnetic phase transition in an entropy-stabilized oxide antiferromagnet, *Phys. Rev. Mater.* **4**, 074405 (2020).
8. Y. Shen, C. N. Saunders, C. M. Bernal, D. L. Abernathy, M. E. Manley, and B. Fultz, Anharmonic Origin of the Giant Thermal Expansion of NaBr, *Phys. Rev. Letters* **125**, 085504 (2020).
9. L.D. Sanjeewa, Y. Liu, J. Xing, R. S. Fishman, M. T. K. Kolambage, M. A. McGuire, C. D. McMillen, J. W. Kolis, and A. S. Sefat, Stacking Faults and Short-Range Magnetic Correlations in Single Crystal Y5Ru2O12: A Structure with Ru+4.5 One-Dimensional Chains, *Phys. Stat. Solidi B* **258**, 20200197 (2021).
10. A. Jafari, B. Klobes, I. Sergueev, D. H. Moseley, M. E. Manley, R. Dronskowski, V. L. Deringer, R. P. Stoffel, D. Bessas, A. I. Chumakov, R. Rüffer, A. Mahmoud, C. A. Bridges, L. L. Daemen, Y. Cheng, A. J. Ramirez-Cuesta, and R. P. Hermann, Phonon spectroscopy in antimony and tellurium oxides, *J. Phys. Chem. A* **124**, 7869 (2020).
11. D. H. Moseley, S. J. Thébaud, L. R. Lindsay, Y. Cheng, D. L. Abernathy, M. E. Manley, and R. P. Hermann, Temperature-dependent lattice dynamics in iridium, *Phys. Rev. Mater.* **4**, 113608 (2020).
12. B. Sun, S. Niu, R. P. Hermann, J. Moon, N. Shulumba, K. Page, B. Zhao, A. S. Thind, K. Mahalingam, J. Milam-Guerrero, R. Haiges, M. Mecklenburg, B. C. Melot, Y.-D. Jho, B. M. Howe, R. Mishra, A. Alatas, B. Winn, M. E. Manley, J. Ravichandran, and A. J. Minnich, High frequency atomic tunneling yields ultralow and glass-like thermal conductivity in chalcogenide single crystals, *Nat. Commum.* **11**, 6039 (2020).

13. T. Rõõm, J. Viirok, L. Peedu, U. Nagel, D.G. Farkas, D. Szaller, V. Kocsis, S. Bordács, I. Kézsmárki, D. L. Kamenskyi, H. Engelkamp, M. Ozerov, D. Smirnov, J. Krzystek, K. Thirunavukkuarasu, Y. Ozaki, Y. Tomioka, T. Ito, T. Datta, and R. S. Fishman, The magnetoelastic distortion of multiferroic BiFeO3 in the canted antiferromagnetic state, *Phys. Rev. B* **102**, 214410 (2020).
14. R. Hanus, J. George, M. Wood M., Y. Cheng, D. E. Abernathy, M. E. Manley, G. Hautier, G. J. Snyder, and R. P. Hermann, Uncovering design principles for amorphous-like heat conduction using two-channel lattice dynamics, *Mat. Today Phys.* **18**, 100344 (2021).
15. F. Ye, Z. Morgan, W. Tian, S. Chi, X. Wang, M. E. Manley, D. Parker, M.A. Khan, J.F. Mitchell, and R.S. Fishman, Canted antiferromagnetic order and spin dynamics in the honeycomb lattice Tb2Ir3Ga9, *Phys. Rev. B* **103**, 184413 (2021).
16. J. P. Male, R. Hanus, G. J. Snyder, and R. P. Hermann, Thermal evolution of internal strain in doped PbTe, *Chem. Mater.* **33**, 4765 (2021).
17. L. Anovitz, M. C. Cheshire, R. P. Hermann, X. Gu, J. M. Sheets, S. L. Brantley, D. R. Cole, E. S. Ilton, D. F. R. Mildner, C. Gagnon, L. F. Allard, and K. C. Littrell, Oxidation and associated pore structure modification during experimental alteration of granite, *Geochimica et Cosmochimicha Acta* **292**, 532 (2021).
18. B. A. Duell, J. Li, P. G. LaBarre, J. Zhang, R. P. Hermann, A. P. Ramirez, and M. A. Subramanian, Structure and electronic properties of CaAl12-xFexO19 hibonites, *J. Solid State Chem.* **291**, 121650 (2020).
19. G. Pokharel, H. S. Arachige, T. J. Williams, A. F. May, R. S. Fishman, G. Sala, S. Calder, G. Ehlers, D. S. Parker, T. Hong, A. Wildes, D. Mandrus, J. A. M. Paddison, and A. D. Christianson, Cluster frustration in the breathing pyrochlore magnet LiGaCr4S8, *Phys. Rev. Lett.* **125**, 167201 (2020).
20. K. Devlin, J. Zhang, J. Fettinger, E. S. Choi, A. Hauble, V. Taufour, R. P. Hermann, and S. Kauzlarich, Deconvoluting the magnetic structure of the commensurately modulated quinary zintl phase Eu11-xSrxZn4Sn2As12, *Inorg. Chem.* **60**, 5711 (2021).
21. W. R. Meier, B. C. Chakoumakos, S. Okamoto, M. A. McGuire, R. P. Hermann, G. D. Samolyuk, S. Gao, Q. Zhang, M. B. Stone, A. D. Christianson, and B. C. Sales, Catastrophic charge density waves in BaFe2Al9, *Chem. Mater.* **33**, 2855 (2021).
22. Y. Shen, C. N. Saunders, C. M. Bernal, D. L. Abernathy, T. J. Williams, M. E. Manley, and B. Fultz, Prediction and observation of intermodulation sidebands from anharmonic phonons in NaBr, *Phys. Rev. B* **103**, 134302 (2021).
23. T. Berlijn, G. Alvarez, D. S. Parker, R. P. Hermann, and R. S. Fishman, Simulating spin waves in entropy stabilized oxides, *Phys. Rev. Res.* **3**, 033273 (2021).
24. R. Juneja, S. Thébaud, T. Pandey, C. A. Polanco, D. H. Moseley, M. E. Manley, Y. Q. Cheng, B. Winn, D. L. Abernathy, R. P. Hermann, L. Lindsay, Quasiparticle twist dynamics in non-symmorphic materials, *Mat. Today Phys.* **21**, 100548 (2021).

Realization of Full Neutron Polarization Control: Next Generation Spherical Neutron Polarimetry for Neutron Scattering

Chenyang Jiang, Oak Ridge National Laboratory

Program Scope

The overarching goal of this project is to enable neutron scattering studies of complex noncollinear magnetic structures and investigations of hybrid correlation functions coupling different degrees of freedom (spin-lattice, spin-orbit, spin-chirality) using full polarization analysis. This will be accomplished by developing next generation Spherical Neutron Polarimetry (SNP) capabilities to be deployed across multiple neutron instruments at the High Flux Isotope Reactor (HFIR) and the Spallation Neutron Source (SNS) at Oak Ridge National Laboratory (ORNL). The new SNP capability will help resolve questions that are otherwise intractable or cannot be unambiguously determined using traditional methods. SNP enables full control over the neutron polarization for both incoming and outgoing neutrons and measures all components of the change in polarization due to the scattering process. The change in polarization contains information on the magnetic structure and dynamics. After validating the SNP capability at HFIR, our goal is to deploy it at the SNS on both direct geometry time-of-flight spectrometers featuring large detector arrays as well as on diffractometers. Ultimately, with the addition of the SNP capability, this project will introduce a program whereby we synergistically examine high scientific-impact systems and develop the analysis tools that will allow for routine use of SNP by neutron facilities users with a clear path leading from experiment to results to publication.

Recent Progress

A prototype SNP device PHitPAD (Portable High-Tc Polarization Analysis Device) has been built at ORNL [1, 2] and initial test was performed on the Polarized Triple-axis Spectrometer (PTAX) at HFIR (Fig. 1). PHitPAD utilizes a combination of adiabatic and non-adiabatic transitions of neutron polarization in magnetic fields to realize the full control of neutron polarization. High-Tc YBCO films create sharp magnetic boundaries between each polarization control section to ensure precise polarization manipulation. A zero-field chamber made of high-permeability mu-metals at the sample position fully decouples the incoming and outgoing neutron polarization, which allows for measuring the neutron

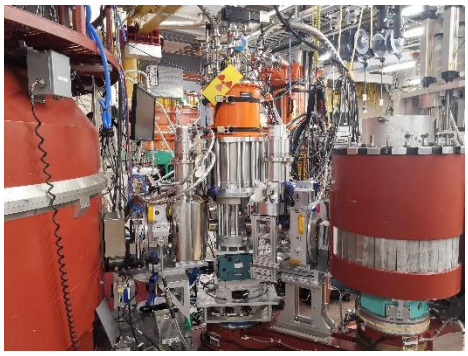

Figure 1. PHitPAD setup on PTAX at HFIR with an orange crystat.

polarization change in each direction and thus enables full polarization analysis. The test on PTAX calibrated the device using a single crystal Si sample and then performed SNP on a couple of single crystal samples with known structures including $BiFeO_3$ and $Ca_2Y_2Cu_5O_{10}$ to demonstrate its validity on magnetic samples. SNP was also conducted on $NiCo_2TeO_6$, a chiral magnet sample, to demonstrate PHitPAD's sensitivity to chiral structures. Preliminary results are shown in Fig. 2.

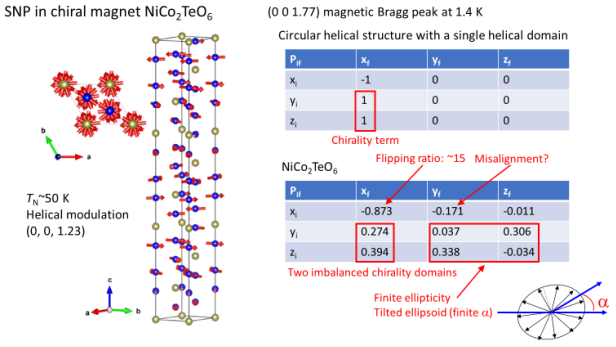

Figure 2. SNP measurements on $NiCo_2TeO_6$

In addition, in SNP all neutron optical components require precise alignment to achieve aberrationless polarization transport. The conventional calibration protocol may not catch all misalignments in the device. The newly developed 3-dimensioinal calibration protocol [3], however, can unambiguously show where the misalignment is, and with this information the SNP device can be easily tuned to compensate for this misalignment. Fig. 3 shows a test of the 3-dimenional calibration protocol with a direct beam on HFIR CG-4B test beamline, which shows largely good polarization transport through the whole instrument.

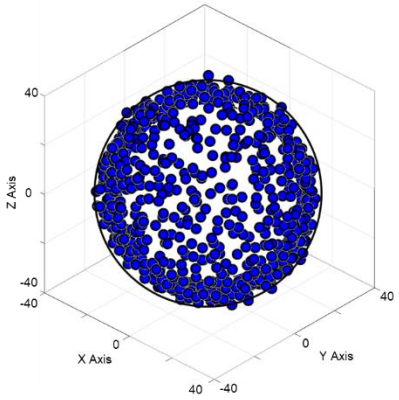

Figure 3. The 3D calibration of PhitPAD on HFIR CG-4B. A perfect device would have all the points on a sphere.

Future Plans

1. PHitPAD is being optimized now and will go back to PTAX early next year. On PTAX, a thorough 3D calibration of the device at different scattering angles will be performed to ensure the consistency of its performance before any real experiment. Meanwhile, we aim to develop a next generation software application that effectively manages both SNP related hardware and beamline related hardware while providing the user with powerful data visualization tools. We expect PHitPAD to go into HIFR user program later next year and will leverage HFIR's strong neutron scattering expertise to choose suitable samples for each experiment.
2. Right now, PHitPAD can only be used on PTAX because PTAX is the only polarized neutron instrument that can do polarization analysis. For some samples like skyirmon lattice systems, using a SANS instrument may be a better option. We want to enable the polarization analysis capability on HFIR GPSANS instrument and perform SNP on this beamline.
3. To date, there is no SNP devices for time-of-flight instruments in the world because the conventional SNP can only deal with monochromatic beams. In order to move

SNP to SNS, a new strategy needs to be developed both theoretically and experimentally. We will seek different options and find the most viable one to extend SNP to Hybrid Spectrometer at SNS. New data analysis software also needs to be developed for the new device.

References

1. Wang, T., S.R. Parnell, W.A. Hamilton, F. Li, A.L. Washington, D.V. Baxter, and R. Pynn, *Compact spherical neutron polarimeter using high-T-c YBCO films*. Rev Sci Instrum, 2016. 87(3)
2. Wang, T., et al. *Developing Wide Angle Spherical Neutron Polarimetry at Oak Ridge National Laboratory*. J. Phys.: Conf. Ser., 2019. 1316 012014.
3. Tosado, J., et al. *A strategy for handling aberration in Spherical Neutron Polarimetry*. J. Phys.: Conf. Ser., 2019. 1316 012015

Publications

1. Ding, L., et al. *Neutron diffraction study of magnetism in van der Waals layered MnBi2n Te3n+ 1*. Journal of Physics D: Applied Physics 54, no. 17 (2021): 174003.

Resolving the Structure and Dynamics of Advanced Materials with Unprecedented Resolution

Fankang Li, Oak Ridge National Laboratory, Oak Ridge, TN, 37831

Program Scope

Quantum materials present a range of remarkable properties with enormous potential for future energy-relevant technologies. Fundamental research to comprehensively understand the interplay of collective modes with quasiparticle dynamics and the discovery/characterization of new electronic phases in such materials is critical for explaining macroscopic physical-chemical properties, such as thermal transport, electrical conductivity, and magnetism. The capability to direct and control the properties of materials at the relevant length, time, and energy scales is essential for the development of next-generation materials for energy sustainability. Even though instrumentation has been advanced dramatically over the past ten years, there are still fundamental challenges to obtaining deeper insights into the structure and dynamics of energy related materials with ultra-high-resolution probes. Revolutionary advances in capabilities associated with neutron techniques, as described in this proposal, will lead to a significant improvement in the understanding of advanced materials. The goal of this project is to develop the next generation neutron scattering techniques by fully using neutron's freedoms, which will ensure the world-leading performance of high-resolution instruments at the High Flux Isotope Reactor (HFIR) of Oak Ridge National Laboratory (ORNL). With this goal, this project will be focused on the following aims:

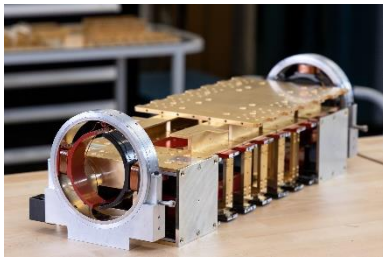

The Inelastic Neutron Spin Echo apparatus developed at ORNL[1].

Specific Aim 1: Develop ORNL's Capabilities and Expertise in the Ultra-High-Resolution Larmor Encoding Methods. As stated by the Basic Energy Sciences Advisory Committee (BESAC, 2020) on "The Scientific Justification for a U.S. Domestic High-Performance Reactor-Based Research Facility", to get deep insight into the quantum materials, the development of Inelastic Neutron Spin Echo (INSE) and Larmor Diffraction (LD) should be prioritized in a high-performance reactor-based neutron source [2]. It states "In fact, several types of polarized neutron scattering instruments can only be constructed at a high-power research reactor (HPRR). These include the neutron Larmor diffractometer, which can be used to very precisely measure lattice parameter variations; the neutron triple-axes spin echo spectrometer, which has extremely good energy resolution (~1 μeV) at large energy transfers and large wave vectors." INSE allows for the linewidth measurements of dispersive quasi-particle excitations, such as phonons and magnons, over the entire Brillouin zone with μeV resolution, which are otherwise inaccessible to neutron or

X-ray spectroscopies, or any other method such as Raman scattering [3]. With similar equipment, LD can also be implemented, permitting high-intensity measurements of lattice constants with a resolution of $\Delta d/d \sim 10^{-6}$, allowing us to investigate the lattice distortion induced by weak interactions such as spin lattice coupling [4].

Specific Aim 2: Develop Collaborations with US Researchers to Ensure a Robust Long-Term User Program for LD and INSE at ORNL. To encourage the scientific user community to use these techniques, I propose to demonstrate their potential applications by utilizing them to investigate the structure and dynamics of several quantum materials. LD and INSE can interrogate these materials with previously inaccessible resolution in momentum and energy. Such experiments may also uncover new routes for accessing and manipulating previously unknown states of quantum matter.

Specific Aim 3: Explore and Develop Novel Concepts and Methods using Polarized Neutrons that Will Underpin Next Generation Neutron Scattering Instrumentation. I will develop new Larmor encoding methods using polarized neutrons and I will also explore the application of entangled neutron probe and Orbital Angular Momentum (OAM) probe in the characterization of quantum materials, such as entanglement and chirality. The success of the project will also pave the way for the future neutron spin echo related instrumentation at the HFIR cold and thermal guide hall.

In addition to the BESAC report, our proposal also addresses the item PRD4-Trust 4b in the report of Basic Research Needs Workshop on Quantum Materials (BRNQM) for Energy Relevant Technology "Develop New Windows into Quantum Materials" [5], which states "To enable new and better windows into quantum materials, the following instrumentation research areas look particularly exciting to pursue:…Advanced photon, electron, and neutron probes, including hybrid probes…" and it explains that "Spectroscopic probes based on THz to x-ray photons, neutrons, and electrons are needed to probe the full range of material response functions, with enhanced efficiency, speed, and resolution". Furthermore, the report states that "New tools to probe solid-state quantum entanglement in spin and orbital sectors" will have great impact.

Recent Progress

Since the project was launched in August of 2021, two full time postdoctoral research associates have been hired. In collaboration with the scientific community in the US, three beamline proposals have been submitted to HFIR to develop and demonstrate the technique outlined in this proposal.

Future Plans

This project will establish the expertise of ORNL in the ultra-high-resolution diffraction and spectroscopy with unprecedented resolution, which allows for the lattice parameter measurements with $\Delta d/d \sim 10\text{-}6$ resolution and linewidth measurements of dispersive quasi-particle excitations over the entire Brillouin zone with μeV resolution. The techniques developed with this

proposal will be routinely accessible by scientific community to study the basic organizing principles and their responses to external perturbations that are at play in quantum materials. To encourage the scientific user community to use these techniques, I will develop collaborations with US researchers to ensure a robust long-term user program at ORNL. The new scattering methods developed with this proposal will form a basis for next generation neutron scattering instrumentation. The success of this project is essential to ensure world-leading performance of high-resolution instruments in future HFIR guide halls and is a necessary step towards new capabilities that will ensure ORNL's scientific leadership in the study of complex materials using the DOE BES funded neutron sources.

References

[1] F. Li, S. R. Parnell, W. A. Hamilton, B. B. Maranville, T. Wang, R. Semerad, D. V. Baxter, J. T. Cremer, and R. Pynn, Superconducting magnetic Wollaston prism for neutron spin encoding, Rev. Sci. Instrum. **85**, 053303 (2014). doi:http://dx.doi.org/10.1063/1.4875984

[2] R. Birgeneau, S. Clark, P. Dai, T. Epps, K. Heeger, D. Hoogerheide, M. Kastner, B. Keimer, D. Louca, P. Lyons *et al.*, The Scientific Justification for a U.S. Domestic High-Performance Reactor-Based Research Facility, 2020.

[3] F. Li and R. Pynn, A novel neutron spin echo technique for measuring phonon linewidths using magnetic Wollaston prisms, J. Appl. Crystallogr. **47**, 1849 (2014). doi:10.1107/S1600576714020597

[4] F. Li, H. Feng, A. N. Thaler, S. R. Parnell, L. Crow, M. Matsuda, F. Ye, T. Kimura, J. A. Fernandez-Baca, and R. Pynn, New capabilities in high-resolution neutron Larmor diffraction at ORNL, J. Appl. Crystallogr. **51**, 584 (2018). 10.1107/s1600576718004211

[5] C. Broholm, F. I., M. J., and M. M., Basic Research Needs Workshop on Quantum Materials For Energy Relevant Technology, 2016.

Publications

N/A

Neutron and x-ray scattering investigations of the influence of short-range correlations, interfaces, and complex disorder on materials properties

S. Rosenkranz, O. Chmaissem*, R. Osborn, D. Phelan, S.G.E. te Velthuis
Argonne National Laboratory; *and Northern Illinois University

Program Scope

Advanced functionality in many crystalline materials derives from the presence of complex disorder, short-range correlations, or interfaces. Materials that harbor such disorder generally exhibit strongly enhanced responses, with electronic, magnetic, optical, and thermal properties that are extremely sensitive to perturbations such as magnetic or electric fields and are of considerable importance for future energy applications. This program develops and utilizes the latest advances in neutron and synchrotron x-ray scattering techniques to study the structural and magnetic correlations of such materials on a range of length and time scales in order to obtain an understanding of the role of heterogeneity. We address important scientific questions regarding phenomena driven or enhanced by atomic and lattice disorder and short-range correlations and intercalation, complex spin correlations, and competing spin, charge and lattice correlations. In particular, we use our previously developed methods for efficient diffuse single crystal diffuse scattering measurements and 3D-ΔPDF analysis to investigate energy conversion materials and ionic conductors, and we combine this with neutron reflectivity to investigate solid electrolyte interfaces. We use diffuse scattering and 3D-ΔPDF analysis and inelastic neutron scattering to determine the origin of structural phase transitions and to study structural correlations of relaxors in the quantum limit. We further utilize single crystal diffuse scattering, inelastic neutron scattering, and polarized neutron reflectivity to investigate the influence of complex spin correlations in anisotropic spin-glassed, frustrated magnets, and thin films and heterostructures exhibiting anomalous magnetic behavior.

Recent Progress

Ionic and Lattice Correlations: Short-range atomic correlations and local distortions embedded in an otherwise long-range ordered crystalline structure play a critical role for many materials properties of importance for energy applications, including thermoelectricity, ionic conductivity, and relaxor ferroelectricity. Our recent development of efficient methods for the measurement of the total scattering in single crystals, comprising both Bragg peaks and diffuse scattering, over full volumes of momentum transfer and its rapid transformation into three-dimensional pair distribution functions provides unprecedented microscopic insight into such subtle structural distortions. Utilizing these methods, we have observed an order-disorder transition in $Na_xV_2O_5$ and obtained a direct, model-free visualization of the short-range ordering. In this prototype battery material, Na-ions sit on partially occupied two-leg ladders within the rigid vanadium oxide framework. The 3D-ΔPDF (Fig. 1) directly shows that at all temperatures, the sodium ions tend to form a zigzag pattern that minimizes Coulomb interactions. The spatial extent of the

sodium correlations can furthermore be extracted from the 3D-PDFs, allowing us to determine correlation lengths from values of 10 Å at room temperature to over 150 Å at 30 K, and to show that, although there appears to be an order-disorder transition at ~230 K, it is really a dimensional crossover from 2D to 3D correlations [11]. In the inorganic perovskite $CsPbBr_3$, we observed rods of diffuse scattering, indicating the presence of short-range 2D correlations. Using inelastic neutron scattering combined with ab-initio molecular dynamics simulations, this was shown to be due to overdamped phonons across entire Brillouin-zone edges, which directly modulate the electronic states and strongly impact the materials opto-electronic properties [6]. We have also combined quasi-elastic neutron scattering, x-ray PDF analysis, and ab-initio molecular dynamics simulations to show that the recently discovered KAg_3Se_2 is a first of its kind, 2D type-I superionic conductor [3].

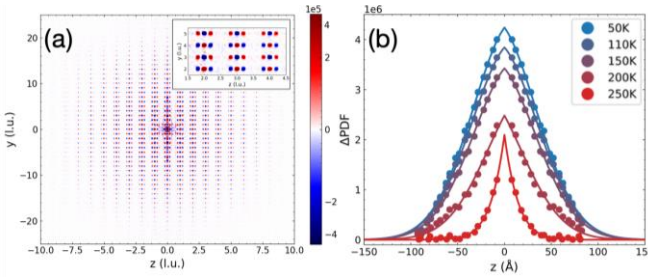

Fig. 1: (a) ΔPDF in the real-space y-z plane at 200K for $Na_{0.45}V_2O_5$. The inset shows the triplet motif explained in [11] (b) Temperature dependence of the ionic correlations along the z-axis fitted to an exponential decay.

Complex Spin Correlations: Diffuse neutron scattering and polarized neutron reflectivity (PNR) provide uniquely detailed insight into phenomena associated with complex spin correlations. For Fe_2TiO_5, which shows Ising-like spin-glass freezing despite having purely Fe^3 spins with no orbital component, our analysis of the magnetic diffuse scattering data measured on *Corelli* revealed the formation of "surfboard-shaped" regions of correlated spins and we showed that the glass transition results from the freezing of transverse fluctuations of these quasi-spins, providing the first example of a purely magnetic van der Waals effect [4].

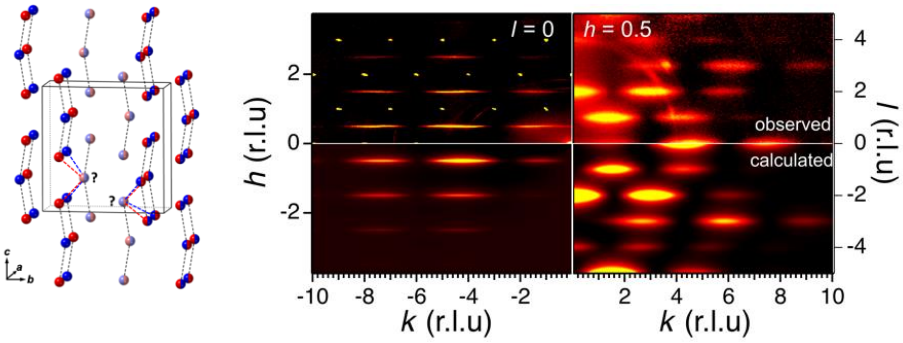

Fig. 2: Observed and calculated (based on model shown on the left) diffuse magnetic scattering from Fe_2TiO_5.

Of great interest is the impact of spin correlations induced at interfaces and the potential impact of topological spin structures on transport properties in heterostructures. We observed a large intrinsic topological anomalous Hall effect (AHE) that emerges at the interface between a ferromagnetic manganite, $La_{0.7}Sr_{0.3}MnO_3$ (LSMO), and a semi-metallic iridate, $SrIrO_3$ (SIO). This AHE originates in the proximity-induced magnetism of the strong spin-orbit coupling iridate, demonstrating that the AHE can be artificially engineer in heterostructures [5]. Polarized Neutron Reflectometry (PNR) and x-ray circular dichroism measurements further reveal significant differences in the magnetic properties of these bilayers depending on the order in

which the layers are grown on the substrate. We observe that a interfacial layer with a net Ir moment is only present when SIO is deposited first on the substrate.

Coupled spin, charge, and lattice correlations: Many phenomena of interest emerge from the simultaneous presence of complex correlations involving spin, charge, and lattice degrees of freedom. A longstanding question is whether metal-insulator transitions (MIT) are primarily due to Mott localization or a Peierls instability. Utilizing single crystal diffuse scattering and performing a detailed 3D-ΔPDF analysis [2], we showed that the 3D structural order in Mo_xVO_2 collapses at x=0.19 while the MIT persists. Below the electronic transition, we find a novel frustrated two-dimensional order with extremely short-range correlations between well-ordered [110] planes. These observations suggest that the MIT is not driven by a Peierls instability alone and confirms the importance of Mott physics. We have also used diffuse neutron scattering to demonstrate that the metal-insulator transition in a trilayer nickelate results from the formation of and intertwined charge and spin density waves [22].

The coexistence and coupling of magnetic and ferroelectric order is important in many applications. Following an elaborate multi-step procedure, we have been able to synthesize the series of $Sr_{1-x}B_xMn_yTi_{1-y}O_3$ compounds. Neutron and x-ray powder diffraction measurements reveal the presence of ferroelectric order with large polarization similar to those of $BaTiO_3$. A detailed investigation of the temperature and pressure dependence further shows a large coupling of magnetic and ferroelectric order and a wide tunability of this coupling as a function of stoichiometry and pressure [19].

Lastly, we continued our investigations of the influence of structural and nematic correlations in hole-doped iron arsenide superconductors. Following our previous discovery of the double-**Q** C_4 magnetic order in a hole doped 112 arsenide compound, we performed a detailed investigation utilizing high-resolution synchrotron x-ray and powder neutron diffraction of the conditions under which this state is stabilized. We found a hidden relation between structural and magnetic properties that enabled us to construct a universal phase diagram capturing the states of all the hole-doped AFe_2As_2 compounds. We further expanded the search for the presence of the C_4 phase in other families of iron-based superconductors. In the 1111-type $La_{1-x}P_xFeAsO$ series, we discovered a complex phase diagram, in which a double-**Q** C_4 collinear magnetic state is stabilized between C_2 stripe antiferromagnetism and a double-**Q** non-collinear C_4 phase, as a function of P substitution. This observation is in agreement with new theoretical predictions, providing unique insight into the universality of the magnetic order across different families of iron pnictides.

Future Plans

Ionic and Lattice Correlations: In order to obtain a better understanding of the mechanisms of ionic conductivity, we plan to combine our diffuse scattering techniques with single-crystal quasi-elastic neutron scattering to investigate the dynamics of ionic correlations. By measuring volumes of 4D-S(**Q**,ω), we obtain the complete momentum dependence of the coherent diffuse

scattering as well as, in some materials, both the coherent and incoherent quasi-elastic linewidths, which provide unprecedented insight into the microscopic diffusion pathways, residence times, and activation energies. We plan to perform initial investigations on the well-known fluorite compound $SrCl_2$ which serves to lay the groundwork for investigating other systems of interest. We will also use neutron reflectivity to investigate Li-intercalation in diffusion in solid state electrolyte films in order to investigate the dependence of interfacial reactivity on electrolyte crystal orientations and crystallinity.

We will investigate the prevalence and impact of 2D structural correlations in perovskite compounds using inelastic and single crystal diffuse scattering to study inorganic and double perovskites. And we also plan to start studies of structural correlations in relaxors in the quantum limit, such as $K_2Li_2Ta_5O_{15,}$ by performing temperature dependent single-crystal diffuse scattering studies and 3D-ΔPDF analysis.

Complex Spin Correlations: To study the effect of magnetic dilution on the anisotropic spin freezing in Fe_2TiO_5, we will measure diffuse neutron scattering from Ga-substituted samples. We will also perform inelastic neutron scattering measurements to investigate the behavior of the spin fluctuations up to the spin freezing temperature. We will also use diffuse neutron scattering to study the spin correlations in the geometrically frustrated magnet $Bi_2Fe_4O_3$ in order to perform a detailed comparison to conventional spin glasses.

The origin of an anomalous Hall effect observed in certain heterostructures and often attributed to a topological Hall effect (THE) will be investigated using PNR. PNR uniquely characterizes the depth-dependent magnetization and provides insight whether behavior resembling THE instead results from the presence of multiple magnetic domains with different coercivities. We will investigate thin films of $SrRuO_3$ as well as various heterostructures exposing ferromagnets to different layers with or without heavy elements that can create interfacial DMI and can induce topological spin textures.

Coupled spin, charge, and lattice correlations: Utilizing single crystal diffuse scattering, we will investigate the structural phase transitions in $BaTiO_3$, $SrTiO_3$, and $NaNO_2$, to address the long-standing debate about the origin of their order parameter, *i.e.*, whether they have order-disorder or displacive character. Using our latest developments in advanced 3D-ΔPDF analysis, we can resolve the question by directly measuring the amplitude of local distortions below the transition.

We will further investigate the evolution and impact of lattice correlations on electronic properties in a number of materials of interest, including vanadates and nickelates. Following our initial studies of Mo-doped VO_2 [2], we will investigate the MIT as a function of other dopants, such as Nb, Cr, and Al, and we will extend our investigations to V_2O_3, another canonical MIT system. We also plan to utilize diffuse scattering and 3D-ΔDPF analysis to investigate the influence of correlated lattice fluctuations on the MIT in perovskite nickelates $RNiO_3$ and to study coupled spin and charge correlations in layered nickelates.

Publications

1. S. Hameed, D. Pelc, Z. W. Anderson, A. Klein, R. J. Spieker, L. Yue, B. Das, J. Ramberger, M. Lukas, Y. Liu, M. J. Krogstad, R. Osborn, Y. Li, C. Leighton, R. M. Fernandes, M. Greven, *Enhanced superconductivity and ferroelectric quantum criticality in plastically deformed strontium titanate*, Nat. Mater. (2021). DOI:10.1038/s41563-021-01102-3
2. M.A. Davenport, M.J. Krogstad, L.M. Whitt, C. Hu, T.C. Douglas, Ni Ni, S. Rosenkranz, R. Osborn, J.M. Allred, *Fragile 3D order in $V_{1-x}Mo_xO_2$*, Phys. Rev. Lett. **127**, 125501 (2021). DOI: 10.1103/PhysRevLett.127.125501
3. A.J.E. Rettie, Jingxuan Ding, Xiuquan Zhou, M.J. Johnson, C.D. Malliakas, N.C. Osti, D.Y. Chung, R. Osborn, O. Delaire, S. Rosenkranz, M.G. Kanatzidis, *A Two-Dimensional Type I Superionic Conductor*, Nat. Mater. (2021). DOI: 10.1038/s41563-021-01053-9
4. P.G. LaBarre, D. Phelan, Y. Xin, F. Ye, T. Besera, T. Siegrist, S.V. Syzranov, S. Rosenkranz, A.P. Ramirez, *Fluctuation-Induced Interactions and the Spin Glass Transition in Fe_2TiO_5*, Phys. Rev. B **103**, L220404 (2021). DOI: 10.1103/PhysRevB.103.L220404
5. M.W. Yoo, J. Tornos. A. Sander, Lin-Fang Lin, N. Mohanta, A. Peralta, D. Sanchez-Manzano, F. Gallego, D. Haskel, J.W. Freeland, D.J. Keavney, Y. Choi, J. Strempfer, X. Wang, M. Cabero, H.B. Vasili, M. Valvidares, G. Sanchez-Santolino, J.M. Gonzalez-Calbet, A. Rivera, C. Leon, S. Rosenkranz, M. Bibes, A. Barthélémy, A. Anane, E. Dagotto, S. Okamoto, S.G.E. te Velthuis, J. Santamaria, J.E. Villegras, *Large intrinsic anomalous Hall effect in $SrIrO_3$ induced by magnetic proximity effect*, Nat. Commun. **12**, 3283 (2021). DOI: 10.1038/s41467-021-23489-y
6. T. Lanigan-Atkins, X. He, M.J. Krogstad, D.M. Pajerowski, D.L. Abernathy, G.N.M.N. Xu, Z. Xu, D.Y. Chung, M.G. Kanatzidis, S. Rosenkranz, R. Osborn, O. Delaire, *Two-Dimensional overdamped fluctuations of the soft perovskite lattice in $CsPbBr_3$*, Nat. Mater. **20**, 977 (2021). DOI: 10.1038/s41563-021-00947-y
7. U. Ruett, J. Almer, P. Kenesei, J-S Park, R. Osborn, Y. Ren, D. Robinson, M. J. Krogstad, S. Rosenkranz, Xuan Zhang, Meimei Li, and K.M. Wiaderek**,** *APS: High-Energy X-rays Expediting Applied and Fundamental Research*, Synchrotron Radiation News **33**, 44 (2021). DOI: 10.1080/08940886.2020.1841498
8. B.R. Ortiz, S.M.L. Teicher, Y. Hu, J.L. Zuo, P.M. Sarte, E.C. Schueller, M.J. Krogstad, S. Rosenkranz, R. Osborn, R. Seshadri, L. Balents, J. He, S.D. Wilson, *CsV_3Sb_5: aA $\mathbb{Z}_2$ Topological Kagome Metal with a Superconducting Ground State,* Phys. Rev. Lett. **125**, 247002 (2020) DOI: 10.1103/PhysRevLett.125.247002
9. Junjie Zhang, D. Phelan, A.S. Botana, Yu-Sheng Cheng, Hong Zheng, M.J. Krogstad, S.G. Wang, Y. Qiu, J.A. Rodriguez-Riveria, R. Osborn, S. Rosenkranz, M.R. Norman, J.F. Mitchell, *Intertwined density waves in a metallic nickelate,* Nat. Commun. **11**, 6003 (2020). DOI: 10.1038/s41467-020-19836-0
10. M. Kauth, S. Rosenkranz, A.H. Said, K.M. Taddei, Th. Wolf, F. Weber, *Soft elastic constants from phonon spectroscopy in hole-doped $Ba_{1-x}(K,Na)_xFe_2As_2$ and $Sr_{1-x}Na_xFe_2As_2$*, Phys. Rev. B. **102**, 144526 (2020). DOI: 10.1103/PhysRevB.102.144526
11. M.J. Krogstad, S. Rosenkranz, J.M Wozniak, G. Jennings, J.P.C. Ruff, J.T. Vaughey, R. Osborn, *Reciprocal Space Imaging of Ionic Correlations in Intercalation Compounds*, Nature Materials **19**, 63 – 68 (2020). DOI: 10.1038/s41563-019-0500-7

12. Bi-Xia Wang, Hong Zheng, E. Krivyakina, O. Chmaissem, Pietro Papa Lopes, J.W. Lynn, L.C. Gallington, Y. Ren, S. Rosenkranz, J.F. Mitchell, and D. Phelan, *Synthesis and characterization of bulk $Nd_{1-x}Sr_xNiO_2$ and $Nd_{1-x}Sr_xNiO_3$,* Phys. Rev. Materials **4**, 084409 (2020).
DOI: 10.1103/PhysRevMaterials.4.084409
13. Hong Zheng, Bi-Xia Wang, D. Phelan, Junjie Zhang, Yang Ren, M.J. Krogstad, S. Rosenkranz, R. Osborn, J.F. Mitchell, *Oxygen Inhomogeneity and Reversibility in Single Crystal $LaNiO_{3-\delta}$,* Crystals **10**, 557 (2020). DOI: 10.3390/cryst10070557
14. J.F. Khoury, A.J.E. Rettie, I. Robredo, M.J. Krogstad, C.D. Malliakas, A. Bergara, M.G. Vergniory, R. Osborn, S. Rosenkranz, D.Y. Chung, M.G. Kanatzidis, *A synthetic route to Ir_2In_8Q (Q = S, Se, Te): Dirac semimetal candidates with re-entrant structural modulations,* J. Am. Chem. Soc. **142**, 6312 (2020). DOI: 10.1021/jacs.0c00809
15. Z. Wang, X. Zhang, J. Xia, L. Zhao, K. Wu,G. Yu, K.L.Wang, X. Liu, S.G.E. te Velthuis, A. Hoffmann, Y. Zhous, W. Jiang, *Generation and Hall effect of skyrmions enabled using nonmagnetic point contacts,* Phys. Rev. B. **100**, 184426 (2019). DOI: 10.1103/PhysRevB.100.184426
16. B.-X. Wang, H. Zheng, Y. Ren, M.J. Krogstad, J.F. Mitchell, D. Phelan, *Single Crystal Growth of Relaxor Ferroelectric $Ba_2PrFeNb_4O_{15}$ by the optical floating zone method*, Crystal Growth and Design, **19**, 7249 – 7256 (2019). DOI: 10.1021/acs.cgd.9b01147
17. D. Phelan, M.J. Krogstad, N.J. Schreiber, R. Osborn, A.H. Said, H. Zheng, S. Rosenkranz, *Acoustic phonon dispersion and diffuse scattering across the valence transition of $(Pr_{0.85}Y_{0.15})_{0.7}Ca_{0.3}CoO_{3-d}$,*
Phys. Rev. B **100**, 054101 (2019). DOI: 10.1103/Phys.RevB.100.054101
18. S.G.E. te Velthuis, *The 14th Joint Magnetism and Magnetic Materials - Intermag Conference*,
AIP Advances **9**, 050401 (2019). DOI: 10.1063/1.5109432
19. K. Chapagain, D.E. Brown, S. Kolesnik, S. Lapidus, B. Haberl, J. Molaison, C. Lin, C. Kenney-Benson, C. Park, J. Pietosa, E. Markiewicz, B. Andrezejeski, J.W. Lynn, S. Rosenkranz, B. Dabrowski, O. Chmaisssem, *Tunable Multiferroic Order Parameters in $Sr_{1-x}Ba_xMn_{1-y}Ti_yO_3$,*
Phys. Rev. Materials **3**, 084401 (2019). DOI: 10.1103/PhysRevMaterials.3.084401
20. H. Zheng, J. Zhang, B. Wang, D. Phelan, M.J. Krogstad, Y. Ren, W.A. Phelan, O. Chmaissem, B. Poudel, J.F. Mitchell, *High pO_2 Floating Zone Single Crystal Growth of the Perovskite Nickelate $PrNiO_3$*, Crystals **9**, 324 (2019). DOI: 10.3390/cryst9070324
21. J.A.W. Straquadine, F. Weber, S. Rosenkranz, A.H. Said, I.R. Fisher, *Suppression of charge density wave order by disorder in Pd-intercalated $ErTe_3$*, Phys. Rev. B **99**, 235138 (2019).
22. Junjie Zhang, D.M. Pajerowski, A.S. Botana, L. Harriger, J. Rodriguez-Rivera, J.P.C. Ruff. N.J. Schreiber, B. Wang, Yu-Sheng Chen, M.R. Norman, S. Rosenkranz, J.F. Mitchell, D. Phelan, *Spin-stripe order in a square planar trilayer nickelate*, Phys. Rev. Lett. **122**, 247201 (2019).
DOI: 10.1103/PhysRevLett.122.247201
23. Z. Sefrioui, Yaohua Liu, C. Leon, S.G.E. te Velthuis, M. Bibes, A. Barthelemy, J. Santamaria, *Novel Functionalities in Oxide Magnetic Tunnel Junctions: Spin Filtering by Interface-Induced Magnetism*, in *Oxide Spintronics*, editor Tamalika Banerjee (Jenny Stanford Publishing, New York, 2019). DOI: 10.1201/9780429468193-7

National School on Neutron and X-ray Scattering

Stephan Rosenkranz[1], Matthias Frontzek[2], Bianca Haberl[2], Michael Manley[3], Uta Ruett[4]

[1]Materials Science Division, Argonne National Laboratory, Lemont, IL 60439
[2]Neutron Scattering Division, Oak Ridge National Laboratory, Oak Ridge, TN 37831
[3]Materials Science and Technology Division, ORNL, Oak Ridge, TN 37831
[4]X-ray Science Division, Argonne National Laboratory, Lemont, IL 60439

Program Scope

The National School on Neutron and X-ray Scattering (NXS) provides a comprehensive introduction to the underlying theory of neutron and synchrotron x-ray scattering and related experimental techniques that are available at national facilities. The program includes both classroom lectures from experts in the field and hands-on experiments. The school plays an important strategic role in educating the United States scientific community in the capabilities of its national neutron and x-ray user facilities. The NXS was initiated at Argonne National Laboratory (ANL) in 1999, but since 2008 is jointly organized by ANL and Oak Ridge National Laboratory (ORNL) with participants spending equal time at both sites. However, due to COVID related travel and access restrictions, NXS was forced to be held in a virtual format for the last two years. NXS distinguishes itself from other topical schools in the United States by providing a broad grounding in the fundamentals of both neutron and x-ray techniques. NXS emphasizes the complementarity of the various structural, spectroscopic, and imaging probes and exposes participants to a wide cross-section of the techniques available at national neutron and x-ray facilities.

Fig. 1: NXS logo composed from the photos of all 2020 participants (credit: Genevieve Martin, ORNL).

Recent Progress

The 22nd and 23rd NXS were held from June 13-27, 2020, and July 12 – 30, 2021, respectively. Interest from the scientific community in the school remains strong with a high oversubscription rate, by a factor of 3 or more. In 2020, 256 students applied from most states of the US as well as from Canada for the nominally 60 seats available. However, just when the review of the applications started, the format of the NXS had to be changed due to the COVID-19 pandemic. The subsequent change on short notice to a virtual format meant that no hands-on training - the pinnacle of the NXS - could be offered. But on the upside, it was possible to admit all applicants (see the collage in Fig.1) and provide them the opportunity to learn the theoretical basics from extended lectures. Because of the larger number of participants and the platform available at the time, interactions were very limited with students not being able to ask questions in person, though questions could be posted in the chat window. In order to enable interactions and networking with lecturers, beamline scientists, and fellow participants, ten parallel interaction 'rooms', setup as bluejeans meetings with students able to talk and enable their camera if they wanted, were offered three times each week in the evenings with scientists and lecturers present. While these rooms led to lively and inspiring interactions and were appreciated by the students, the feedback received at the end of NXS clearly revealed that more direct interaction during the lectures and hands-on experiments were dearly missed by students, lecturers, and all scientists participating in the school. However, the students were very thankful that the school took place, when many other programs were canceled during the first year of the pandemic.

While NXS in 2021 still had to be held in a virtual format due to continuing travel and site access restrictions, APS at ANL and SNS and HFIR at ORNL all offered remote user experiments by the time the school took place. Based on the lessons learned and feedback received from NXS2020, the virtual format for NXS2021 was therefore adapted to allow for more interactions of the students with lecturer and staff scientists and to

Fig. 2: Participants and organizers of the NXS2021 (credit: Genevieve Martin, ORNL).

provide practical experience via remote experiments. The latter however again imposed a limit of 60 participants (shown in Fig. 2), out of 197 applications received in 2021, as was also the case for previous regular onsite schools. Because the students and lecturers were spread across all continental US time zones as well as one student from Hawaii, there was a reduced number of hours available for lectures and experiments each day. NXS2021 was therefore extended to three weeks, with the first week focused on introductory lectures and the second and third weeks in the more traditional format of being focused on ANL and ORNL respectively, with lectures covering more advanced topics and remote experiments. For most of the lectures a 'flipped' classroom format was utilized, whereby students were instructed to watch the recorded lectures from the previous year ahead of time, followed by live sessions where lecturers could revisit the most important points and students had ample time to directly ask questions. Though demanding on the student's efforts, this flipped classroom concept led to lively interactive sessions. Further online tools such as Slack for persistent questions/answers, Gather.town for social interaction and allowing students to present posters of their research (Fig. 3), and Microsoft forms for daily feedback were used. The remote experiments were performed in small groups of 4-5 students. Each student was assigned 8 experiments out of 46 different experiments offered, taking into consideration the students' preferences while also ensuring they cover a wide range of techniques across all facilities. Using various online platforms, students could interact with the beamline scientists, analyze data, and for many experiments remotely control the instruments. At the APS, some experiments further utilized Hololens and HMT-1 headsets that provided the students a live view of the facility, beamline, and experiment control and data analysis through the experimenter's eyes. The feedback for NXS2021 and in particular the remote practical experience was very positive, though the format to watch prerecorded lectures ahead of time and the extended duration over three weeks was generally regarded as to demanding for the students.

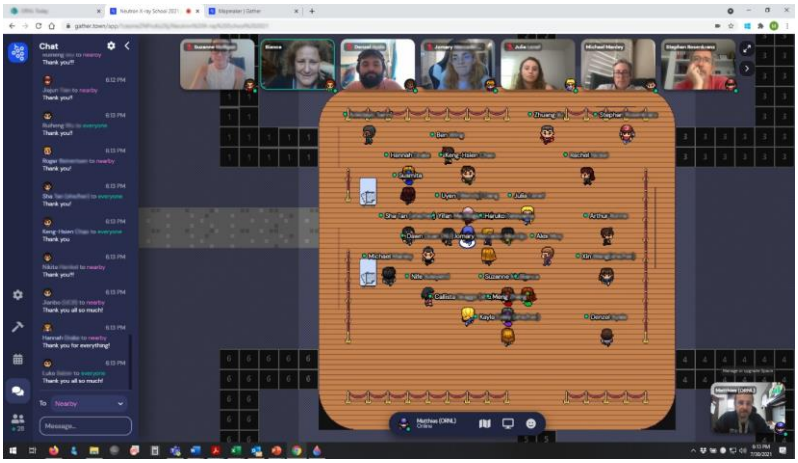

Fig. 3: Example of a busy evening in Gather.town.

To date, a total of 1322 students have attended NXS, not including NXS2020 when all applicants were admitted and no experiments were offered. While students are selected solely based on qualifications and merit evidenced in their application, the yearly NXS

cohort are very diverse and represent a wide range of scientific areas. The national character of the school is also reflected in the wide geographic distribution of the participants that have attended. Participating students have represented 178 unique North American colleges and universities, spread over 49 different states, Washington DC, Puerto Rico, Canada, and Mexico. About 18% of the participants were students at schools in EPSCoR states. The distribution of the participants over the different states or territories generally tracks the distribution of the applicants.

The long-term impact of NXS was most recently assessed in 2019 through a survey sent to participants from all previous schools, 1999-2018, supplementing an earlier survey conducted in 2014. These surveys show that a large fraction of NXS alumni used at least one DOE-funded facility as part of their thesis research, and many are still using these facilities, see Fig. 4. A large number of NXS Alumni are now faculty at U.S. Universities and an equal number have staff positions at U.S. National Laboratories, in programmatic and facilities divisions (Fig. 5), highlighting the impact NXS has in training future users of, and beamline scientists at, national neutron and x-ray facilities.

Future Plans

Based on feedback received in previous years, NXS will be held again for a period of two weeks, with dates chosen to minimize overlap with the academic year, other schools, and conferences, yet coinciding with the operation of the three facilities involved. If conditions in 2022 allow, the school will be held again in person with students spending one week at ANL and one week at ORNL. The 24th NXSchool is planned to be held July 11-22, 2022. Because of the foreseen upgrade of the APS in 2023, experimental sessions will be recorded in 2022 as the base for meaningful instructions and introduction into the data analysis to provide enhanced virtual synchrotron x-ray experiments even when APS is not running.

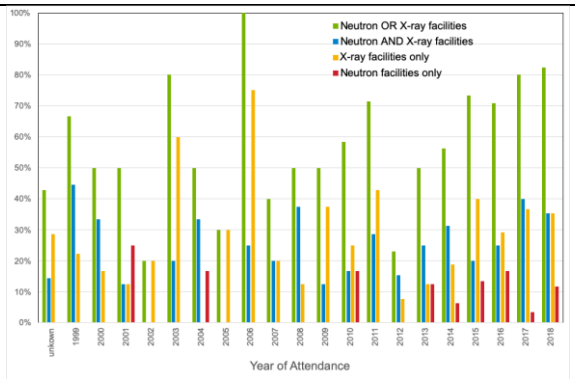

Fig. 4: Percentages of 1999-2018 participants who are still using neutron and or x-ray facilities.

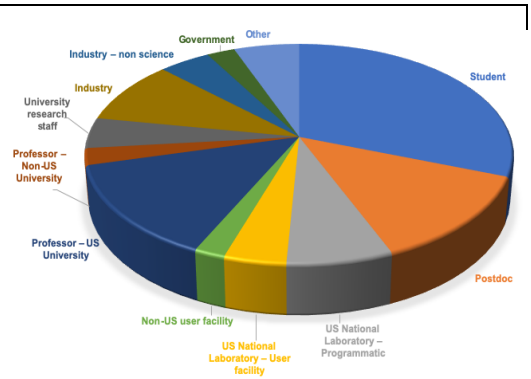

Fig. 5: Distribution of positions held in 2019 of NXS 1999-2018 participants.

Publications

Matthias Frontzek, Bianca Haberl, Michael E. Manley, Uta Ruett, Stephan Rosenkranz, *The 22nd National School on Neutron and X-ray Scattering 2020 – Upsides of going virtual*, Neutron News **31**, 4-6 (2020). DOI: 10.1080/10448632.2020.1822694

Matthias Frontzek, Bianca Haberl, Michael E. Manley, Stephan Rosenkranz, Uta Ruett, *The 23rd National School on Neutron & X-ray Scattering 2021 – virtual school with remote experiments*, Neutron News *in print*

Neutron Scattering Studies of Unconventional Superconductors

John M. Tranquada, Genda Gu, Cedomir Petrovic, and Igor A. Zaliznyak
Condensed Matter Physics and Materials Science Division
Brookhaven National Laboratory, Upton, NY 11973-5000

Program Scope

We combine exploratory synthesis, crystal growth, and neutron scattering techniques to address key questions associated with strong interactions in quantum materials, from high-temperature superconductors to magnetic semi-metals. In particular, how can we properly understand itinerant antiferromagnetism, and what is the role of intertwined orders in cuprate and iron-based superconductors? Can one exploit the interaction of spin-polarized itinerant states with local magnetic moments to obtain unprecedented responses to external stimuli? Advanced synthesis techniques are used to discover new model compounds, and high-quality crystals are grown of the most interesting materials. We exploit the latest neutron-scattering technologies available at national neutron user facilities, such as the Spallation Neutron Source and the High Flux Isotope Reactor, to obtain direct information on spin correlations and atomic displacements necessary to provide transformative answers to these questions. One such technology, in whose development we have actively participated, is time-of-flight, polarized, inelastic neutron spectroscopy. Complementary characterizations and theoretical analysis are performed in collaboration with other groups in the Condensed Matter Physics and Materials Science Division, especially using the National Synchrotron Light Source II and the Center for Functional Nanomaterials.

Recent Progress

Charge stripes and superconductivity in cuprates: Analysis of neutron scattering measurements of the temperature-dependent appearance of one-dimensional spin excitations in stripe ordered $La_{1.67}Sr_{0.33}NiO_4$ [8] led to us to the recognition that antiphase spin stripes cause a decoupling (through geometric frustration) of the spin degrees of freedom within the charge stripes from the surrounding order. Taking this lesson and applying it to cuprates leads to a new understanding of the "hourglass" spin excitation spectrum observed in superconducting cuprates, including $La_{2-x}Ba_xCuO_4$ (LBCO) with x = 1/8 [76]. The absence of low-energy spin excitations at the antiferromagnetic wave vector indicates that the spin excitations on the charge stripes must be gapped. The gap magnitude is indicated by the energy at which spin excitations appear at the antiferromagnetic wave vector, commonly interpreted as the neck of the hourglass. This argument leads to a picture of charge stripes as hole-doped 2-leg spin ladders, which are known to exhibit a spin gap associated with singlet-triplet spin excitations and pairing of holes.

Antiphase Josephson coupling between charge stripes would lead to pair-density-wave (PDW) superconducting order [16]. Collaborative transport measurements have now provided direct evidence for PDW order in LBCO with x = 1/8 [A]. Evidence that Zn impurities locally pin PDW correlations has also been obtained [98].

Charge-stripe correlations are also observed in $La_{2-x}Sr_xCuO_4$ [77,100], but because of differences in the structural symmetry from LBCO, it has been less clear what might cause pinning of charge stripes. We have now demonstrated by neutron scattering that the structure of the parent cuprate La_2CuO_4 has lower symmetry than previously assumed, such that orthogonal Cu-O bonds are inequivalent, which can lead to charge-stripe pinning when doped with holes [74].

Electronic properties of the bulk and surface states of $Fe_{1+y}Te_{1-x}Se_x$. By combining polarized neutron scattering with scanning angle-resolved photoemission spectroscopy and microprobe composition and resistivity measurements, we characterized the electronic state of $Fe_{1+y}Te_{1-x}Se_x$ [69]. This led us to establish a phase diagram in which the superconductivity is observed only at lower Fe concentration, in association with distinct antiferromagnetic correlations, while the coexisting topological surface state occurs only at higher Te concentration. We find that $Fe_{1+y}Te_{0.55}Se_{45}$, a composition for which a topological surface state was initially reported, is located very close to both phase boundaries, which explains the inhomogeneity of superconducting and topological states detected in the follow-up experiments. Our results demonstrate the compositional control required for use of topological Majorana zero modes in practical applications and pave the way for translational engineering of $Fe_{1+y}Te_{1-x}Se_x$ based topological superconductor materials.

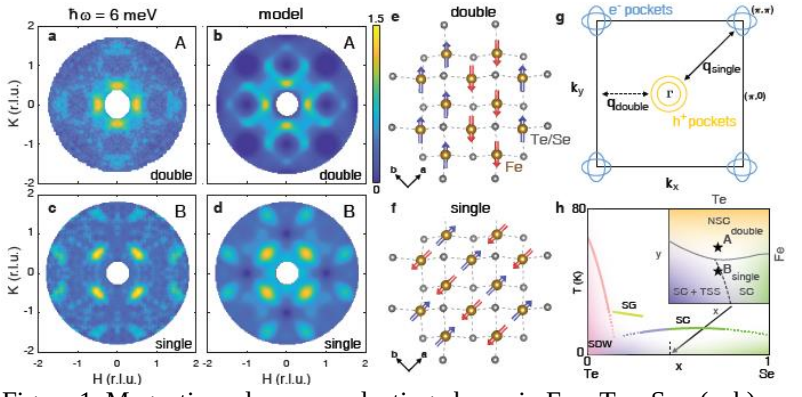

Figure 1. Magnetic and superconducting phases in $Fe_{1+y}Te_{1-x}Se_x$. (a, b) Magnetic neutron scattering (P||Q, spin-flip channels) at 5K for non-superconducting (NSC) and superconducting (SC) samples A and B, respectively, at 6(1) meV. The color bar indicates absolute neutron scattering intensity from 0 to 1.5 mbarn/sr/meV/f.u. (c, d) Model fit of the neutron scattering patterns in (a, b), respectively. The scattering for the NSC sample A reveals double-stripe (q_{double}) magnetism (e), while for SC a single-stripe (q_{single}) pattern (f). (g) Schematics of the Fermi surface in two-Fe unit cell indicating q_{single} and q_{double} wave-vectors. (h) Temperature-composition and Fe-Te (insert) phase diagrams. Stars show the average chemical composition of $Fe_{1+y}Te_{1-x}Se_x$ samples A and B.

Topology and strong correlations in intermetallic and 2D van der Waals (vdW) materials. As part of the exploratory materials effort, numerous Dirac and Weyl materials have been synthesized (typically as single crystals) and characterized with a variety of techniques. For example, LaAlGe is a type-II Weyl material in which very small effective electronic masses have been inferred from measurements of quantum oscillations in magnetic fields up to 35 T at the

National High Magnetic Field Laboratory [68]. Fe_3Sn_2, containing Fe layers with a breathing Kagome lattice structure, exhibits magnetic skyrmions at room temperature that are detectable by thermoelectric measurements [B]. Small-angle neutron scattering measurements revealed the variation of ferromagnetic domain texture with applied magnetic field, and its correlation with anisotropic magnetoresistance [3]. The discovery of $EuZnSb_2$ [14] provides a platform for investigating the interaction of charge fluctuations, localized Eu magnetic moments, and Dirac states with Sb orbital character. Other examples of 2D vdW materials that have been synthesized and characterized in the last two years include $Mn_3Si_2Te_6$ [35,73,102], 2H-$Co_{0.22}TaS_2$ [72], 2H-$Mn_{0.28}TaS_2$ [71], $FeCr_2Te_4$ [7,70], VI_3 [4], $CrCl_3$ [6], $Fe_{3-x}GeTe_2$ [42] and $Cr_2Ge_2Te_6$ [27].

Signatures of coupling between spin waves and Dirac fermions have been investigated in antiferromagnetic semimetal $YbMnBi_2$. The inelastic neutron scattering measurements of magnetic excitations revealed finite spin-wave lifetimes consistent with a direct coupling of magnetic excitations to Dirac charge carriers [10]. In contrast with the large broadening of magnetic spectra observed in antiferromagnetic metals such as the iron pnictides, here the spin waves exhibit a small but resolvable intrinsic width, consistent with our theoretical analysis. Accounting for the Dirac fermion dispersion specific to $YbMnBi_2$ leads to predicted signatures, such as the nearly wave-vector-independent damping, which was observed in the experiment. While its effect on spin waves is weak due to the vanishing density of states for Dirac fermions, the spin-fermion coupling constant refined from the comparison of our data with theory is quite large, implying potentially significant impact of magnetism on charge transport.

Future Plans

Polarized neutron scattering study of magnetic correlations across superconducting and non-superconducting phases of $Fe_{1+y}Te_{1-x}Se_x$ in the topological regime at $x<0.45$. Our recent studies including polarized measurements at HYSPEC of $Fe_{1+y}Te_{0.55}Se_{0.45}$ have established a composition-dependent phase diagram of $Fe_{1+y}(Te_{1-x}Se_x)$, where local magnetism greatly impacts the emergence of superconductivity and the topological phase. This phase diagram (Fig. 1h) is isomorphous to a diagram of correlated quantum phenomena in the strong spin-orbit regime, which predicts a wide variety of topological states (including Weyl semimetal and axion insulator) that have not been identified so far in $Fe_{1+y}(Te_{1-x}Se_x)$. This comparison inspires our planned further investigations of this system. The previous measurements were performed on $FeTe_{0.55}Se_{0.45}$, which is at the boundary of quantum and topological phase transitions (Fig. 1h), and on samples both inside the coherent superconductor and incoherent metal phases. In follow-up work, we plan to undertake full neutron polarization analysis of the low-energy magnetic excitations in non-superconducting (NSC) $Fe_{1+y}Te_{1-x}Se_x$, where topological band structure is disrupted by the local magnetism associated with slight Fe off-stoichiometry, and superconducting (SC) samples, in the strong spin-orbit regime, $x<0.45$, where topological superconductivity exists. As a first step, we will address these questions by performing polarized neutron measurements on SC and NSC $FeTe_{1-x}Se_x$ system with $x=0.3$.

Neutron scattering signatures of possible Weyl state and spin-fermion coupling in layered antiferromagnetic semi-metals. In the *A/R*Mn*X*$_2$ (*A* = Ca, Sr; *R* = Yb, Eu; *X* = Bi, Sb) materials, the *X* layers hosting itinerant Dirac electrons are separated by strongly-correlated magnetic Mn-*X* layers, which order antiferromagnetically, near, or above room temperature. The coupling of Dirac charge carriers and Mn magnetism can lead to novel physics, including Weyl semi-metallic behavior, which can be induced by the canting of the Mn moments that breaks time reversal symmetry and induces in-plane ferromagnetism (FM). However, our polarized and unpolarized diffraction measurements on a prototypical representative of the family, $YbMnBi_2$, revealed no spin-canting, albeit measurable spin-fermion coupling was observed through spin-wave damping [C]. Here, we plan to carry out polarized neutron diffraction study of sister materials, $CaMnBi_2$ and $YbMnSb_2$, where spin canting indicative of Weyl-state formation was reported based on bulk magnetometry measurements. In both cases, the putative in-plane spin-canting is associated with an anomaly in electrical conductivity. Neutron refinement of magnetism in these materials is fundamental to establish the Weyl physics. Using neutron scattering, we will also search for the signatures of spin-fermion coupling in spin-wave spectra of $YbMnSb_2$, following up on our previous work on $YbMnBi_2$. *A/R*$MnSb_2$ compounds have smaller (compared to Bi) spin-orbit coupling (SOC) on the 2D Sb square net. This implies closed, or reduced, SOC-induced gap near the Dirac point, which is favorable for coupling to magnons.

Lattice dynamics, structural stability, and thermoelastic properties of perovskites. In our recent work [15,75], an understanding of the unusual lattice dynamics and negative thermal expansion of ScF_3-type empty perovskites was developed based on the concept of Coulomb Floppy Networks (CFNs). This understanding led to a quantitative description of empty perovskites, which is in excellent agreement with experiment. In future work, we plan to apply the CFN description to the equation of state, V(P,T) of ScF_3 and explain the colossal pressure-induced softening observed in this material close to structural phase transition. We will also undertake additional neutron diffraction measurements, under pressure, of the equation of state and the (P, T) phase diagram of ScF_3 and confront the new results with the CFN theory. Finally, we will extend the CFN description to other perovskite classes with the goal to develop an intuitive description of lattice properties of $SrTiO_3$, which is important for understanding the low-carrier-density superconductivity observed in this material at low doping.

References

A. P. M. Lozano, Tianhao Ren, G. D. Gu, A. M. Tsvelik, J. M. Tranquada, and Qiang Li, "Phase-sensitive evidence of pair-density-wave order in a cuprate," arXiv:2110.05513.

B. Qianheng Du, Myung-Geun Han, Yu Liu, Weijun Ren, Yimei Zhu, and Cedomir Petrovic, Adv. Quantum Technol. **3**, 2000058 (2020).

C. A. Sapkota, L. Classen, M. B. Stone, A. T. Savici, V. O. Garlea, Aifeng Wang, J. M. Tranquada, C. Petrovic, I. A. Zaliznyak. Signatures of coupling between spin waves and Dirac fermions in $YbMnBi_2$. Phys. Rev. B **101**, 041111(R) (2019).

Publications

1. Zhixiang Hu, D. Graf, Yu Liu, and C. Petrovic, "Three-dimensional Fermi surface and small effective masses in Mo8Ga41," Appl. Phys. Lett. **116**, 202601 (2020).

2. Yangmu Li, Jie Wu, Fernando Camino, G. D. Gu, Ivan Bozovic, and John M. Tranquada, "Large surface conductance and superconductivity in topological insulator microstructures," Appl. Phys. Lett. **115**, 173507 (2019).

3. Yangmu Li, Qi Wang, Lisa DeBeer-Schmitt, Zurab Guguchia, Ryan D. Desautels, Jia-Xin Yin, Qianheng Du, Weijun Ren, Xinguo Zhao, Zhidong Zhang, Igor A. Zaliznyak, Cedomir Petrovic, Weiguo Yin, M. Zahid Hasan, Hechang Lei, and John M. Tranquada, "Magnetic-Field Control of Topological Electronic Response near Room Temperature in Correlated Kagome Magnets," Phys. Rev. Lett. **123**, 196604 (2019).

4. Yu Liu, Milinda Abeykoon, and C. Petrovic, "Critical behavior and magnetocaloric effect in VI3," Phys. Rev. Research **2**, 013013 (2020).

5. Yu Liu, Zhixiang Hu, and C. Petrovic, "Anisotropic magnetocaloric effect and critical behavior in CrSbSe3," Phys. Rev. B **102**, 014425 (2020).

6. Yu Liu and C. Petrovic, "Anisotropic magnetocaloric effect and critical behavior in CrCl3," Phys. Rev. B **102**, 014424 (2020).

7. Yu Liu, R. J. Koch, Zhixiang Hu, Niraj Aryal, Eli Stavitski, Xiao Tong, Klaus Attenkofer, E. S. Bozin, Weiguo Yin, and C. Petrovic, "Three-dimensional Ising ferrimagnetism of Cr-Fe-Cr trimers in FeCr2Te4," Phys. Rev. B **102**, 085158 (2020).

8. A. M. Merritt, D. Reznik, V. O. Garlea, G. D. Gu, and J. M. Tranquada, "Nature and impact of stripe freezing in La1.67Sr0.33NiO4," Phys. Rev. B **100**, 195122 (2019).

9. S. E. Nikitin, Tao Xie, A. Podlesnyak, and I. A. Zaliznyak, "Experimental observation of magnetic dimers in diluted Yb:YAlO3," Phys. Rev. B **101**, 245150 (2020).

10. A. Sapkota, L. Classen, M. B. Stone, A. T. Savici, V. O. Garlea, Aifeng Wang, J. M. Tranquada, C. Petrovic, and I. A. Zaliznyak, "Signatures of coupling between spin waves and Dirac fermions in YbMnBi2," Phys. Rev. B **101**, 041111 (2020).

11. A. Sapkota, Y. Li, B. L. Winn, A. Podlesnyak, Guangyong Xu, Zhijun Xu, Kejing Ran, Tong Chen, Jian Sun, Jinsheng Wen, Lihua Wu, Jihui Yang, Qiang Li, G. D. Gu, and J. M. Tranquada, "Electron-phonon coupling and superconductivity in the doped topological crystalline insulator (Pb0.5Sn0.5)1−xInxTe," Phys. Rev. B **102**, 104511 (2020).

12. E. G. Sergeicheva, S. S. Sosin, D. I. Gorbunov, S. Zherlitsyn, G. D. Gu, and I. A. Zaliznyak, “Unexpected magnetic phase in the weakly ordered spin-1/2 chain cuprate Sr2CuO3,” Phys. Rev. B **101**, 201107 (2020).

13. J. M. Tranquada, Guangyong Xu, and I. A. Zaliznyak, “Magnetism and superconductivity in Fe1+yTe1−xSex,” J. Phys. Condens. Matter **32**, 374003 (2020).

14. Aifeng Wang, Sviatoslav Baranets, Yu Liu, Xiao Tong, E. Stavitski, Jing Zhang, Yisheng Chai, Wei-Guo Yin, Svilen Bobev, and C. Petrovic, “Magnetic mixed valent semimetal EuZnSb2 with Dirac states in the band structure,” Phys. Rev. Research **2**, 033462 (2020).

15. David Wendt, Emil Bozin, Joerg Neuefeind, Katharine Page, Wei Ku, Limin Wang, Brent Fultz, Alexei V. Tkachenko, and Igor A. Zaliznyak, “Entropic elasticity and negative thermal expansion in a simple cubic crystal,” Sci. Adv. **5**, aay2748 (2019).

16. Daniel F. Agterberg, J.C. Seamus Davis, Stephen D. Edkins, Eduardo Fradkin, Dale J. Van Harlingen, Steven A. Kivelson, Patrick A. Lee, Leo Radzihovsky, John M. Tranquada, and Yuxuan Wang, “The Physics of Pair-Density Waves: Cuprate Superconductors and Beyond,” Annu. Rev. Condens. Matter Phys. **11**, 231–270 (2020).

17. T. A. Assefa, Y. Cao, J. Diao, R. J. Harder, W. Cha, K. Kisslinger, G. D. Gu, J. M. Tranquada, M. P. M. Dean, and I. K. Robinson, “Scaling behavior of low-temperature orthorhombic domains in the prototypical high-temperature superconductor La1.875Ba0.125CuO4,” Phys. Rev. B **101**, 054104 (2020).

18. N. Auvray, B. Loret, S. Benhabib, M. Cazayous, R. D. Zhong, J. Schneeloch, G. D. Gu, A. Forget, D. Colson, I. Paul, A. Sacuto, and Y. Gallais, “Nematic fluctuations in the cuprate superconductor Bi2Sr2CaCu2O8+δ,” Nat. Commun. **10**, 5209 (2019).

19. Lu Chen, Ziji Xiang, Colin Tinsman, Bin Lei, Xianhui Chen, G. D. Gu, and Lu Li, “Spontaneous Nernst effect in the iron-based superconductor Fe1+yTe1−xSex,” Phys. Rev. B **102**, 054503 (2020).

20. Kevin A. Cremin, Jingdi Zhang, Christopher C. Homes, G. D. Gu, Zhiyuan Sun, Michael M. Fogler, Andrew J. Millis, D. N. Basov, and Richard D. Averitt, “Photoenhanced metastable c-axis electrodynamics in stripe-ordered cuprate La1.885Ba0.115CuO4,” Proc. Natl. Acad. Sci. USA **116**, 19875–19879 (2019).

21. Zengyi Du, Hui Li, Sang Hyun Joo, Elizabeth P. Donoway, Jinho Lee, J. C. Seamus Davis, Genda Gu, Peter D. Johnson, and Kazuhiro Fujita, “Imaging the energy gap modulations of the cuprate pair-density-wave state,” Nature **580**, 65–70 (2020).

22. K. Fujita, I. Drozdov, Z. Du, H. Li, S.-H. Joo, J. Lee, G. Gu, P. D. Johnson, and T. Valla, "Combined spectroscopic imaging STM and ARPES study of different gaps measured in the cuprate phase diagram," Phys. Rev. B **101**, 045136 (2020).

23. Qiang Gao, Hongtao Yan, Jing Liu, Ping Ai, Yongqing Cai, Cong Li, Xiangyu Luo, Cheng Hu, Chunyao Song, Jianwei Huang, Hongtao Rong, Yuan Huang, Qingyan Wang, Guodong Liu, Genda Gu, Fengfeng Zhang, Feng Yang, Shenjin Zhang, Qinjun Peng, Zuyan Xu, Lin Zhao, Tao Xiang, and X. J. Zhou, "Selective hybridization between the main band and the superstructure band in the Bi2Sr2CaCu2O8+δ superconductor," Phys. Rev. B **101**, 014513 (2020).

24. S. Gheidi, K. Akintola, A. C. Y. Fang, Shyam Sundar, A. M. Cote, S. R. Dunsiger, G. D. Gu, and J. E. Sonier, "Absence of μSR evidence for magnetic order in the pseudogap phase of Bi2+xSr2−xCaCu2O8+δ," Phys. Rev. B **101**, 184511 (2020).

25. Z. Guguchia, D. Das, C. N. Wang, T. Adachi, N. Kitajima, M. Elender, F. Brückner, S. Ghosh, V. Grinenko, T. Shiroka, M. Müller, C. Mudry, C. Baines, M. Bartkowiak, Y. Koike, A. Amato, J. M. Tranquada, H.-H. Klauss, C. W. Hicks, and H. Luetkens, "Using Uniaxial Stress to Probe the Relationship between Competing Superconducting States in a Cuprate with Spin-stripe Order," Phys. Rev. Lett. **125**, 097005 (2020).

26. Jing Guo, Yazhou Zhou, Cheng Huang, Shu Cai, Yutao Sheng, Genda Gu, Chongli Yang, Gongchang Lin, Ke Yang, Aiguo Li, Qi Wu, Tao Xiang, and Liling Sun, "Crossover from two-dimensional to three-dimensional superconducting states in bismuth-based cuprate superconductor," Nat. Phys. **16**, 295–300 (2020).

27. Myung-Geun Han, Joseph A. Garlow, Yu Liu, Huiqin Zhang, Jun Li, Donald DiMarzio, Mark W. Knight, Cedomir Petrovic, Deep Jariwala, and Yimei Zhu, "Topological Magnetic-Spin Textures in Two-Dimensional van der Waals Cr2Ge2Te6," Nano Lett. **19**, 7859–7865 (2019).

28. Xinguo Hong, Matt Newville, Yang Ding, Tetsuo Irifune, Genda Gu, and Ho-Kwang Mao, "Distinct intermediate states in the isostructural R−3m phase of the topological insulator Bi2Se3 at high pressure," Phys. Rev. B **101**, 214107 (2020).

29. Ali A. Husain, Matteo Mitrano, Melinda S. Rak, Samantha Rubeck, Bruno Uchoa, Katia March, Christian Dwyer, John Schneeloch, Ruidan Zhong, G. D. Gu, and Peter Abbamonte, "Crossover of Charge Fluctuations across the Strange Metal Phase Diagram," Phys. Rev. X **9**, 041062 (2019).

30. Lingyuan Kong, Shiyu Zhu, Michael Papaj, Hui Chen, Lu Cao, Hiroki Isobe, Yuqing Xing, Wenyao Liu, Dongfei Wang, Peng Fan, Yujie Sun, Shixuan Du, John Schneeloch, Ruidan

Zhong, Genda Gu, Liang Fu, Hong-Jun Gao, and Hong Ding, “Half-integer level shift of vortex bound states in an iron-based superconductor,” Nat. Phys. **15**, 1181–1187 (2019).

31. Jooseop Lee, Karel Prokeš, Sohee Park, Igor Zaliznyak, Sachith Dissanayake, Masaaki Matsuda, Matthias Frontzek, Stanislav Stoupin, Greta L. Chappell, Ryan E. Baumbach, Changwon Park, John A. Mydosh, Garrett E. Granroth, and Jacob P. C. Ruff, “Charge density wave with anomalous temperature dependence in UPt2Si2,” Phys. Rev. B **102**, 041112(R) (2020).

32. J. Q. Lin, H. Miao, D. G. Mazzone, G. D. Gu, A. Nag, A. C. Walters, M. Garcia-Fernandez, A. Barbour, J. Pelliciari, I. Jarrige, M. Oda, K. Kurosawa, N. Momono, Ke-Jin Zhou, V. Bisogni, X. Liu, and M. P. M. Dean, “Strongly Correlated Charge Density Wave in La2−xSrxCuO4 Evidenced by Doping-Dependent Phonon Anomaly,” Phys. Rev. Lett. **124**, 207005 (2020).

33. B. Loret, N. Auvray, G. D. Gu, A. Forget, D. Colson, M. Cazayous, Y. Gallais, I. Paul, M. Civelli, and A. Sacuto, “Universal relationship between the energy scales of the pseudogap phase, the superconducting state, and the charge-density-wave order in copper oxide superconductors,” Phys. Rev. B **101**, 214520 (2020).

34. Yongchang Ma, Dong Wu, Cuimin Lu, and Cedomir Petrovic, “The electric pulses induced multi-resistance states in the hysteresis temperature range of 1T-TaS2 and 1T-TaS1.6Se0.4,” Appl. Phys. Lett. **116**, 171906 (2020).

35. L. M. Martinez, H. Iturriaga, R. Olmos, L. Shao, Y. Liu, Thuc T. Mai, C. Petrovic, Angela R. Hight Walker, and S. R. Singamaneni, “Enhanced magnetization in proton irradiated Mn3Si2Te6 van der Waals crystals,” Appl. Phys. Lett. **116**, 172404 (2020).

36. A. M. Merritt, J.-P. Castellan, T. Keller, S. R. Park, J. A. Fernandez-Baca, G. D. Gu, and D. Reznik, “Low-energy phonons in Bi2Sr2CaCu2O8+δ and their possible interaction with electrons measured by inelastic neutron scattering,” Phys. Rev. B **100**, 144502 (2019).

37. A. M. Merritt, A. D. Christianson, A. Banerjee, G. D. Gu, A. S. Mishchenko, and D. Reznik, “Giant electron–phonon coupling of the breathing plane oxygen phonons in the dynamic stripe phase of La1.67Sr0.33NiO4,” Sci. Rep. **10**, 11426 (2020).

38. Ana Milosavljevic, Andrijana Solajic, Bojana Visic, Marko Opacic, Jelena Pesic, Yu Liu, Cedomir Petrovic, Zoran V. Popovic, and Nenad Lazarevic, “Vacancies and spin–phonon coupling in CrSi0.8Ge0.1Te3,” J. Raman Spectrosc., 1–8 (2020), https://onlinelibrary.wiley.com/doi/abs/10.1002/jrs.5962.

39. Matteo Mitrano, Sangjun Lee, Ali A. Husain, Minhui Zhu, Gilberto de la Pena Munoz, Stella X.-L. Sun, Young Il Joe, Alexander H. Reid, Scott F. Wandel, Giacomo Coslovich, William Schlotter, Tim van Driel, John Schneeloch, G. D. Gu, Nigel Goldenfeld, and Peter

Abbamonte, “Evidence for photoinduced sliding of the charge-order condensate in La1.875Ba0.125CuO4,” Phys. Rev. B **100**, 205125 (2019).

40. Y. Nambu, J. Barker, Y. Okino, T. Kikkawa, Y. Shiomi, M. Enderle, T. Weber, B. Winn, M. Graves-Brook, J. M. Tranquada, T. Ziman, M. Fujita, G. E. W. Bauer, E. Saitoh, and K. Kakurai, “Observation of Magnon Polarization,” Phys. Rev. Lett. **125**, 027201 (2020).

41. Toshinori Ozaki, Lijun Wu, Genda Gu, and Qiang Li, “Ion irradiation of iron chalcogenide superconducting films,” Supercond. Sci. Technol. **33**, 094008 (2020).

42. Se Young Park, Dong Seob Kim, Yu Liu, Jinwoong Hwang, Younghak Kim, Wondong Kim, Jae-Young Kim, Cedomir Petrovic, Choongyu Hwang, Sung-Kwan Mo, Hyung-jun Kim, Byoung-Chul Min, Hyun Cheol Koo, Joonyeon Chang, Chaun Jang, Jun Woo Choi, and Hyejin Ryu, “Controlling the Magnetic Anisotropy of the van der Waals Ferromagnet Fe3GeTe2 through Hole Doping,” Nano Lett. **20**, 95–100 (2020).

43. Bryan Rachmilowitz, He Zhao, Hong Li, Alexander LaFleur, J. Schneeloch, Ruidan Zhong, Genda Gu, and Ilija Zeljkovic, “Proximity-induced superconductivity in a topological crystalline insulator,” Phys. Rev. B **100**, 241402(R) (2019).

44. T. J. Reber, X. Zhou, N. C. Plumb, S. Parham, J. A. Waugh, Y. Cao, Z. Sun, H. Li, Q. Wang, J. S. Wen, Z. J. Xu, G. Gu, Y. Yoshida, H. Eisaki, G. B. Arnold, and D. S. Dessau, “A unified form of low-energy nodal electronic interactions in hole-doped cuprate superconductors,” Nat. Commun. **10**, 5737 (2019).

45. Ian Robinson, Tadesse A. Assefa, Yue Cao, Genda Gu, Ross Harder, Evan Maxey, and Mark P. M. Dean, “Domain Texture of the Orthorhombic Phase of La2−xBaxCuO4,” J. Supercond. Nov. Magn. **33**, 99–106 (2020).

46. D. Santos-Cottin, M. Padlewski, E. Martino, S. Ben David, F. Le Mardele, F. Capitani, F. Borondics, M. D. Bachmann, C. Putzke, P. J. W. Moll, R. D. Zhong, G. D. Gu, H. Berger, M. Orlita, C. C. Homes, Z. Rukelj, and Ana Akrap, “Probing intraband excitations in ZrTe5: A high-pressure infrared and transport study,” Phys. Rev. B **101**, 125205 (2020).

47. Sehun Seo, Heesung Noh, Ning Li, Jianyi Jiang, Chiara Tarantini, Ruochen Shi, Soon-Gil Jung, Myeong Jun Oh, Mengchao Liu, Jongmin Lee, Genda Gu, Youn Jung Jo, Tuson Park, Eric E. Hellstrom, Peng Gao, and Sanghan Lee, “Artificially engineered nanostrain in FeSexTe1-x superconductor thin films for supercurrent enhancement,” NPG Asia Mater. **12**, 7 (2020).

48. Resta A. Susilo, Bo Gyu Jang, Jiajia Feng, Qianheng Du, Zhipeng Yan, Hongliang Dong, Mingzhi Yuan, Cedomir Petrovic, Ji Hoon Shim, Duck Young Kim, and Bin Chen, “Band gap crossover and insulator–metal transition in the compressed layered CrPS4,” npj Quantum Mater. **5**, 58 (2020).

49. T. Valla, I. Pletikosic, I. K. Drozdov, and G. D. Gu, "Reconstruction of the Bi2Sr2CaCu2O8+δ Fermi surface," Phys. Rev. B **100**, 241112(R) (2019).

50. T. Valla, I. K. Drozdov, and G. D. Gu, "Disappearance of superconductivity due to vanishing coupling in the overdoped Bi2Sr2CaCu2O8+δ," Nat. Commun. **11**, 569 (2020).

51. Siyuan Wan, Qiangqiang Gu, Huazhou Li, Huan Yang, J. Schneeloch, R. D. Zhong, G. D. Gu, and Hai-Hu Wen, "Twofold symmetry of proximity-induced superconductivity in Bi2Te3/Bi2Sr2CaCu2O8+δ heterostructures revealed by scanning tunneling microscopy," Phys. Rev. B **101**, 220503(R) (2020).

52. Zhenyu Wang, Jorge Olivares Rodriguez, Lin Jiao, Sean Howard, Martin Graham, G. D. Gu, Taylor L. Hughes, Dirk K. Morr, and Vidya Madhavan, "Evidence for dispersing 1D Majorana channels in an iron-based superconductor," Science **367**, 104–108 (2020).

53. Qi Wang, Qianheng Du, Cedomir Petrovic, and Hechang Lei, "Physical Properties of Half-Heusler Antiferromagnet MnPtSn Single Crystal," Chin. Phys. Lett. **37**, 027502 (2020).

54. J. Wu, A. T. Bollinger, X. He, G. D. Gu, H. Miao, M. P. M. Dean, I. K. Robinson, and I. Bozovic, "Angle-Resolved Transport Measurements Reveal Electronic Nematicity in Cuprate Superconductors," J. Supercond. Nov. Magn. **33**, 87–92 (2020).

55. Hui Yan, Nozomi Shirato, Xiangde Zhu, Daniel Rosenmann, Xiao Tong, Weihe Xu, Cedomir Petrovic, Volker Rose, and Evgeny Nazaretski, "X-ray Assisted Scanning Tunneling Microscopy and Its Applications for Materials Science: The First Results on Cu Doped ZrTe3," Crystals **9**, 588 (2019).

56. R. Yang, M. Corasaniti, C. C. Le, Z. Y. Liao, A. F. Wang, Q. Du, C. Petrovic, X. G. Qiu, J. P. Hu, and L. Degiorgi, "Spin-Canting-Induced Band Reconstruction in the Dirac Material Ca1−xNaxMnBi2," Phys. Rev. Lett. **124**, 137201 (2020).

57. T. Yilmaz, G. D. Gu, E. Vescovo, K. Kaznatcheev, and B. Sinkovic, "Photon energy and polarization-dependent electronic structure of Cr-doped Bi2Se3," Phys. Rev. Materials **4**, 024201 (2020).

58. Yijun Yu, Liguo Ma, Peng Cai, Ruidan Zhong, Cun Ye, Jian Shen, G. D. Gu, Xian Hui Chen, and Yuanbo Zhang, "High-temperature superconductivity in monolayer Bi2Sr2CaCu2O8+δ," Nature **575**, 156–163 (2019).

59. Wenjie Zhang, Peipei Wang, Brian Skinner, Ran Bi, Vladyslav Kozii, Chang-Woo Cho, Ruidan Zhong, John Schneeloch, Dapeng Yu, Genda Gu, Liang Fu, Xiaosong Wu, and Liyuan Zhang, "Observation of a thermoelectric Hall plateau in the extreme quantum limit," Nat. Commun. **11**, 1046 (2020).

60. Wenjie Zhang, Peipei Wang, Genda Gu, Xiaosong Wu, and Liyuan Zhang, "Negative longitudinal magnetothermopower in the topological semimetal ZrTe5," Phys. Rev. B **102**, 115147 (2020).

61. Yigui Zhong, Jianyu Guan, Jin Zhao, Cenyao Tang, Zhicheng Rao, Haijiang Liu, Jian-hao Zhang, Sen Li, Zhengyu Weng, Genda Gu, Yujie Sun, and Hong Ding, "Anomalous doping evolution of nodal dispersion revealed by in situ ARPES on continuously doped cuprates," Phys. Rev. B **100**, 184504 (2019).

62. Shiyu Zhu, Lingyuan Kong, Lu Cao, Hui Chen, Michael Papaj, Shixuan Du, Yuqing Xing, Wenyao Liu, Dongfei Wang, Chengmin Shen, Fazhi Yang, John Schneeloch, Ruidan Zhong, Genda Gu, Liang Fu, Yu-Yang Zhang, Hong Ding, and Hong-Jun Gao, "Nearly quantized conductance plateau of vortex zero mode in an iron-based superconductor," Science **367**, 189–192 (2020).

63. Dana Capitano, Zhixiang Hu, Yu Liu, Xiao Tong, Dmytro Nykypanchuk, Donald DiMarzio, and Cedomir Petrovic, "Synthesis and Characterization of Ultrathin $FeTe_2$ Nanocrystals," ACS Omega **6**, 10537–10546 (2021).

64. Qianheng Du, Huixia Fu, Junzhang Ma, A. Chikina, M. Radovic, Binghai Yan, and C. Petrovic, "Surface conductivity in antiferromagnetic semiconductor CrSb2," Phys. Rev. Research **2**, 043085 (2020).

65. Qianheng Du, Lijun Wu, Huibo Cao, Chang-Jong Kang, Christie Nelson, Gheorghe Lucian Pascut, Tiglet Besara, Theo Siegrist, Kristjan Haule, Gabriel Kotliar, Igor Zaliznyak, Yimei Zhu, and Cedomir Petrovic, "Vacancy defect control of colossal thermopower in FeSb2," npj Quantum Mater. **6**, 13 (2021).

66. Qianheng Du, Xiao Tong, Yu Liu, and C. Petrovic, "Suppression of thermal conductivity and electronic correlations in Fe1−xRuxSb2 ($0 \leq x \leq 0.6$)," Appl. Phys. Lett. **11**8, 171904 (2021).

67. Qianheng Du and Cedomir Petrovic, "Optimal carrier concentration for FeSb2 colossal thermopower," Appl. Phys. Lett. **118**, 233901 (2021).

68. Zhixiang Hu, Qianheng Du, Yu Liu, D. Graf, and C. Petrovic, "High Fermi velocities and small cyclotron masses in LaAlGe," Appl. Phys. Lett. **117**, 222410 (2020).

69. Yangmu Li, Nader Zaki, Vasile O. Garlea, Andrei T. Savici, David Fobes, Zhijun Xu, Fernando Camino, Cedomir Petrovic, Genda Gu, Peter D. Johnson, John M. Tranquada, and Igor A. Zaliznyak, "Electronic properties of the bulk and surface states of Fe1+yTe1−xSex," Nat. Mater. **20**, 1221–1227 (2021).

70. Yu Liu, Hengxin Tan, Zhixiang Hu, Binghai Yan, and C. Petrovic, "Anomalous Hall effect in the weak-itinerant ferrimagnet FeCr2Te4," Phys. Rev. B **103**, 045106 (2021).

71. Yu Liu, Zhixiang Hu, Eli Stavitski, Klaus Attenkofer, and C. Petrovic, “Three-dimensional ferromagnetism and magnetotransport in van der Waals Mn-intercalated tantalum disufide,” Phys. Rev. B **103**, 144432 (2021).

72. Yu Liu, Zhixiang Hu, Eli Stavitski, Klaus Attenkofer, and C. Petrovic, “Magnetic critical behavior and anomalous Hall effect in 2H−Co0.22TaS2 single crystals,” Phys. Rev. Research **3**, 023181 (2021).

73. Yu Liu, Zhixiang Hu, Milinda Abeykoon, Eli Stavitski, Klaus Attenkofer, Eric D. Bauer, and C. Petrovic, “Polaronic transport and thermoelectricity in Mn3Si2Te6 single crystals,” Phys. Rev. B **103**, 245122 (2021).

74. A. Sapkota, T. C. Sterling, P. M. Lozano, Yangmu Li, Huibo Cao, V. O. Garlea, D. Reznik, Qiang Li, I. A. Zaliznyak, G. D. Gu, and J. M. Tranquada, “Reinvestigation of crystal symmetry and fluctuations in La2CuO4,” Phys. Rev. B **104**, 014304 (2021).

75. Alexei V. Tkachenko and Igor A. Zaliznyak, “Empty perovskites as Coulomb floppy networks: Entropic elasticity and negative thermal expansion,” Phys. Rev. B **103**, 134106 (2021).

76. J. M. Tranquada, “Cuprate superconductors as viewed through a striped lens,” Adv. Phys. **6**9, 437–509 (2020).

77. John M. Tranquada, Mark P. M. Dean, and Qiang Li, “Superconductivity from Charge Order in Cuprates,” J. Phys. Soc. Jpn. **90**, 111002 (2021).

78. I. A. Zaliznyak, E. Bozin, and A. V. Tkachenko, “Comment on “Colossal Pressure-Induced Softening in Scandium Fluoride,” Phys. Rev. Lett. **126**, 179601 (2021).

79. Michael E. Berkowitz, Brian S. Y. Kim, Guangxin Ni, Alexander S. McLeod, Chiu Fan Bowen Lo, Zhiyuan Sun, Genda Gu, Kenji Watanabe, Takashi Taniguchi, Andrew J. Millis, James C. Hone, Michael M. Fogler, Richard D. Averitt, and D. N. Basov, “Hyperbolic Cooper-Pair Polaritons in Planar Graphene/Cuprate Plasmonic Cavities,” Nano Lett. **21**, 308–316 (2021).

80. F. Boschini, M. Minola, R. Sutarto, E. Schierle, M. Bluschke, S. Das, Y. Yang, M. Michiardi, Y. C. Shao, X. Feng, S. Ono, R. D. Zhong, J. A. Schneeloch, G. D. Gu, E. Weschke, F. He, Y. D. Chuang, B. Keimer, A. Damascelli, A. Frano, and E. H. da Silva Neto, “Dynamic electron correlations with charge order wavelength along all directions in the copper oxide plane,” Nat. Commun. **12**, 597 (2021).

81. Damianos Chatzopoulos, Doohee Cho, Koen M. Bastiaans, Gorm O. Steffensen, Damian Bouwmeester, Alireza Akbari, Genda Gu, Jens Paaske, Brian M. Andersen, and Milan P.

Allan, “Spatially dispersing Yu-Shiba-Rusinov states in the unconventional superconductor FeTe0.55Se0.45,” Nat. Commun. **12**, 298 (2021).

82. Shaobo Cheng, Xing Li, Changsong Xu, Yu Liu, Marco Beleggia, Lijun Wu, Wenbin Wang, Cedomir Petrovic, Laurent Bellaiche, Jing Tao, and Yimei Zhu, “Coexistence and Coupling of Multiple Charge Orderings and Spin States in Hexagonal Ferrite,” Nano Lett. **21**, 5782–5787 (2021).

83. Yi Xue Chong, Xiaolong Liu, Rahul Sharma, Andrey Kostin, Genda Gu, K. Fujita, J. C. Seamus Davis, and Peter O. Sprau, “Severe Dirac Mass Gap Suppression in Sb2Te3-Based Quantum Anomalous Hall Materials,” Nano Lett. **20**, 8001–8007 (2020).

84. M. Corasaniti, R. Yang, Z. Hu, M. Abeykoon, C. Petrovic, and L. Degiorgi, “Evidence for correlation effects in noncentrosymmetric type-II Weyl semimetals,” Phys. Rev. B **104**, L121112 (2021).

85. Sanja DjurdjicMijin, A. M. Milinda Abeykoon, Andrijana Solajic, Ana Milosavljevic, Jelena Pesic, Yu Liu, Cedomir Petrovic, Zoran V. Popovic, and Nenad Lazarevic, “Short-Range Order in VI3,” Inorg. Chem. **59**, 16265–16271 (2020).

86. S. Djurdjic Mijin, A. Baum, J. Bekaert, A. Solajic, J. Pesic, Y. Liu, Ge He, M. V. Milosevic, C. Petrovic, Z. V. Popovic, R. Hackl, and N. Lazarevic, “Probing charge density wave phases and the Mott transition in 1T − TaS2 by inelastic light scattering,” Phys. Rev. B **103**, 245133 (2021).

87. Peng Fan, Fazhi Yang, Guojian Qian, Hui Chen, Yu-Yang Zhang, Geng Li, Zihao Huang, Yuqing Xing, Lingyuan Kong, Wenyao Liu, Kun Jiang, Chengmin Shen, Shixuan Du, John Schneeloch, Ruidan Zhong, Genda Gu, Ziqiang Wang, Hong Ding, and Hong-Jun Gao, “Observation of magnetic adatom-induced Majorana vortex and its hybridization with field-induced Majorana vortex in an iron-based superconductor,” Nat. Commun. **12**, 1348 (2021).

88. Tim Gazdic, Ivan Maggio-Aprile, Genda Gu, and Christoph Renner, “Wang-MacDonald d-Wave Vortex Cores Observed in Heavily Overdoped Bi2Sr2CaCu2O8+δ,” Phys. Rev. X **11**, 031040 (2021).

89. Shunsuke Hasegawa, Shohei Hayashida, Shinichiro Asai, Masato Matsuura, Zaliznyak Igor, and Takatsugu Masuda, “Nontrivial temperature dependence of magnetic anisotropy in multiferroic Ba2MnGe2O7,” Phys. Rev. Research **3**, L032023 (2021).

90. Xinguo Hong, Matt Newville, Yang Ding, Dongzhou Zhang, Tetsuo Irifune, Genda Gu, and Ho-Kwang Mao, “Origin of the isostructural electronic states of the topological insulator Bi2Te3,” Phys. Rev. B **102**, 134110 (2020).

91. T E Kidd, P V Lukashev, L Stuelke, C Gorgen, S Roberts, G Gu, and A J Stollenwerk, “Diffusion energy barrier of Au on Bi2Se3: theory and experiment,” Phys. Scr. **96**, 125708 (2021).

92. Dong Seob Kim, Jung Yun Kee, Ji-Eun Lee, Yu Liu, Younghak Kim, Namdong Kim, Choongyu Hwang, Wondong Kim, Cedomir Petrovic, Dong Ryeol Lee, Chaun Jang, Hyejin Ryu, and Jun Woo Choi, “Surface oxidation in a van der Waals ferromagnet Fe3−xGeTe2,” Curr. Appl. Phys. (2021).

93. Chung Koo Kim, Jonathan D. Denlinger, Asish K. Kundu, Genda Gu, and Tonica Valla, “Absence of a Dirac gap in ferromagnetic Crx(Bi0.1Sb0.9)2−xTe3,” J. Appl. Phys. **129**, 083902 (2021).

94. T. Konstantinova, L. Wu, W. G. Yin, J. Tao, G. D. Gu, X. J. Wang, Jie Yang, I. A. Zaliznyak, and Y. Zhu, “Photoinduced Dirac semimetal in ZrTe5,” npj Quantum Mater. **5**, 80 (2020).

95. Tatiana Konstantinova, Lijun Wu, Weiguo Yin, Jing Tao, Genda Gu, Igor Zaliznyak, and Yimei Zhu, “Photoinduced Topological Insulator to Dirac Semimetal Transition in ZrTe5,” Microsc. Microanal. **27**, 2718–2719 (2021).

96. Asish K. Kundu, Genda Gu, and Tonica Valla, “Quantum Size Effects, Multiple Dirac Cones, and Edge States in Ultrathin Bi(110) Films,” ACS Appl. Mater. Interfaces **13**, 33627–33634 (2021).

97. Man Li, Nan Xu, Jianfeng Zhang, Rui Lou, Ming Shi, Lijun Li, Hechang Lei, Cedomir Petrovic, Zhonghao Liu, Kai Liu, Yaobo Huang, and Shancai Wang, “Quantization of the band at the surface of charge density wave material 2H-TaSe2,” Chinese Phys. B **30**, 047305 (2021).

98. P. M. Lozano, G. D. Gu, J. M. Tranquada, and Qiang Li, “Experimental evidence that zinc impurities pin pair-density-wave order in La2−xBaxCuO4,” Phys. Rev. B **103**, L020502 (2021).

99. Nathan J. McLaughlin, Hailong Wang, Mengqi Huang, Eric Lee-Wong, Lunhui Hu, Hanyi Lu, Gerald Q. Yan, Genda Gu, Congjun Wu, Yi-Zhuang You, and Chun-hui Rita Du, “Strong Correlation Between Superconductivity and Ferromagnetism in an Fe-Chalcogenide Superconductor,” Nano Lett. **21**, 7277–7283 (2021).

100. H. Miao, G. Fabbris, R. J. Koch, D. G. Mazzone, C. S. Nelson, R. Acevedo-Esteves, G. D. Gu, Y. Li, T. Yilmaz, K. Kaznatcheev, E. Vescovo, M. Oda, T. Kurosawa, N. Momono, T. Assefa, I. K. Robinson, E. S. Bozin, J. M. Tranquada, P. D. Johnson, and M. P. M. Dean, “Charge density waves in cuprate superconductors beyond the critical doping,” npj Quantum Mater. **6**, 31 (2021).

101. Ana Milosavljevic, Andrijana Solajic, Bojana Visic, Marko Opacic, Jelena Pesic, Yu Liu, Cedomir Petrovic, Zoran V. Popovic, and Nenad Lazarevic, "Vacancies and spin–phonon coupling in CrSi0.8Ge0.1Te3," J. Raman Spectrosc. **51**, 2153–2160 (2020).

102. Rubyann Olmos, Jose A. Delgado, Hector Iturriaga, Luis M. Martinez, Christian L. Saiz, L. Shao, Y. Liu, C. Petrovic, and Srinivasa R. Singamaneni, "Critical phenomena of the layered ferrimagnet Mn3Si2Te6 following proton irradiation," J. Appl. Phys. **130**, 013902 (2021).

103. Nicola Poccia, Shu Yang Frank Zhao, Hyobin Yoo, Xiaojing Huang, Hanfei Yan, Yong S. Chu, Ruidan Zhong, Genda Gu, Claudio Mazzoli, Kenji Watanabe, Takashi Taniguchi, Gaetano Campi, Valerii M. Vinokur, and Philip Kim, "Spatially correlated incommensurate lattice modulations in an atomically thin high-temperature Bi2.1Sr1.9CaCu2.0O8+y superconductor," Phys. Rev. Materials **4**, 114007 (2020).

104. Bryan Rachmilowitz, He Zhao, Zheng Ren, Hong Li, Konrad H. Thomas, John Marangola, Shang Gao, John Schneeloch, Ruidan Zhong, Genda Gu, Christian Flindt, and Ilija Zeljkovic, "Coulomb blockade effects in a topological insulator grown on a high-Tc cuprate superconductor," npj Quantum Mater. **5**, 72 (2020).

105. T. J. Reber, J. D. Rameau, C. Petrovic, Hasnain Hafiz, M. Lindroos, A. Bansil, and P. D. Johnson, "Superconducting pairing mechanism in CeCoIn5 revisited," Phys. Rev. B **102**, 205112 (2020).

106. Y. Shen, G. Fabbris, H. Miao, Y. Cao, D. Meyers, D. G. Mazzone, T. Assefa, X. M. Chen, K. Kisslinger, D. Prabhakaran, A. T. Boothroyd, J. M. Tranquada, W. Hu, A. M. Barbour, S. B. Wilkins, C. Mazzoli, I. K. Robinson, and M. P. M. Dean, "Charge Condensation and Lattice Coupling Drives Stripe Formation in Nickelates," Phys. Rev. Lett. **126**, 177601 (2021).

107. T. Valla, P. Pervan, I. Pletikosi´c, I. K. Drozdov, Asish K. Kundu, Zebin Wu, and G. D. Gu, "Hole-like Fermi surface in the overdoped non-superconducting Bi1.8Pb0.4Sr2CuO6+δ," Europhys. Lett. **134**, 17002 (2021).

108. Dongfei Wang, Jens Wiebe, Ruidan Zhong, Genda Gu, and Roland Wiesendanger, "Spin-Polarized Yu-Shiba-Rusinov States in an Iron-Based Superconductor," Phys. Rev. Lett. **126**, 076802 (2021).

109. Dongfei Wang, Ruidan Zhong, Genda Gu, and Roland Wiesendanger, "Surface orbital order and chemical potential inhomogeneity of the iron-based superconductor FeTe0.55Se0.45 investigated with special STM tips," Phys. Rev. Research **3**, L032055 (2021).

110. Yan-Ting Wang, Jay C. LeFebvre, Ethan Y. Cho, Stephen J. McCoy, Hao Li, Genda Gu, Kazuo Kadowaki, and Shane A. Cybart, "Fabrication of Bi2Sr2CaCu2O8+x ab-Plane Josephson Junctions by a Focused Helium Ion Beam," IEEE Trans. Appl. Supercond. **31**, 1–4 (2021).

111. R. Yang, M. Corasaniti, L. Wu, Q. Du, Y. Zhu, C. Petrovic, and L. Degiorgi, "Ingredients for enhanced thermoelectric power at cryotemperatures in the correlated semiconductor CoSbS revealed by its optical response," Phys. Rev. B **103**, L161111 (2021).

112. Nader Zaki, Genda Gu, Alexei Tsvelik, Congjun Wu, and Peter D. Johnson, "Time-reversal symmetry breaking in the Fe-chalcogenide superconductors," Proc. Natl. Acad. Sci. USA **118**, e2007241118 (2021).

113. He Zhao, Hong Li, Lianyang Dong, Binjie Xu, John Schneeloch, Ruidan Zhong, Minghu Fang, Genda Gu, John Harter, Stephen D. Wilson, Ziqiang Wang, and Ilija Zeljkovic, "Nematic transition and nanoscale suppression of superconductivity in Fe(Te,Se)," Nat. Phys. **17**, 903–908 (2021).

114. Yuying Zhu, Menghan Liao, Qinghua Zhang, Hong-Yi Xie, Fanqi Meng, Yaowu Liu, Zhonghua Bai, Shuaihua Ji, Jin Zhang, Kaili Jiang, Ruidan Zhong, John Schneeloch, Genda Gu, Lin Gu, Xucun Ma, Ding Zhang, and Qi-Kun Xue, "Presence of s-Wave Pairing in Josephson Junctions Made of Twisted Ultrathin Bi2Sr2CaCu2O8+x Flakes," Phys. Rev. X **11**, 031011 (2021).

115. M. Zonno, F. Boschini, E. Razzoli, S. K. Y. Dufresne, M. Michiardi, M. X. Na, T. M. Pedersen, S. Gorovikov, S. Gonzalez, G. Di Santo, L. Petaccia, M. Schneider, D. Wong, P. Dosanjh, Y. Yoshida, H. Eisaki, R. D. Zhong, J. A. Schneeloch, G. D. Gu, A. K. Mills, S. Zhdanovich, G. Levy, D. J. Jones, and A. Damascelli, "Ubiquitous suppression of the nodal coherent spectral weight in Bi-based cuprates," Phys. Rev. B **103**, 155109 (2021).

Fingerprinting Macromolecular Flow and Deformation with Neutrons

Yangyang Wang
Center for Nanophase Materials Sciences, Oak Ridge National Laboratory

Program Scope

Flow and deformation of macromolecules is ubiquitous in nature and industry, and a clear understanding of this phenomenon at both macroscopic and microscopic length scales is of fundamental and practical importance. Historically, the development of neutron scattering techniques has provided powerful tools for investigating the microscopic details of polymer motions in the quiescent state. However, the application of neutron scattering to polymers undergoing mechanical deformation and flow has not achieved a satisfactory status and is strewn with practical and theoretical difficulties. The objective of this project is to *unearth the full potential of small-angle neutron scattering (SANS) and neutron spin-echo spectroscopy (NSE) for understanding the flow and deformation behavior of polymers at the molecular level, by directly addressing the key scientific issues in anisotropic scattering*. To realize this goal, we have pursued the following three specific aims: (1) Establish protocols to reconstruct 3D anisotropic structures from 2D SANS spectra; (2) Develop new methods to examine dynamic fluctuations and viscoelastic "fingerprints" of polymers under deformation by exploiting the spherical harmonic expansion technique and taking advantage of the time-of-flight neutrons at the Spallation Neutron Source; and (3) Reveal real-space anisotropic structures via a new Fourier transform platform. These developments will allow us to address some of the most important scientific questions regarding the application of neutron scattering to polymer rheology.

Recent Progress

Quantification of flow-induced demixing in polymer blends: Flow-induced mixing, demixing, and phase transition phenomena in polymeric liquids are ubiquitous and practically important [1-4]. Small-angle neutron scattering by such systems often yields exotic scattering patterns, with the most famous example being the so-called "butterfly patterns". Despite the intense experimental and theoretical efforts since the 1980s, a clear understanding of these complicated phenomena has not been obtained and a systematic framework for quantitative analysis of those scattering patterns has not been developed. Previously, we successfully demonstrated how the spherical harmonic expansion technique could be employed to quantitative analyze the SANS spectra from deformed polymers, where the scattering was dominated by the single-chain structure factor [5-8]. In a more recent development [9], we show that the large concentration fluctuations of polymeric liquids under deformation and flow can be quantitatively studied by applying the spherical harmonic expansion technique to small-angle neutron scattering.

The basic idea of the spherical harmonic expansion analysis is to $I(\boldsymbol{Q}) = \sum_{l,m} I_l^m(Q) Y_l^m(\boldsymbol{\Omega})$, where $I(\boldsymbol{Q})$ is the measured scattering intensity and $I_l^m(Q)$ is the spherical harmonic expansion coefficient corresponding to each $Y_l^m(\boldsymbol{\Omega})$. This approach allows us to decompose the measured 2D

scattering spectrum into components with different symmetry. Because of the axial symmetry of the uniaxial extension problem, all the $m \neq 0$ terms and the odd l terms are forbidden. It follows that $I(\boldsymbol{Q}) = \sum_{l:\text{even}} I_l^0(Q) Y_l^0(\theta,\phi)$, with $Y_l^0(\theta,\phi) = \Theta_l(\theta) = \sqrt{2l+1} P_l(\cos\theta)$. More details about the data analysis procedure can be found in refs. [5-9]. The physical interpretation of such an expansion is that each coefficient $I_l^0(Q)$ represents the Q-dependent deformation anisotropy corresponding to the spherical harmonic function $Y_l^0(\theta,\phi)$. $I_0^0(Q)$ represents the isotropic component whereas $I_2^0(Q)$ is the leading term of the anisotropic components.

Using a series of binary polymer blends, we show in a recent work [9] that the emergence of the butterfly patterns is caused by the change of sign in the leading anisotropic component of the small-angle spectrum, when the scattering is dominated by intermolecular correlation associated with flow-induced demixing (Fig. 1). The increasing fluctuations of concentration are evidenced by the enhancement of the isotropic component of the scattering spectrum in the zero-angle limit and peak shift of the leading anisotropic coefficients towards low Q. Additionally, the spherical harmonic expansion framework permits real-space analysis of anisotropic scattering length density correlation in a convenient form. This new approach provides a concrete venue for quantitative studies of phase transitions of fluids under deformation and flow via SAS techniques, where mainly qualitative approaches were previously employed.

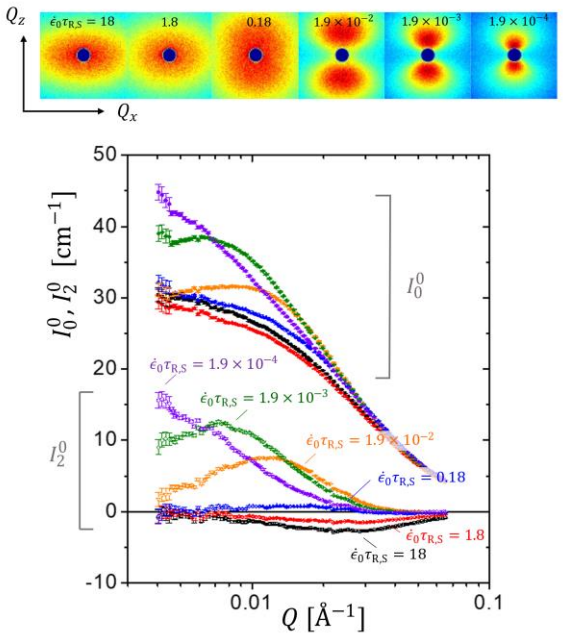

Figure 1. Top panel: SANS spectra of polymer blends after uniaxial stretching to $\lambda = 1.8$ with different engineering strain rates $\dot{\epsilon}_0$. The product of $\dot{\epsilon}_0$ and the Rouse time of the short chain $\tau_{R,S}$ is displayed on each spectrum. The stretching is along the z axis. Bottom panel: Expansion coefficients $I_0^0(Q)$ (filled symbols) and $I_2^0(Q)$ (open symbols) for all the samples.

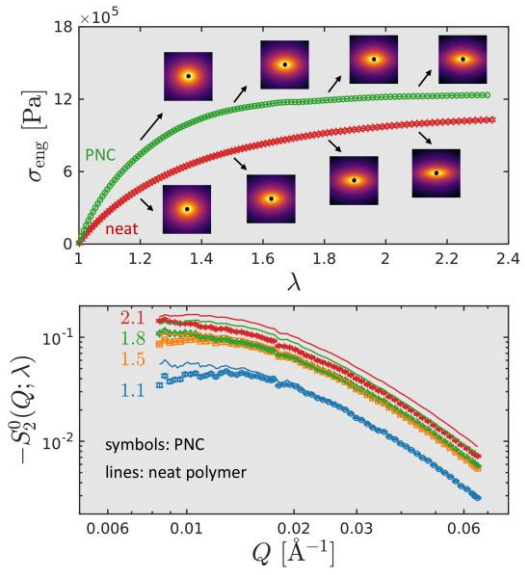

Figure 2. The upper panel illustrates the mechanical reinforcement in the PNC. The bottom panel shows quantitative analysis of the SANS spectra, where the neat polymer and PNC exhibit similar structural anisotropy.

Microscopic reinforcement mechanism in deformed polymer nanocomposites: Polymer nanocomposites (PNCs) exhibit many superior macroscopic properties than their individual

building blocks, the matrix polymer and the nanoparticle (NP). However, the molecular mechanism leading to the strong enhancement of macroscopic properties remains largely unresolved. Early studies argued an enhancement in the matrix polymer deformation to accommodate the non-deformable NP phase in PNCs to satisfy the overall macroscopic deformation [10]. Although such a concept of strain amplification is widely used by the PNC community, microscopic experiments regarding its existence have been inconclusive and controversial. Our recent work [11] helps to shed light on this longstanding problem. With proper polymer deuteration, the average scattering length density of the matrix polymer can be matched with that of the NP phase. At the zero-average-contrast point, the anisotropic structures of deformed polymers can be quantitatively determined by SANS with the spherical harmonic expansion technique. A combination of SANS and rheology [11] demonstrates the polymer deformation dominates the stress response of PNCs (Fig. 2). Despite a substantial mechanical reinforcement in the deformed PNC, a lack of molecular overstraining in the polymer phase has been identified. This observation cannot be explained by the NP-NP contribution but is consistent with the hydrodynamic effect of particles where a redistribution of the strain field in the polymer matrix is envisioned. This finding helps to clarify the molecular origin of the mechanical reinforcement in deformed PNCs and provides a new perspective for understanding the influence of NPs on the structure and dynamics of the polymer phase.

Development of a rotatable sliding plate shear cell: To overcome the limitations of the current rheo-SANS shear cells and establish protocols for reconstructing 3D anisotropic structures from 2D SANS spectra, we have developed a rotation transformation method based on spherical harmonic expansion analysis [12]. The basic idea is to perform rheo-SANS experiments on a sliding plate shear cell with a central rotary axis along the flow direction. By rotating the shear cell, all the spherical harmonic expansion coefficients of the anisotropic structure factor can be determined from measurements on a finite number of planes. Based on this concept, a rotatable sliding-

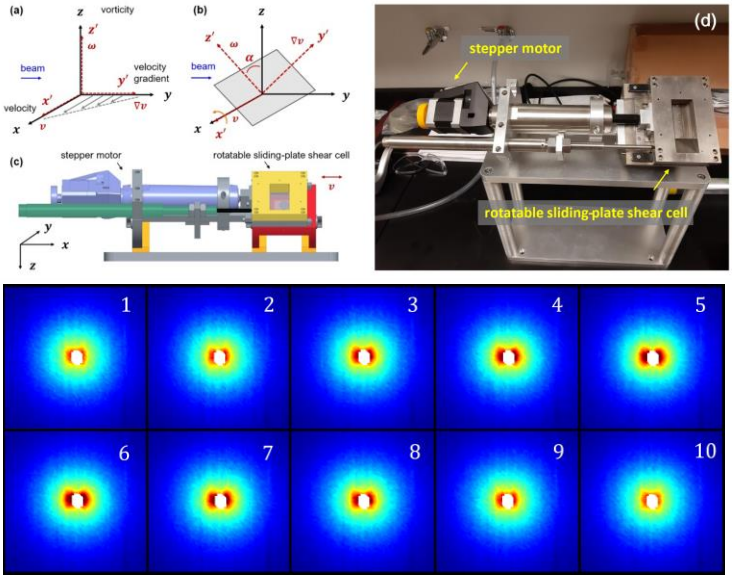

Figure 3. Schematic representation of the coordinate system setup and the rotatable sliding-plate shear cell. (a) In the initial state, the sample reference frame (x', y', z') and the laboratory reference frame (x, y, z) are aligned. x' is the velocity direction, y' is the velocity gradient direction, and z' is the vorticity direction. The incident neutron beam is along the y axis. (b) Rotation of the sample (shear cell) along the x axis. (c) Conceptual design of the rotatable sliding-plate shear cell. (d) The sliding-plate shear cell that has been constructed at ORNL. Bottom panel: evolution of SANS spectra within one period of steady oscillatory shear for a deformed polymer blend.

plate shear cell (Fig. 3) have been constructed and tested at the EQ-SANS beamline of SNS/ORNL. The new sample cell overcomes the difficulties associated with the traditional shear cells, including beam size, sample aspect ratio, sample viscosity, and path length problems. The successful demonstration of this new sample environment provides a powerful technique to understand the rheological behavior of polymeric materials using neutron scattering.

Future Plans

We plan to further explore the benefits of the recently developed rotatable sliding plate shear cell and study the connection between the viscoelastic response of polymers and the measured SANS spectra by performing time-resolve SANS/large-amplitude oscillatory shear experiments. Secondly, building upon the success of real-space analysis for flow-induced demixing in polymer blends [9], we will carry out further real-space investigations of large-scale conformations of deformed polymers using SANS and computer simulations. Lastly, a specific aim of this project is to explore the nonequilibrium dynamics of deformed polymers using neutron spin-echo spectroscopy. We have proposed a method to circumvent the doppler effect in order to properly carry out such experiments. Nevertheless, much is unknown about the dynamics in the deformed state. To inform the design of our neutron scattering experiments, we will first investigate the nonequilibrium dynamics using computer simulations. This work is a logical extension of our recent computational and experimental work on liquid dynamics in the equilibrium state [13,14], where we explored new model independent approaches for data analysis. The results of this theoretical/computational investigation will provide guidance for the design and interpretation of neutron spectroscopy experiments under flow and deformation.

References

[1] E. Helfand and G. H. Fredrickson, Phys Rev Lett **62**, 2468 (1989).
[2] R. Larson, Rheologica Acta **31**, 497 (1992).
[3] S. Milner, Phys Rev Lett **66**, 1477 (1991).
[4] H. Ji and E. Helfand, Macromolecules **28**, 3869 (1995).
[5] Z. Wang, et al., Phys. Rev. X **7**, 031003 (2017).
[6] C. N. Lam, et al., Phys Rev Lett **121**, 117801 (2018).
[7] W.-S. Xu, J.-M. Y. Carrillo, C. N. Lam, B. G. Sumpter, and Y. Wang, ACS Macro Lett **7**, 190 (2018).
[8] G.-R. Huang, B. Wu, Y. Wang, and W.-R. Chen, Phys. Rev. E **97**, 012605 (2018).
[9] Y. Wang, W. Wang, K. Hong, and Y. Liu, Macromolecules **54**, 3531-3542 (2021).
[10] L. Mullins and N. R. Tobin, J. Appl. Polym. Sci. **9**, 2993 (1965).
[11] R. Sun, et al., Phys. Rev. Lett. **126**, 117801 (2021).
[12] G.-R. Huang, et al., Phys. Rev. **E** 96, 022612 (2017).
[13] Z. Shen, J. Ma, J.-M. Y. Carrillo, W.-R. Chen, B. G. Sumpter, and Y. Wang, Phys. Rev. E **104**, 024503 (2021).
[14] J. Ma, et al., Phys. Rev. E **103**, 022609 (2021).

Publications

1. J. Ma, J.-M. Y. Carrillo, C. Do, W.-R. Chen, P. Falus, Z. Shen, K. Hong, B. G. Sumpter, and Y. Wang, "Spatial correlations of entangled polymer dynamics," Phys. Rev. E **104**, 024503 (2021).
2. Y. Wang, W. Wang, K. Hong, and Y. Liu, "Quantification of deformation-induced concentration fluctuations in polymeric liquids by small-angle neutron scattering," Macromolecules **54**, 3531-3542 (2021).
3. R. Sun, M. Melton, N. Safaie, R. C. Ferrier, Jr., S. Cheng, Y. Liu, X. Zuo, and Y. Wang, "Molecular view on mechanical reinforcement in polymer nanocomposites," Phys. Rev. Lett. **126**, 117801 (2021).
4. Z. Shen, J. Ma, J.-M. Y. Carrillo, W.-R. Chen, B. G. Sumpter, and Y. Wang, "Spatiotemporal mapping of mesoscopic liquid dynamics," Phys. Rev. E **103**, 022609 (2021).
5. Y. Wang, W. Wang, K. Hong, C. Do, W.-R. Chen, "Quantitative examination of a fundamental assumption in small-angle neutron scattering studies of deformed polymer melts," Polymer **204**, 122698 (2020).
6. G.-R. Huang, J.-M. Y. Carrillo, Y. Wang, C. Do, L. Porcar, B. G. Sumpter, W.-R. Chen, "An Exact Inversion Method for Extracting Orientation Ordering from Small-Angle Scattering," Phys. Chem. Chem. Phys. **23**, 4120-4132 (2021).
7. G.-R. Huang, Y. Wang, C. Do, and W.-R. Chen, "Spatial correlation functions of paracrystals with radial symmetry," Phys. Rev. E, **102**, 032110 (2020).

Author Index

Allred, Jared M. 9
Andersen, Ken 3
Azoulay, Jason 73
Bates, Frank S. 106
Batista, Cristian 119
Birol, Turan 61
Bockstaller, Michael R. 13
Cao, Huibo 201
Chandran, K. S. Ravi 17
Cheong, S.-W. 22
Chmaissem, O. 226
Choi, Joshua J. 89
Christianson, Andrew 207
Dai, Pengcheng 28
DeCaluwe, Steven C. 34
Delaire, Olivier 38
Eskildsen, Morten R. 43
Fernandes, Rafael 61
Fishman, R. S. 214
Frandsen, Benjamin 48
Frontzek, Matthias 232
Fullerton, Eric 164
Fultz, Brent 52
Gilbert, Dustin A. 56
Greven, Martin 61
Gu, Genda 237
Gu, Xiaodan 69, 73
Haberl, Bianca 232
Halász, Gábor 207
Helgeson, Matthew E. 80
Hermann, R. P. 214
Jalan, Bharat 61
Jiang, Chenyang 220
Jiang, Hongchen 92
Karim, Alamgir 13
Ke, Xianglin 85
Kiryukhin, V. 22
Lee, Seung-Hun 89
Lee, Young 92
Leighton, Chris 61
Li, Fankang 223
Li, Mingda 97, 102
Lodge, Timothy P. 106
Louca, Despina 111
Luscombe, Christine 138
Mandrus, David 207
Manley, Michael 214, 232
Matyjaszewski, Krzysztof 13
May, Andrew 207
Moulé, Adam J. 114
Mourigal, Martin 119
Olsen, Bradley 124
Osborn, R. 226
Paddison, Joseph 207
Perahia, Dvora 129
Petrovic, Cedomir 237
Phelan, D. 226
Plumb, Kemp 135
Pozzo, Lilo D. 138
Reznik, Dmitry 142
Richards, Jeffrey J. 147
Riggleman, Robert A. 178
Rodriguez, Efrain E. 151
Rosenkranz, Stephan 226, 232
Ross, Kate A. 156
Ruett, Uta 232
Schneider, Gerald J. 159
Sinha, Sunil K. 4, 164
Sirenko, A. 22
Swan, James 170
Taylor, Jonathan 5
te Velthuis, S. G. E. 226
Tisdale, William 170
Tranquada, John M. 237
Underhill, Patrick T. 80
Wang, Yangyang 253
Wen, Jiajia 92
Wilson, Stephen D. 174
Winey, Karen I. 178
Xie, Weiwei 182
Yang, Junjie 188
Zaliznyak, Igor A. 237
Zhang, Yang 192

Participants List

Name	Email	Organization
Abernathy, Doug	abernathydl@ornl.gov	Oak Ridge National Laboratory
Aczel, Adam	aczelaa@ornl.gov	Oak Ridge National Laboratory
Allred, Jared	jmallred@ua.edu	University of Alabama
Andersen, Ken	andersenkh@ornl.gov	Oak Ridge National Laboratory
Anderson, Zachary	and01942@umn.edu	University of Minnesota
Bates, Frank	bates001@umn.edu	University of Minnesota
Batista, Cristian	cbatist2@utk.edu	University of Tennessee
Birol, Turan	tbirol@umn.edu	University of Minnesota
Bockstaller, Michael	bockstaller@cmu.edu	Carnegie Mellon University
Cao, Zhiqiang	zhiqiang.cao@usm.edu	University of Southern Mississippi
Cao, Huibo	caoh@ornl.gov	Oak Ridge National Laboratory
Cavalcante, Lucas	lsrcavalcante@ucdavis.edu	University of California, Davis
Chandran, Ravi	ravi.chandran@utah.edu	University of Utah
Cheong, Sang-Wook	sangc@physics.rutgers.edu	Rutgers University
Chmaissem, Omar	chmaissem@anl.gov	Northern Illinois Univ./Argonne Nat. Lab
Choi, Joshua	jjc6z@virginia.edu	University of Virginia
Christen, Hans	christenhm@ornl.gov	Oak Ridge National Laboratory
Christianson, Andrew	christiansad@ornl.gov	Oak Ridge National Laboratory
Dai, Pengcheng	pdai.utk@gmail.com	Rice University
Das, Bhaskar	dasb@umn.edu	University of Minnesota
DeCaluwe, Steven	decaluwe@mines.edu	Colorado School of Mines
de la Cruz, Clarina	delacruzcr@ornl.gov	Oak Ridge National Laboratory
Delaire, Olivier	olivier.delaire@duke.edu	Duke University
Do, Seunghwan	seunghwando@gmail.com	Oak Ridge National Laboratory
Do, Changwoo	doc1@ornl.gov	Oak Ridge National Laboratory
Doucet, Mathieu	doucetm@ornl.gov	Oak Ridge National Laboratory
Duan, Chunruo	cd22@rice.edu	Rice University
Eskildsen, Morten	eskildsen@nd.edu	University of Notre Dame
Feng, Erxi	fenge@ornl.gov	Oak Ridge National Laboratory
Feng, Yiping	yiping.feng@science.doe.gov	Department of Energy
Fernandes, Rafael	rfernand@umn.edu	University of Minnesota
Fernandez-Baca, Jaime	fernandezbja@ornl.gov	Oak Ridge National Laboratory
Fishman, Randy	fishmanrs@ornl.gov	Oak Ridge National Laboratory
Frandsen, Benjamin	benfrandsen@byu.edu	Brigham Young University
Fullerton, Eric	efullerton@ucsd.edu	University of California, San Diego
Fultz, Brent	btf@caltech.edu	California Institute of Technology
Gao, Shang	gaos2@ornl.gov	Oak Ridge National Laboratory
Gilbert, Dustin	dagilbert@utk.edu	University of Tennessee
Graf, Matthias	matthias.graf@science.doe.gov	Department of Energy
Greven, Martin	greven@umn.edu	University of Minnesota
Gu, Xiaodan	xiaodan.gu@usm.edu	University of Southern Mississippi
Gu, Genda	ggu@bnl.gov	Brookhaven National Laboratory

Guo, Jiasen	jgvr7@umsystem.edu	University of Missouri, Columbia
Halász, Gábor	halaszg@ornl.gov	Oak Ridge National Laboratory
He, Lilin	hel3@ornl.gov	Oak Ridge National Laboratory
He, Xing	xing.he@duke.edu	Duke University
Helgeson, Matthew	helgeson@ucsb.edu	University of California, Santa Barbara
Hermann, Raphael	hermannrp@ornl.gov	Oak Ridge National Laboratory
Hoffmann, Christina	choffmann@ornl.gov	Oak Ridge National Laboratory
Hu, Xiao	xh5fe@virginia.edu	University of Virginia
Hu, Zhixiang	zhixiang@bnl.gov	Brookhaven National Laboratory
Jakobi, Bruno	bjakob1@lsu.edu	Louisiana State University
Jalan, Bharat	bjalan@umn.edu	University of Minnesota
Jiang, Chenyang	jiangc@ornl.gov	Oak Ridge National Laboratory
Jiang, Hong-Chen	hcjiang@stanford.edu	SLAC National Accelerator Laboratory
Jones, Braedon	braedon.c.jones@gmail.com	Brigham Young University
Karim, Alamgir	akarim3@central.uh.edu	University of Houston
Ke, Xianglin	kexiangl@msu.edu	Michigan State University
Kerch, Helen	Helen.kerch@science.doe.gov	Department of Energy
Kiryukhin, Valery	vkir@physics.rutgers.edu	Rutgers University
Krivyakina, Elena	ekrivyakina@anl.gov	Northern Illinois University
Lee, Young	youngsl@stanford.edu	Stanford University and SLAC
Lee, Ho Nyung	hnlee@ornl.gov	Oak Ridge National Laboratory
Lee, Seunghun	shlee@virginia.edu	University of Virginia
Leighton, Chris	leighton@umn.edu	University of Minnesota
Lessner, Eliane	eliane.lessner@science.doe.gov	Department of Energy
Li, Mingda	mingda@mit.edu	Massachusetts Institute of Technology
Li, Fankang	frankli@ornl.gov	Oak Ridge National Laboratory
Li, Yu	yu.li@anl.gov	Argonne National Laboratory
Littrell, Ken	littrellkc@ornl.gov	Oak Ridge National Laboratory
Liu, Qingsong	qingsongliu2025@u.northwestern.edu	Northwestern University
Lodge, Tim	lodge@umn.edu	University of Minnesota
Longbons, Grace	glongbon@nd.edu	University of Notre Dame
Louca, Despina	louca@virginia.edu	University of Virginia
Mamontov, Eugene	mamontove@ornl.gov	Oak Ridge National Laboratory
Mandrus, David	dmandrus@utk.edu	Oak Ridge National Laboratory
Manley, Michael	manleyme@ornl.gov	Oak Ridge National Laboratory
Marshall, Madalynn	mm3092@chem.rutgers.edu	Rutgers University
May, Andrew	mayaf@ornl.gov	Oak Ridge National Laboratory
Mohottalalage, Supun	ksupuns@g.clemson.edu	Clemson University
Moseley, Duncan	moseleydh@ornl.gov	Oak Ridge National Laboratory
Moulé, Adam	amoule@ucdavis.edu	University of California, Davis
Mourigal, Martin	mourigal@gatech.edu	Georgia Institute of Technology
Nguyen, Thanh	ngutt@mit.edu	Massachusetts Institute of Technology
Olsen, Bradley	bdolsen@mit.edu	Massachusetts Institute of Technology

Osborn, Raymond	rosborn@anl.gov	Argonne National Laboratory
Paddison, Joe	paddisonja@ornl.gov	Oak Ridge National Laboratory
Pandey, Sudip	spandey@physics.ucsd.edu	University of California, San Diego
Perahia, Dvora	dperahi@g.clemson.edu	Clemson University
Petrovic, Cedomir	petrovic@bnl.gov	Brookhaven National Laboratory
Phelan, Daniel	dphelan@anl.gov	Argonne National Laboratory
Plumb, Kemp	kemp_plumb@brown.edu	Brown University
Pozzo, Lilo	Dpozzo@uw.edu	University of Washington
Price, Eliza	ekprice@mit.edu	Massachusetts Institute of Technology
Rawot Chhetri, Top	tbrawotchettri@crimson.ua.edu	University of Alabama, Tuscaloosa
Reznik, Dmitry	dmitry.reznik@colorado.edu	University of Colorado, Boulder
Richards, Jeffrey	jeffrey.richards@northwestern.edu	Northwestern University
Riggleman, Robert	rrig@seas.upenn.edu	University of Pennsylvania
Ringler, John	john.ringler@colostate.edu	Colorado State University
Rodriguez, Efrain	efrain@umd.edu	University of Maryland
Rosenkranz, Stephan	srosenkranz@anl.gov	Argonne National Laboratory
Sarte, Paul	pmsarte@ucsb.edu	University of California, Santa Barbara
Saunders, Claire	csaunder@caltech.edu	Caltech
Schneeloch, John	jas9db@virginia.edu	University of Virginia
Schneider, Gerald	gjschneider@lsu.edu	Louisiana State University
Schwartz, Andrew	andrew.schwartz@science.doe.gov	Department of Energy
Sefat, Athena	Athena.Sefat@science.doe.gov	Department of Energy
Shen, Zhiqiang	shenz@ornl.gov	Oak Ridge National Laboratory
Singh, Deepak	singhdk@missouri.edu	University of Missouri, Columbia
Sinha, Sunil	ssinha@physics.ucsd.edu	University of California, San Diego
Sirenko, Andrei	sirenko@njit.edu	New Jersey Institute of Technology
Srinivasan, Ramana	u1072681@utah.edu	University of Utah
Sterling, Tyler	ty.sterling@colorado.edu	University of Colorado, Boulder
Stone, Matthew	stonemb@ornl.gov	Oak Ridge National Laboratory
Taylor, Jonathan	Jonathan.Taylor@esss.se	European Spallation Source ERIC
te Velthuis, Suzanne	tevelthuis@anl.gov	Argonne National Laboratory
Thiyagarajan, Pappannan	p.thiyagarajan@science.doe.gov	Department of Energy
Tisdale, Will	tisdale@mit.edu	Massachusetts Institute of Technology
Tranquada, John	jtran@bnl.gov	Brookhaven National Laboratory
Tucker, Matt	tuckermg@ornl.gov	Oak Ridge National Laboratory
Underhill, Patrick	underp3@rpi.edu	Rensselaer Polytechnic Institute
Wang, Yangyang	wangy@ornl.gov	Oak Ridge National Laboratory
Watkins, Erik	ebw@lanl.gov	Los Alamos National Laboratory
Wen, Jiajia	jwen11@stanford.edu	SIMES, SLAC National Laboratory
Williams, Travis	williamstj@ornl.gov	Oak Ridge National Laboratory
Wilson, Stephen	stephendwilson@ucsb.edu	University of California, Santa Barbara
Wilson, Lane	lane.wilson@science.doe.gov	Department of Energy
Winey, Karen	winey@seas.upenn.edu	University of Pennsylvania

Wu, Wenjie	wwu25@central.uh.edu	University of Houston
Xie, Weiwei	weiwei.xie@rutgers.edu	Rutgers University
Xie, Oliver	oxie@mit.edu	Massachusetts Institute of Technology
Xu, Xianghan	xx80@physics.rutgers.edu	Rutgers University
Yang, Junjie	jyang@njit.edu	New Jersey Institute of Technology
Yang, Yi	yiy042@ucsd.edu	University of California, San Diego
Zaliznyak, Igor	zaliznyak@bnl.gov	Brookhaven National Laboratory
Zhai, Yue	yuezhai@andrew.cmu.edu	Carnegie Mellon University
Zhang, Yang	zhyang@illinois.edu	University of Illinois at Urbana-Champaign
Zhang, Yuxuan	zhangy6@ornl.gov	Oak Ridge National Laboratory
Zhang, Bo	zhan5777@umn.edu	University of Minnesota